STATE OF CALIFORNIA • DEPARTMENT OF TRANSPORTATION
TECHNICAL REPORT DOCUMENTATION PAGE
DRISI-2011 (REV 10/1998)

1. REPORT NUMBER CA21-3021	2. GOVERNMENT ASSOCIATION NUMBER	3. RECIPIENT'S CATALOG NUMBER
4. TITLE AND SUBTITLE Fiber Optic Monitoring of Base Grouted Piles		5. REPORT DATE July, 2021
		6. PERFORMING ORGANIZATION CODE
7. AUTHOR R.A. Yeskoo, K. Soga		8. PERFORMING ORGANIZATION REPORT NO. n/a
9. PERFORMING ORGANIZATION NAME AND ADDRESS UC Berkeley Berkeley CA.		10. WORK UNIT NUMBER
		11. CONTRACT OR GRANT NUMBER Contract No. 65A0645
12. SPONSORING AGENCY AND ADDRESS California Department of Transportation (Caltrans) Division of Research, Innovation & System Information, MS-83 2963 R Street, Sacramento CA 95816		13. TYPE OF REPORT AND PERIOD COVERED Final Report
		14. SPONSORING AGENCY CODE

15. SUPPLEMENTARY NOTES

A separate report, referenced below, describes the execution of the post-grouting test program that utilized distributed fiber-optic strain sensing.

A. Boeckmann, J.E. Loehr, and T. Shantz, (June, 2021) Post-grouting of Drilled Shafts: Evaluation and Recommendations for Deployment (CA21-2865), California Dept. of Transportation, https://dot.ca.gov/programs/research-innovation-system-information/research-final-reports

16. ABSTRACT
This report documents the field application of distributed fiber-optic strain (DFOS) sensing for measuring strain in drilled shaft foundations. Nine 5-foot diameter reaction shafts and four 3-foot diameter test shafts were subjected to base grouting. Following several weeks of set-up the test shafts were then loaded from the top in a conventional quasi-static load test. Distributed fiber optic strain sensing techniques were used to measure strain along the entire shaft length along four separate fiber optic cables. These strain measurements were compared to those of vibrating-wire (VW) strain gauges at multiple depths. While DFOS could not match VW gauge's resolution, the strain estimates of each method compared very favorably. Comparisons are provided for reaction and test shafts during grouting and for test shafts during static load testing. A major advantage of DFOS sensing is that it provides a near continuous estimate of strain along the entire fiber-optic cable length.

The report also addresses practical aspects of DFOS for field work including installation methods, field splicing of fiber-optic cables, and the use of an interrogator device to make strain estimates. A laboratory testing program is described that investigates the accuracy of DFOS when strain varies during the typical 5-minute sampling interval required by the interrogator. DFOS sensing requires a separate fiber-optic cable to measure temperature since the frequency shift in reflected light that is the basis of DFOS methods is also temperature dependent.   These fiber-optic based temperature measurements are compared against a dense array of thermistor based measurements in several of the shafts.

17. KEYWORDS Fiber optic, Brillouin, strain gauge, strain sensing, grouting, drilled shaft, CIDH, load-test, foundation, bridges, variable strain effect, fiber Bragg grating, temperature sensing	18. DISTRIBUTION STATEMENT No restrictions.		
19. SECURITY CLASSIFICATION (of this report) Unclassified	20. NUMBER OF PAGES 195 pages		21. COST OF REPORT CHARGED

Reproduction of completed page authorized.

ADA Notice For individuals with sensory disabilities, this document is available in alternate formats. For alternate format information, contact the Forms Management Unit at (916) 445-1233, TTY 711, or write to Records and Forms Management, 1120 N Street, MS-89, Sacramento, CA 95814.

DISCLAIMER STATEMENT

Fiber Optic Monitoring of Base Grouted Piles

R. A. Yeskoo[1] and K. Soga[2]

July 7, 2021

1. PhD student, University of California, Berkeley
2. Professor, University of California, Berkeley

Table of Contents

1. Introduction

Base grouting of piles generally refers to a range of methods to introduce grout under pressure to the tip of a deep foundation element. Most commonly employed on large diameter drilled shafts, the goal of base grouting is to improve the performance of the pile during loading. There remains debate within the geotechnical community regarding contribution of the specific combination of mechanisms that contribute to the improvement, with the apportionment split between ground improvement at the tip, pre-mobilization of tip displacements, and pre-mobilization of shaft resistance (FHWA 2017, Day et. al. 2015, Ruiz 2008). Regardless of the mechanism, an increase in the stiffness of the foundation element's response under loading has been observed in load tests, as compared to un-grouted piles in the same stratigraphy.

Base grouting has been performed on production foundation projects throughout Europe for many decades; however, it has been slow to be adopted within the United States. Continuing testing and research on the practice in the U.S. is ongoing, both in the academic and public sector, to refine the design guidelines of successful base grouting programs and improve the quality assurance / control of grout delivery during construction (FHWA 2017). The California Department of Transportation (Caltrans) formed a research team to explore the use of base grouting of piles on future Caltrans deep foundations. The research team, under the leadership of Tom Schantz, is comprised of members from the University of Missouri (Erik Loehr and Andy Boeckmann), and members from the University of California, Berkeley (Kenichi Soga and Andrew Yeskoo). The University of Missouri team has focused its efforts on development of the design and reliability of base grouting, while the Berkeley team has focused on exploration of the use of Distributed Fiber Optic Sensing (DFOS) as a complimentary or alternative method for strain measurements during grouting and load testing.

Quality assurance and control (QA/C) during production base grouting is typically performed by monitoring the grout delivery to the pile, including pressure and volumetric flow rate, as well as movement of the top of the pile (FHWA 2017, Mullins 2016). Additional measurements such as pile base movements and point strain within the pile are occasionally incorporated into a small portion of test piles. However, these methods are not typically used on the production scale

except for the most critical projects. Distributed fiber optic sensing of strain within the pile can offer a relatively inexpensive method to incorporate distributed strain measurements within test and production piles as another means to monitor the performance of the pile during base grouting. The variable nature of grout delivery at the base of the pile and the potential for blockages to develop during grouting pose the very real risk that grout pressures and flows observed at the surface are not being transmitted to the base as intended. The addition of DFOS as a cost-effective way to incorporate strain measurements into base grouting can greatly reduce the uncertainty associated with the grouting process and improve the specification and engineering acceptance of base grouted piles in production.

This report presents the results of the Berkeley team's research during the project. Chapter 2 contains a summary of survey results from European engineers and contractors regarding their opinions and practices for base grouting of piles. Chapter 3 presents the results of a lab testing program performed to explore the effect on transient (non-constant) strains during fiber optic readings. Chapter 4 summarizes the field experiment and the equipment and installation. Chapter 5 provides a summary of the fiber optic strain measurements taken during base grouting. Chapter 6 provides a summary of the fiber optic strain measurements taken during load testing. Chapter 7 presents a discussion of some of the observations made regarding the data, including a comparison of the fiber optic strain data with strain data from conventional vibrating wire strain gauges. Finally, Chapter 8 is a conclusion to the report, including a summary of the use of fiber optics for monitoring of base grouting and recommendations for future work.

Two additional reports were produced from the Berkeley team's work on this project. The first is focused on a summary and analysis of thermal measurements taken during curing on five of the reaction shafts during the base grouting project. The second presents results and analysis of fiber optic monitoring of a soil anchor load test in southern California.

Field Test Overview

The primary phase of the research testing was a field trial consisting of the installation of thirteen drilled shafts, each approximately 35-feet deep below ground surface. The piles were

divided into four three-foot-diameter test piles and nine five-foot-diameter reaction piles. The nine reaction piles were installed in a 3x3 grid, 28-feet on center, with the smaller test piles located in the center of each quadrant of four reaction piles. The test site was located approximately 18 miles north of Sacramento, California, within the Caltrans right-of-way at the junction of CA State Routes 99 and 77. A satellite image of the test site from Google Earth, taken August 28, 2019, is shown in Figure 1-1. The grid of the nine reaction piles can faintly be seen within the satellite image and are marked with a red box in the figure.

Figure 1-1: Satellite image of the field test site in August 2019 (Google Earth)

Several types of measurements and observations were taken during the construction of the piles, including scans of the drilling fluid-filled borehole wall, measurements of the base hardness of the drilled borehole, and measurements of the integrity of the pile concrete after pour. The integrity methods used on the project included thermal monitoring during curing using both distributed fiber optics and a commercial monitoring system, cross-hole sonic logging (CSL), and Gamma-Gamma logging (GGL).

Following construction of the piles, twelve of the piles were base grouted including all of the reaction piles and three of the four test piles. Three base grouting delivery methods were used

on the project. These include an open-type system (tube-à-manchette), a closed-type system (rubber bladder), and a proprietary expansion cell system (RIM-Cell by Loadtest). The delivery grout pressure and volume were recorded by an in-line data logger between the grout plant and the pile. Movements of the pile were measured using a combination of dial gauges and survey methods of points at the top of the pile and tell-tales extending to the bottom of the pile. Mechanical strains within the pile were measured using vibrating wire strain gauges as well as distributed fiber optic strain cable. Temperatures within the pile were also measured using distributed fiber optic thermal monitoring. A photo showing the typical site setup of the various monitoring systems during base grouting is shown in Figure 1-2.
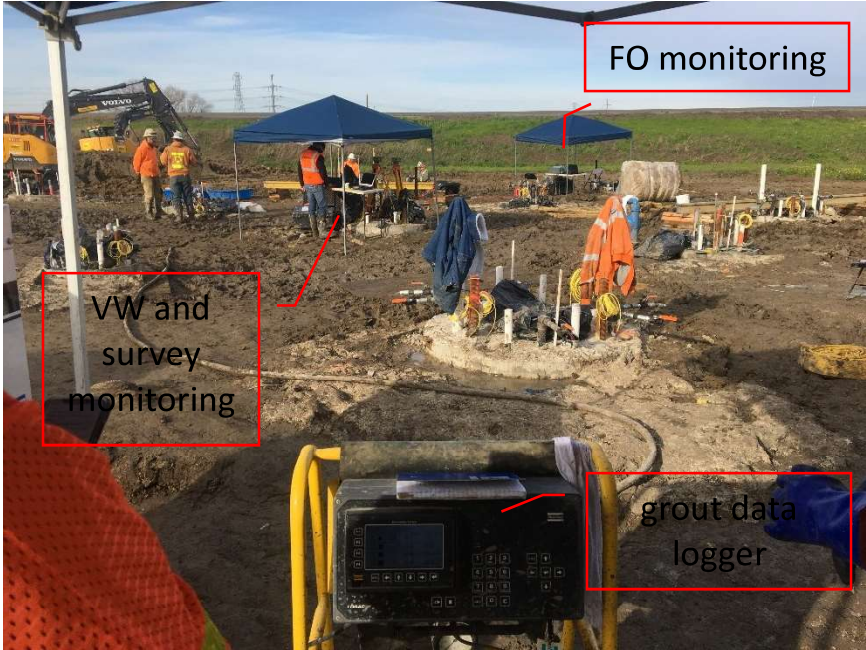

Figure 1-2: Monitoring systems during base grouting

After the base grouting was complete, the four test shafts were load tested. The axial loads were imposed on the test pile using four hydraulic jacks, connected to the four surrounding reaction piles through a steel load frame. A photo of the load test frame is shown in Figure 1-3.

Figure 1-3: Load test frame

Displacement and strain measurements were taken in the manner as described above for base grouting, with additional measurements taken of top displacements of the pile using LVDTs and the hydraulic jack pressure and associated load on the pile were taken during the load test.

Overview of Fiber Optic Monitoring

Fiber optic monitoring refers to a variety of different sensing techniques which allow the interaction of light along a fiber optic cable to be used to measure various physical parameters along the cable length. The systems are broadly divided into point-based sensing systems and distributed systems (Kechavarzi et al., 2016; Soga and Luo, 2018). The first category includes Extrinsic Fabry-Perot interferometers and Fiber Bragg Gratings (FBGs). These incorporate optical reflectors or etched treatments along the fiber optic cable, allowing the measurement of physical parameters at the sensing points. In the case of FBG systems, multiple sensing treatments can be installed along the same cable, allowing for a quasi-distributed sensing system. The second category of Distributed Fiber Optic Sensing (DFOS) relies on the fiber optic cable itself as a sensing instrument. When light is sent through a fiber optic cable, several types of scattering occur to a small proportion of the light's power while traveling within the fiber core. Of the scattering within the cable, a small subportion of the scattered light is reflected back towards the source, a phenomenon called backscattering. By carefully recording differences in the backscattered light, measurements of physical phenomenon can be made

along the cable. The types of DFOS technologies are divided by the type of scattering that they rely upon. These are divided into Raman scattering, which is proportional to temperature changes, Rayleigh scattering, which is proportional to vibration or dynamic rate-of-strain, and Brillouin scattering, which is proportional to strain and temperature changes. A diagram illustrating this phenomenon is shown in Figure 1-4.
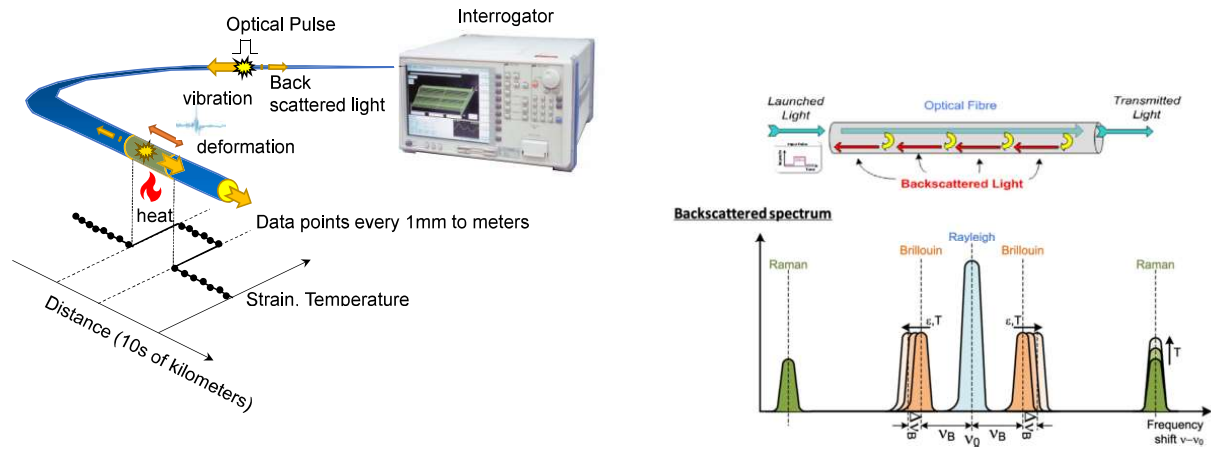

Figure 1-4: Backscattered light phenomenon (after Kechavarzi et al., 2016)

For civil engineering applications, FBG and Brillouin based sensing systems are the most common for measurements of strain and temperature. A brief overview of how these technologies function is presented below.

Fiber Bragg Grating (FBG) Sensing

Fiber Bragg Grating sensing relies on discrete sensing points created within a fiber optic cable by creating evenly spaced etchings, referred to as gratings, within the fiber optic core. The spacing of the fiber optic gratings is designed to correspond and interact with a specific wavelength of light. When a broadband light pulse is passed through the fiber optic cable, each grating will create a reflection back to the source of its signature wavelength, allowing the remainder of the light to continue propagating down the cable in the original direction of travel. This principle is illustrated in Figure 1-5.
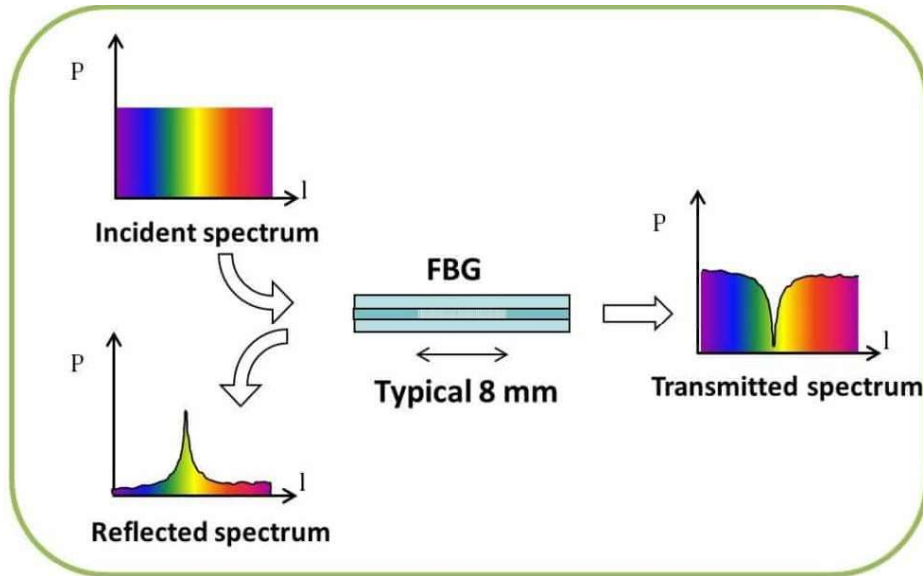
9

Figure 1-5: Spectral reflection and shadowing of FBG (image credit: FBGS)

Extension or contraction of the cable containing a grating results in a proportional increase or decrease in the spacing of the grates, shifting the reflected wavelength. This principle is illustrated in Figure 1-6. The shift in the wavelength is proportional to strain (either mechanically generated or thermally generated, or both).
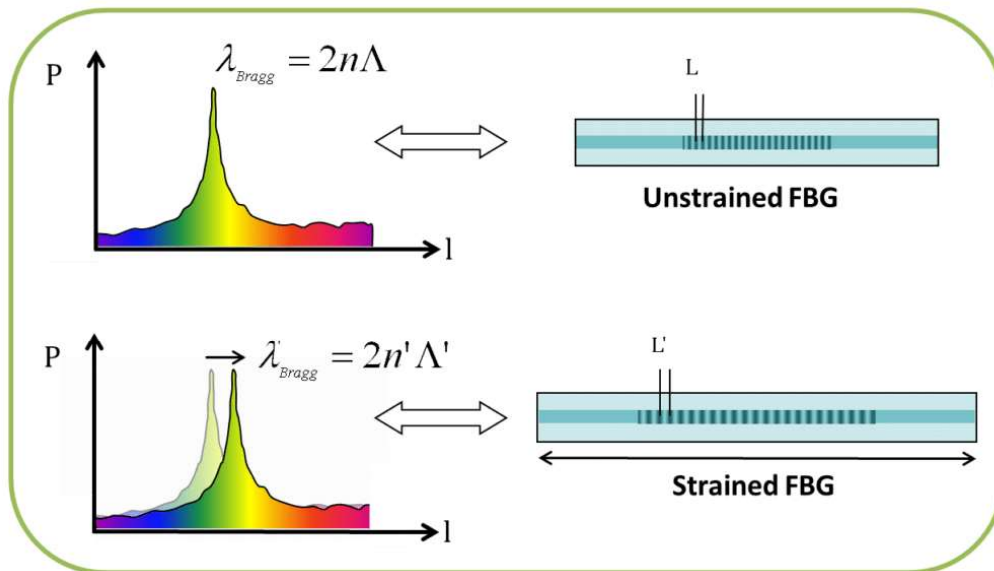

Figure 1-6: FBG central and strained wavelength (image credit: FBGS)

Multiple gratings can be included on a continuous length of fiber, so long as their central wavelengths are spaced far apart enough to allow for identification of the signal for each

discrete sensor, including as they shift within their measurement range. Commercial analyzers can track the wavelength peaks along the fiber optic cable dynamically and include the ability to enter calibration factors to convert from wavelength to temperature or strain. Strain sensors along the fiber are created by allowing the surrounding strains to be transferred into the grating. Temperature sensors along the fiber take the opposite approach, physically preventing external strains from being applied to the grating and using the thermal coefficient of the fiber to convert thermal strain to temperature change. Since the strain sensors are also subjected to thermal strain, it is often prudent to co-locate a temperature sensor with each strain sensor to allow later correction for the thermal strains.

The sensing points themselves can either be etched directly onto a fiber optic cable, either at standardized or custom spacing, or can be housed within stand-alone sensor packages which are networked together using standard fiber optic cable. The sensor housings can be tailored to match the function and form of more conventional point-based sensors, such as vibrating wire strain gauges. However, they are often much more expensive than vibrating wire sensors. FBG sensors offer the benefit of being unaffected by electronic or magnetic interference, as well as functioning without any electrical current at the sensing locations.

Distributed Brillouin Strain and Temperature Sensing

Distributed Brillouin sensing relies on backscattered light signals generated along the length of a fiber optic cable. As a light pulse travels down the fiber optic cable, it interacts with minute changes in density fluctuations within the fiber core. Standard single-mode telecommunications fiber optic cable contains these fluctuations as a result of their manufacturing – no specialized fiber core is required for the majority of Brillouin sensing. Certain high resolution Brillion technologies rely on specialized non-linear fibers with additional density fluctuations introduced during manufacturing. However, these fibers are not commonly deployed in long distances or common applications within civil engineering.

The density fluctuations scatter a small amount of light within the fiber, including a portion which propagates back towards the source. The Brillouin scattering phenomena results in a change in the photon energy, corresponding to a shift in the frequency of the scattered light.

The frequency shift from the source light is referred to as the Brillouin frequency shift, and it is this shift that is recorded by the measurement instrument (i.e., analyzer). The shift is proportional to small changes in material density and varies linearly with applied longitudinal strain along the fiber core, either thermal or mechanical.

The Brillouin scattering effect occurs naturally within the fiber optic core at low energies, a phenomenon called spontaneous Brillouin scattering. The strength of the scattered signal can be magnified by introducing a "pump" light pulse from the opposite end of the fiber, an approach called stimulated Brillouin scattering. This increases the resolution of the measurement. The use of spontaneous or stimulated Brillouin scattering are the fundamental difference between a Brillouin Optical Time Domain Reflectometry (BOTDR) or a Brillouin Optical Time Domain Analysis (BOTDA) fiber optic sensing analyzer. BOTDR only requires connection to one end of the sensing fiber optic cable and the strain resolution (measurement repeatability) is about 20-30 $\mu\varepsilon$, depending on the analyzer. Because of its use of stimulated Brillouin scattering, BOTDA requires a continuous loop within the sensing cable with the benefit of an increase in frequency (strain/temperature) sensitivity. The strain resolution (measurement repeatability) is about 2-5 $\mu\varepsilon$, again depending on the specific analyzer.

In commercial Brillouin fiber optic analyzers, the system both generates the light pulse to send into the sensing cable as well as records the Brillouin frequency response. The reflected light is recorded periodically with time, with the arrival time of the reflection used to localize the reflection source along the fiber based on the speed of light within the core. The regularity of how often a reading point is recorded determines the readout spacing of the analyzer – that is how often along the fiber a single measurement is taken. The readout spacing of the analyzer used in this study was 0.25 m; that is, strain/temperature data is given every 0.25 m.

The pulse width, or how long a section within the fiber is occupied by the light at any given time, determines the spatial resolution of the analyzer. This can be thought of as the length over which the strain or temperature measurement is taken within the fiber, although differences in the "shape" of the pulse mean that it is often not an exact linear average along the interval. The spatial resolution of the commercial analyzer used in this study was 0.75 m.

This means that each data point is a strain of 0.75 m gauge length. In other words, it is a weighted average strain of ±0.375 m from the data point.

While taking a reading, most commercial analyzer designs only record the light response within a single frequency band at a time. The way that a complete reading is taken is by "sweeping" the recorded frequencies within a set window and a gain (scattered light power)-frequency-distance plot is produced, as shown in Figure 1-7. The figure plots the spectrum data around the frequency range where Brillouin scattering is occurring.

Figure 1-8 shows the spectrum plot of gain versus frequency at a given sensing point along the fiber. It is common to take multiple readings at each frequency interval and average the results to reduce the associated noise in the reading (this is performed automatically by the analyzer). Using this plot generated for each sensing point along the fiber, the Brillouin frequency peak for each point is identified. As described earlier, the Brillouin peak frequency is related to strain, either mechanical or thermal. The figure shows one reading in white and another reading in pink. The shift in the peaks of the two curves are related to change in strain or temperature at that sensing point on the fiber.

For a given reading, Brillouin peak frequency can be identified at each sensing point and Figure 1-9 shows a plot of Brillouin peak frequency versus distance. The output of the analyzer will be a 2D matrix with the distance from the analyzer in the first column and the peak Brillouin frequency in the second. Although a single Brillouin peak frequency value is presented in the common output of the analyzer (Figure 1-9), each point along the fiber has an entire power spectrum with amplitudes of each scanned frequency within the reading window (Figure 1-8). The combination will produce a 3D plot like the one shown in Figure 1-7.
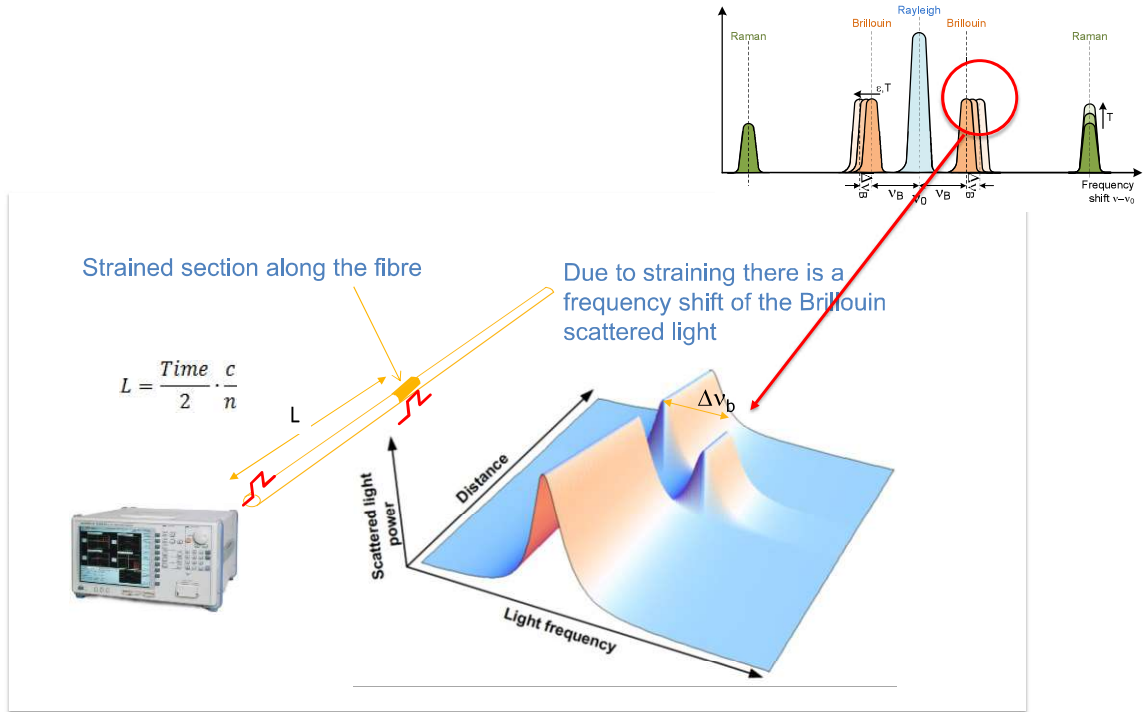
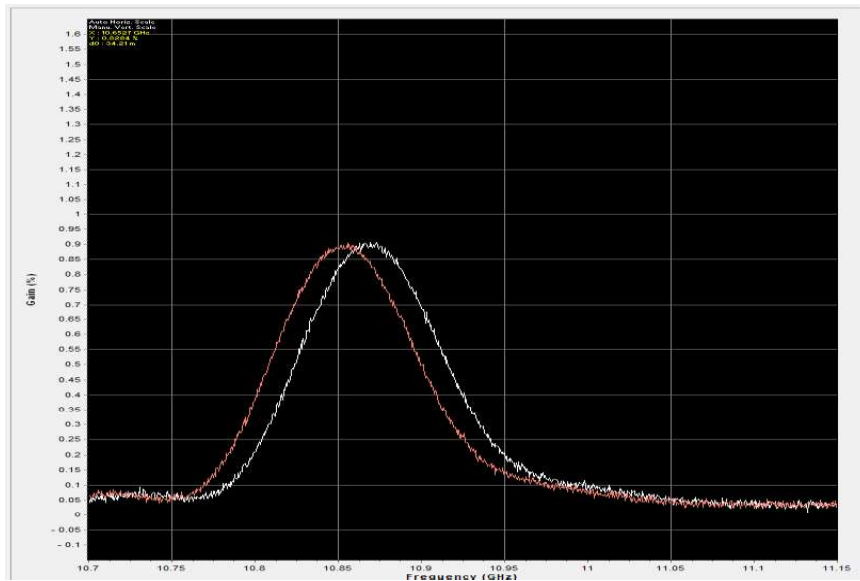*Figure 1-7: 3D power spectrum along the fiber*

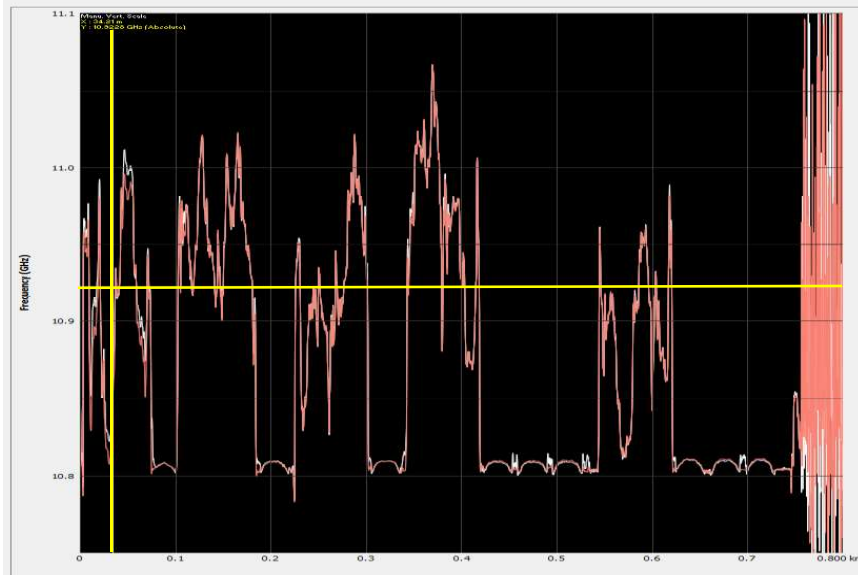*Figure 1-8: Gain (amplitude) vs. Frequency for a single reading point*

14

Figure 1-9: Peak Brillouin Frequency vs. Distance Along Fiber

In Figure 1-9, the peak Brillouin frequency along the length of the sensing fiber is shown for two separate readings, displayed in white and pink. The differences in frequency between the two points indicate areas along the fiber that had changes in strain or temperature between the early and later reading, with the difference in frequency linearly corresponding to a specific change in strain or temperature. The yellow crosshair on the figure is used to narrow in on a single reading point along the fiber. As described earlier, the frequency power spectrum for the two readings at this point are shown in Figure 1-8. The values for the two readings in the previous figure represent the calculated peak frequencies of the power spectrum; however, to generate the reading the power was recorded for every frequency step within the scanning window of 10.7 GHz to 11.15 GHz. Since it can take several minutes to complete a reading for the entire frequency range, this method of Brillouin sensing can be sensitive to changes in strain or temperature during the reading interval. A detailed exploration of this effect on the final reading is presented in Chapter 3.

Since the change in Brillouin peak frequency is proportional to changes in both mechanical strain and temperature along the fiber, it is necessary to compensate for the thermal effect for monitoring projects where the temperature along the sensing fiber fluctuate during the observation period. The approach is to use specialized cable designs to either tightly bond the

15

fiber optic core to applied external mechanical strains, or to completely debond the fiber optic core from external mechanical strains. In the first case, several specialized fiber cable designs have been developed to accommodate a wide range of applications. These include extremely thin packaging for high strain sensitivity, all the way to steel-sheathed cables designed to survive the high temperatures and pressures in downhole oil and gas applications. In all cases, the cables must be carefully designed and manufactured to reliably transfer strains from the exterior of the cable to the fiber optic core within. Any slippage or non-linearity in the strain transfer can greatly affect the fidelity of the measurements along the fiber, often to an unknown or un-correctable degree. The strain cable used in this study is shown in Figure 4-3. In the second case, several standard telecommunications fiber optic cables are manufactured with a "loose-tube" design. While the specific layering and materials vary among manufacturers, this refers to a strain-decoupling layer within the cable, often either a gap or a viscous gel. Changes in the Brillouin frequency in temperature fibers can be assumed to be due only to thermal changes in the fiber; however, testing and calibration is recommended to confirm the strain decoupling of new fiber designs. The temperature cable used in this study is shown in Figure 4-1.

2. European Base Grouting Practitioner Survey

The base grouting practice within the United States has been developing at an increasing pace, led in large part by academic research by several universities across the country as well as the adoption by several construction firms. However, the use of base grouting is still relatively localized on a project-by-project basis and is not widely familiar to many developers, designers, and foundation contractors. At the same time, the base grouting practice in the United Kingdom is comparatively well-established and is actively employed by several engineering firms and contractors in areas of challenging soil conditions.

An online survey on post-grouted shaft construction practice in the UK was conducted to capture some of the approaches and opinions of the practitioners there. We received responses from four consultants (Respondents A-D) and two contractors (Respondents E-F). This section of the report summarizes their replies to the survey, in their own words where possible. While the identities of the participants have been anonymized, the specific opinions and responses that they have given are indicated using parenthetical citations.

The specific questions included in the survey are included in the Appendix. This section of the report also incorporates information obtained from published documents and internal documents provided by collaborating companies.

General

Regarding the benefits of base grouting:

- The primary geotechnical purpose of post-grouting is to reduce pile settlement (stiffer response) under vertical load ("give confidence in mobilizing a high end-bearing resistance at small pile settlement (i.e. compatible with mobilization of shaft friction) (A)".
- A non-geotechnical benefit is that "the construction team tends to apply greater focus and attention to detail during pile construction, due to the greater complexity introduced by the post-grouting process." and "it makes a well-built pile even better" (B)

The primary barriers preventing more widespread adoption of post-grouting in the industry are:

- Limited understanding - "Lack of understanding by consultants and there are only a few competent piling contractors. (A)" "There a limited number of designers in the UK with suitable experience to design and specify base grouting. (C)"
- Extra effort - "many contractors think it is more trouble than it is worth due to the extra effort and constraints it imposes. (C)" "Lack of clarity on the actual benefits of the process, complication of the construction process by the introduction of additional activities (E)"
- Lack of robust acceptance criteria. (D)
- Cost (D).
- Misplaced belief - "Base grouting is only required if the base cannot be adequately cleaned: in other words that base-grouting is itself some kind of remedial grouting process. (B) "Honestly in the design stage when it is not required and design out in many cases where practical. (F)
- Other concerns – "In seismic zones the 'precompression' effect in the pile shaft that is created during base grouting could be lost. (B)."

There is need of "a program of education about the processes involved and the improvements seen in shaft resistance/displacement as a result of post-grouting. (B)" and to evaluate "the impact on cost and program of base grouting vs the benefits (e.g. increased stiffness and capacity).) (F)"

Mechanisms

The base grouting of bored piles has been used effectively to improve the pile (tip and shaft) response to the applied load through the following three main mechanisms: (1) compaction of loose material at the base resulting in stiffer bearing response, (2) negative shaft resistance resulting in stiffening effect by load reversal when vertically loaded downward (3) formation of grout socket at the bottom of pile due to migration of grout upwards around pile shaft, resulting in cohesion between the shaft and the surrounding soil. The combined effects will give stiffer response at working loads for a given permissible settlement.

Concerning the increase in the overall pile stiffness, Respondent (A) describes "the main mechanism (when using small volumes of grout in dense sands) is really "pre-stressing" or "pre-loading" the pile, giving a reversal of shaft friction and a locked-in load at the pile toe. As a result of grout injection, the pile will move upwards (mobilizing its shaft friction in reverse direction to conventional top-down loading), perhaps 5mm. A given volume of grout will produce equal and opposite reaction forces from shaft and end-bearing. When the pile is

subsequently loaded at the head, shaft friction and end-bearing are mobilized from their new load origins (induced by the base grouting). Because of a pre-load, a higher proportion of the ultimate load is carried in shaft friction."

The ultimate capacity remains unchanged, but the overall pile "stiffness" is much higher. Herein, the definition of ultimate capacity is "the theoretical "ultimate" – when load-settlement becomes asymptotic." "Using the code definition of ultimate, i.e., what is mobilized at a settlement of 5 or 10% of base diameter, then this capacity is increased by base grouting (A)".

a) Reversal of shaft friction

The mechanism of the "reversal of shaft friction" is discussed by three out of five respondents (A, B and C). "Shaft grouting can improve the shaft resistance by increasing lateral stresses a little and base grouting can compress the shaft a little, causing reversal of shear up the shaft and some pre-compression in the shaft. In shorter pile this is manifest when there is measured uplift of the top of the pile. Thus post-grouting provides a little more positive shaft resistance when the pile sustains load imposed from the top. (B)" "Pre-loading the pile from at the base causing a reversal of shaft friction. (C)"

b) Base resistance increase

Another mechanism given is on base resistance - "pre-load pile base or consolidate base (C, D, E and F). Typically the latter only in order to stiffen pile response under load." "Pressure of grout permeates/compacts loosened material to re-instate in situ stress state. (D)" "For piles with loose soils at the base, there may be some increase in base stiffness to compaction. (C)" This is in line with contractors stating that "If the base of the piles is properly constructed, it is not possible to actually inject much grout. It can however ensure that any disturbance can be restored." (E) "Main mechanisms, in order of performance. 1. pre-mobilize base capacity (important in piles that rely heavily on the end bearing capacity, particularly under working conditions), 2. Ensure effective base contact (important where there is a heavy reliance on end bearing and base cleanliness cannot be guaranteed by the piling operation), 3. Remedy to any loosening of the strata at and around the pile base that may have been caused during the pile

excavation. Good quality construction techniques should not require this. 4. Quality assurance, pre-loading of pile at the base and measurement of its response prior to incorporation (F)"

c) Other mechanisms

"Only if grout volume is so large that it increases the effective diameter of the base, or shaft. (A)"

"We inadvertently shaft grout portions of the pile in some situations, giving us higher ultimate capacity (C)."

General Considerations

a) Cases considered to conduct post grouting

Post-grouting is conducting for a case with very large column loads with small allowable foundation settlement.

- "It has been valuable when a small number of large diameter and relatively deep, drilled shafts are required, eg to support very large column loads in medium dense to dense sands (below water table) and the allowable foundation settlement is small (typically large buildings/towers or some types of large span bridge structures) (A)."
- "Where imposed load per pile is high and where there is little opportunity for providing redundancy in group action. Also where consistency of base performance is required (B)"
- "There can be efficiencies in using base grouting for heavily loaded piles where excessive settlement is governing design and where lengthening piles is not attractive for some reason (e.g. a discrete bearing layer, equipment limitations)." (C)
- "Long piles or piles where less settlement is needed at working load or where base takes significant portion of load (E)"
- "In end bearing piles in rock or very dense sands (such as the Thanet Sand underlying London). (F)"

The issue of water-bearing sand has been highlighted. "It has been found that piles founded in water-bearing sands can have bases that are difficult to clean consistently. Under working conditions, a poorly cleaned base will mean that, if the shaft resistance is overcome by the imposed loads, that pile will settle more than adjacent piles where the base has been more effectively cleaned. The base grouting process can be used to identify poorly cleaned pile bases and remedial action taken. (B)" Carrying out base cleaning may (SPERW 2016): (a) soften the soil at the base such as in the case of sandy clays and clayey silts; (b) be difficult to achieve

consistent outcomes such as in the case of mudstones and chalks because of the big variation in their properties and or in the case of water-laden silts and sands; and, (c) require a special drilling bucket designed for this purpose and not a general boring tool, thus, base cleaning increases the costs and reduces the productivity of pile construction.

An increase in the confidence of the pile performance is considered for post grouting. "Most effective for heavily loaded piles in water-bearing sands where there is little track record in construction and performance. The process of post-grouting in such situations forces a program of constructability and load trials. That disciplined approach then reduces the potential for excessive foundation settlements in previously untried ground conditions. (B)" "There may be advantages in base grouting for resiliency/additional confidence where no actual capacity benefit at working load is accounted for. (C)"

b) Cases considered not to conduct post grouting

The following cases are considered not to use post grouting.

- Shallow bearing stratum – "for situations when the bearing stratum is shallow, the pre-grouting is ineffective (if the available shaft friction is too small). (A)
- Basement excavation or stress relief – "if basement excavation is carried out after base grouting, and the soil heaves around the pile, then much of the improvement can be lost, since the "pre-load" effect is lost." (A) Where piles are located within basements, stress relief due to removal of overburden may reduce the capacity of a grouted pile. Research indicates that the unloading effect is likely to be a function of changes in the mean stress rather than a change in vertical stress. (SPERW)
- Piles in pile-enhanced raft foundations – "there is a requirement to have piles working as settlement reducers, close to geotechnical yield. (B)"
- Highly constrained sites – "not particularly suitable due to the multiple 'waves' of activity required at each pile location. (C)"
- A non-redundant single pile (C)
- Well-constructed piles in dense granular material (E)
- On walls – "I have twice seen it specified, but unsuccessfully implemented as it is not possible to generate any uplift. (E)"

Soil Conditions

a) Suitable for post grouting

Soil conditions suitable for post-grouting are:

- "Dense to medium dense sands, overlain by relatively competent soils (interbedded stiff clays/medium dense sands). (A)"
- "Water bearing sands" (B)
- "Dense silty sands" (C)
- "Relatively permeable soils. (D)"
- "Loose silty material could benefit if there is sufficient overburden to be able to apply a meaningful pressure" (E)

b) Not suitable for post grouting

Soil conditions not suitable for post-grouting are:

- Clay – "I would not recommend base grouting in clays." (B) "Not recommended in low permeability soils as grouting will just raise pore pressure rather than consolidate material." (D)
- In soils "where there was sufficient experience in cleaning pile bases effectively without base grouting." (B)
- Heavily fractures/voided rock or large size granular materials such as coarse gravel, where it may be difficult to confine the grout and there will be significant loss to the surrounding soil (F)

One respondent (A) describes "Some novel base grouting (e.g. "Expander-body" base grouting, where the bottom of the shaft and the toe is effectively expanded) can be effective across a wider range of soils, e.g. loose to medium dense silts and sands (but I do not have direct experience of these systems.)"

Design

a) Approach

Eurocode 7: Geotechnical design is used for pile design. It adopts a limit state design philosophy with partial factors (i.e. Load and Resistance Factor Design). Partial factors are applied to the actions (Permanent and variable actions, favorable and unfavorable), ground parameters and resistances (base, shaft (compression), shaft (tension)). To derive the design resistances of a piled foundation, a model factor is also applied to the shaft and base resistance calculated using characteristic values of soil properties. The value of the model factor is 1.4 but may be reduced to 1.2 if the resistance is verified by a maintained pile load test to the calculated unfactored

ultimate resistance. The philosophy is to check the stability with two different combinations of partial factors as follows:

i.   Combination 1 - Partial factors are applied to actions and model. Those for ground strength parameters and resistance factors are unity
ii. Combination 2 - Partial factors are applied to model and ground resistances. Those for actions (expect for unfavorable variable actions) and ground strength parameters are unity.

Further details can be found in the ICE Specification for Piling and Embedded Retaining Walls (SPERW) (3rd edition, 2016), which is the UK's technical specification for piling and embedded walling works.

Many respondents state that they have not seen any useful code guidance for post-grouted pile design and they use internally developed ones. "Past pile load test data (within own records, or published papers) is important, but site-specific issues also must be assessed. (A)"

b) Methods
  • The "Fleming" method – "uses independent hyperbolic load-settlement curves for shaft and base, together with elastic shortening of the concrete shaft. It has an empirical basis (derived from circa 4000 pile tests), but is also sound theoretically (see Geotechnique paper, published in 1992). Past pile load test data is most appropriate. (A)
  • Method 1 - The base capacity factor is estimated from empirically derived equation that is developed from a series of past pile load tests. The capacity factor is related to (i) SPT N blow counts, (ii) limit pressure from Menard pressuremeter testing, and (iii) the fines content. (D)
  • Method 2 - The end bearing resistance is estimated from the limit pressure from Menard pressuremeter test with a compression resistance factor given in Eurocode 7 Part 2. The correction for confining pressure is conducted.
  • Yeats and O'Riordan (1989) The design and construction of large diameter base grouted piles in Thanet Sand at Blackwall Yard, London, Proc. Intl. Conf. on Piling and Deep Foundations, London, Vol. 1, pp. 455-461, Balkema. (B)

c) Design parameter characterization

Many respondents describe that pressuremeter data is useful to evaluate design parameters for base grouting. Others include CPT, SPTs and shear wave velocity measurements.

  • Pressuremeter testing was employed and an empirical correlation developed. (C)

- Empirically calibrated equations based on pressuremeter data and pile test data. Eurocode 7 gives some guidance on the use of Menard pressuremeter. (D)
- CPTs and pressuremeter tests are useful, SPT's much less so as we are normally dealing with dense to very dense, deep sand strata. (B)
- Either geophysics (Go measurement) or pressuremeter (G at intermediate strain amplitude, circa 0.1%) are helpful to derive the base stiffness characteristics, but an allowance for some pile construction disturbance is necessary (which requires past pile load tests, for piles constructed with similar means/methods in similar ground/groundwater conditions). (A)
- Can also use SPT. (D)

d) Other design considerations

- "Osterberg/Bi-directional load cell tests provide the most useful data (by far)" (A)
- Eurocode 7 also requires Serviceability Limit State (SLS) conditions to be checked and typically a factor of safety is applied in the calculated shaft resistance to limit the pile movement. However, in base-grouted pile, this check is not required. "This gave significantly enhanced capacities at working load. (C)"
- "When using drilled shafts/bored piles in sands without base grouting, designers use very conservative assumptions (depends on perception of site-specific risks, given the ground/groundwater conditions and local experience); e.g. ignore end-bearing, or use a very high factor of safety on end-bearing (>3). At working load, a common check is to assume a factor of safety of 1.5 on shaft only, and check that this factored resistance is less than the working load. When base grouting is used then the assumptions are less conservative. It is difficult to generalize, but typically assumed pile resistances at working loads for base grouted piles can increase by 1.5 to 2 times that for non- base-grouted piles (sometimes with the limit being the structural capacity of the pile shaft)." (A)
- "Load testing of grouted and non-post-grouted piles enable better estimation of ultimate capacity than textbook/code guidance. Without load testing, there is unlikely to be any difference in the estimation of the geotechnical capacity of a single pile. The essence of post-grouting is to provide piles which settle less under working loads than non- post-grouted piles: there is little difference in ultimate capacity." (B)
- "We were happy to use 900mm diameter test pile data to inform up to 1500mm or even 1800mm diameter pile design. Soil conditions, specifically the strata at the pile toe need to be consistent to be confident in translating results across. Pile length has a big impact on the measurable effects (can you move the pile head?) and thus we have 'long' central London type base grouted piles and 'short' East London type." (C)
- There are numerous published relationships between end bearing and pressuremeter, CPT & SPT tests but these do not always correlate to achievable base capacity in practice and design often relies on experience of achievable base capacity. Much of this work is

based on relatively short base grouted piles (<40m) We have found recently that some of these 'limits' are highly conservative for deep piles (40m+)" (F)

Grout

a) Mixture
   - Cement – CEM I and CEM II are the most commonly used in grout mixes. CEM I products are with higher strength than CEM II products. Since not large strength is required, CEM II products may be better but they have different constituents that might affect its properties. More information about cement constituents and related properties can be found in (En B. 197-1 (2000). The choice of the cement would depend on the required grout properties stated in the project specification.
   - W/C ratios – No one responded to the ranges of the water-cement ratio they use for the grout. But typically W:C of 0.5:1 to gain a strength of 25N/mm² once cured. The "grout needs to be viscous, but able to flow (A)"
   - Bentonite – Bentonite is mainly used to minimize bleed water out of the grout, especially in high w/c ratio grouts. Bentonite is rarely used in base grouting, "unless the grout is to provide some form of low permeability function (A)" "If low permeability is required, then lab testing to show the relationship between bentonite/cement ratio, water/cement ratio, strength and permeability will enable choice of bentonite proportion to be agreed (B)". Many respondents have no experience of using bentonite in grout mixes. With deeper piles it becomes more difficult to flush lines and injection tubes can get blocked but bentonite cement mix with lower strength could prevent this. Bentonite reduces the bleed from the mix and thus prevents a build-up of solids in the pipes. Bentonite and water should be mixed first as cement will retard the bentonite from hydration. It is considered that more research is needed to examine the benefit of adding bentonite.
   - Admixtures (e.g. plasticizers, etc.) – Admixtures are used; some plasticizers are used in small doses (E). This is a matter for the grout supplier and the pile constructor and "we have traditionally shied away from this given the lack of any body of experience demonstrating performance. (C)" One respondent (D) says no admixtures used, whereas another respondent (A) says "commonly used."

b) Grout testing and approvals

   - Grout strength – UCS – 25N/mm2 @ 25 days – Three 100 mm cube samples per pile, testing one at 7 days and two at 28 days. +/- 2 standard deviations from an agreed mean value from pre-construction grout trials. (B) SPERW (2016) requires measuring the compressive strength of the grout material in accordance with BS EN 12390-3. For example, minimum characteristic cylinder and cube strengths are 20 and 25 N/mm2, respectively, after 28 days. Minimum three cubes to be tested at 7 days (achieving half the required compressive strength) and another three cubes to be tested at 28 days per pile.

- Bleed testing – water bleeding less than 5% and only one test replicate per pile. +/- 2 standard deviations from an agreed mean value from pre-construction grout trials., (B) If excessive bleed is suspected, then introduce anti-bleed additives to suit (B)
- Specific gravity not less than 1.84 ±5%.
- Marsh cone – Marsh cone efflux time maximum of 45 ±5% sec. Although this test might be used as an indicator, high flowability/low viscosity grout material might not be a good indicator for the suitability of the grout to be pumped, especially under high pressure and/or for deep piles. The requirement was set for ordinary Portland Cement (OPC) which is no longer available in the UK market whereas Cem I and Cem II tend to have a finer particle size and hence they thicken much more quickly than OPC did.
- Other considerations include "Pumpability (B)"

c) Varying grout mixture during the post grouting phase

In general, the grout mixture does not change during the post-grouting phase (B, C, D, E). Some respondents state that this happens when the following occurs.

- Grout mixture is changed occasionally less viscous followed by more viscous. (A)
- If remedial grouting, then triple-pass grouting with progressive modification of w/c ratio, up or down depending upon the nature of the problem is commonplace. (B)
- Left to contractor. In general no, but I have seen site teams make changes at times. (C)

d) Responsibilities for grout mix design specifications

Piling Contractor (A, C, D, E) or Grouting specialist (B) specifies grout mix, whereas Design Engineer specifies key parameters (UCS, Bleed, Specific Gravity, Viscosity) and reviews the proposed grout mix (C, D).

Grouting Operation

a) Delivery systems

- Tube-a-manchette and U-tubes (A, B, C, D, E and F)
- Jacking plates (A, B)
- Sand and gravel packs (B).

b) Recommended systems

- Flushable U tubes formed of gas barrel equipped with sleeve ports (B)
- Tube-a-manchette: usually better control and facility to re-grout more than once. (A). Gives the ability to carry out the repeat cycles (E)
  - The grouting circuits are independent and should have two TAMs at base of the pile. The TAMs should have drilled holes with a minimum diameter of 8 mm.

- o The base of the TAMs shall be positioned 50mm above the base of the reinforcement cage with a tolerance of -25mm/+0mm.
- For base grouting, the most reliable system appears to be by sleeve port within a sand and gravel pack help within an expamet body tack-welded to a steel plate upon which the concrete of the body of the pile is then placed by tremie. (B) More reliable if the ports are within a sand and gravel zone where the sleeve is bound to function and open fully under grout pressure. (B)
- For shaft grouting, the gas barrel has diameter compatible with the packer system so that grout can be delivered to the correct elevation within the piles. (B)

c) Not recommended systems

- Rubber bladder - usually too prone to damage/leaks. (A)
- Drill and grout- too time consuming/poor control (if pile is deep) (A) The drilling operation can damage the pile and there is a risk of losing drill bits (F)
- Tube-a-manchettes/sleeve ports embedded in pile concrete can have variable performance and may not open or cause excessive segregation and blocking of grout flow that cannot be remedied without post-drilling and packer grouting. (B)

- Tube-a-manchettes due to the uncertainty that you build in by using them. It is difficult to ensure you get them in the right place, and the cracking procedure is difficult to monitor and verify. It also adds another wave of works at the pile. (C)

d) Timing of base grouting after pile construction and necessary actions

- A minimum of 2 days and a maximum of 8 weeks after casting of the pile but not greater than 4 weeks after completion of the last pile.
- "Typically several days (up to a week) elapse before base grouting can commence. (A)"
- "Piles to be base grouted within 2 weeks of construction (E)."
- "TAMs should be cracked, in preparation of subsequent grouting, within 2 days up to two weeks after concerting and the cracking pressure shall be recorded. The earlier the cracking takes place, the better to ensure successful cracking as the concrete would not have developed much strength." "The grouting operations should not then start until before three hours after cracking. These three hours are required to allow dissipation of pre-water pressure developed from cracking. The exact time of pore water pressure dissipation can be estimated using pressuremeter test." (C)
- If base grouting is to take place within a sand or gravel-filled pack beneath a steel plate, then the grouting process can take place within any reasonable time after concrete placement: usual governed by the overall foundation construction program. (B)
- If sleeve ports are used within the body of the pile, then grouting normally proceeds within 3 days of concrete placement in the pile. (B)
- Base grouting date is arbitrary but usually set so it doesn't end up at the end of the program. (D)

e) Multiple stages of grouting

- Minimum values on secondary injections should normally not be specified. (SPERW)
- One respondent prefers incremental stages to get controlled pile head uplift. (A). For example, 1hr between end of one round and the start of the next. 3hr between start of one round and the start of the next. (D) However, another respondent describes that "It is specified but often fails as no grout can get in on 2nd or 3rd rounds. (D)"
- Another respondent (B) states that "re-injection only if there has been an under-supply at a given port, and then only if that under-supply has not been compensated by grout-take recorded at adjacent circuits. (B)"
- No more than 2 cycles should be attempted, ideally not on the same day. This would normally result in the Engineer downrating the pile. (E)
- The time between two rounds of grout should be greater than one hour and the time between the starts of two round of grout should not be less than three hours. The grouting tubes shall be flushed with water after each grouting round. If one or more of the grouting criteria were not achieved; then, the pile shall be re-grouted within 24 hours. (C)
- If any of these criteria are not met during the first grouting phase, then the pile shall be re-grouted, up to a limit of three grouting operations including the initial operation. A minimum of 3 hours shall be allowed between the commencement of one round of grouting to the next and also a minimum of 1 hour shall be allowed between the end of one round of grouting and the commencement of the next round of grouting. (C)
- If the criteria are not met as a result of any secondary or tertiary grouting, then a non-conformance shall be raised within 24hrs of base grouting. (C)
- Consideration should be given to limiting stages if suitable monitoring (in particular strain) is employed. (F)

f) Concerns and quality control

- Grout loss with minimal pile heave
  - Grout volume (A, D)
  - Pressure (carefully controlled) (A, C, D)
  - Residual pressure (D)
  - Incremental pile head heave (only a few mm). (A, C)
  - Tell-tales showing base movement for 'long' piles (C, D)
- Meeting the specified test parameters and measuring the success of the base grouting operation. We now incorporate sensors into such piles wherever possible to assess the actual effect of the base grouting rather than rely on crude parameters of grout take/pressure and pile uplift (which may not be measured in some cases) (F)
- Blockages and grout segregation/excessive bleeding. (B) As pile designs become deeper it has become increasingly difficult to flush grout out of the injection tubes. The high pressures at depth squeezes the water out of the grout mix which can lead to blockages.

Blockages can impede or prevent the successful base grouting of the pile. To avoid segregation (i.e., separation of cement/bentonite from the grout mix), it is recommended to avoid
- o Pauses while carrying out grouting operation as pauses may allow grout particles to be settled/deposited at the bottom of the lines.
- o Variable pumping pressure that may cause expansion and contraction of the grout tubes leading to squeezing out the solid particles from of the gout suspension.
- The lack of ability to actually know where the grout has gone, and how much actually gets spread across the base as opposed to spreading in "fingers" across the base of the pile until it reaches the edge and runs vertically up the shaft. (E)
- Base contamination – where the pile is constructed under support fluid, concrete will be placed by tremie. Grouting pipework should be kept clear of the base of the tremie to allow free flow of concrete and congestion of pipework needs to be minimized to prevent trapping debris at the pile base (SPERW)
- Pile slippage – delays in boring in a pile can lead to a build-up in the filter cake on the wall of the pile if bentonite support fluid has been used. This has been observed to result in uplift of the pile at very low grout pressures. If this is apparent, grouting should be stopped and the pile re-grouted a minimum of 24 hours after the initial grouting (SPERW)
- Hydro-fracture – high grout pressures can cause soil layers to lift and separate resulting in large grout losses. This is indicated by a drop in grout pressure with a corresponding increase in grout take. By using slow rates of grout injection and viscous grouts of a paste consistency, this problem can usually be avoided. (SPERW). Pumping rates to be low enough to allow the grout pressure to increase steadily; hence, minimizing the potential of soil fracturing and heaving.

g) Pile shaft and base inspection and/or sampling/probing

It is considered that pile base quality shall be used as a main criterion in the ranking system for accepting piles that would not be load tested in the field. Base inspection tests shall include (i) Base hardness test and (ii) Base cleanliness test at least four locations around the perimeter of the pile and one location at the center of the pile. The performance of bored base grouted piles is a function of base build up and base grouting. Material build-up at the pile base from material deposited from the pile sides and from the support fluid suspension may occur between checking of pile base hardness following pile base cleaning and commencement of concrete placement.

Base hardness tests are carried out using a weighted tape provided at the following time: (i) Immediately after the support fluid is exchanged, (ii) Immediately after the final base cleaning;

(iii) Immediately prior to reinforcement cage installation; and (iv) Immediately before concreting. The weighted tape shall be fabricated from a short section of a rebar welded to a square section approximately 100mm x 100mm of 20mm thick steel plate weighing approximately 1kg. The acceptance is based on the grading of the weight performance such as hard/sudden impact, slight embedment of the weight into soil, or the weight sinking slowly making base difficult to detect.

Base build up tests involve measurement material build-up, which is defined as the level of the base of pile immediately after base cleaning (e.g. within 10mins) minus the level of the base of pile immediately prior to concreting. The test is carried out at the same times and five locations as the base hardness. When a build-up is greater than certain amount depending on the base hardness test results, the contractor shall consider taking the re-bar cage out and re-clean. If the pile base is not re-cleaned, the base grouting criteria shall be achieved to allow a sign-off of the pile capacity. If base grouting criteria are not achieved, the pile base shall be cored (samples taken of concrete, grout and ground) and re-base grouted by means of packer system to demonstrate a sound base. Where a build-up of less than a certain amount is observed, the pile can be completed. The Engineer may use a base grouting scoring system to assess the pile base quality.

Monitoring

a) Parameters monitored

Automated and continuous data loggers are common. Over-sampling is desirable and is agreed with the grouting specialist at the outset. Monitored parameters are:

- Pile head movement (All)
- Pile tip movement (C, D, E, F)
- Pile strains (B, C, D, F)
- Grouting volume (All)
- Grout flow (A, B, C, D, F)
- Minimum grouting pressure (All)
- Maximum grouting pressure (A, B, C, E, F)
- Residual pressure/time (All)

b) Acceptance criteria

- Pile head movement – Typical values are to be not less than 0.2mm (GEOGUIDE 2003-8 DRG) or 0.3 mm (SPERW 2016) nor greater than 2mm. The movement is measured by (a) two independent methods such as using linear variable differential transformer (LVDT) and a dial gauge that measure the uplift relative to a stable external reference frame, or (b) measuring the base uplift using an extensometer system at an elevation 0.5m above the pile base to avoid local interaction between the extensometer and the cracked concrete close to base grout tube.
- Tip movement >0.3mm an elevation 0.5m above the pile base using 2 retrievable extensometers installed within separate tubes (in addition to the base grouting tubes) cast into each pile. The uplift at the pile base shall not exceed 2.0 mm.
- Noticeable strain – Pairs of vibrating wire strain gauges mounted on sister bars attached to the pile cage arranged across a pile diameter. These strain gauges shall be located at 1m above the pile base. The strain gauges shall have a resolution of better than $0.5\mu\varepsilon$. Measurements of strain shall be recorded at the following times: a. before concrete casting, b. during cracking of the TAMs and c. during base grouting.
- Pressure >30bar – Typically, not less than 30 bar and not greater than 70 bar for each grouting circuit. In the case of secondary injections, minimum values normally not specified. (SPERW). Pressure measurements shall only be accepted if a minimum volume of 5 liters of grout (after allowing for the compliance of the delivery system) has been injected.
- Residual pressure – A residual grout pressure of 15 bar should be held at least 2 minutes on each grouting circuit without the addition of any other grout material. (SPERW)
- Volume>25 l/circuit (100 l/pile) (D).
- Back sight measurements of the grouting frame shall be taken from both ends of the frame, both before and after the base grouting operation and at other times if the frame is suspected to have moved. The resolution of the reading shall be better than or equal to 0.01mm. The supports of the reference beam shall be at least 3 pile diameters apart.
- Currently no method to know where grout is. (D).
- New guidance is needed on how to assess the success or otherwise of base grouting on deep piles/drilled shafts (40m+) where there is little possibility of measuring upward pile movement during the base grouting operation. (F)

c) Grout volume monitoring

Grout volume is calculated by the amount injected based on flowmeter using a computerized system. Typically for 1500 mm-diameter pile, a minimum grout volume of 100 liters per pile (i.e., 25 liters/circuit when four circuits are used). For piles having a diameter greater than 1500 mm, the recommended minimum grout volume is scaled upward according to the base area, e.g., 144 liters total grout volume for a 1800mm-diameter pile. Larger grout volumes (>>25

liters/circuit) are typically injected while grouting the base using the first pair of opposite circuits. In such a case, the grout is expected to fill most of the base and the grout volume to be injected through the second pair of opposite circuits will be less than 25 liters/circuit; however, the volume should not be less than 5liters/circuit. If less than 5 liters/circuit is injected, the injected grout may be assumed to accommodate the expansion in the circuit due to pressurization and not due to grout injected at the base. Thus, the tube-a-manchettes at this circuit should be re-cracked with water and the grout is re-injected.

d) Pressure monitoring

Pressure monitoring is at the surface (pile head and pump) (A, B). Checks are made (pre-grouting) to quantify the grout head (pressure) losses through the delivery system. (A) An estimate of pressure dependent resistance to flow is often carried out using horizontal pipework at ground level. (B) Self-weight of the vertical grout column needs to be included in such estimates. (B).

e) Actions taken if the pile fails criteria

- Check grout records (has hydraulic fracture occurred?) (A)
- Re-examine the structural design to establish whether the reserve of safety on shaft capacity exceeds 1.3 to 1.5 under working conditions. If a pile can theoretically perform adequately, inform the client of the technical decision. If the client unhappy with the technical decision, then establish whether additional non-grouted piles can be installed or whether there is a reasonable chance of success in carrying out remedial grouting to achieve a satisfactory pile. (B)
- Downrating the pile (E)
- Investigate, design review and assess data available. This is when strain measurement data is highly valuable. (F)

f) Pile ranking system

A pile ranking system has been developed by one of the consultants as a criterion to be used in accepting grouted piles that would not be load tested in the field and did not meet one or more of the base grouting criteria as per project specification. This system was developed when it was found grouted piles may meet the load-settlement behavior required in project specification when load tested in the field, even though these piles did not meet one or more of

the base grouting criteria as per project specification. The ranking system comprised of five main criteria in ranked order as follows.

1. Pile Uplift.
2. Base Stiffness
3. Maximum grout pressure
4. Residual Grout Pressure, which is the sustained grout pressure over two minutes.
5. Grout Volume

For a pile of interest, scores (both positive and negative) are given for each criterion. If one or more of the base grouting criteria as per project specification has not met, then a certain minimum score is required to consider the pile acceptable.

Load Testing of Base Grouted Piles

a) Objectives

Pile load testing of grouted and non-post-grouted piles enable "better estimation of ultimate capacity than textbook/code guidance. Without load testing, there is unlikely to be any difference in the estimation of the geotechnical capacity of a single pile. (B)

- "Load tests on previously untried ground conditions are essential. In some ground conditions there is sufficient post-grouted pile test data to enable design to proceed on the basis of historic records. However even in those cases, constructability trials are desirable, and the results of such trials compared with the historic constructability records: construction durations, grout pressures, volumes of grout-take etc." (B)
- "Occasionally, preliminary (sacrificial) tests are specified for base grouted piles, if the costs can be justified (needs a lot of piles and a large potential saving or if a local regulator insists); it is far more common to rely on past load test data." (A)
- "Generally there is a load testing program on which the design will rely and receive feedback. Such test piles can often be selected in foundation locations where the governing load case has the least effect on working loads: for example towards the center of a foundation where the governing load case is dominated by environmental loads such as wind or seismic." (B)
- "Without a load test it is difficult to assess the impact on stiffness that based grouting has had." "Our design would prescribe load relevant load testing and in most cases include preliminary/sacrificial pile tests" (F)

b) Tested proportion

- "As per Eurocode 7. Sacrificial and production pile tests. Representative 1% of production piles, i.e. if mixed diameters then selection of 1% needs to account for this." (D)
- With suitable preliminary testing working test can be excluded in some cases and working tests are typically carried out on up to 1% of piles when appropriate. Design Eurocodes dictate the test type required based on the design approach used. (F)

c) Test methods

- "Osterberg/Bi-directional load cell tests can produce "most useful data (by far)"" (A)
- "Use a bi-directional load test on a non-base grouted pile at a reduced diameter (up to 50%) provides same means/methods used for installation." (A)
- "Pile diameter not more than double the test pile diameter." (E)
- "The use [of] 900mm diameter test pile data to inform up to 1500mm or even 1800mm diameter pile design. Soil conditions, specifically the strata at the pile toe need to be consistent to be confident in translating results across. Pile length has a big impact on the measurable effects (can you move the pile head?) and thus we have 'long' central London type base grouted piles and 'short' East London type." (C)
- "In addition to base stiffness, the ultimate capacity of shaft and base is also needed, usually shaft stiffness does not vary significantly (but base stiffness does, due to means/method influences)." (A)
- Based on our recent experience of very heavily loaded and deep base grouted piles we now question the use of bi-directional load tests in accurately assessing the capacity of such piles. The use of twin plates (built into the pile) jacked apart close to the pile base will, in may soils, have an effect on the vertical effective stress at the pile toe. The effective stress local to the pile toe (overburden) dominates the idealized base capacity 'punching' failure mechanism. Our recent experience using a top loaded reaction system has produced base capacities and shaft capacities close to the base well in excess of what has previously been reported in the Thanet Sands of London, UK. (F)

Project Responsibilities

- Contractors – The piling contractor is responsible for the design of the grout delivery system, once the system type has been chosen (A). But some contractors use specialty grouting contractors who will design the system/method from the top of the grout tube. (C) The cage manufacturer will have an influence over the grout tube detailing (shop drawings to be reviewed by designer engineer). (C), "Our specialist grouting division do design the system and brief the site team on how to use it." (F)
- Designers – The designer will have had detailed discussion and agreement with the pile supplier about the means and methods to be adopted in pile construction (B). These include number of TAM ports vs pile base area, maximum injection pressure, and grout system compliance, i.e. expansion or lack thereof under pressure. (D)

Method Statement (Specifications)

The method statement for post grouted shafts shall at least include the following (SPERW 2016; GEOGUIDE 2003-8 DRG):

- Previous experience and curricula vitae of key personnel carrying out the grouting process to ensure they are competent and appropriately trained.
- Description of grout constituents.
- Details of grout delivery system including list of all equipment used in mixing and injecting the grout (e.g., the number and alignment of grout circuits; location and alignment of tube-a- manchettes; and packers, method of measuring friction losses in the tubes/packers).
- Detailed methods of quality control on grout material, including sampling scheme (i.e., cubes number and size and sampling intervals) and target properties to be investigated (i.e., density, flow and bleed of the grout).
- Grout injection system in details including the identification of: the number and alignment of grout circuits; location and alignment of tube-a-manchettes; and packers. If there is a requirement to grout up or otherwise backfill grouting tubes following base grouting operations, then this shall be stated in the project specification.
- Quality control procedures on the grouting process (i.e., measuring grout take, which should be automatic with real-time data capture, and include a physical method of checking grout take at the end of injection of each circuit, method of measuring grout pressures which should include a continuous record; calibration certificates for pressure gauges; typical electronic record for grouting, which shall include data of grout take, grout pressure, residual pressure, times of grouting and pile uplift for each grouting circuit; typical continuous records of grout pressure and pile uplift shall also be included, target minimum, maximum and residual grout pressures for each grout injection). Details of the measurement system shall be submitted by the contractor with the tender and shall be subject to acceptance by the contract administrator
- Methods for cleaning pile base and checking its quality. Although this requirement was mentioned in SPERW (2016) notes for guidance (Section C) and not in the main specifications (Section B).

3. Fiber Optic Laboratory Testing – Measurements During Variable Strain

Distributed fiber optics offer a near-unprecedented distribution and density of strain measurement along the installed route. However, with this dramatic increase in range and coverage comes an associated drawback of a long reading time. Rather than readings being taken over a matter of seconds, many commercial distributed fiber optic interrogators require minutes to complete a distributed reading. During this reading time, it is unclear from the manufacturer's product specifications how the optical system and associated algorithms deal with changing strains along the fiber length during the reading interval. A laboratory test of a popular commercial distributed fiber optic strain sensing system was conducted to examine the effect of reading time on interpreted strain data over a range of varying strain.

Test Approach and Setup

The main criteria of the test are to be able to apply a controlled, measured, and linearly variable displacement along a length of fiber optic cable with time. To maximize the benefit of the test and the applicable strain ranges, the original test plan was to include multiple fiber optic loops of varying lengths, each attached to the same linear actuator. In this design, applying a single displacement could produce multiple strain ranges, depending on the length of each fiber loop. Over a series of visits to the Pacific Earthquake Engineering Research Center (PEER) at the UC Berkeley Richmond Field Station, several potential test setups and orientations were explored with the PEER researchers. The original test design called for the fibers to be oriented vertically - offering the benefit of the self-weight of the fiber contributing to pre-tensioning the fibers. Unfortunately, no area with both adequate headroom and an easily accessible fixed point was available. The option of fixing the top cable pulley to the lab gantry crane was considered but was abandoned due to safety concerns related to access. Ultimately, it was decided to switch to a horizontal orientation of the fiber optic cables with two loops with a length ratio of roughly 1:2, as shown in Figure 3-1.

The test setup was oriented to the south face of the strong wall in building 484 at the Richmond Field Station. The pulleys were attached using threaded rods into the existing anchor holes in

the strong wall blocks, while the clamping mechanism was assembled using steel members at the east end of the Single Degree of Freedom shake table. A component diagram of the test layout is shown in Figure 3-1.
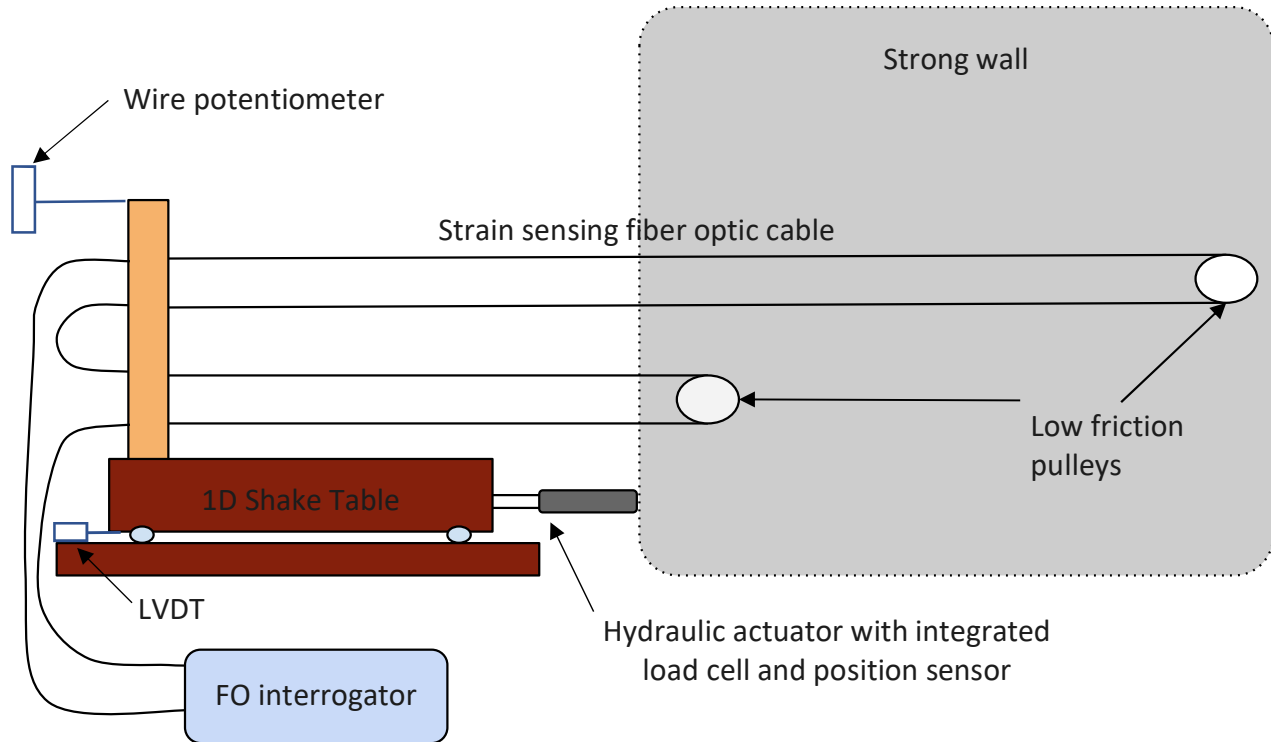
Figure 3-1: Component diagram of the test layout

The pulleys, as shown in Figure 3-2, were selected to be made of a low friction material to allow the cable to rotate around the pulley axis freely. The pulleys were 6" in diameter; chosen based on the center-to-center clamp spacing as well as ensuring a large enough curvature to prevent the risk of signal loss or breakage in the fiber optic cable during testing. The pulleys had a circular cross-section channel ~¼" deep to route the cable within. The pulleys were mounted vertically using a threaded rod in the anchor holes in the first and last blocks of the strong wall. The clamps and pulley heights were selected to have the cable arms as close to horizontal as possible. Nuts were installed on the threaded rod to prevent the pulleys from moving along the bar, although a small gap was left between the nuts and pulleys to allow free rotation of the pulley on the bar.

Figure 3-2: Photo of Loop 2 (long loop) pulley mounted on strong wall

Each clamping mechanism was made of two separate pieces of wood (see Figure 3-3). The first was a vertical length of 2x12 lumber, connected to a stack of cross steel members that were bolted to a horizontal extension from the shake table. This vertical board provided the clamping face for all four loops. Adhesive discs of 40-grit sandpaper were adhered to the face of the 2x12 along the four cable paths to increase the friction between the wood and the cable. Four 11.25" long wood boards (custom planed lumber 2" x 5") were then bolted to the clamping face of the lumber using 1⁄2" diameter bolts with fender washers to distribute the clamping load along the board. A triangular channel was cut into the centerline of each board using a table saw with the blade tilted at a 45° angle, then smoothing the lip using a hand plane. Various depths of the channel were tested to maximize the clamping force while avoiding crushing (and potentially damaging) the cable. A final depth of the channel of 3mm (for the 5mm diameter cable) was chosen. The clamping bolts were tightened in an alternating pattern to ensure the clamping force was applied symmetrically. During the tightening of the clamps, the fiber optic cable was pulled taught by hand to remove slack in the system and apply an initial pretension to the cable. The bolts were then tightened to 10 foot-lbs using a torque wrench to ensure an even clamping force between all four boards. Tell-tale marks were made on each cable at the front and rear of the clamp to provide a visual check of any slippage of the cable during the test.

Figure 3-3: Photo of wood clamp setup at far corner of 1D shake table

In addition to the fiber optic strain measurements taken during the test, four other instruments were used to monitor the test procedure, as shown in Figure 3-1. The first pair was the displacement sensor and load cell, which were incorporated into the hydraulic piston attached to the shake table. Although these instruments were not installed specifically for our test, the data from these were recorded and used to control the movement of the shake table. The second pair of instruments were two displacement gauges attached near the clamping mechanism. The first, an LVDT, was attached at the base of the shake table to measure the linear displacement of the cable directly beneath the clamping mechanism. The second, a wire pot potentiometer, was attached at the top of the clamping mechanism to the wall via a wire to measure any differential movement between the base of the shaking table and the top of the clamp. The potential sources of the differential movement identified prior to testing were movement within the horizontal bolt connections (the holes were oversized compared to the bolts) and bending of the stack of x-connectors that the cable boards were clamped to. Prior to installation, each potentiometer was calibrated for a range of 0.3" to 1.8", allowing a functional range of 1.5". With the fiber optic cables slack, the table was also checked for linearity and error over the range of desired displacement rates. An achievable displacement rate of 1mm was established and was set as a lower threshold in the testing plan. The table was then

centered at approximately 0.3" in the stroke of the potentiometers and the cable was tensioned by hand and clamped.

Test Program

A three-part test program consisting of three primary set points and two intermediate points was designed to explore a range of strain combinations. The baseline zero for the test was established after setting the zero setpoint of the fixed table and pre-tensioning the fiber optic cables by hand in the clamps. From the baseline, target setpoints of 10 mm and 20 mm displacement were established. In between these setpoints, intermediate points of 5 mm and 15 mm were also established to provide an average value of the primary setpoints. The primary and intermediate setpoints, as well as the calculated associated strains, are presented in Table 3-1. A large range of strains was chosen to test (ranging from 0-2466 µε) to explore the effect of different magnitudes of frequency (strain) shift during the fiber optic readings. The first phase of the test was taking steady (constant) strain readings at the 3 primary setpoints (pretension, 10 mm, 20 mm). Once the primary setpoints were taken, additional steady readings were taken at the intermediate setpoints (this step was postponed as there was concern that the actuator may not achieve precise displacements of 10 and 20 mm during testing).

Table 3-1: Proposed primary and secondary test setpoints

	Loop 1 Installed length: 8.11m	Loop 2 Installed length: 15.75m
Displacement (mm)	Strain (microstrain)	Strain (microstrain)
0 (pretension)	0	0
5	*617*	*317*
10	1233	635
15	*1850*	*952*
20	2466	1270

The second phase of the test consisted of fiber optic strain readings taken while first ascending, then descending, between the primary setpoints over a 5 minute (300 second) constant displacement rate. The 3 ramp intervals were 0 – 10 mm, 0 - 20 mm, and 10 - 20 mm.

The third phase consisted of fiber optic strain readings taken while changing the strain rapidly (over 10 seconds) between setpoints at the 2.5 minute point in the reading. The same intervals as in the second phase testing were used. For all individual test, as well as the holds, 3 readings using the fiber optic analyzer were taken to capture any potential scatter or variance in repeatability.

The fiber optic strain readings were taken using a commercial fiber optic BOTDA analyzer (Omnisens DITEST). The fiber optic analyzer settings were carefully controlled to reliably complete each reading within exactly 5 minutes, +/- 2 seconds. Since the settings directly affect the later interpretation of the fiber optic strain data, both the scanning window and frequency step of the analyzer were selected using the minimum values to provide the best achievable frequency resolution, given the reading time constraint. The fiber optic analyzer settings are presented in Table 3-2.

Table 3-2: Fiber optic analyzer read settings

Sensor length (m)	100
Spatial resolution (m)	0.75
Sampling interval (m)	0.25
Measurement step (MHz)	0.2
Start manual scan (GHz)	10.87
Stop manual scan (GHz)	11.06
Averaging (profile)	2000

Based on the above settings, the analyzer performed a scan in 951 steps, with an approximate duration of 0.315 seconds per frequency step (based on the 5 minute read time - it is unknown if a portion of the read time at the beginning or end is used for the system function outside of the reading duration). Based upon this timing, the readings for the control and the other measurement data acquisition system were taken at 10 Hz.

Deviation from Test Program

Three deviations were encountered during the test program. The first, which was expected based on preliminary testing with the 1D shake table control system, was that the actuators were not reliably reaching the input test points. This may have been due to a miscalibration

within the control system, or potentially from the extra load imparted on the system by the tension from the fiber optic cables. However, the deviation from the setpoint was repeatable in a series of test cycles and was therefore considered acceptable for the purposes of this project.

The second deviation was that a linear (non-constant) difference was observed between the displacement measurements at the base of the shake table and the top of the clamping apparatus. While this was not entirely unexpected and was the motivation for including the two measurement points in the first place, it provided an unforeseen challenge in selecting which displacement to use in the subsequent analysis of the fiber optic strain data. The identified options were to use the bottom displacement, the top displacement, or a linear interpolation between the two. Given the various system design components and the fact that most of the opportunities for relative movement were low in the system, making a linear interpolation potentially inappropriate, it was decided to use the top displacement for analysis.

The final and most significant deviation involved an interruption to the proposed test program. During the initial cycle testing (0 – 10 mm), a loud noise occurred in the laboratory, and it was observed that a separate hydraulic jack unrelated to the fiber optic test had fully extended itself, significantly tilting the structural specimen that it was attached to. While the cause for this issue was unknown but suspected to be a valve leak somewhere in the hydraulic system, these concerns dictated that the fiber optic test be halted and postponed to a later date. As a result, the subsequent analysis is based on the first 3 load cycles and not the originally proposed test program.

Results and Data Analysis

A preliminary reading taken prior to the pretensioning of the fiber optic cable was made to establish the amount of pretension applied to the cable. The average applied pretension was 395 $\mu\varepsilon$ on the short loop (loop 1) and 463 $\mu\varepsilon$ on the long loop (loop 2). The processed strain data for the pretension is presented in Figure 3-4. The difference in the strain between the two loops is due to the variation in the manual pretension prior to clamping. The amount of tension was based on manual grip, simulating the common pretensioning practice for fiber optic cables in the field.
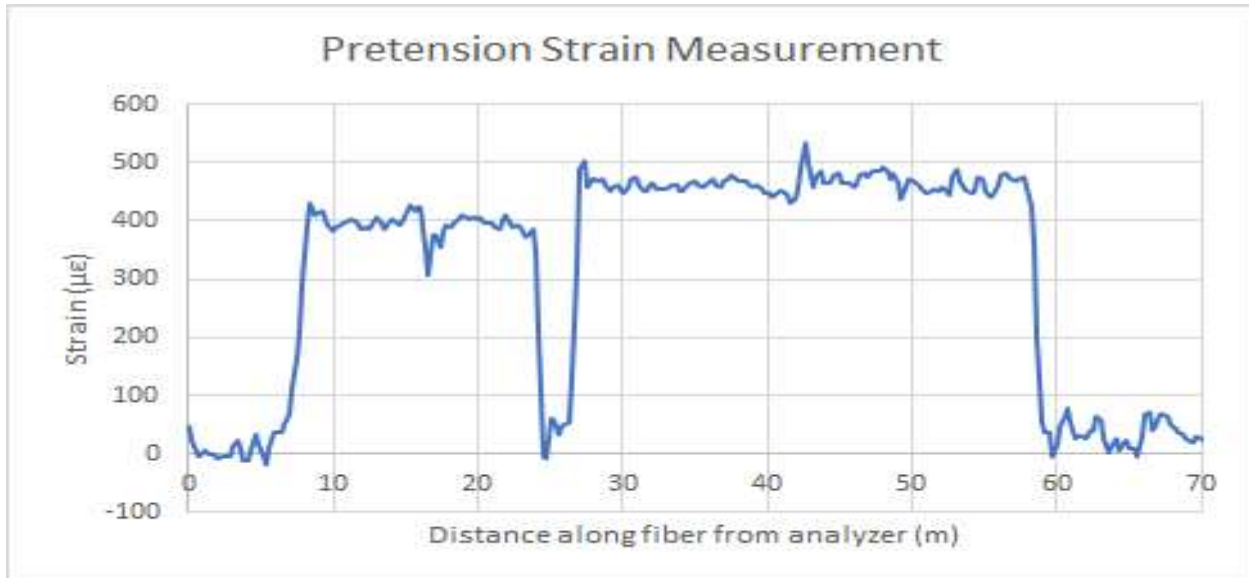
Figure 3-4: Strain measurement after initial manual pretension of fiber loops

Due to the edge effects within the spatial resolution of the analyzer, 0.5 m at each clamp was removed from subsequent processing, as well as the strain gradient around the pulley turnarounds. Loop 1 is indexed as 8.678-16.08 m (A) and 16.59-23.992 m (B) from the analyzer, while Loop 2 is indexed as 27.566-41.859 m (A) and 43.390-57.684 m (B) from the analyzer.

The first 2 load cycles were performed ramping from 0 (pretension) to 10 mm displacement. The top displacement potentiometer indicated that an actual displacement of 8.135 mm was achieved, with repeatability between the two cycles of 0.005 mm. Readings at the 10 mm setpoint (1 cm target, 8.135 mm actual) and 0 mm were taken between cycles. The associated strain measurements are presented in Figure 3-5. It is noted that the measured peak strains in Loop 1 and 2 were within 4 and 8%, respectively, of the calculated equivalent strains based on the displacement measurements.
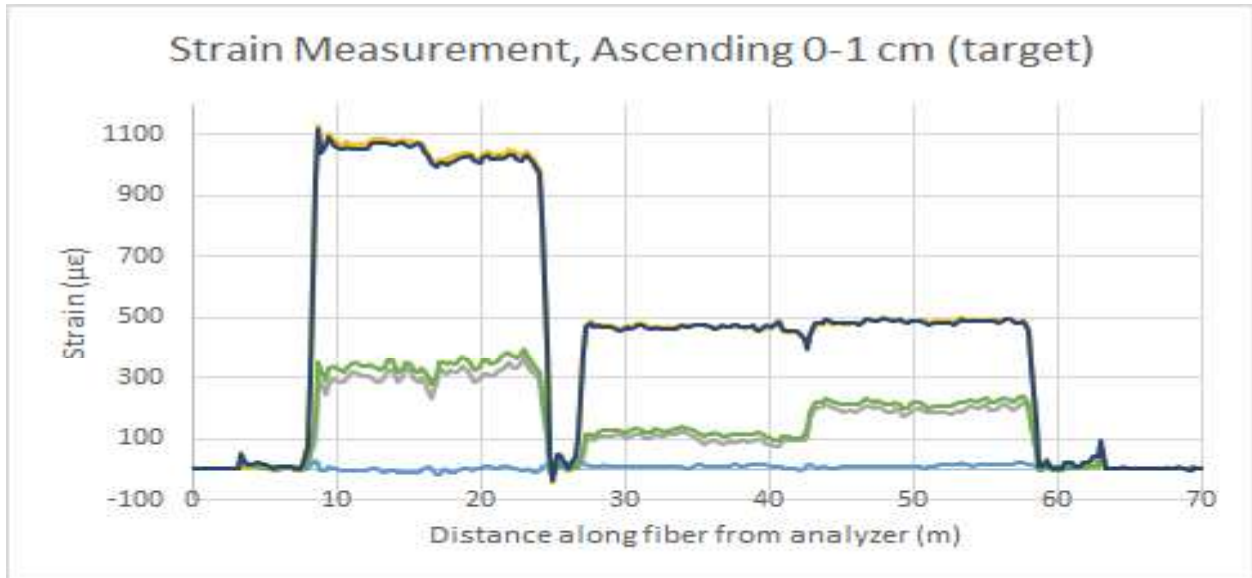
Figure 3-5: Ascending strain measurements, run 1 (grey) and 2 (green)

As shown in Figure 3-5, the higher lines represent the static strain measurements at 10 mm
(target) displacement, while the intermediate lines represent the readings taken during the two
ramp cycles (run 1 (grey line) and run 2 (green line) in Figure 3-5). It is clear that the
intermediate strains do not represent an average (visually halfway) of the applied strains during
the ramp cycle, indicating that the reported strain measurements were taken at different times
during the 5 minute load. The Brillouin peak frequency values during the two ramp readings
from 0 - 10 mm (target) are shown in Figure 3-6. Comparing the order of the Brillouin
frequency, from smallest to largest, to the overall percentage of the total applied strain, it can
be observed that an increase in the 3 starting frequencies correlate to the magnitude of the
strain measurement during the transient reading. Since the strain is increasing linearly, this
intuitively supports that the lower frequency portions of the fiber are being interrogated by the
analyzer earlier than sections with higher frequency.
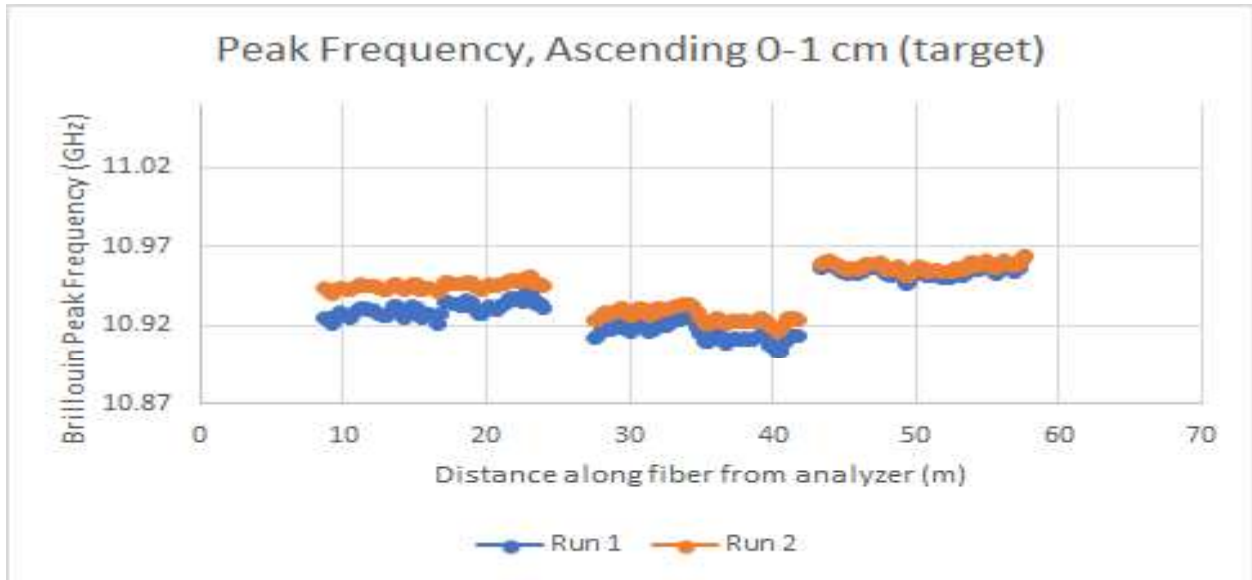
Figure 3-6: Peak frequency during two ascending strain reads

Based upon correspondence with the fiber optic analyzer manufacturer, it is understood that the analyzer sweeps from the bottom of the frequency sensing window to the top in the prescribed measurement step. This would indicate that sections along the fiber where the Brillouin backscatter is at a lower frequency would be read earlier in the read interval than those at a higher frequency. This can be represented visually by plotting the measured strain against the associated frequency, as shown in Figure 3-7, and an approximately linear trend in the data can be observed. The scatter in the data is within the system repeatability of approximately +/- 20 µε. The linear trend can become even more evident if we separate the readings from the two loops and add the measured strain values at the 0 and 10 mm (target) displacements, forcing them through the minimum and maximum limits of the frequency sweep window. This is shown in Figure 3-8 for loop 1 and Figure 3-9 for loop 2. The strain readings during the ramp cycle plot linearly depending on their peak frequency between the minimum and maximum window frequency limits and the associated minimum and maximum strain (measured in static readings).

45
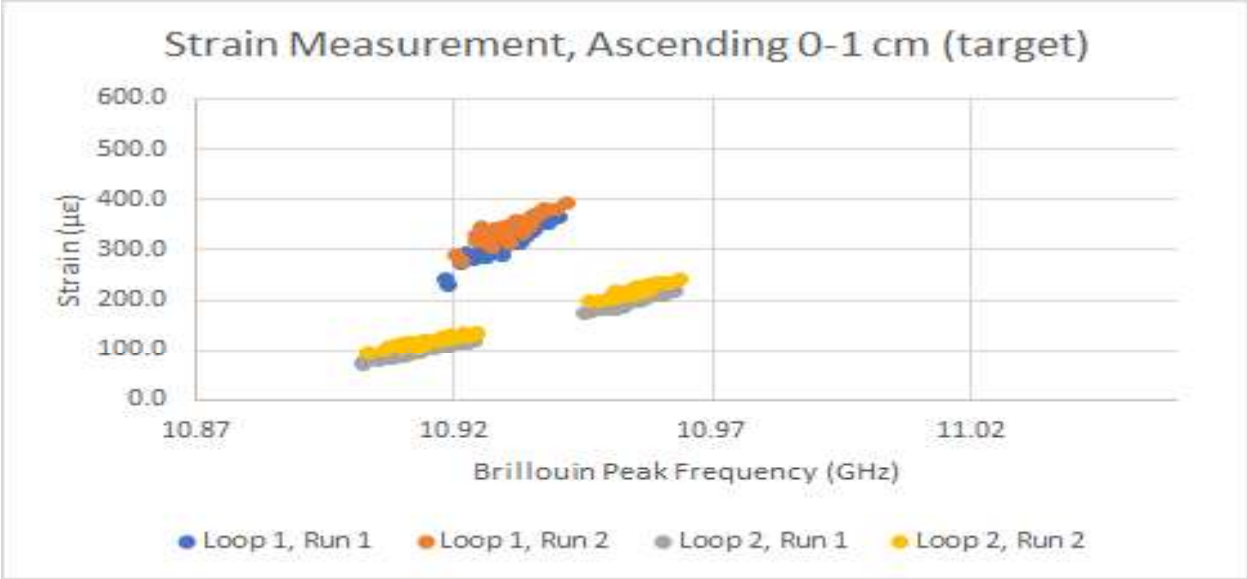
Figure 3-7: Strain vs. peak frequency during ascending read
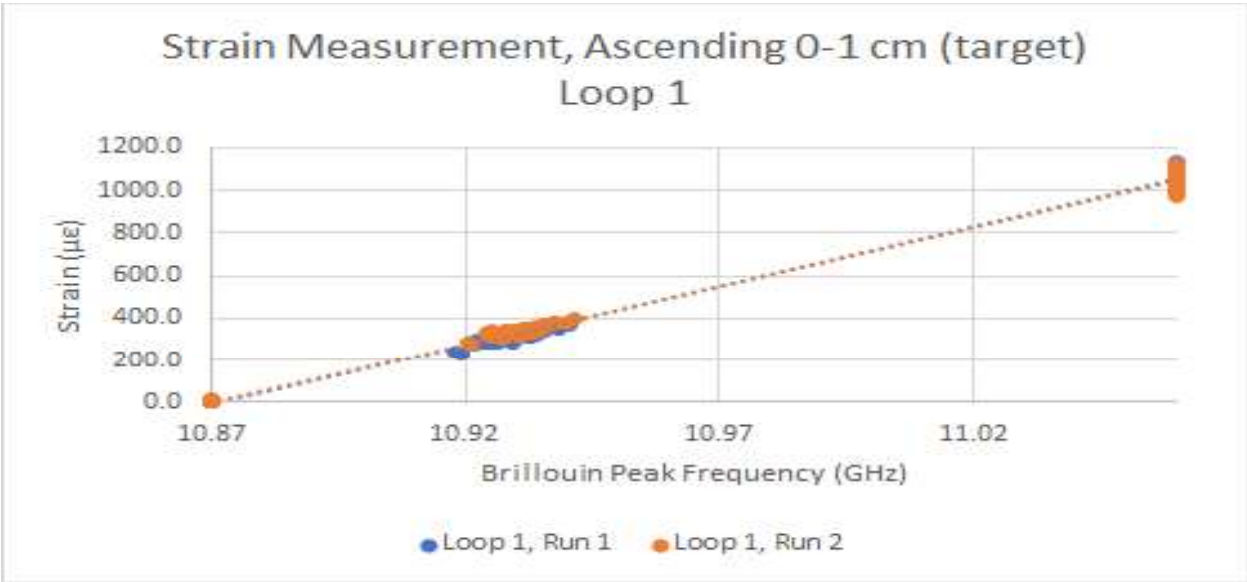
Figure 3-8: Strain vs. peak frequency during ascending reads, Loop 1
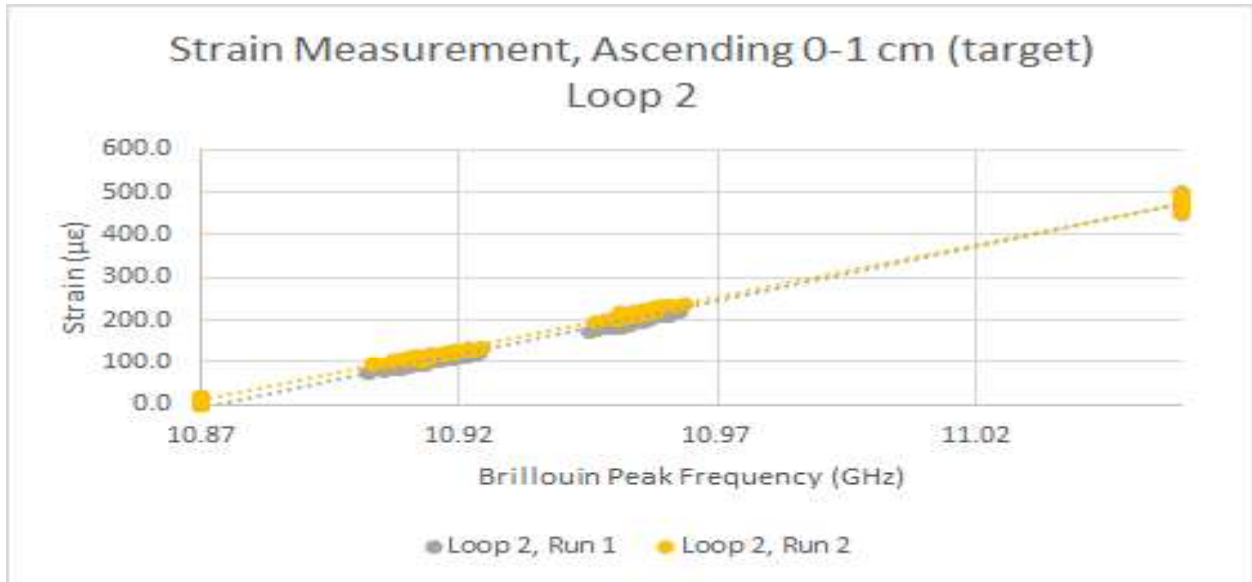
Figure 3-9: Strain vs. peak frequency during ascending reads, Loop 2

A third load cycle was performed ramping down from 10 - 0 mm. In this case, the trends observed in the two ascending load tests were reversed. Figure 3-10 shows the strain profiles at 10 mm displacement (blue line), 5 mm displacement (red line) and 0 mm displacement (grey line). It is noted that in the final descending load cycle, the fixed table overran the 0 cm setpoint, resulting in a negative strain relative to the pretension baseline. The strain vs. peak frequency plot during descending read is given in Figure 3-11 for loop 1 and Figure 3-12 for loop 2. Again, the strain readings during the ramp cycle plot linearly depending on their peak frequency between the minimum and maximum window frequency limits and the associated minimum and maximum strain (measured in static readings).
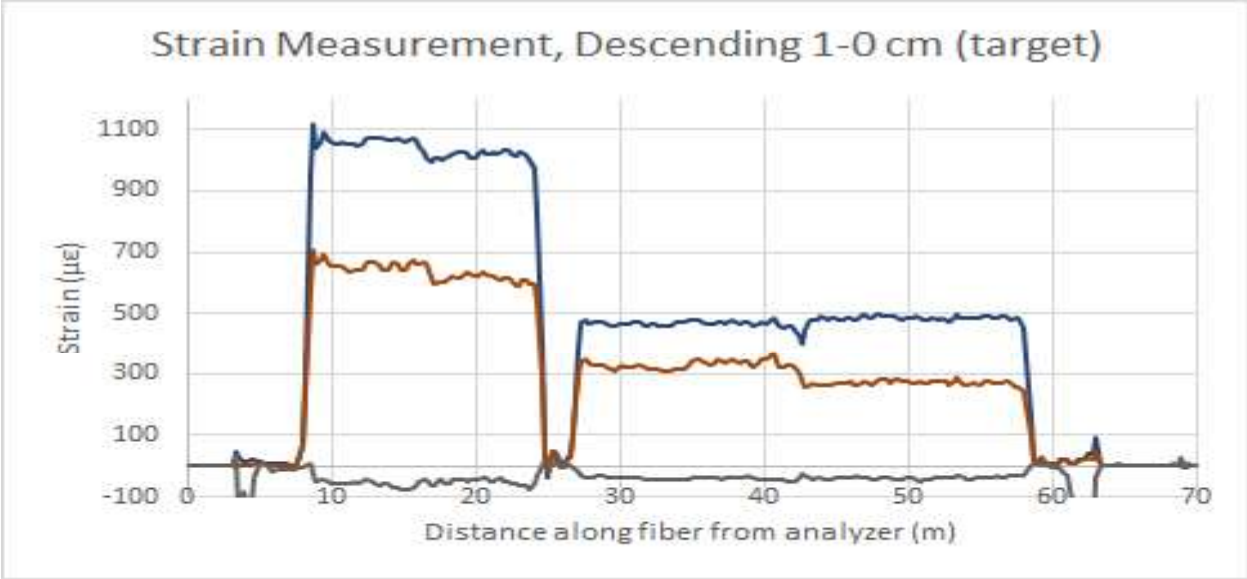
Figure 3-10: Descending strain measurements (brown)
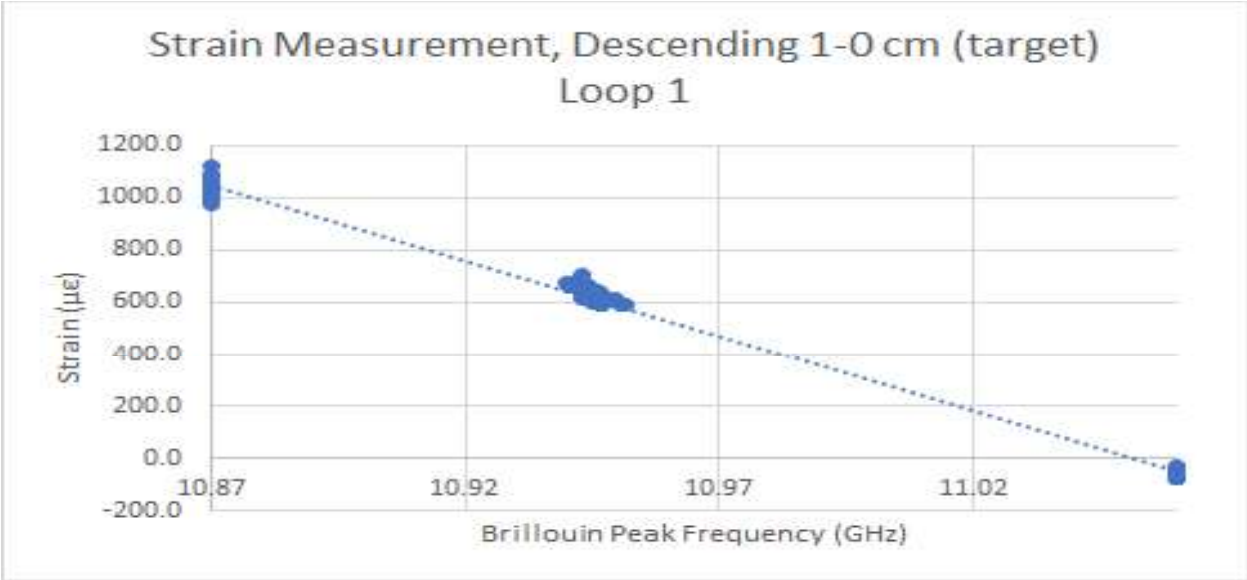
Figure 3-11 Strain vs. peak frequency during descending read, Loop 1

48
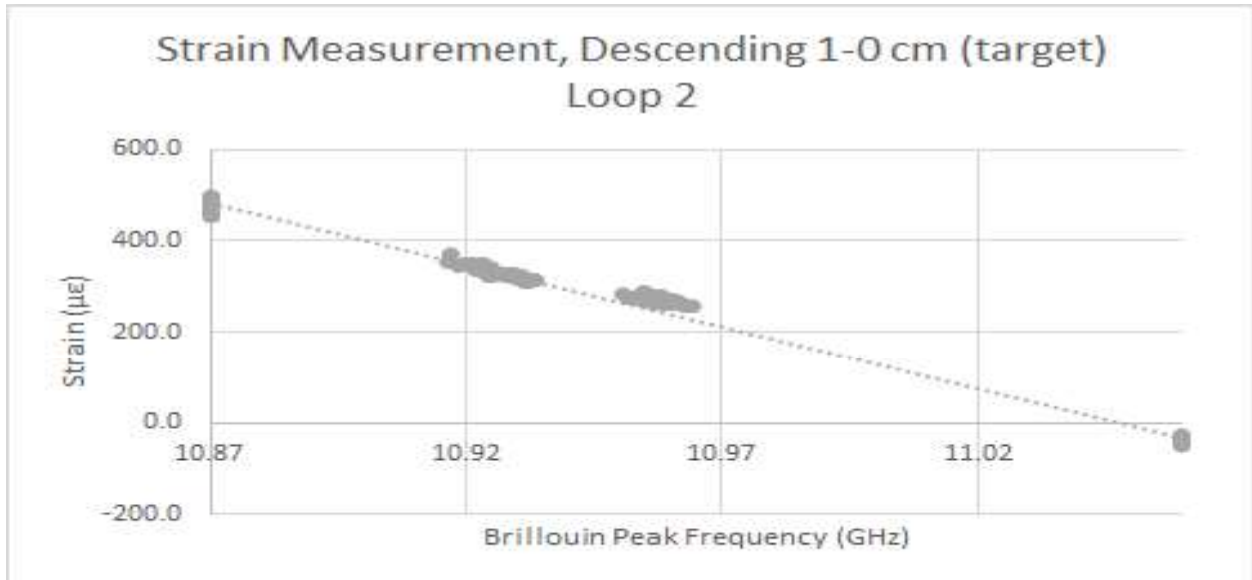
Figure 3-12: Strain vs. peak frequency during descending read, Loop 2

Summary

As was initially suspected based on previous laboratory and field testing using the commercial fiber optic analyzer, the strain profile from a single reading taken during transient strains cannot be treated to represent the average strain along the fiber during the reading time. Instead, the resultant strain is a function of the Brillouin peak frequency, where it falls within the analyzer sweeping window, and the actual strain measurement at that time.

A preliminary literature review did not reveal any previous discussion of this limitation of the use of distributed fiber optic strain sensing during transient loading. This represents a potentially major caveat that must be incorporated in the presentation and analysis of any distributed fiber optic data during transient (or even suspected transient) loading. The correction of such data may be possible, but at this point this would rely on the assumption that the strain field is uniform along each interval of fiber (in our case, Loop 1 and Loop 2). There are several cases in which this can be true, such as suspended fiber in tension (relative displacement between two points), or uniform axial loading, such as in a vertical column. In these cases, the data can be linearized between the starting and ending frequency scans, and the approximate equivalent strain can be chosen at any time within the reading interval.

For installations of fiber optic cables in non-uniform strain fields, such as elements in bending or undergoing differential loading, the above processing technique can allow for an estimate of the time when each strain reading along the fiber was taken during the reading interval, but the strain profile cannot be collapsed to a single time since the potential range at each point is unknown.

For this challenge, three possible recommendations for potentially removing or addressing this error in the future have been identified:

- Whenever possible, hold the load constant during the fiber optic analyzer reading interval. For example, during load tests of structural elements, measure and hold the load constant rather than providing a controlled pressure (which can decrease with diminishing load).
- Reprogram the fiber optic analyzer to perform its averaging over all frequencies in the reading window, rather than at each frequency step. In this way, for a hypothetical 500 step reading sweep, all 500 frequency steps would be performed, then repeated multiple times over the averaging input. This would produce a true average over the reading interval, as well as potentially allow for statistical analysis of the distribution of the frequency peaks at each point, potentially allowing for the back calculation of the associated strain range during the reading interval (this would depend on the signal-noise ratio for each individual read which is not published).
- Select an analyzer with a faster reading time. The development of a Brillouin-based distributed fiber optic strain analyzer at Berkeley is ongoing, which can achieve sub-1 second reading intervals.

Short of implementing one of the above recommendations or development of another technique to address this potential shortfall of distributed fiber optic strain reading, it is important that practitioners recognize this behavior of fiber optic analyzers and incorporate this understanding into the presentation and analysis of distributed fiber optic strain data. While distributed fiber optic strain sensing still offers a good deal of value in many civil engineering applications where changes in strain are on time periods far in excess of the reading interval (months-years), there are several instances where strains cannot be treated as constant in the minutes-long reading intervals of fiber optic analyzers. Further testing and

analysis are required to determine if it is possible to correct more accurately for this error using current measurement equipment.

4. Field Installation

Overview of Monitoring Program

The fiber optic monitoring portion of the larger drilled shaft instrumentation program consists of thermal and strain monitoring in all thirteen of the installed drilled shafts. The thermal monitoring was performed using distributed fiber optic sensing, while the strain monitoring was performed predominantly using distributed fiber optic sensing with one additional shaft instrumented with point-based fiber optic sensors. The distributed fiber optic sensing was performed using Brillouin optical time domain analysis (BOTDA) and Brillouin optical time domain reflectometry (BOTDR). The point-based fiber optic sensing was performed using Fiber Bragg Grating (FBG) sensors. All the distributed cables were installed in loops; both a necessity for BOTDA interrogation as well as for redundancy in the case of a cable breakage during installation. The FBG strings were installed in individual vertical strings.

The thermal monitoring was divided by breadth. Five shafts (reaction shafts R1, R2, R3, R7, R9) were instrumented with three temperature loops to facilitate thermal monitoring during concrete curing. The remaining eight shafts were instrumented with a single temperature loop to allow for later correction to the fiber optic strain data, if determined necessary.

The strain monitoring consisted of two tightly-buffered strain loops installed in each of the thirteen shafts. In addition, test shaft T2 had two point-based FBG fiber optic strings installed to measure strain. Strain measurements were taken during the grouting phase, as well as during the four load tests.

A summary of the pile types and dates of installation, grouting and load testing is shown in Table 4-1.

Table 4-1: Post grouted research project pile summary

Pile	Diameter	Grout System	Date Installed	Date Grouted	Date Load Tested
R1	5'	RIM Cell	Dec. 19, 2018	Feb. 6, 2019	-
R2	5'	Open-type	Jan. 10, 2019	Feb. 7, 2019	-
R3	5'	Closed-type	Jan. 10, 2019	Feb. 4, 2019	-
R4	5'	Open-type	Dec. 21, 2018	Feb. 6, 2019	-
R5	5'	Closed-type	Jan. 9, 2019	Feb. 5, 2019	-
R6	5'	Open-type	Jan. 10, 2019	Feb. 8, 2019	-
R7	5'	Closed-type	Jan. 2, 2019	Feb. 5, 2019	-
R8	5'	Open-type	Jan. 3, 2019	Feb. 7, 2019	-
T1	3'	None	Jan. 4, 2019	-	Feb. 23, 2019
T2	3'	RIM Cell	Jan. 9. 2019	Feb. 6, 2019	Feb. 28, 2019
T3	3'	Open-type	Jan. 8, 2019	Feb. 7, 2019	Mar. 4, 2019
T4	3'	Closed-type	Jan. 4, 2019	Feb. 5, 2019	Feb. 21, 2019

Fiber Optic Cables

Three types of cable were used for the fiber optic monitoring program – a distributed thermal cable, a distributed strain cable, and a point-based strain cable. The distributed cables consist of a standard telecommunications single mode fiber optic cable, prepared in either a loose-tube (thermal) or tightly-buffered (strain) cable packaging. The point-based strain cable is a fiber optic cable with optical gratings etched into the fiber at prescribed frequencies and spacing.

a) Thermal Cable (distributed)

The distributed temperate cable chosen for the project is an 8 mm diameter standard outdoor telecommunications cable manufactured by Belden, part number FSSC004N0. A schematic cross section of the cable is shown in Figure 4-1 and a photo of the cable is shown in Figure 4-2.
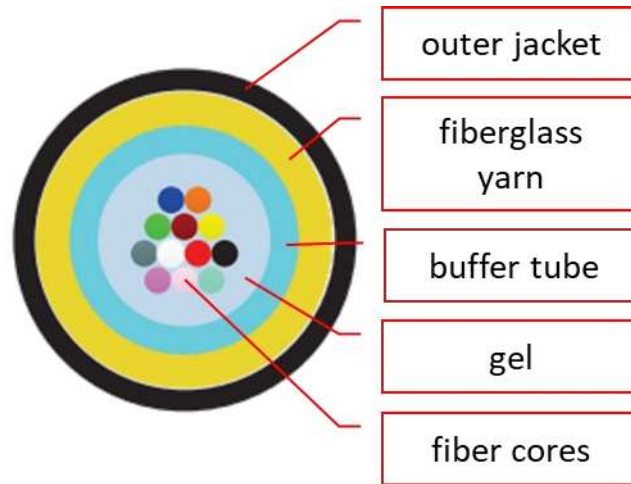
Figure 4-1: Schematic cross section of Belden 8 mm thermal cable (diagram credit: Belden Optical Fiber Catalog)

Figure 4-2: Photo of Belden 8 mm thermal cable (photo credit: Belden Optical Fiber Catalog)

The cable is a non-armored, loose tube cable with four single mode fibers in a gel-filled tube. The tube is then wrapped in a fiberglass yarn and coated with a polyethylene jacket. The gel provides a physical strain break in the cable design, preventing externally applied strains on the outer jacket from being transferred to the optical cables within. Although each cable contains four fibers, only one fiber was utilized in the temperature monitoring. The main functional parameters of the cable are listed in Table 4-2.

Table 4-2: Belden 8 mm temperature cable technical specifications

Brillouin Center Frequency (GHz)	10.84
Average Loss (dB/km)	0.3
Curvature Radius (mm)	160
Temperature Coefficient (MHz/°C)	1.100

b) Strain Cable (distributed)

The distributed strain cable chosen for the project is a 5 mm diameter armored cable manufactured by the NanZee Sensing Technology Co., part number NZS-DSS-C02. A schematic cross section of the cable is shown in Figure 4-3 and a photo of the cable is shown in Figure 4-4.
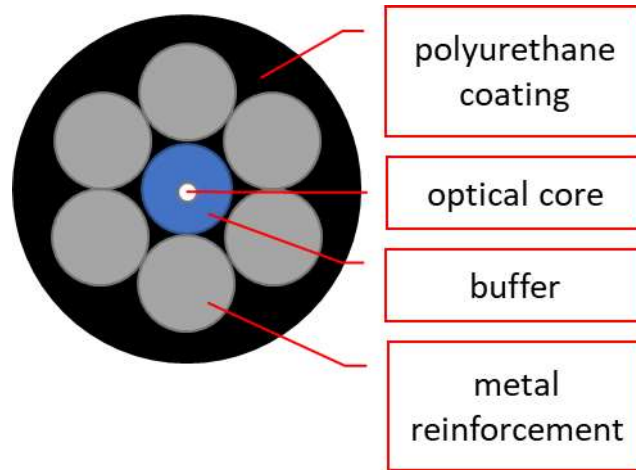
Figure 4-3: Schematic cross section of Nanzee 5 mm strain cable
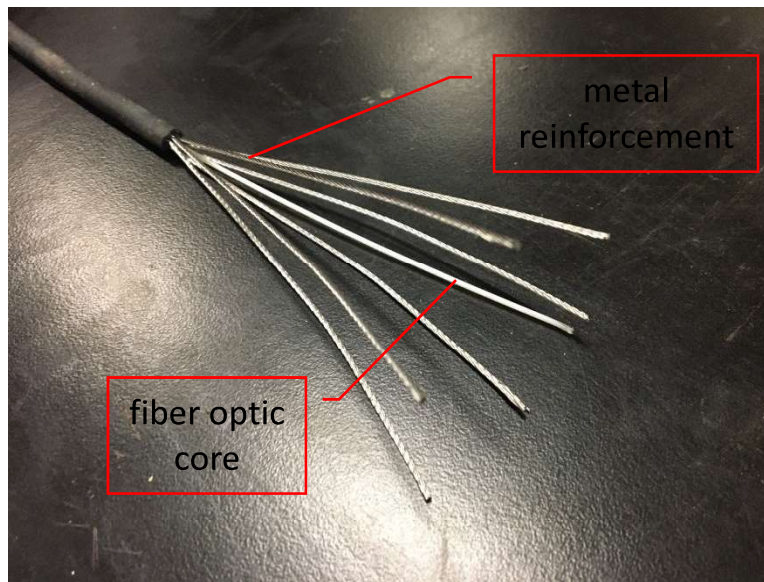
Figure 4-4: Photo of Nanzee 5 mm strain cable

This cable was chosen for its linear performance during the magnitudes of strain anticipated during the monitoring program, as well as its robustness and ease of use during installation and connection. The cable consists of a single-mode fiber optic core, tightly wound within a spiral of six braided steel cables, then wrapped in a tight polyurethane outer sheath. As opposed to

thermal cable, it is necessary for strain cable to have a tightly bonded design to ensure that applied strain to the exterior sheath is transferred in a predictable and linear manner through the intermediate layers into the central fiber optic core. The main functional parameters of the cable are listed in Table 4-3.

Table 4-3: Nanzee 5 mm distributed strain cable technical specifications

Brillouin Center Frequency (GHz)	10.850
Average Loss (dB/km)	0.201
Curvature Radius (mm)	18
Strain Coefficient (MHz/$\mu\varepsilon$)	0.04998
Temperature Coefficient (MHz/°C)	1.775

c) Strain Cable (point-based)

The point-based FBG sensor cable chosen for the project is a draw tower grating produced by FBGS, part number LBL-1550. A schematic cross section of the cable is shown in Figure 4-5 and a photo of the cable is shown in Figure 4-6.
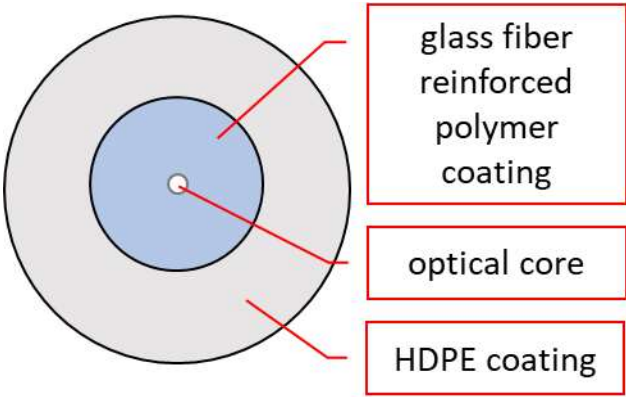
Figure 4-5: Schematic cross section of FBGS strain cable
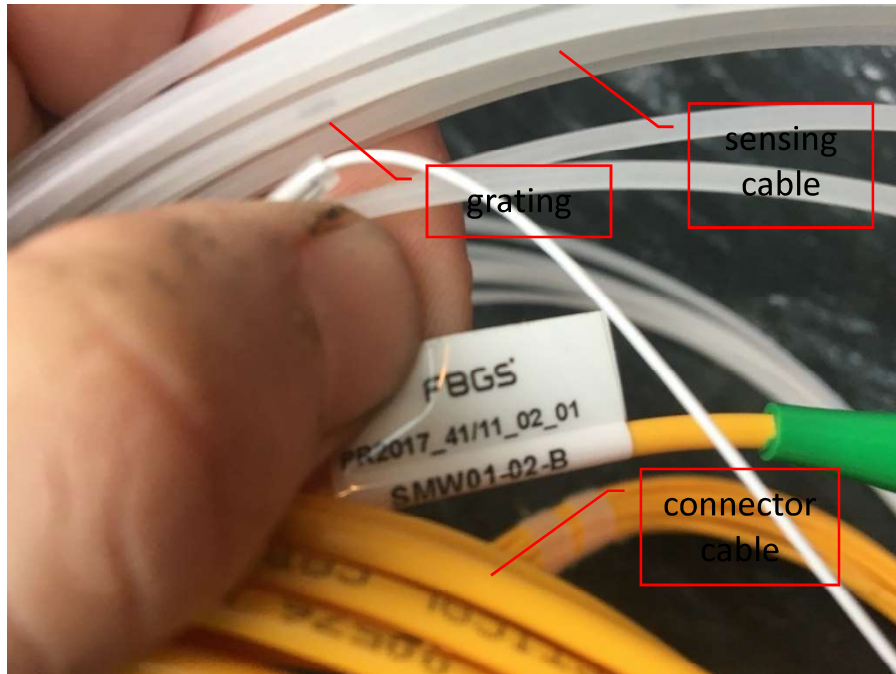
Figure 4-6: Photo of FBGS strain cable (white) and connector cable (yellow)

The fiber consists of standard 20m lengths with FBG points etched at regular one meter spacing (20 sensors for a total sensing length of 19m). Once prepared, the fiber is then drawn in 1 mm of glass fiber reinforced polymer (GFRP) coated by 2mm of HDPE. The grating frequency spacing is standardized to fit within the standard sensing wavelength window of 1510 nm to 1590 nm. This allows the product to be offered as a standard off-the-shelf item, reducing the cost by several times as compared to a bespoke FBG sensor string. For our project application, we specified one 20 m pre-manufactured string into two, 9 m sensing lengths with 10 gratings each. The main functional parameters of the cable are listed in Table 4-4.

Table 4-4: FBGS strain cable technical specifications

Center Wavelength Range (nm)	1510-1590
Absolute Wavelength Accuracy (nm)	≤ 0.5
Relative Wavelength Accuracy (nm)	≤ 0.3
Grating Length (mm)	8.0
Strain Sensitivity ($\Delta\lambda/(\lambda \cdot \Delta\varepsilon)$)	7.8 $\mu\varepsilon^{-1} \cdot 10^{-7}$
Temperature Sensitivity ($\Delta\lambda/(\lambda \cdot \Delta T)$)	6.5 $K^{-1} \cdot 10^{-6}$

Fiber Optic Analyzers

Three fiber optic analyzers were utilized during the field monitoring. Two of the analyzers were used for distributed strain and temperature readings, while the third was used for point-based strain readings. All of the fiber optic analyzers rely on a separate control laptop, running specific software for interfacing with the unit and controlling the associated readings. Power during monitoring was provided through a dedicated inverter generator with a battery surge protector and power supply to protect against power loss during monitoring.

a) Omnisens VISION Dual

The primary fiber optic analyzer used on the project was a commercial distributed strain sensing box produced by Omnisens SA of Switzerland, as shown in Figure 4-7. This analyzer in a Brillouin scatting based distributed sensing unit, capable of performing readings in both Brillouin Optical Time Domain Analysis (BOTDA) and Brillouin Optical Time Domain Reflectometer (BOTDR) modes.
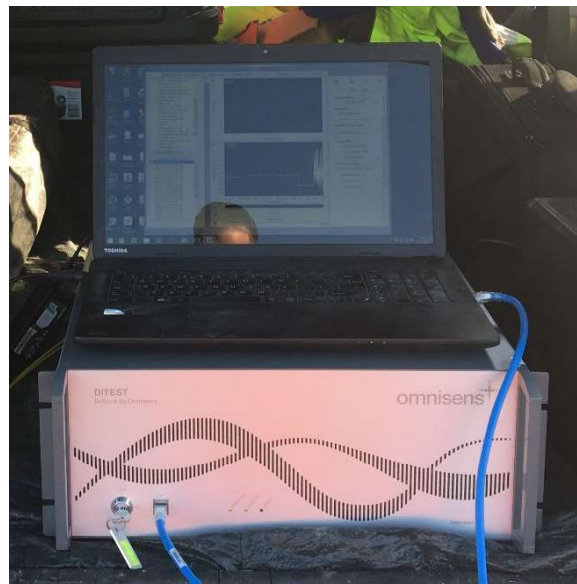
Figure 4-7: Omnisens fiber optic analyzer and control laptop during thermal readings

When operating in BOTDA mode, the analyzer is connected to both ends of the fiber optic cable, forming a continuous loop from the analyzer. A signal is sent through the sensing port into the cable, while a pump is sent from the other end to stimulate (increase) the magnitude of the Brillouin scattering in the cable. This allows the system to have a smaller spatial

resolution and a higher associated strain/temperature resolution while operating in this mode. For this project, most distributed readings were taken using the Omnisens unit operating in BOTDA mode.

BOTDR mode allows measurements to be taken using a connection to a single end of the fiber optic cable. This allows readings to be taken in the event of a breakage or damage to the cable during installation or preparation for testing. Three breakages occurred during the monitoring program which resulted in the need to switch from BOTDA to BOTDR mode. The single ended readings come with an associated increase in the spatial resolution (from 0.75 m to 1 m) and decrease in the strain/temperature resolution.

In both modes, the reading time for the chosen project settings was slightly below 5 minutes. The analyzer takes readings by sweeping in frequency within the user-defines reading window, starting at the lowest frequency, performing a series of readings, averaging the results for that frequency, and then stepping to the next higher frequency. The effect of this approach on the reading and the time-representation during non-constant strains is explored in the laboratory testing section of this report (Chapter 3).

The analyzer settings used for the Omnisens readings are presented in Table 4-5.

Table 4-5: Omnisens fiber optic analyzer reading settings

Frequency Step (MHz)	0.5
Frequency Start (GHz)	10.70
Frequency Stop (GHz)	11.15
Averaging	2000
Sampling Interval (m)	0.30
Sampling Interval (m)	0.30
Spatial Resolution, BOTDA (m)	0.75
Spatial Resolution, BOTDR (m)	1.00

b) ALICIA

The ALICIA fiber optic analyzer (see Figure 4-8) is a research-based analyzer, first developed in Professor Kenichi Soga's research group at the University of Cambridge in 2015. It is a single ended system; only connecting to one end of the sensing fiber optic installation. While the

system approach relies on the same Brillouin scattering based distributed sensing as the Omnisens analyzer, most closely mimicking it in BOTDR mode, the unique ALICIA system architecture uses digital methods for signal processing rather than the analog frequency sweeping method of the Omnisens analyzer. This results in much faster data acquisition speed, with readings taken in 1-2 seconds as opposed to 5 minutes. The system has an effective spatial resolution of 1 m with a sampling interval of 0.02 m. Being a research-based system, the system design requires the use of separate components in addition to a control laptop to function, rather than the integrated single box employed by the Omnisens analyzer. While this allows for flexibility during lab testing and system development, work is ongoing to develop the system into a single box.

Figure 4-8: ALICIA fiber optic analyzer during load test

c) Micron Optics SM130

The Micron Optics SM130 (Figure 4-9) is an FBG optical interrogator, capable of simultaneously reading up to four channels of FBG strands. Each channel is individually calibrated with the manufacturer-provided central frequency for all the FBG sensing nodes in the string. The interrogator then uses these calibration factors to calculate the frequency shift, which is then converted into differential strain. The control software tracks the peak frequency of each grating continuously during monitoring at a maximum scanning frequency of 2 KHz. For this

project, data was saved at a 1 second frequency during monitoring. The wavelength accuracy of the analyzer is 1 pm, which for the strain sensitivity of the FBGS cable, corresponds to a strain resolution of 0.8 με.

Figure 4-9: Micron Optics SM130 FBG interrogator (photo credit: Micron Optics)

Cable Installation

a) Preparation

All the fiber optic monitoring cables were precut to length prior to pile installation. For the distributed thermal and strain cables, a minimum of an extra 8 m beyond the pile length was included in each run to allow for splicing and connection at the pile head. Each pile was instrumented with a minimum of one thermal loop and two strain loops. A summary of the installed fiber optic instrumentation is presented in Table 4-6.

Table 4-6: Fiber optic sensing cable by pile

Pile Designation	Temperature Cable	Strain Cable
T1,T3, T4, R4, R5, R6, R8	1 distributed loop	2 distributed loops
R1, R2, R3, R7, R9	3 distributed loops	2 distributed loops
T2	1 distributed loop	2 distributed loops, 2 FBG verticals

The fiber optic cable was installed on site by attaching it to the reinforcement cage. The decision was made to install the cable after delivery to the field, rather than at the yard, to

reduce the chance of a breakage of the fiber during picking, transportation, and placement on cribbage.

b) Distributed fiber optic cable installation

Prior to cable installation, within every pile each vertical reinforcement bar was assigned a designation based on its type and location. A primary hollow bar (HB1) was spray painted for reference, with all subsequent bars numbered sequentially clockwise looking down on the cage from the top. For the reaction piles which had solid bars (SB) in addition to hollow bars, the numbering followed the same convention with the first solid bar clockwise of HB1 given the primary solid bar designation SB1. A schematic diagram of the vertical reinforcement bar numbering is shown in Figure 4-10.
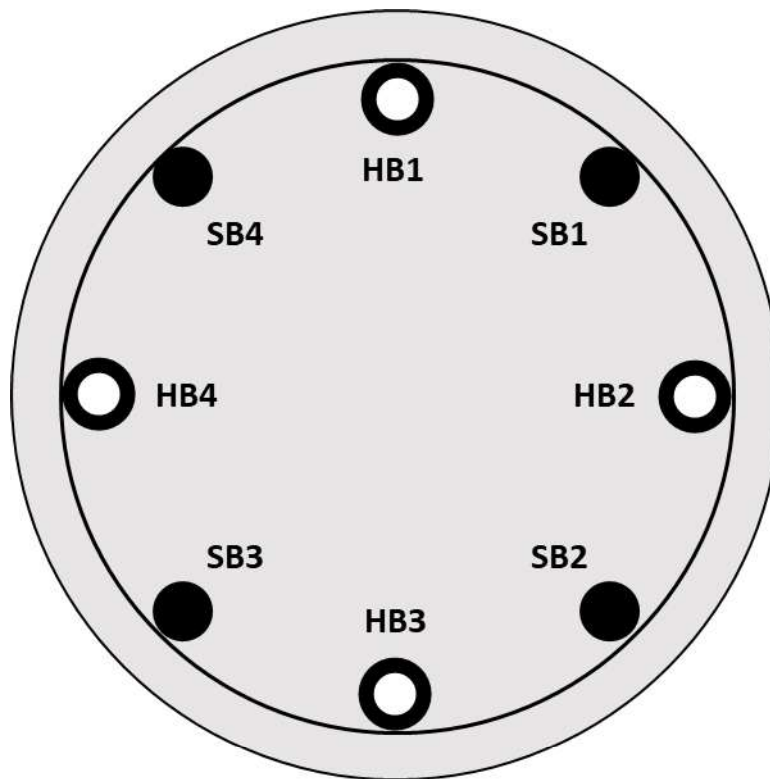
Figure 4-10: Schematic diagram of vertical reinforcement bar labeling convention, looking down from the top of the pile

For the distributed sensing cables (both strain and temperature), each pile was instrumented with a continuous cable run, measured to accommodate the number of loops planned for the specific pile. A diagram of a typical cable installation is shown in Figure 4-11 (reinforcement

spacing and number of horizontals are not to scale). While each pile had several fiber optic loops, for simplicity the figure shows the routing of just a single loop (down, 1.5 circumferential loops, up).
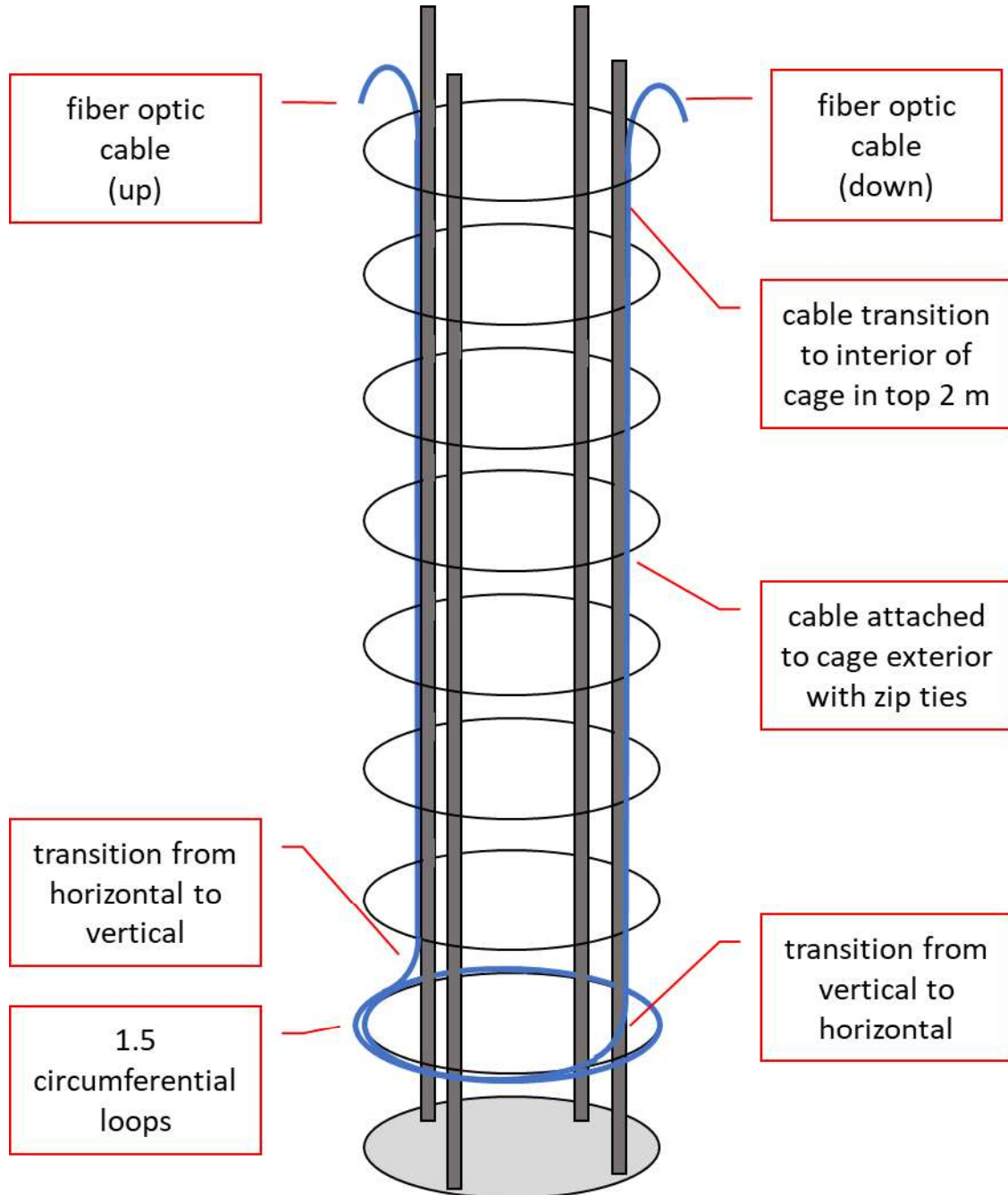
Figure 4-11: Fiber optic cable routing for a single loop

At the beginning of each cable, 4 m of cable was left coiled at the pile head to allow for connection to the cable during monitoring. The first vertical of the cable was then unreeled along a vertical bar from the top to the bottom of the cage. The cable was routed inside of the cage for the top 2 m to prevent damage to the cable from the rigging during the final hoist of the cage prior to installation in the borehole. After the top 2m, the cable was routed through the horizontal reinforcement and continued along the vertical bar on the outside of the cage, attached every three feet to the crossing horizontal loop using industrial zip ties. Care was taken to ensure that all slack was pulled out of the cable as it was installed, as well as to make sure that the cable rested flat on the exterior of the cage without any kinks or sharp bends which could break the cable during hoisting or installation.
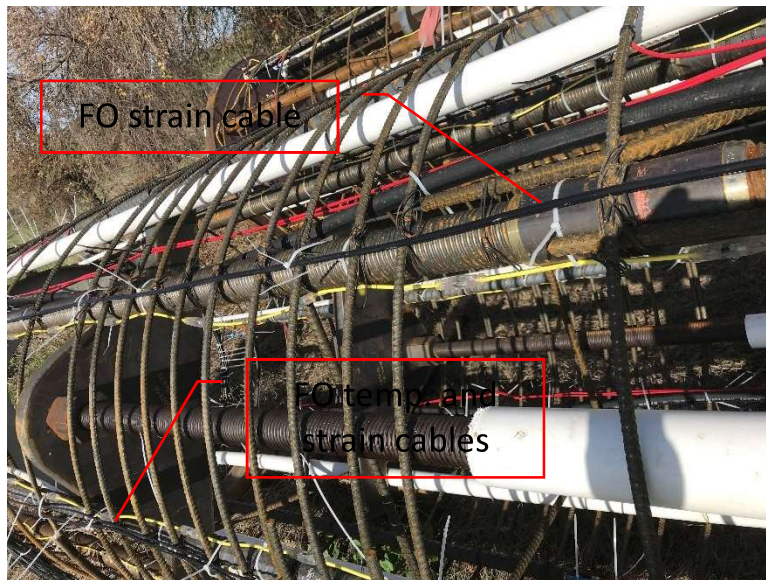
Figure 4-12: Instrumentation installed on reinforcement cage

At the bottom of the cage, each distributed fiber optic cable was routed from the vertical bar to the bottom or second to bottom horizontal reinforcement, as shown in Figure 4-11 (the schematic diagram introduced earlier). Zip ties were placed just above and below the bend to control the radius of the cable throughout the bend. The cable was then routed in 1.5 circumferential loops, circling the pile counterclockwise, before being routed back up the vertical bar opposite the first. Figure 4-13 shows the transition of a strain fiber optic cable from

64

a vertical bar to the horizontal circumferential loops, as well as several previously installed fiber optic cables encircling the bottom.
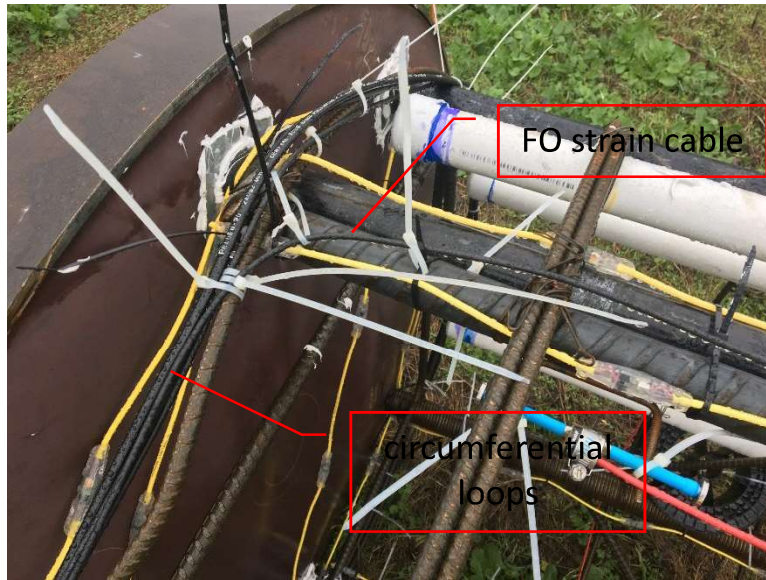
Figure 4-13: Fiber optic strain cable transitioning to circumferential loop at the bottom of the reinforcement cage

At the top of the pile, the cable was once again routed inside the cage 2 m below the top horizontal bar. This setup – the vertical "down", 1.5 circumferential loops, and a vertical "up" – constitutes a single loop, as shown in Figure 4-11. For piles with multiple loops of the same type, 7 m of cable was left between each loop to allow for reconnection in the event of a fiber break within the pile. The installation of all the fiber optic cable on the cage took approximately 2-3 hours after delivery to site with 2 researchers. Figure 4-14 shows the top of a reinforcement cage prepared for lifting into the pile bore with all cabling coiled and secured to the top bars. The fiber optic cable bundles are black, while the red cable are the conventional strain gauges and the yellow cables are the conventional thermal wire.

Figure 4-14: All instrumentation wiring installed and coiled, cage prepared for final pick

c) FBG cable installation

On pile T2, two FBG strands were installed in addition to the distributed thermal and strain fiber optic cables, following the vertical routing of two previously installed distributed strain cables. Since the FBG strands are single ended, no circumferential loops were included at the bottom of the pile. Due to the fragility of the glass polymer reinforcement on the exterior of the cable, the FBG cable was routed on the interior of the cage and attached using zip ties. One of the cables was kinked on the reinforcement during installation, causing the fiber to break and rendering that string inoperable for monitoring.

d) Instrumented cage installation and concreting

In every cage, there would be 1-2 fiber verticals, which were inaccessible due to the way the cage was supported on the cribbing. In these cases, the excess cable was coiled and attached to the side of the cage at the end of the last circumferential loop, as shown in Figure 4-15.

Figure 4-15: Cable reel attached to the bottom of the cage on vertical inaccessible when cage was on the ground

After the cage was lifted vertical and oriented over the pile bore, the coil was detached, and the cable was installed with zip ties along the appropriate vertical bar as the cage was lowered into the bore, as shown in Figure 4-16. This method is the same as how fiber optic cables would be installed on subsequent cages for multi-section piles.

Figure 4-16: Installation of final fiber optic cable vertical during lowering of reinforcement cage

Following the lowering of the cage, all fiber optic and conventional sensor cables were routed out of two PVC pipes to protect the cables from bending or damage during later pile work. The

cable was then bundled and placed into heavy duty plastic bags to protect them during concreting.

At the completion of the pile concreting, the temperature and strain cables were spliced together and FC connectors were connected to the remaining 2 free ends. A photo of the field setup for splicing the fiber optic cables after the piles were installed is shown in Figure 4-17. The field setup was laid out on a portable folding table. Disinfecting wipes were used to carefully clean the cable ends of mud and dirt, as well as wipe down the table. The tools on the left of the table were used to remove the outer layers of the fiber optic cables include a pipe cutter, cable snips, wide and needle nose pliers, a matte knife, and wire strippers. The yellow-handled tools in the upper center part of the table were used to prepare the fiber core – stripping any protective coating and buffer to expose the core. The core was cleaned with a sterile wipe wetted with alcohol (center top, left). The core was cleaved (center bottom, left), then installed in the holder within the splicer (center, right). The process was repeated for the other section of fiber which was being spliced.

Figure 4-17: Photo of the field setup and tools used for splicing fiber optic cables from the piles

A close-up of the strain cable being prepared for splicing with a protection tube is shown in Figure 4-18. The FC connectors allowed the fiber optic cables to be connected to the analyzer channels or to each other using double-ended connectors.
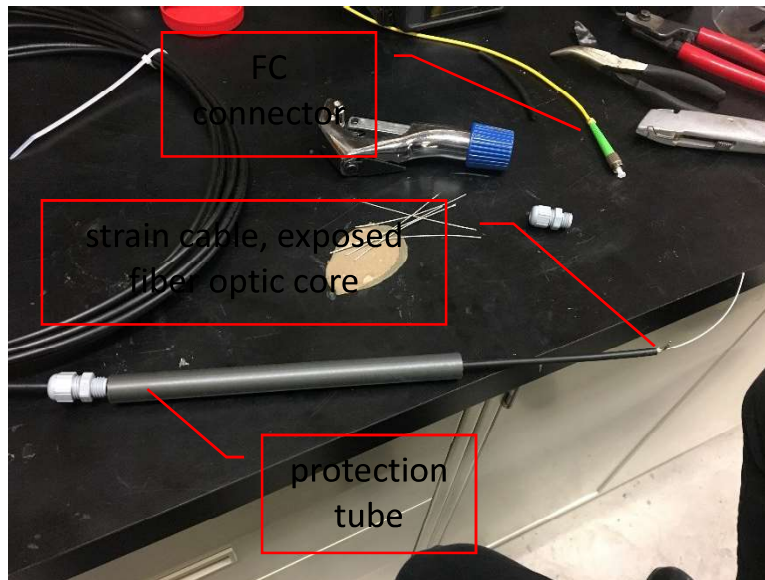
Figure 4-18: Nanzee 5mm strain cable prepared for splicing with plastic protection tube and FC connector

The splicing process entails carefully removing the protective sheathing around the fiber optic strand, cleaving the end of the fiber optic cable to a 90° face, splicing the two cable cores together using a fiber optic fusion splicer, and securing a protective sheath around the completed splice. A photo of a splice between the strain cable and an FC connector patch cable is shown in Figure 4-19. This photo was taken of a splice performed in the lab between the Nanzee 5 mm cable and an FC connector patch cable. The image on the screen shows a close-up view of the two fiber optic cores which are aligned and measured for squareness of the cut. Any incompatibility of the angle of the two cuts will result in an error from the splicer and the fiber would have to be recut.

Figure 4-19: Fujikura fusion splicer, joining strain cable (left) and FC patch cable (right)

The maximum optical loss for each splice was set at 0.1 dB – any splice over this value would be cut and repeated. A photo of the same cable shown in Figure 4-19 after the splice is completed is shown in Figure 4-20.

Figure 4-20: Photo of completed splice between strain cable (left) and FC patch cable (right)

Following the completion of the splice, continuity was confirmed through all connections using an Optical Time Domain Reflectometer (OTDR) testing device. This allows for testing of both the continuity of the splice as well as checking for any breaks or sharp bends in the fiber optic cable

in the pile. A photo of the OTDR readout of the previous splice is shown in Figure 4-21. The readout shows the reflectance of the splice, as well as the loss along the cable length. This cable has a large reflectance at the end since it is a bare cut (no splice or termination), causing the reading to fail in this scan. Attaching another splice to the other end greatly diminishes the reflection at the opposite end.
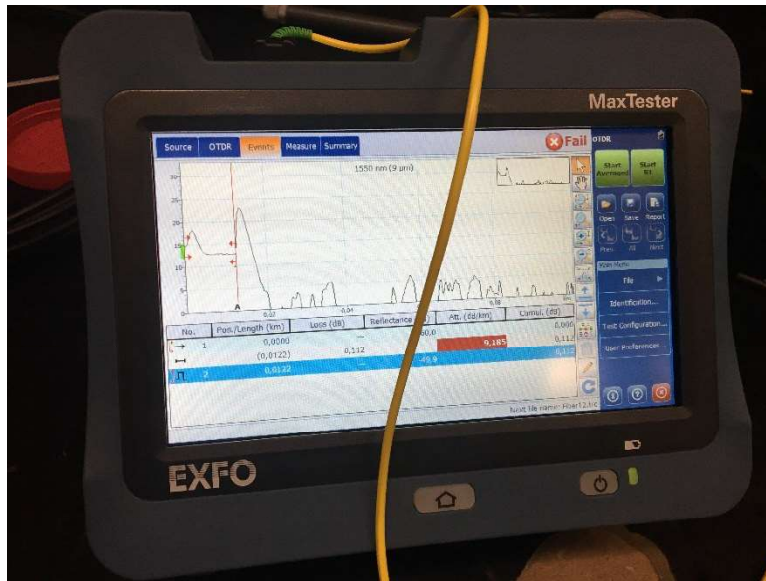
Figure 4-21: OTDR readout of a fiber optic splice and length of cable

None of the installed distributed fibers were broken during installation, including a section of temperature cable that was pinched between the reinforcement and cribbing during handling of the cage prior to picking. A photo of the kink in the cable is shown in Figure 4-22. After the cage was repositioned, an integrity test was performed on the cable using the OTDR which showed no breakage or loss at the pinch point.

Figure 4-22: Thermal fiber optic cable pinched under reinforcement during handling prior to installation

The only breakage of a cable occurred during the load test of test pile T3. During the penultimate unload cycle, the load frame, which had previously lifted off its cribbing due to the high reaction force from the applied load, settled onto a section of thermal cable which had shifted slightly during the test. The cable was caught on a sharp edge between the two steel pieces, severing the fiber optic core. A close-up of the break is shown in Figure 4-23.
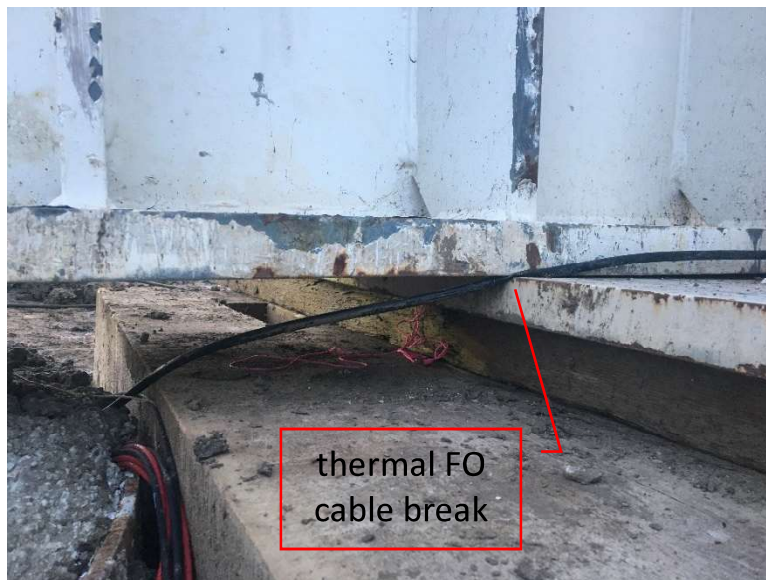
Figure 4-23: Thermal fiber optic cable severed by load frame

The splice and protection system used to join cable loops and attach FC connectors proved to be robust. Of the 39 splices installed for the monitoring program, only 2 splices experienced failures. In both cases, this was due to a strong pull being exerted on the fiber optic cable, for instance someone tripping on the cable and jerking the splice apart as they stumbled.

5. Measurements During Grouting

Overview

Following the installation of the thirteen drilled shafts, twelve of the shafts were base grouted using three different grout delivery methods (RIM Cell, Open-type and Close-type). Distributed fiber optic measurements of strain and temperature were taken during the grouting process. A summary of the base grouting program is shown in Table 5-1.

Table 5-1: Pile base grouting program summary

Pile	Diameter	Grout System	Date Grouted
R1	5'	RIM Cell	Feb. 6, 2019
R2	5'	Open-type	Feb. 7, 2019
R3	5'	Closed-type	Feb. 4, 2019
R4	5'	Open-type	Feb. 6, 2019
R5	5'	Closed-type	Feb. 5, 2019
R6	5'	Open-type	Feb. 8, 2019
R7	5'	Closed-type	Feb. 5, 2019
R8	5'	Open-type	Feb. 7, 2019
R9	5'	Closed-type	Feb. 4, 2019
T2	3'	RIM Cell	Feb. 6, 2019
T3	3'	Open-type	Feb. 7, 2019
T4	3'	Closed-type	Feb. 5, 2019

<u>Grouting</u>

Each pile was grouted progressively, clearing each delivery circuit with water before switching to grout and cycling through the different circuits, as necessary. The grout pressure was measured by an automated data logger immediately downstream of the grout plant, as well as at a manually read dial gauge placed on the feed line at the final connection at the pile head. Separate readings of grout volume and pile head and base displacements were read using a combination of automated and manual systems. This report focuses on the strain measured by the distributed fiber optic sensors installed within the piles. A separate report by the University of Missouri team provides an in-depth discussion into the grouting design, methodology, and analysis for the project.

<u>Fiber Optic Measurements</u>

Measurements

For the distributed fiber optic monitoring, the strain and temperature fiber optic loops in each shaft were interrogated during the base grouting. Prior to the start of grouting, the strain and temperature loops were spliced together to form a continuous fiber line for each pile. In all cases, the sensing side of the analyzer was connected to the strain side of the fiber optic line. The readings were taken using the commercial Omnisens analyzer. All the readings were taken in the loop BOTDA mode with the exception of those for pile R5 which had a broken splice, necessitating using the single-ended BOTDR mode for the readings. A minimum of three readings were taken prior to the commencement of grouting to serve as a baseline. Readings during grouting were taken based on the progression of the grout progress, with the grout line dial pressure gauge at the top of the pile noted at the start of each reading. Each reading took approximately five minutes to perform, with the grout pressure fluctuating during the interrogation time. A minimum of three readings were taken after the conclusion of grouting to observe the strain decay in the pile after the supply pressure was released.

Data analysis

The raw output of each fiber optic reading is a series of frequency values at increasing distances away from the sensing side of the analyzer. The first step necessary to process the raw data into engineering units is to "index" the 1 dimensional data set to specific locations within the pile; both radially (by reinforcement bar) and depth in the pile (measured as depth below the top of casing, TOC). The data set is first divided by a set of estimated cuts based on recorded lengths of fiber installed for each fiber optic loop, including the 1.5 circumference at the base of each pile. The frequency record is then converted into either strain or temperature using a linear transformation by the strain or temperature coefficient to create a preliminary record with depth. Further fine tuning of the vertical position of each loop is then performed by comparing the records to each other over the monitoring period, identifying strain and temperature gradients that can be used to refine the assigned depth of each individual monitoring point.

Temperature change effect

Prior to final processing of the strain profiles, the temperature changes as measured by the thermal fiber optic lines was evaluated to determine if thermal compensation of the strain measurements was necessary. Changes in excess of 1-3 MHz from the baseline were observed in the thermal fiber optic cables, corresponding to a thermal fluctuation of 0.9-2.7° C. Converting into strain using the thermal coefficients of the strain cable, this corresponds to an associated range of thermally-induced strains of 32-96 με. For illustration, the temperature readings taken during the base grouting of shaft R2 (open-type system) are shown in Figure 5-1
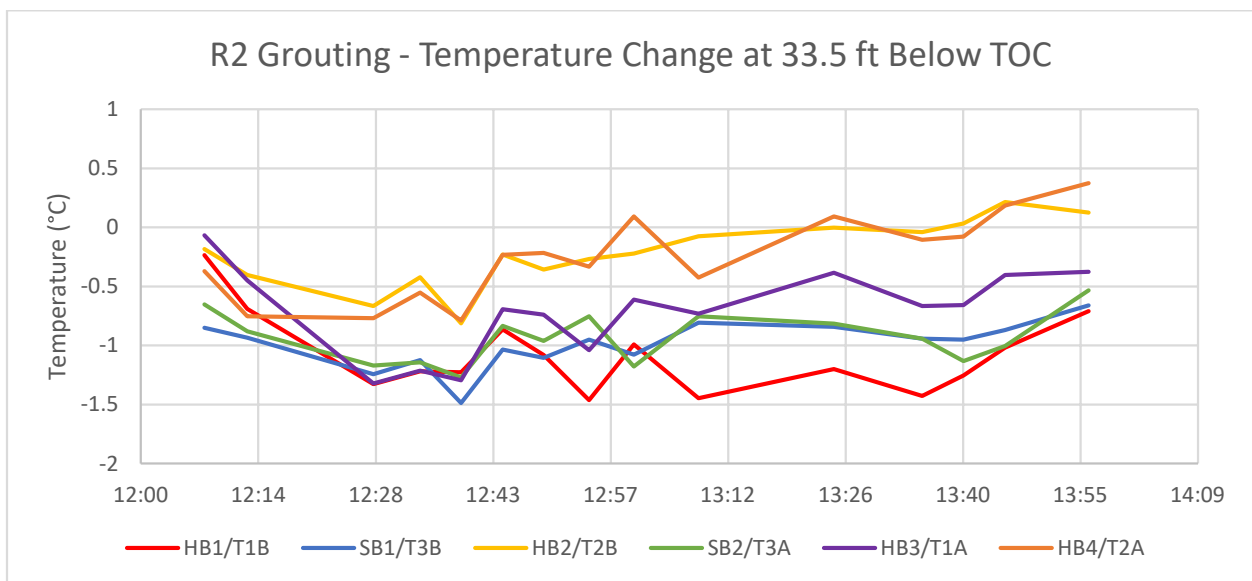
Figure 5-1: Temperature change in shaft R2 during grouting

As can be seen in the figure, temperatures in the shaft dropped by up to 1.5° C within the first half hour of monitoring. The recorded thermal changes were not uniform across the pile and were likely due to circulation of the water and grout in the vertical delivery tubes, with the largest variations recorded in the fibers closest to the active tubes. The grout delivery system for the open-type in 5' piles consisted of 3 separate loops – one roughly in the center of the shaft and 2 on either side. The lowest recorded temperature readings on hollow bars 2 and 4 were on the axis of the shaft perpendicular to the loops, making them the bars farthest from the flowing water and grout. The initial drop observed on hollow bars 2 and 4 correspond to the

time when water and grout were circulating in the middle grout circuit – the temperature rebound back to 0 is after the return valve was closed.

Based on the high observed temperature variation, thermal compensation was performed on all strain readings taken during grouting. For strain fibers with a co-located temperature fiber, the temperature compensation was performed directly using the readings from the associated fibers. For strain fibers without a directly corresponding temperature fiber, the average of the two closest temperature fibers were used to calculate the compensation value.

Results

The presentation of the strain measurements during grouting for each shaft are divided by grouting system.

RIM Cell

a) Reaction Shaft R1

Reaction Shaft R1 was grouted on February 6, 2019. The grout data logger record of pressure and volume at the grout plant is presented in Figure 5-2. After some problems with the grout plant, including a pressure spike 9:46, grouting of the pile began at 9:51. The pressure was initially attempted to be held at 200 psi at 9:52, after which subsequent holds were attempted at 600 psi at 10:08 and 800 psi at 10:16. At 800 psi, a vent cap at the top of the pile burst off and a stream of water was released, dropping the pressure in the line to 250 psi and pumping was stopped. The measured volumes are not adjusted for the initial flush or grout in the lines and therefore represent an upper bound of the volumes placed at the pile base.
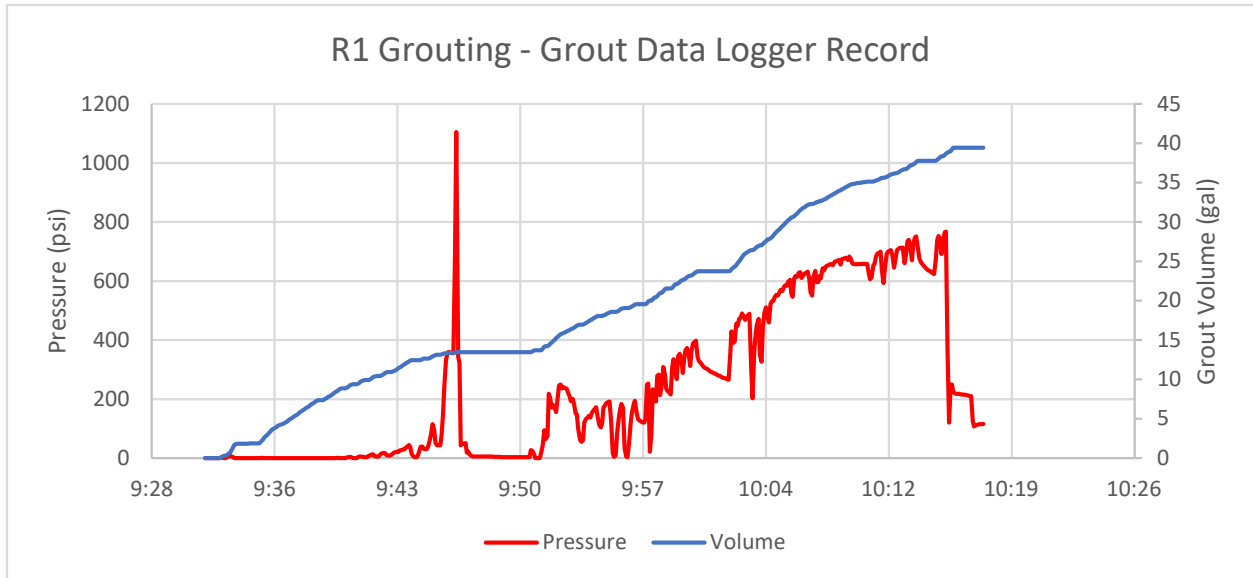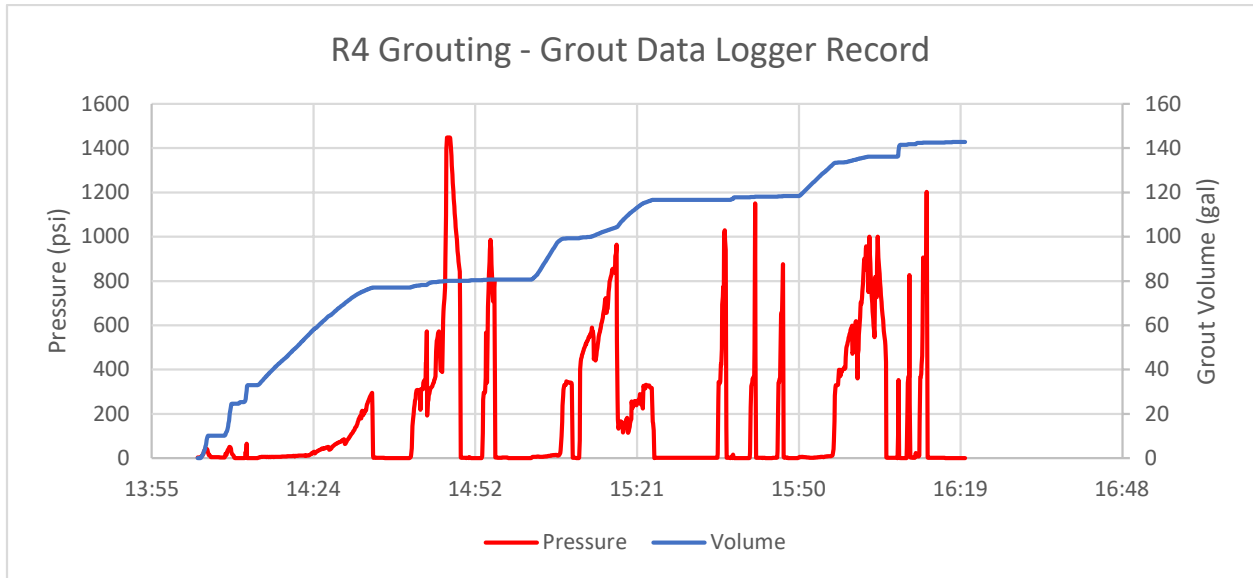
Figure 5-2: R1 grouting, grout data logger record

The fiber optic record for shaft R1 is divided into 4 strain verticals and 6 temperature verticals. The raw frequency and segment divisions are shown in Figure 5-3.
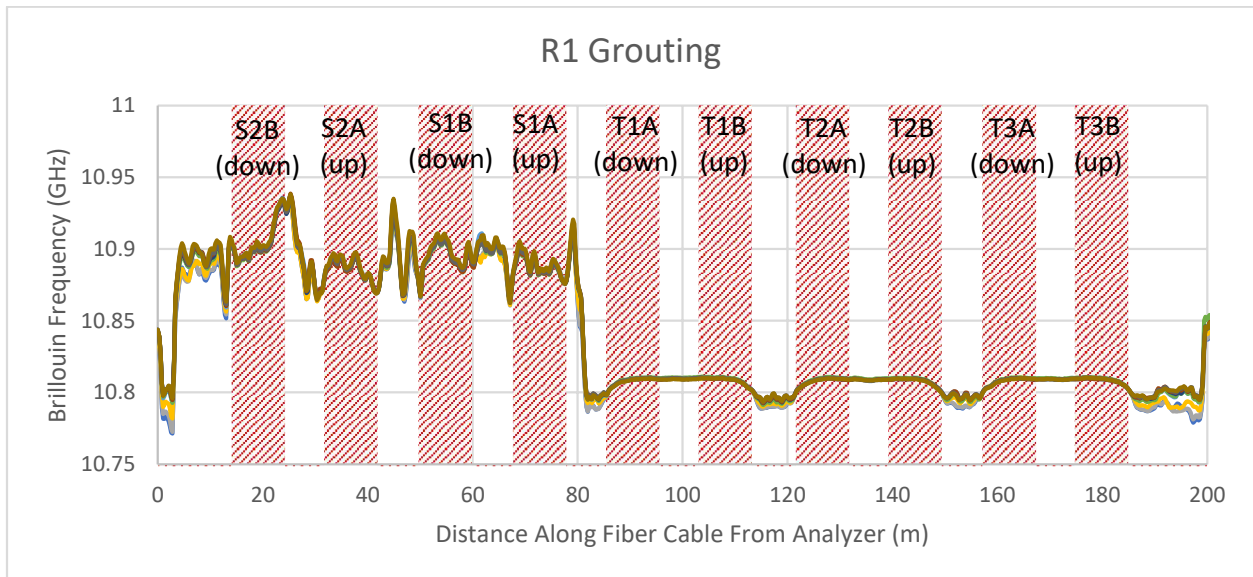
Figure 5-3: R1 grouting, raw Brillouin frequency
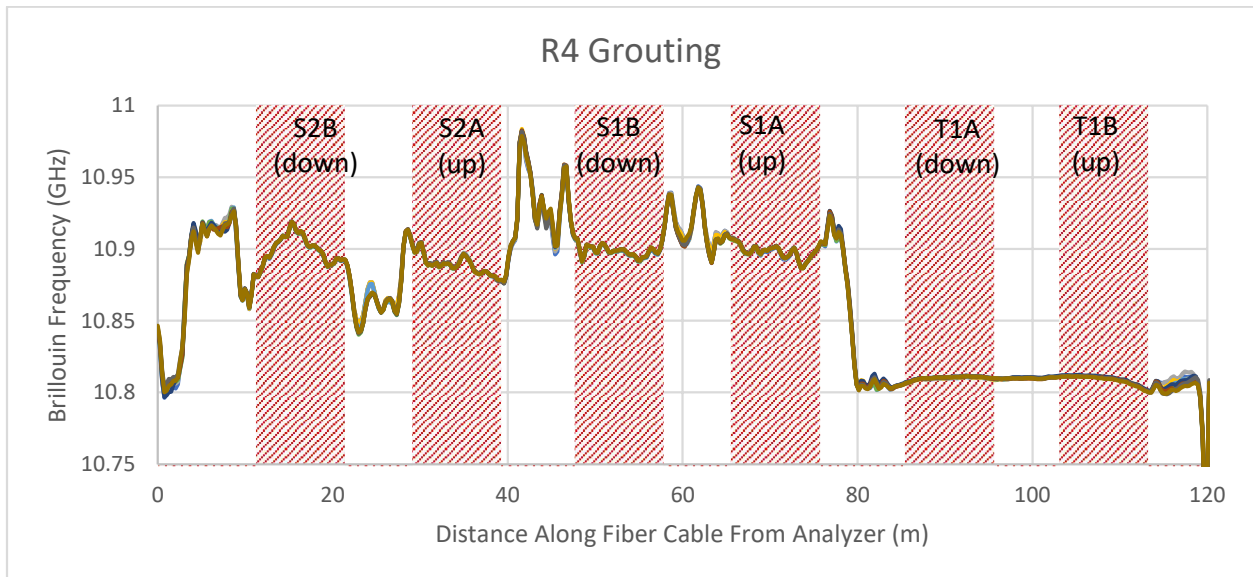
The measured vertical strains with time at a depth of 33.5 feet below the top of casing (TOC), approximately 1 pile diameter (5 feet) above the base, are presented in Figure 5-4. This figure shows an initial peak in vertical strain of 40 to 60 με at 9:58, when the associated grouting pressure was fluctuating around 300 psi. The strains across the pile then decreased to under 20

78

με, despite increasing grout pressure, until they fell dramatically after the vent cap burst. The final reading after the release of pressure shows tension developed in the pile from 0 to 60 με.
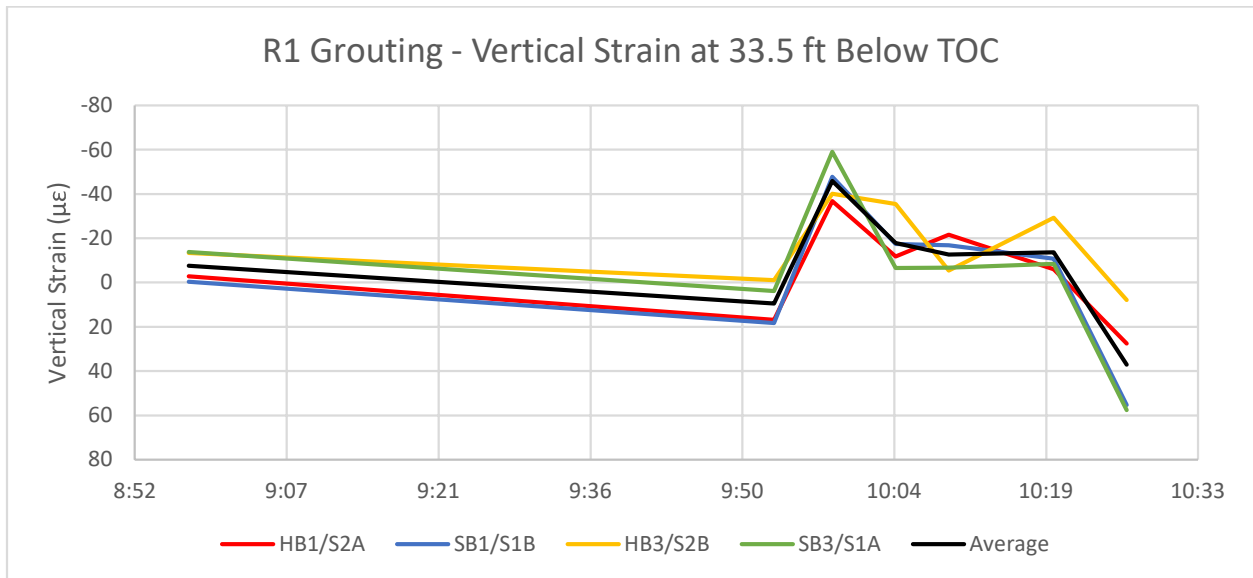
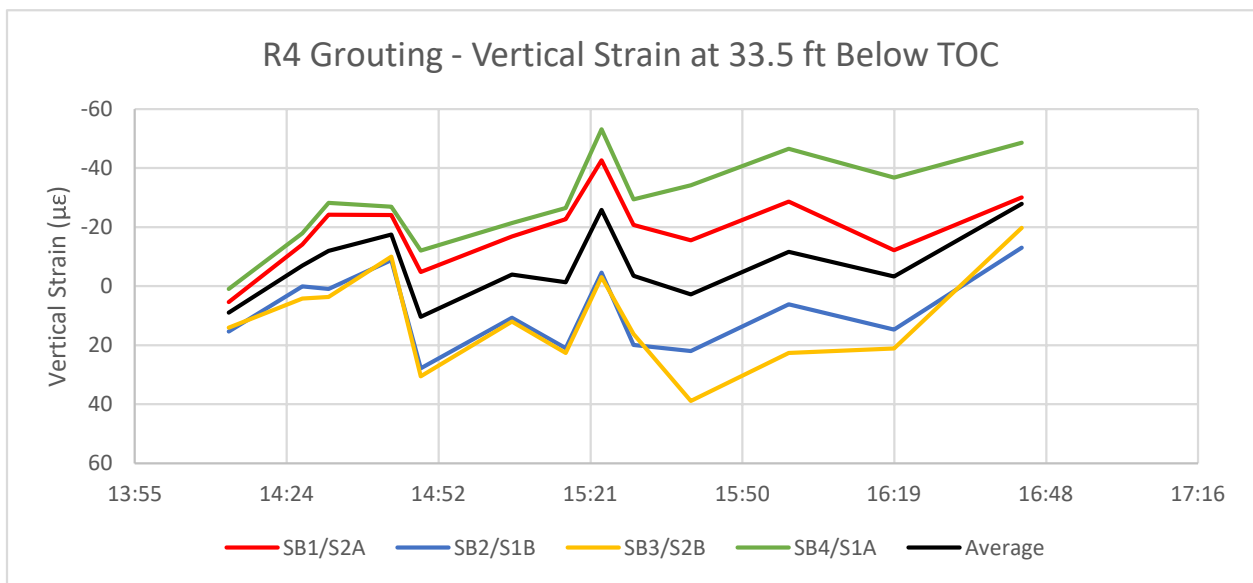*Figure 5-4: R1 grouting, vertical strains at 33.5 feet below TOC*

Figure 5-5 through Figure 5-7 show the vertical strains with depth in the pile at 9:58 (~300 psi), 10:09 (~600 psi), and 10:18 (after pressure release). Figure 5-5 shows that the initial vertical strain peak around 9:58 averaged 50 με in compression and extended through most of the length of the pile before beginning to drop off at 10 feet below TOC. Looking at the 10:09 plot, the average vertical strain in the pile has decreased to below 25 με in compression, with tension developing in SB1. After the grout pressure is released, the entire pile is put into tension with average strains of just below 50 με measured through a depth of 15 feet below TOC. The measured average strain profiles are more or less uniform with depth, indicating limited shaft friction development. The change in strain indicates that the pile was in compression at 300 psi grout pressure. However, the pile experienced decrease in stress with time even the grouting pressure increased. When the grout pressure was released, the pile is experiencing tension, suggesting that the RIM cell is pulling the pile downwards. Further investigation is needed to interpret the data of this pile.
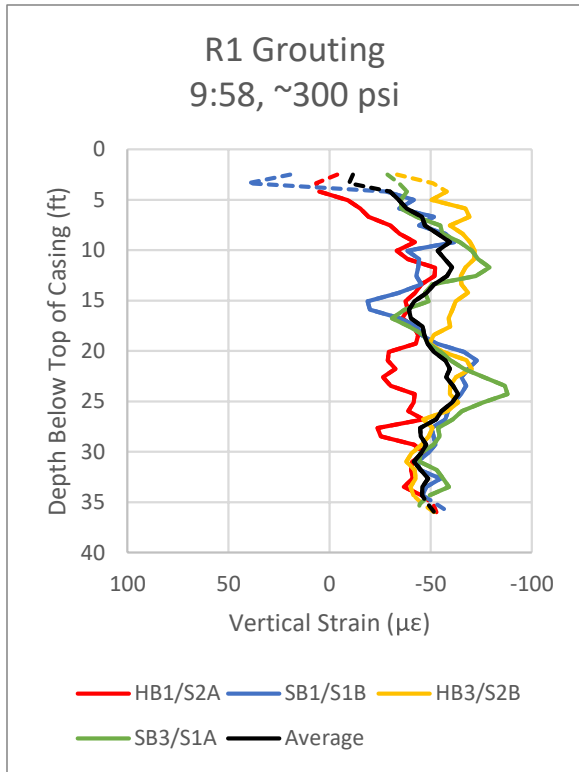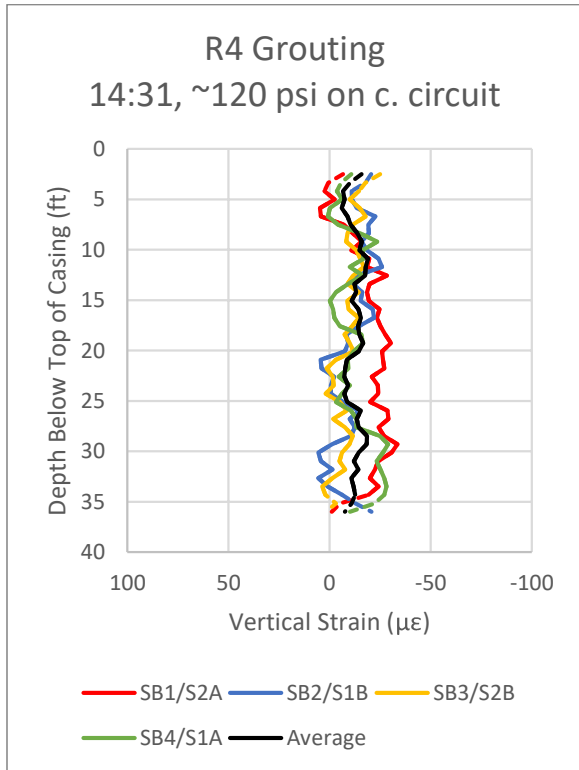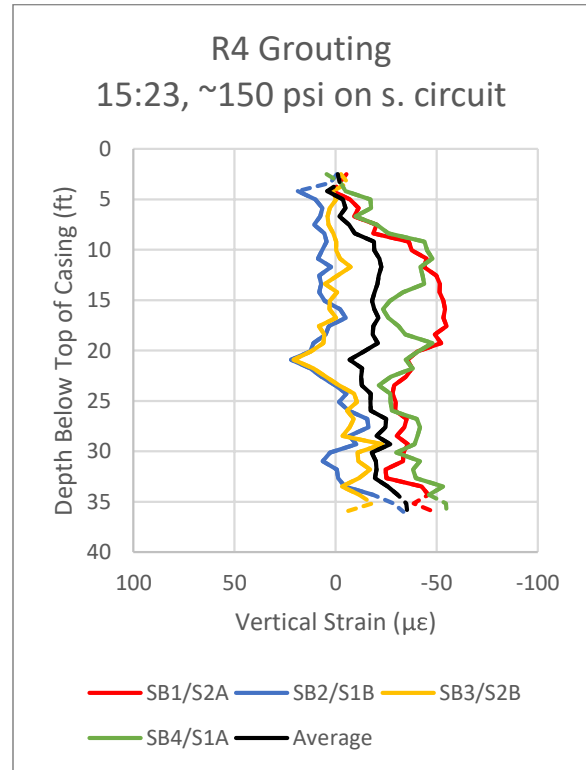
Figure 5-5: Vertical strain profile at 9:58 (~300 psi)
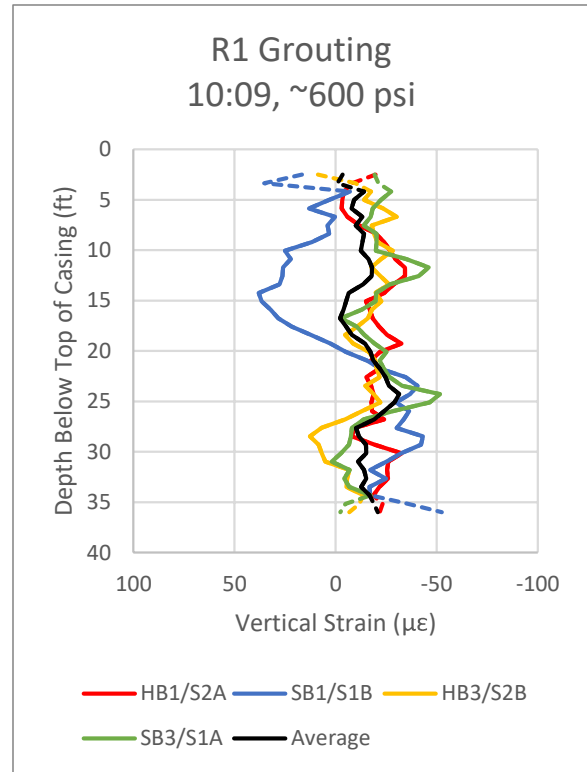
Figure 5-6: Vertical strain profile at 10:09 (~600 psi)
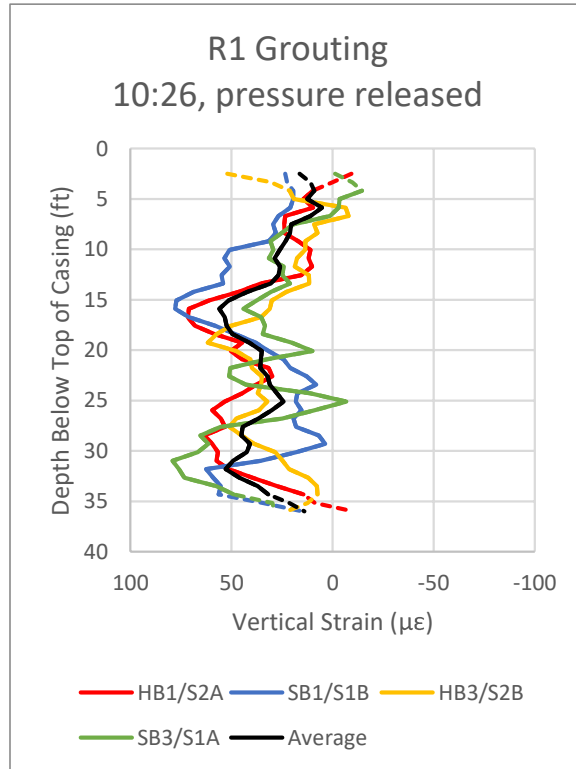
Figure 5-7: Vertical strain profile at 10:26 (after pressure release)

b) Test Shaft T2

Test Shaft T2 was grouted on February 6, 2019. The grout data logger record of pressure and volume at the grout plant is presented in Figure 5-8. Grouting of the pile with all return valves commenced at 12:08. An initial pressure hold was performed at 400 psi at 12:11. A second hold at 600 psi at 12:14 was performed with pressures fluctuating widely between 500 and 700 psi. A peak pressure of 965 psi was observed at 12:24 prior to a vent cap burst at 12:27 at which point the pressure dropped to 0 psi and pumping was stopped. The measured volumes are not adjusted for the initial flush or grout in the lines and therefore represent an upper bound of the volumes placed at the pile base.
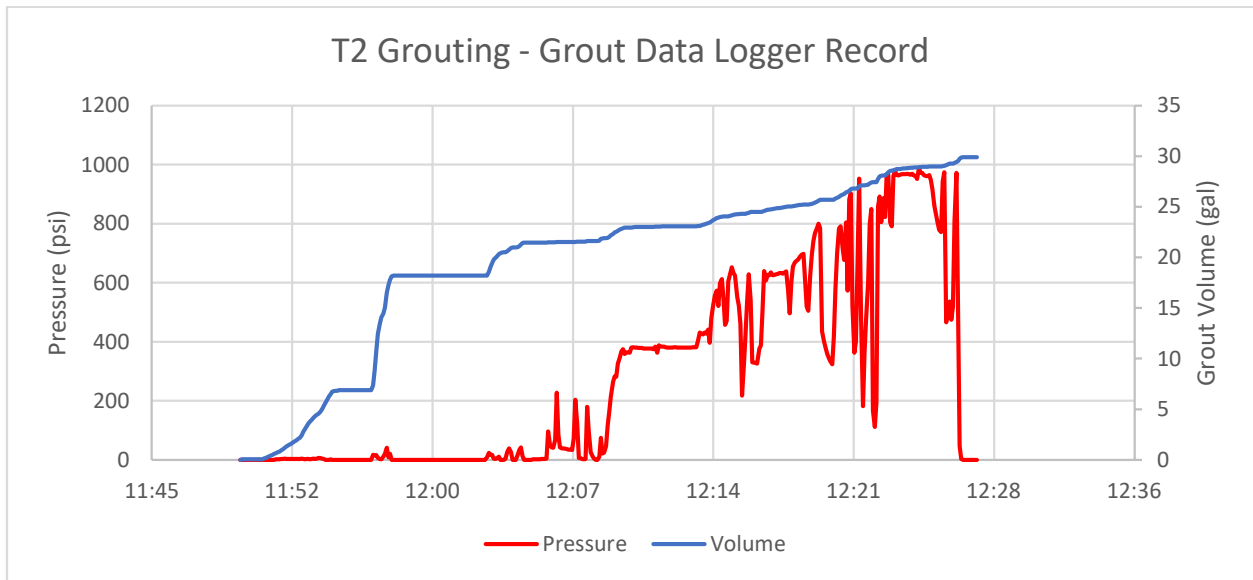
Figure 5-8: T2 grouting, grout data logger record

The fiber optic record for shaft T2 is divided into 4 strain verticals and 2 temperature verticals. The raw frequency and segment divisions are shown in Figure 5-9.
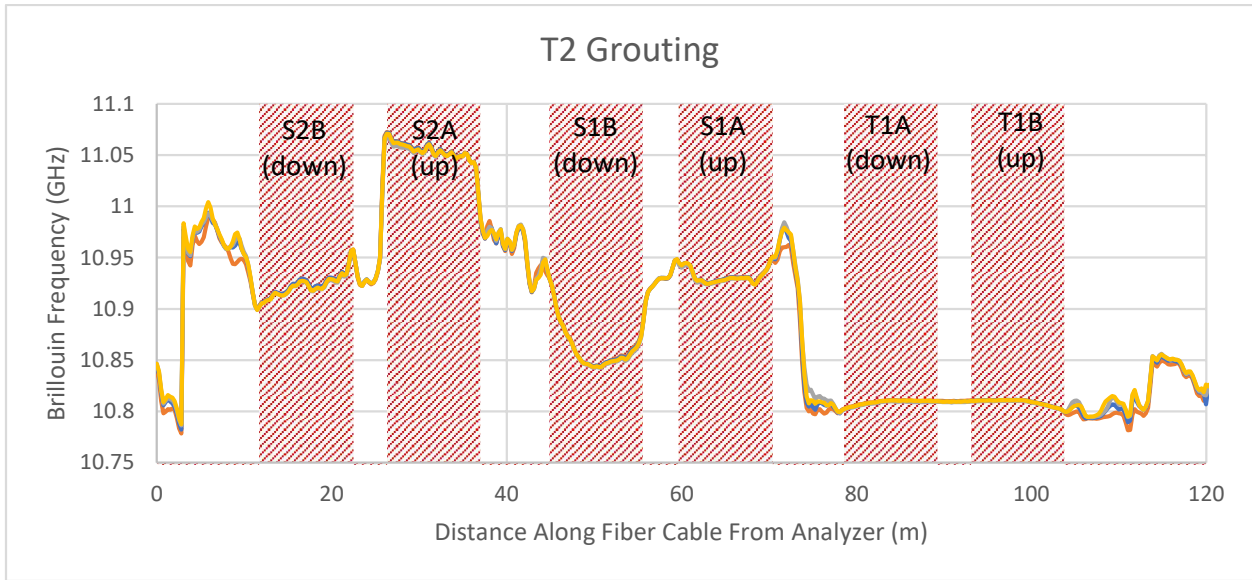
Figure 5-9: T2 grouting, raw Brillouin frequency

The measured vertical strains with time at a depth of 34.4 feet below the top of casing (TOC) are presented in Figure 5-10. This figure shows a peak vertical strain of 100 με in compression at 12:25, when the associated grouting pressure was approximately 965 psi before the vent cap burst. The peak strain on the other verticals were lower in magnitude and occurred at lower pressure, indicating a shifting strain distribution within the pile during grouting. After release of the vent cap, the strains returned to an average value just below 20 με.
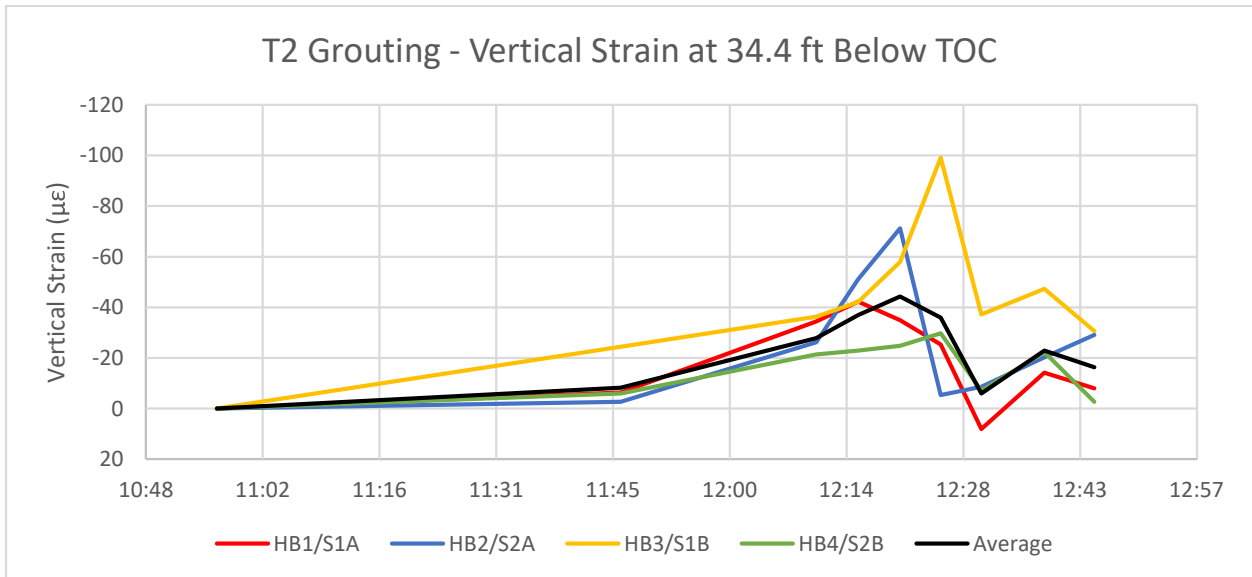
Figure 5-10: T2 grouting, vertical strains at 34.4 feet below TOC

82

Figure 5-11 through Figure 5-13 show the vertical strains with depth in the pile at 12:15 (~600 psi), 12:25 (~965 psi), and 12:44 (after pressure release). Figure 5-11 shows a compressive strain increase in all the verticals extending approximately 20 feet from the base of the pile. The reading at 12:25 (Figure 5-12), the final reading prior to the vent cap bursting, shows a significant strain concentration on one quadrant of the pile with strains on all sides extending to within 5 feet of the TOC. Following the release of pressure, Figure 5-13 shows average residual strains centered just above 0 $\mu\varepsilon$, with variation of on the order of 30-50 $\mu\varepsilon$ throughout the pile. In Figure 5-11, the strain profiles are increasing with depth, indicating some negative friction development during grouting. By the Figure 5-12, the strain has become non-uniform, indicating a significant load concentration on the side of HB3. This could potentially be due to a variation in the loading being applied by the RIM cell, or potentially a difference in the friction resistance along one side of the shaft. In Figure 5-13, the compressive strains at the bottom of the pile have been released; however there appears to still be approximately 20 $\mu\varepsilon$ of compressive strain in the center of the pile, potentially indicating a locked-in negative friction.
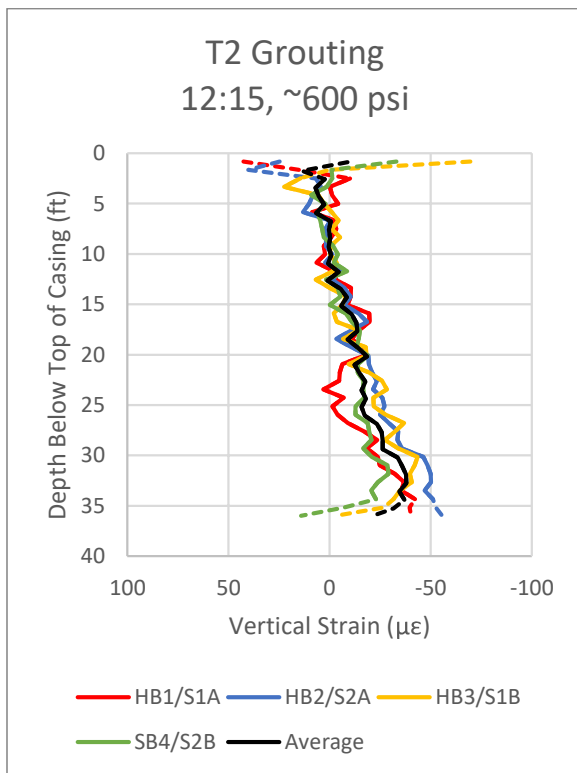
Figure 5-11: Vertical strain profile at 12:15 (~600 psi)
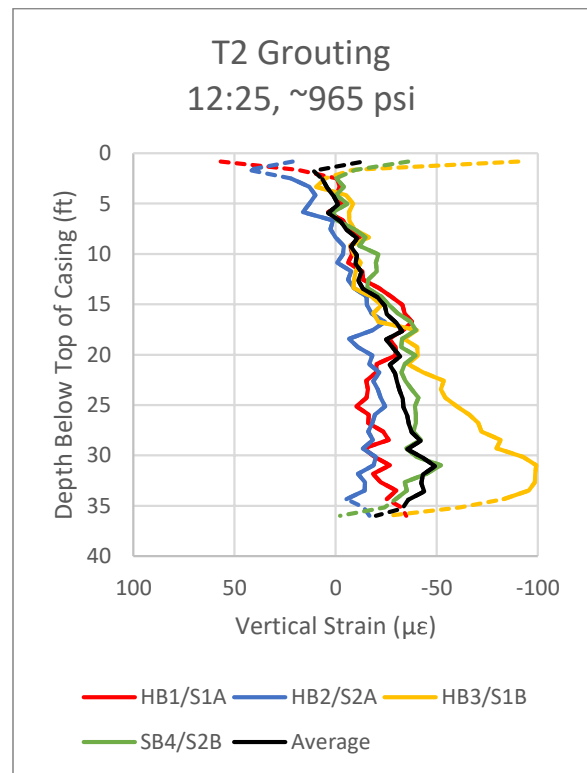
Figure 5-12: Vertical strain profile at 12:25 (~965 psi)
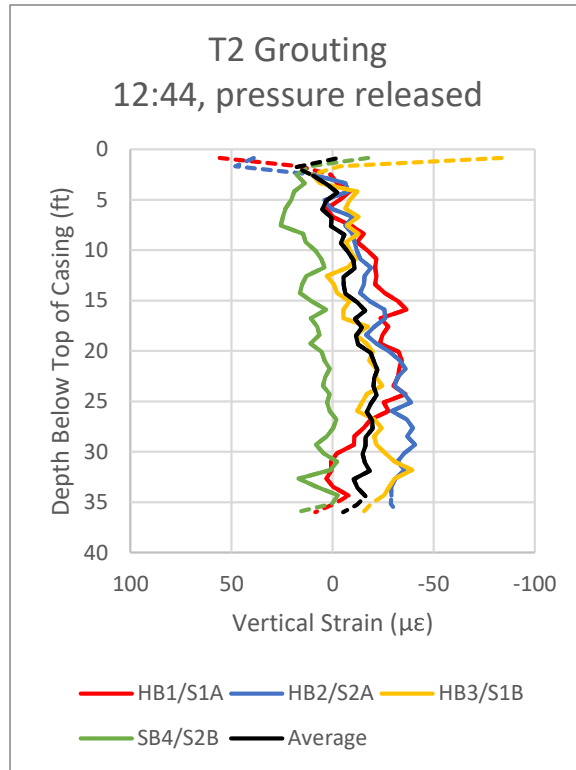
Figure 5-13: Vertical strain profile at 12:44 (after pressure release)

Open-Type (tube-à-manchette)

c) Reaction Shaft R2

Reaction Shaft R2 was grouted on February 7, 2019. The grout data logger record of pressure and volume at the grout plant is presented in Figure 5-14. Grouting was performed on three circuits, with the center circuit primed and grouted first. Grouting on the center circuit with the return valve closed began at 12:10 and continued to 13:08, at which time grouting was switched to the south circuit. The south circuit was grouted for approximately 4 minutes from 13:23 to 13:27. At 13:27, grouting was switched to the north circuit. The north circuit was grouted from 13:33 to 13:47, at which time grouting was ceased. The measured volumes are not adjusted for the initial flush or grout in the lines and therefore represent an upper bound of the volumes placed at the pile base.
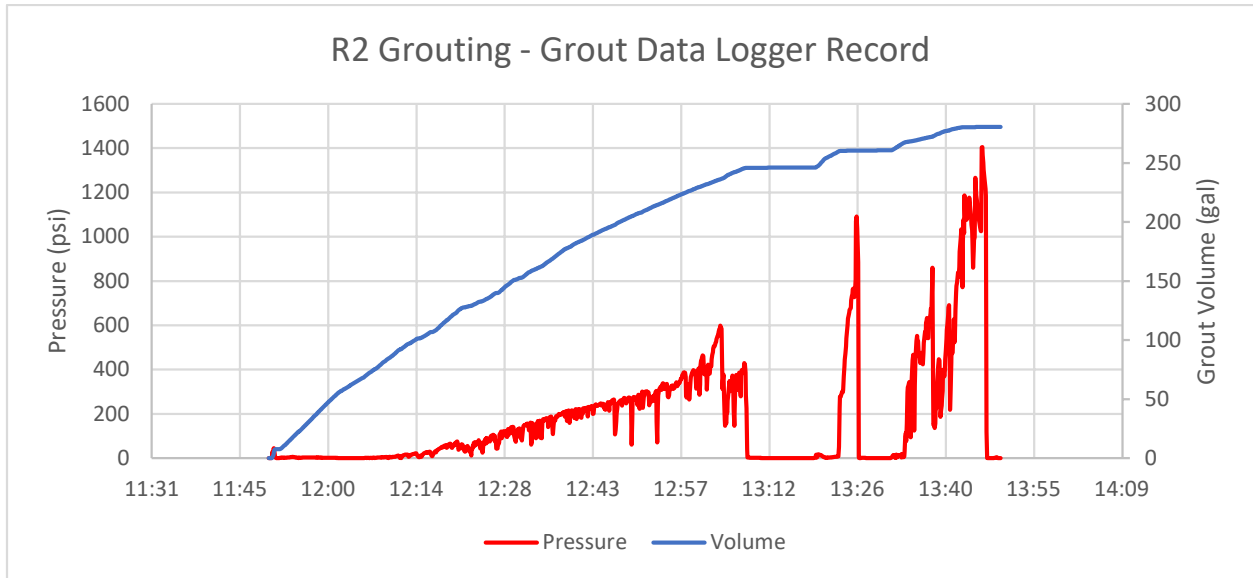
Figure 5-14: R2 grouting, grout data logger record

The fiber optic record for shaft R2 is divided into 4 strain verticals and 6 temperature verticals. The raw frequency and segment divisions are shown in Figure 5-15.
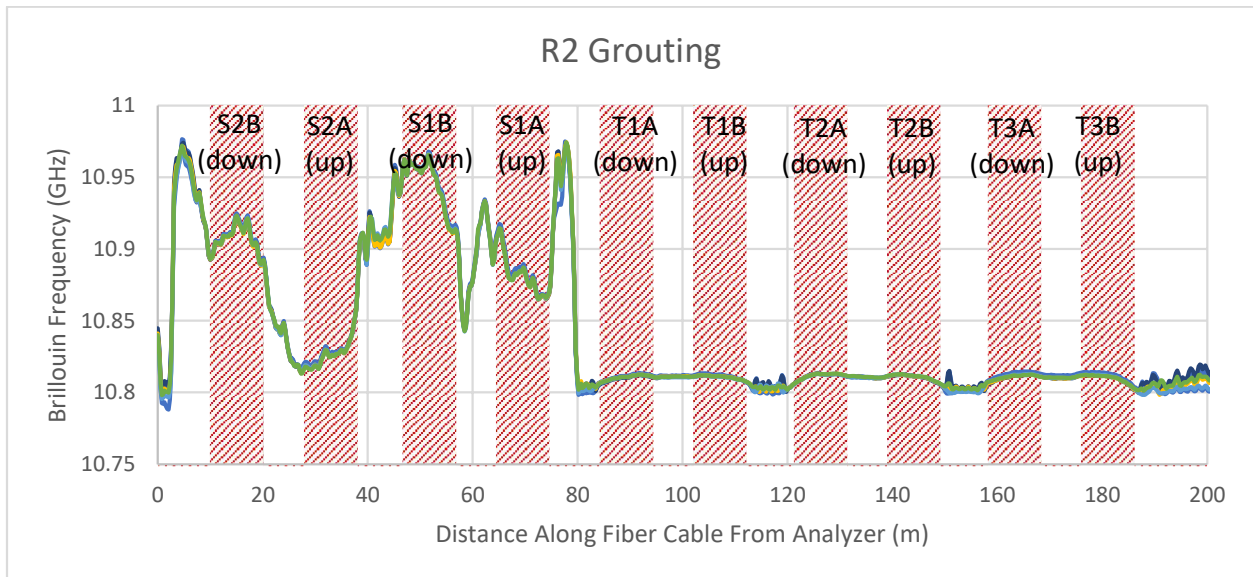
Figure 5-15: R2 grouting, raw Brillouin frequency

The measured vertical strains with time at a depth of 33.5 feet below the top of casing (TOC), approximately 1 pile diameter (5 feet) above the base, are presented in Figure 5-16. This figure shows a peak in vertical strain of approximately 45 με in compression on SB4 between 12:44 and 13:00, when the associated grouting pressure was rising between 200 and 350 psi. Once

85

grouting was ceased on the center circuit at 13:08, the average strain remained between 10 and 25 µε. The strains on SB1, which were shown as approximately 35 µε in tension shortly after the start of the water and grout flush, showed an increase of 25 µε in compression during the final grouting on the north circuit, potentially indicating that the grout injection at this point was still having an effect at the base of the pile. The final readings after the pressure was released show little immediate decay of the prior strains.
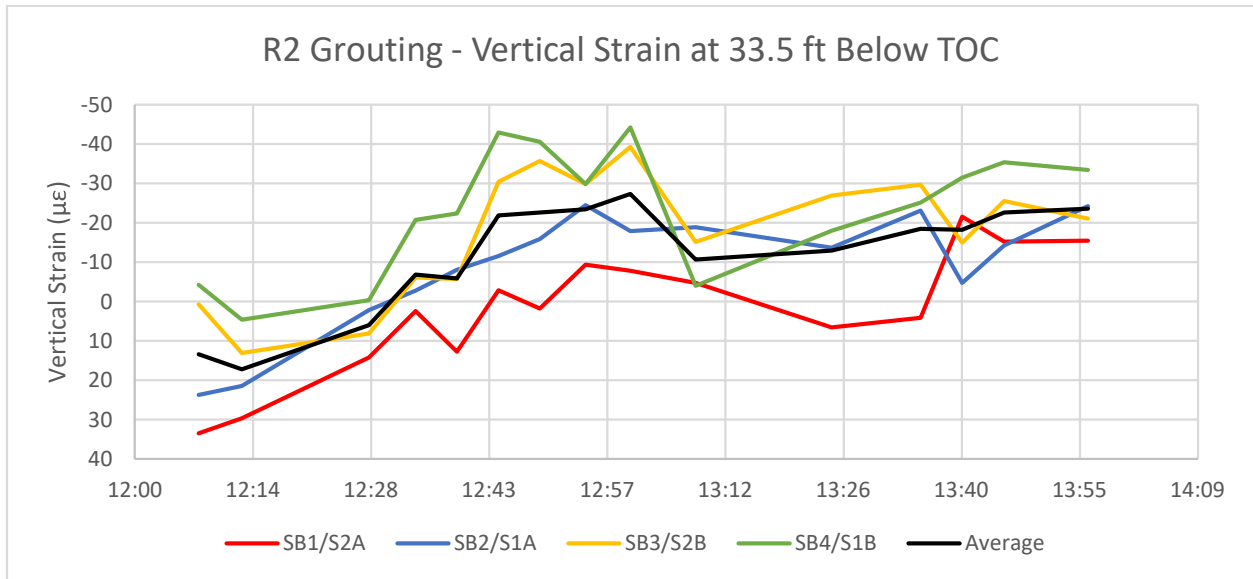
Figure 5-16: R2 grouting, vertical strains at 33.5 feet below TOC

Figure 5-17 through Figure 5-19 show the vertical strains with depth in the pile at 13:00 (~350 psi on center circuit), 13:40 (~350 psi on north circuit), and 13:56 (after pressure release). Figure 5-17 shows that the vertical strain at the bottom peak around 13:00 averaged 30 µε and extended up to 20 feet below TOC, except for SB3 which had 15 µε through to the TOC. Looking at the 13:00 plot of Figure 5-18, the average vertical strain in the pile has decreased to below 20 µε, with the spike on SB1 mentioned above extending less than 10 feet above the base of the pile. In Figure 5-19, 10 minutes after the grout pressure was released, the pile has a linear average strain with a peak value of approximately 25 µε, reducing to 0 by 5 feet below TOC. In all three figures, the strain profiles increase with depth, indicating the development of some negative friction during grouting. However, the strains reach their highest value early in the grouting on the first injection circuit, with lower strain values after switching to the other

circuits and after pressure release, indicating that the additional injections are not generating a proportional increase in load at the base of the pile. This may be due to blockage of the subsequent ports or migration of further grout injection away from the base of the pile.
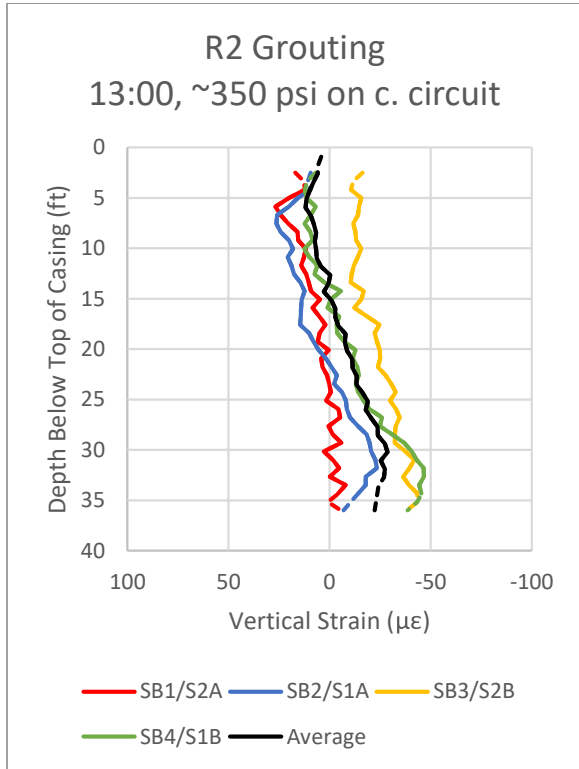
Figure 5-17: Vertical strain profile at 13:00 (~350 psi)
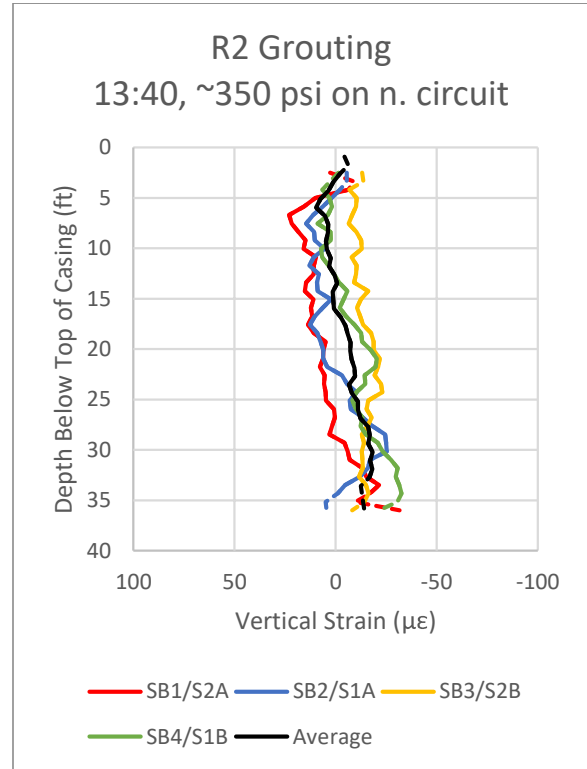


Figure 5-18: Vertical strain profile at 13:40 (~350 psi)
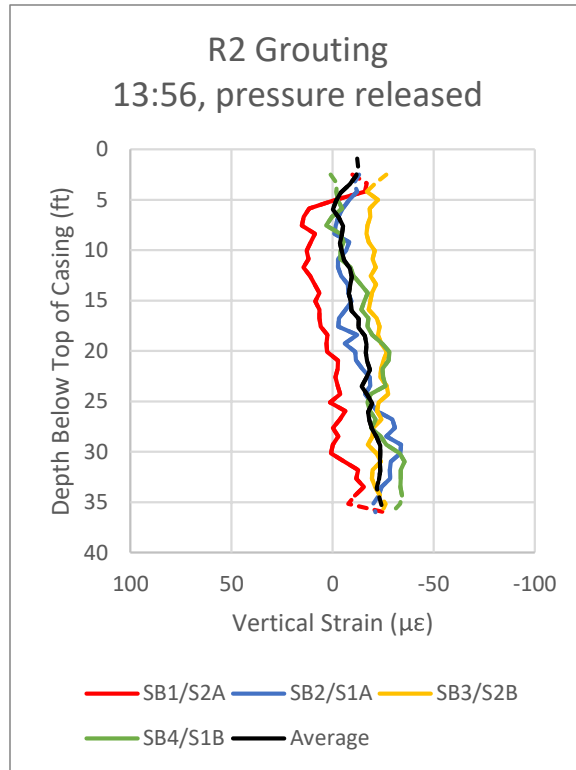
Figure 5-19: Vertical strain profile at 13:56 (after pressure release)

d) Reaction Shaft R4

Reaction Shaft R4 was grouted on February 6, 2019. Grouting was performed on three circuits, with the center circuit primed and grouted first. The grout data logger record of pressure and volume at the grout plant is presented in Figure 5-20. Grouting on the center circuit began at 14:05, with multiple starts and stops as leaks developed and pressure spikes were observed at the grout plant. The grout line was switched to the south circuit at 15:03 and continued until 15:42 with multiple pressure spikes at or above 1000 psi, at which point the grout line was switched to the north circuit. Grouting on the north circuit was performed from 15:56 to 16:09, at which point grouting was halted on the pile. The measured volumes are not adjusted for the initial flush or grout in the lines and therefore represent an upper bound of the volumes placed at the pile base.

Figure 5-20: R4 grouting, grout data logger record

The fiber optic record for shaft R4 is divided into 4 strain verticals and 2 temperature verticals. The raw frequency and segment divisions are shown in Figure 5-21.

Figure 5-21: R4 grouting, raw Brillouin frequency

The measured vertical strains with time at a depth of 33.5 feet below the top of casing (TOC), approximately 1 pile diameter (5 feet) above the base, are presented in Figure 5-22. The figure shows an initial increase in average vertical strain of approximately 20 με in compression at 14:31 and 14:43, when the associated grouting pressure was approximately 295 psi. The next

major strain spike is observed at 15:23, after pumping had switched to the south circuit with a pressure dropping sharply from 900 psi to 150 psi. At this time water was noted returning from HB2 (not connected to any of the grout circuits). Although this spike was observed on all strain verticals, SB2 and SB3 were observed to be in slight tension while SB 1 and SB4 were observed in compression, implying that there was non-uniform loading at the base of the pile. The strains roughly plateaued during pumping on the north circuit. However, they showed a sharp increase of an average of 22 µε in compression approximately 30 minutes after the stop of pumping. It is unclear to what this rise in strain is attributed to.

Figure 5-22: R4 grouting, vertical strains at 33.5 feet below TOC

Figure 5-23 through Figure 5-25 show the vertical strains with depth in the pile at 14:31 (~120 psi on center circuit), 15:23 (~150 psi on south circuit), and 16:43 (after pressure release). Figure 5-23 shows that there was moderate vertical strain development during pumping on the center circuit, with average strains of less than 20 µε and peaks on SB1 not exceeding 30 µε. In Figure 5-22, after the large pressure drop on the south circuit, large strains exceeding 50 µε have developed between 10 and 20 feet below TOC on SB1. Looking closer at the data, the strain increase in this area was roughly linear during pumping, implying that the grouting is affecting this zone within the pile. In Figure 5-23, after grouting has ceased, the residual strains

in the bottom portion of the pile are below 50 µε with the shallow compression on SB1 in excess of 70 µε.

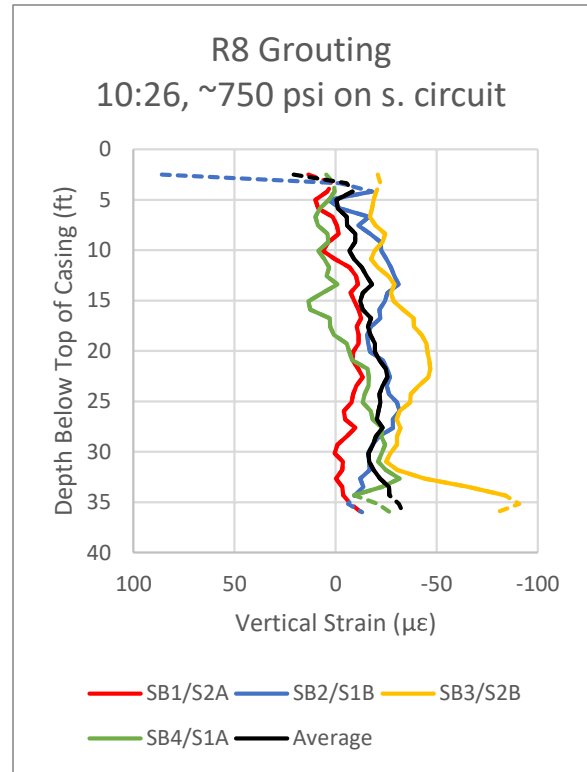Figure 5-23: Vertical strain profile at 14:31 (~120 psi)

Figure 5-24: Vertical strain profile at 15:23 (~150 psi)
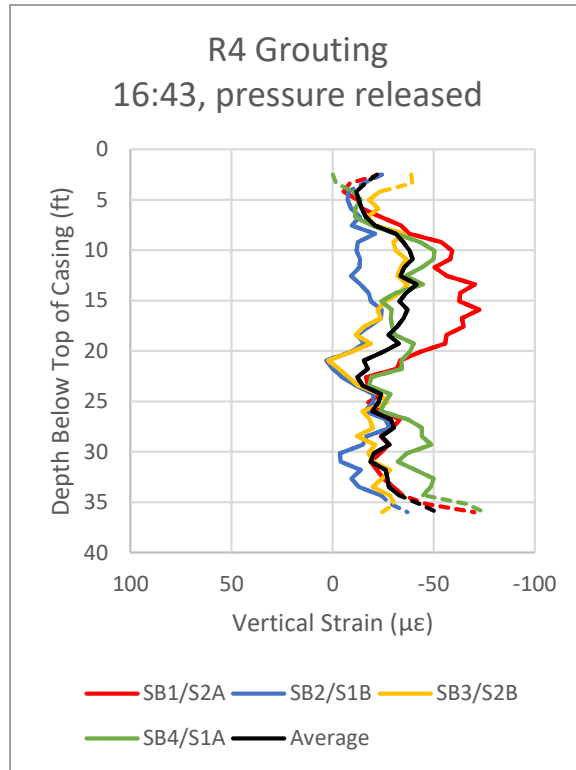
Figure 5-25: Vertical strain profile at 16:43 (after pressure release)

e) Reaction Shaft R6

Reaction Shaft R6 was grouted on February 8, 2019. The grout data logger record of pressure and volume at the grout plant is presented in Figure 5-26. Grouting was performed on three circuits, with the center circuit primed and grouted first. Grouting on the center circuit began at 9:01 and continued through 9:59. The grout line was switched to the south circuit at 9:59 and continued until 10:35, at which point the grout line was switched to the north circuit. Grouting on the north circuit was performed from 10:46 to 10:51, at which point grouting was halted on the pile. The measured volumes are not adjusted for the initial flush or grout in the lines and therefore represent an upper bound of the volumes placed at the pile base.
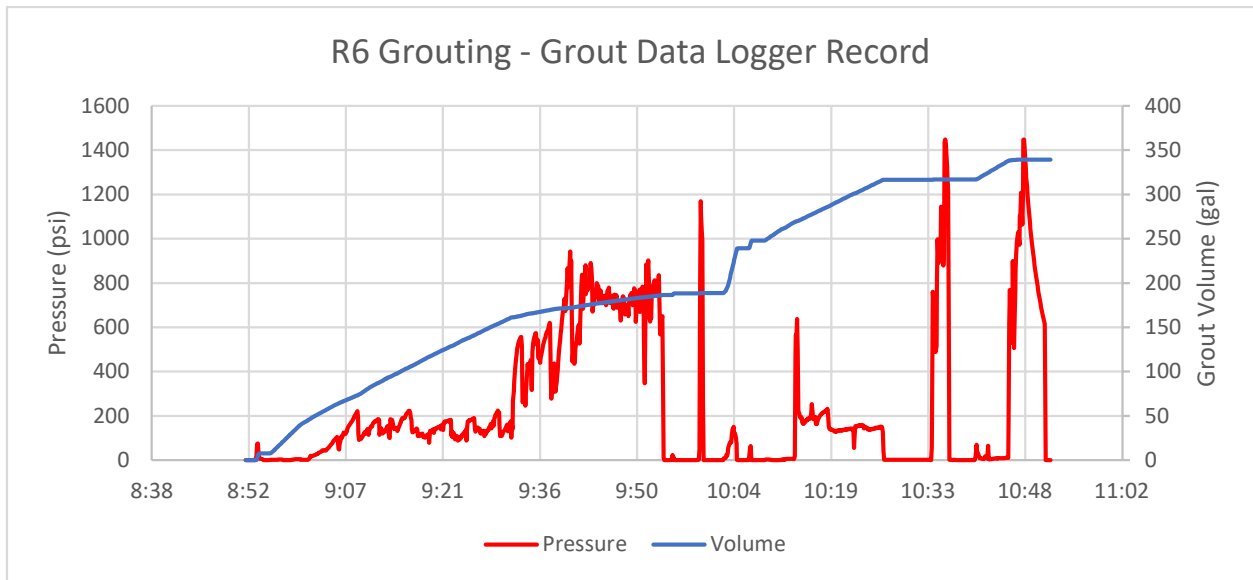
Figure 5-26: R6 grouting, grout data logger record

The fiber optic record for shaft R6 is divided into 4 strain verticals and 2 temperature verticals. The raw frequency and segment divisions are shown in Figure 5-27.
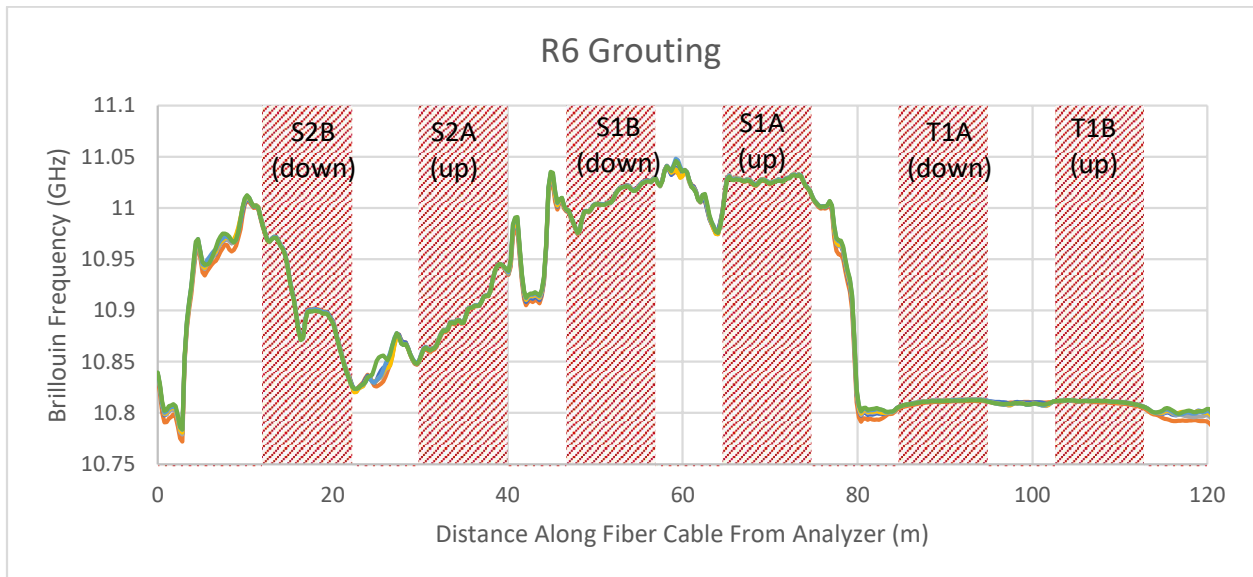
Figure 5-27: R6 grouting, raw Brillouin frequency

The measured vertical strains with time at a depth of 33.5 feet below the top of casing (TOC), approximately 1 pile diameter (5 feet) above the base, are presented in Figure 5-28. This figure shows an initial increase in the vertical strain to approximately 50 με in compression at 9:35 on SB4, when the associated grouting pressure was approximately 475 psi. Compressive strains on

SB4 increased again at 10:15, immediately after pumping had switched to the south circuit. Strains in SB1 and SB3 were generally consistent with those on SB4 during this time, with strains on SB2 remaining at or just below 0 µε. A major drop in compressive strain was observed at 11:00 on all 4 verticals immediately following the venting of all circuit valves on the pile after the conclusion of grouting. These strains rebounded somewhat in further readings, with a final measured average strain in the pile of 20 µε, +/- 20 µε at 11:22.
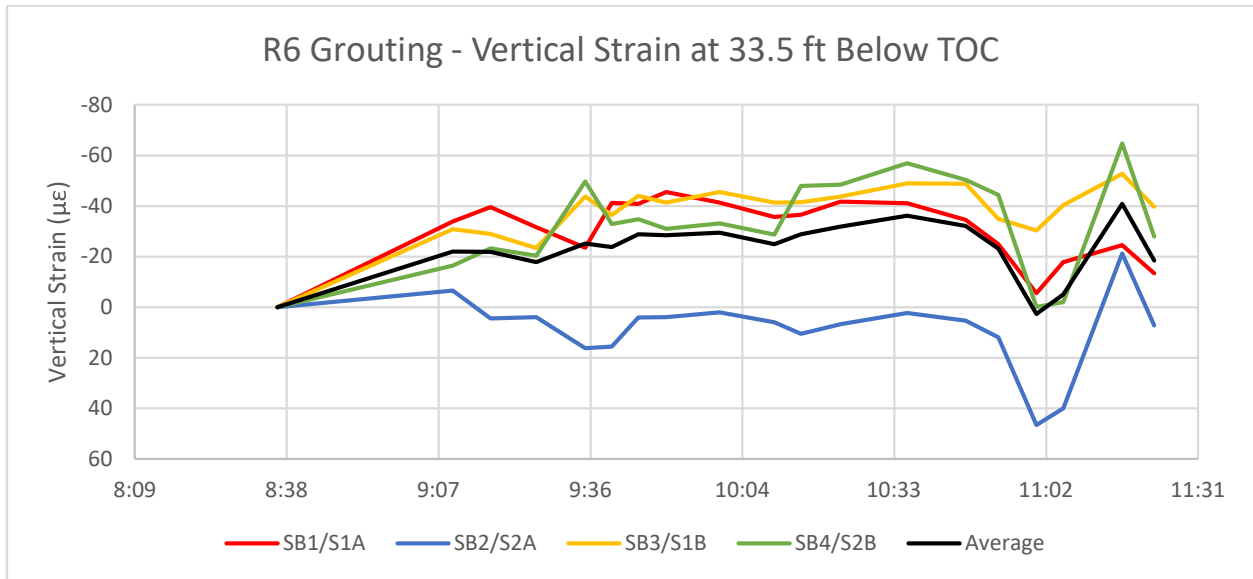
Figure 5-28: R6 grouting, vertical strains at 33.5 feet below TOC

Figure 5-29 through Figure 5-31 show the vertical strains with depth in the pile at 9:35 (~475 psi on center circuit), 10:36 (~1200 psi on south circuit), and 11:22 (after pressure release). Figure 5-29 shows vertical strain development on SB4 during pumping on the center circuit, with compressive strain of 50 µε above the base of the pile roughly constant to 18 feet below TOC. SB3 showed approximately half the corresponding strain, with SB1 and SB2 showing approximately 0 strain. In Figure 5-30, by 10:36, the compressive strain on SB4 remain just above 50 µε above the base with strains increasing on all other verticals with the exception of SB2. In Figure 5-31, after grouting was halted and the pressure in the circuits was released, SB3 and SB4 maintained approximately 37 µε above the base with compressive strains extending upward into the pile to a depth of 20 feet below TOC. The wide variation in compressive strains suggests that the grouting pressures at the base may have been uneven, resulting in bending

development in the lower 20 feet of the pile. After the pressure release, the strain differential decreases to a spread of less than 45 µɛ, as compared to a previous peak differential of approximately 75 µɛ during grouting.
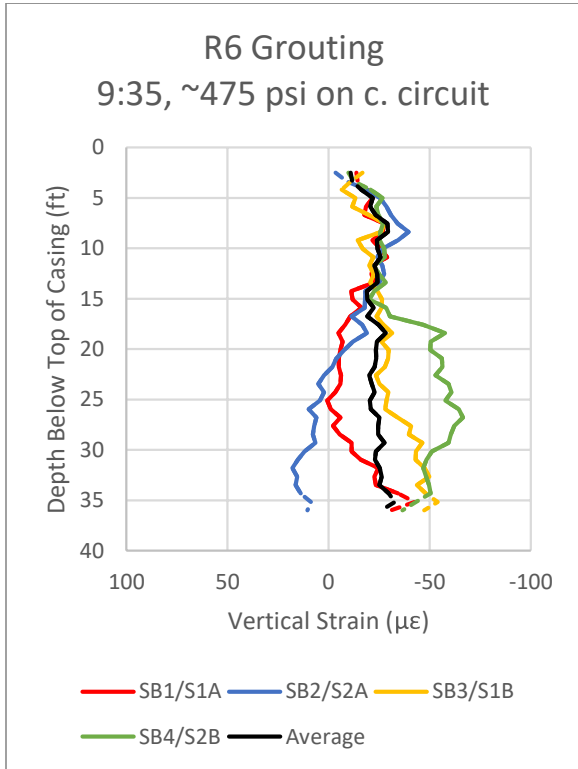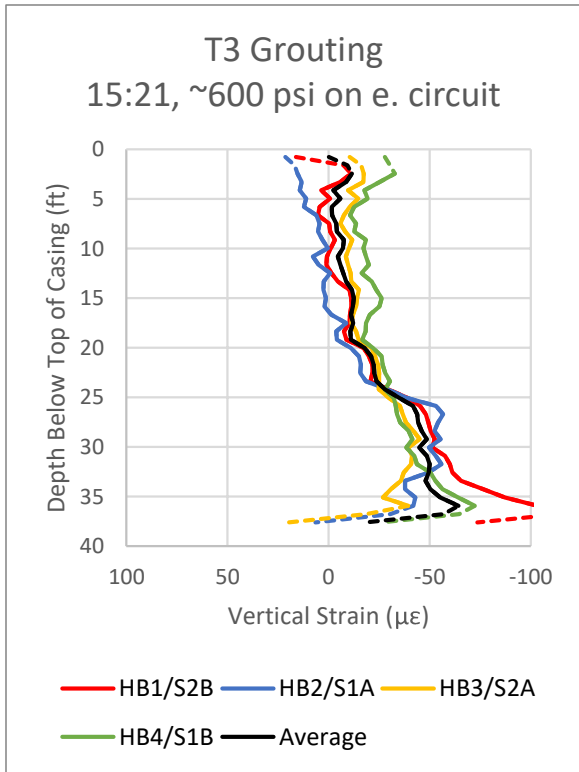

Figure 5-29: Vertical strain profile at 9:35 (~475 psi)
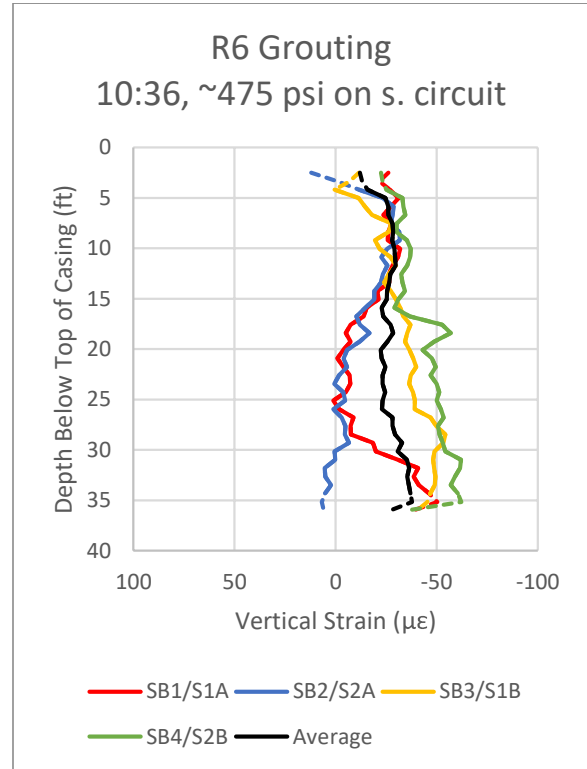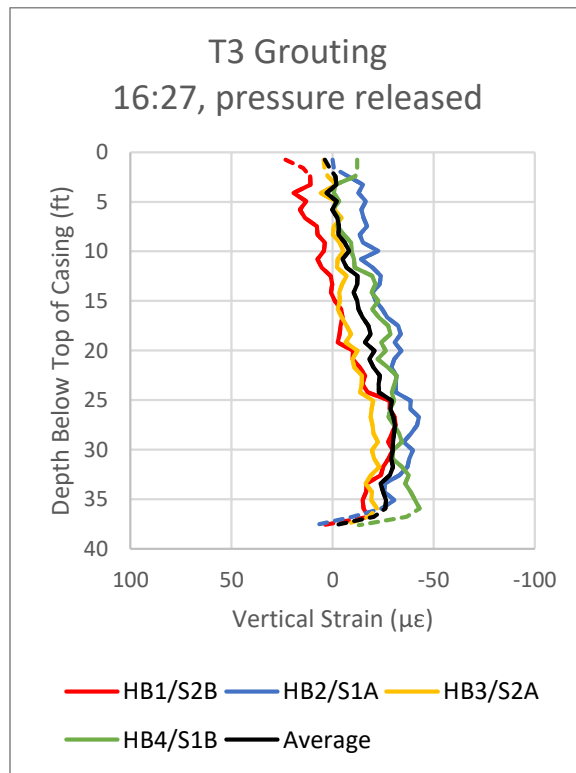

Figure 5-30: Vertical strain profile at 10:36 (~475 psi)
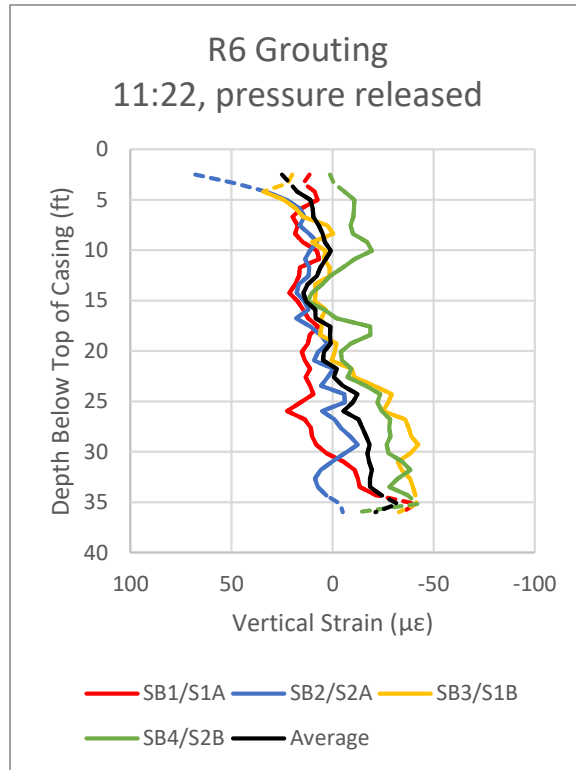
Figure 5-31: Vertical strain profile at 11:22 (after pressure release)

f) Reaction Shaft R8

Reaction Shaft R8 was grouted on February 7, 2019. The grout data logger record of pressure and volume at the grout plant is presented in Figure 5-32. Grouting was performed on three circuits, with the center circuit primed and grouted first. Grouting on the center circuit with the return valve closed was performed from 9:21 to 10:05. The grout line was switched to the south circuit and was grouted from 10:17 through 10:28. The grout line was then switched to the north circuit, which was grouted from 10:43 to 10:49, after which grouting was concluded. The measured volumes are not adjusted for the initial flush or grout in the lines and therefore represent an upper bound of the volumes placed at the pile base.
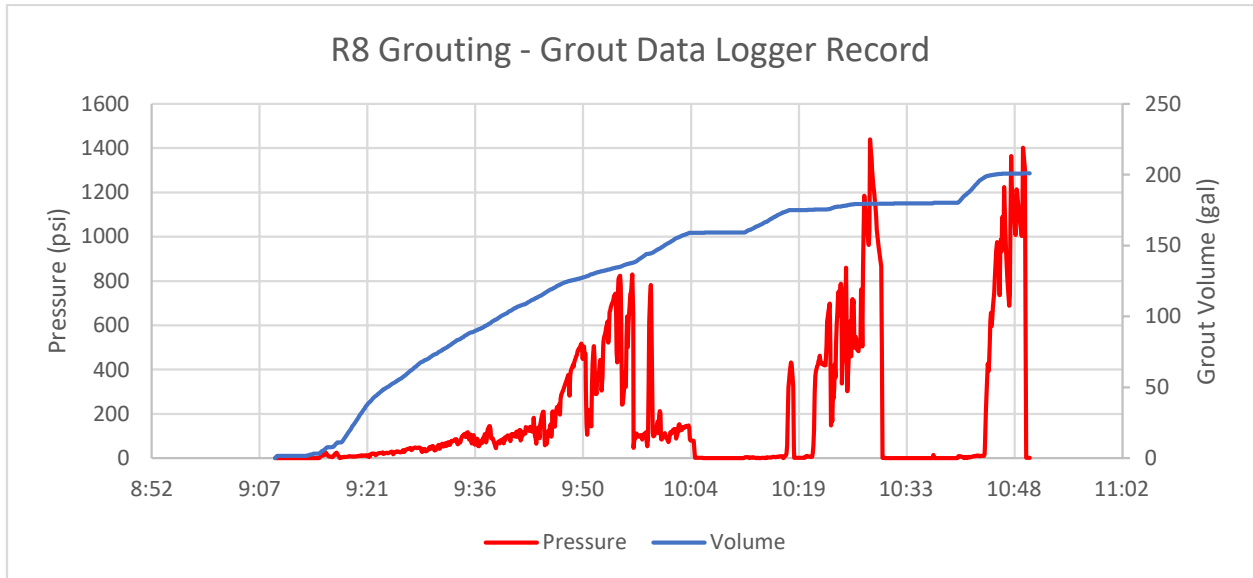
Figure 5-32: R8 grouting, grout data logger record

The fiber optic record for shaft R8 is divided into 4 strain verticals and 2 temperature verticals. The raw frequency and segment divisions are shown in Figure 5-33.
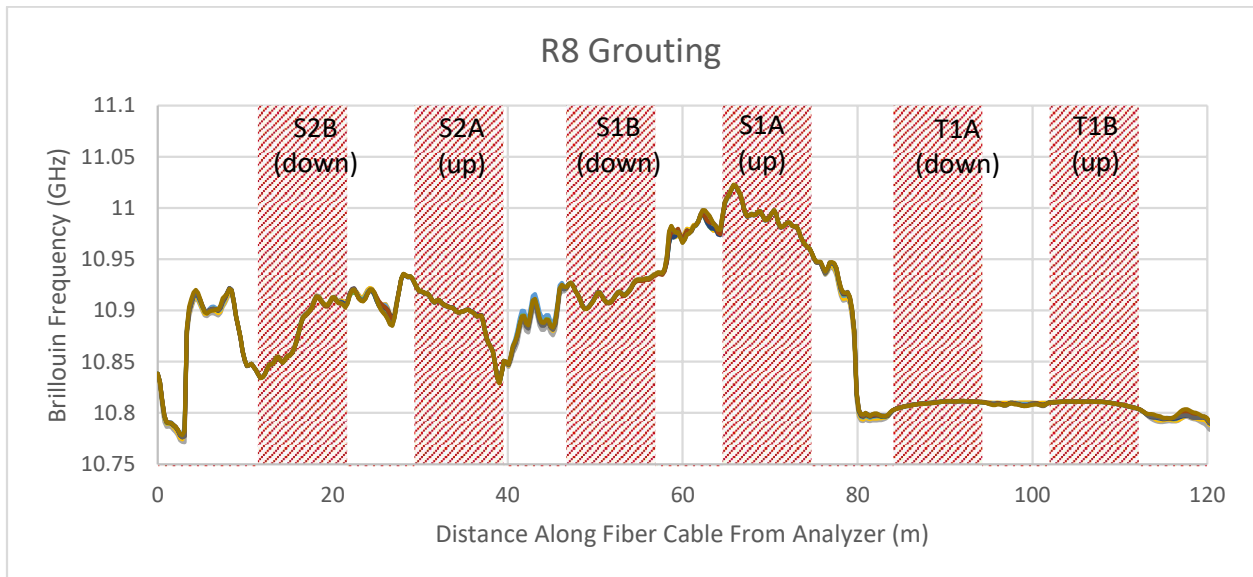
Figure 5-33: R8 grouting, raw Brillouin frequency

The measured vertical strains with time at a depth of 33.5 feet below the top of casing (TOC), approximately 1 pile diameter (5 feet) above the base, are presented in Figure 5-34. The figure shows an initial peak in vertical compressive strain of approximately 60 με at 9:54 on SB3, when the associated grouting pressure had dropped from 750 psi to 300 psi on the center circuit.

Strains on SB3 continued to be the highest of the four verticals, peaking at 65 με at 10:26 with a pressure of 750 psi on the south circuit, just prior to switching to the north circuit. The strains in the other three verticals remained relatively constant through grouting with variations within +/- 20 με of 0.
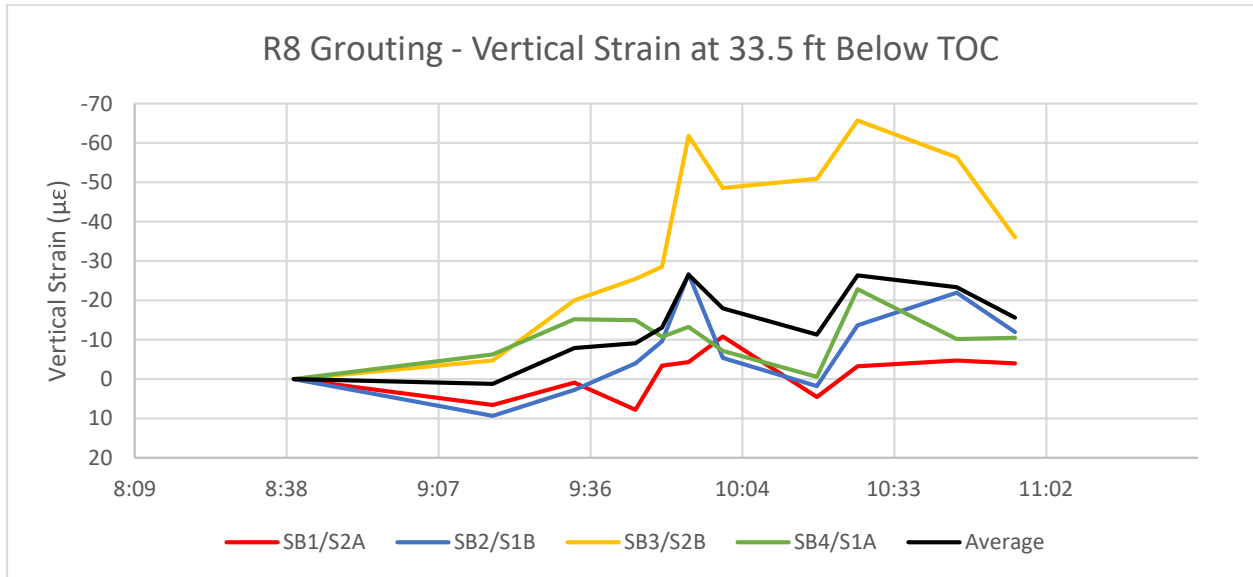
Figure 5-34: R8 grouting, vertical strains at 33.5 feet below TOC

Figure 5-35 through Figure 5-37 show the vertical strains with depth in the pile at 9:54 (~300 psi on center circuit), 10:26 (~750 psi on south circuit), and 10:56 (after pressure release). Figure 5-35 shows an "s" curve of compressive strain developing in SB3, with compressive strain of 70 με above the base of the pile decreasing to 30 με at 30 feet below TOC before increasing again to just below 50 με at 20 feet below TOC. The next Figure 5-36 shows the compressive strain in SB3 above the bottom of the pile further increasing to 84 με, with the strains in the other three verticals remaining below 25 με. In Figure 5-37, by the final reading at 10:26, much of the strain in the bottom of the pile had been lost; however, a strong strain differential of approximately +/- 40 με had developed in the top 15 feet of the pile. It is not clear from site observations what introduced this wide differential at the conclusion of grouting. The initial linear strain along the pile in Figure 5-35 implies that some negative skin friction was developed early on in the pile grouting. However, this trend did not clearly persist through the end of grouting and pressure release.
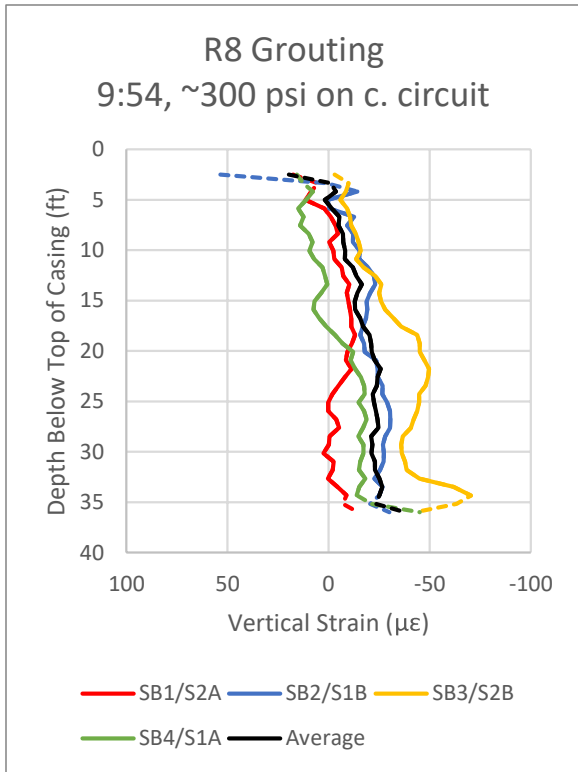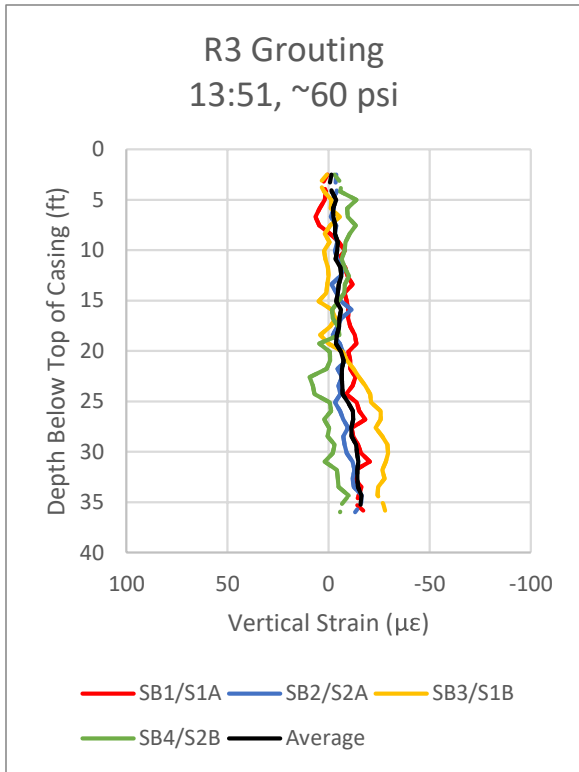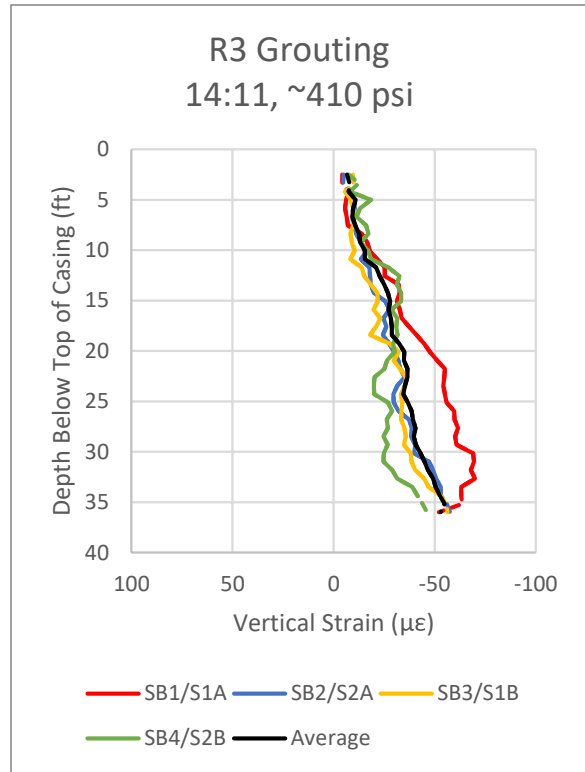
Figure 5-35: Vertical strain profile at 9:54 (~300 psi)

Figure 5-36: Vertical strain profile at 10:26 (~750 psi)
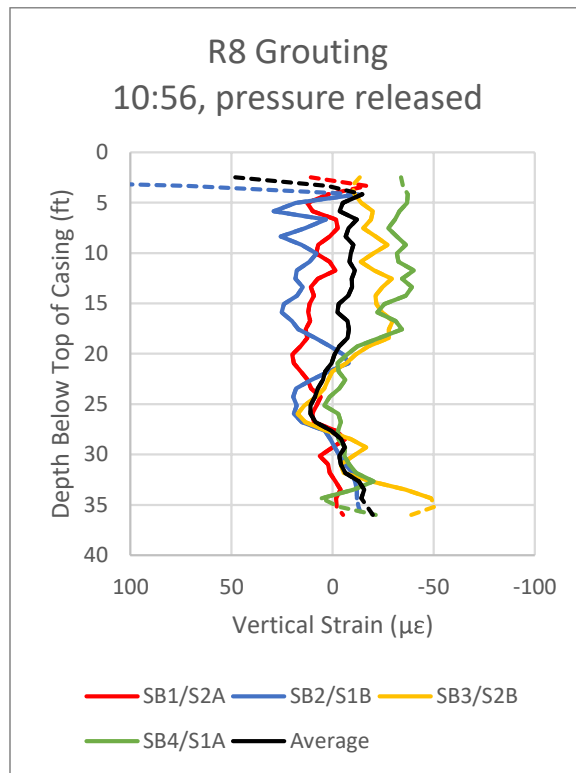
Figure 5-37: Vertical strain profile at 10:56 (after pressure release)

Test Shaft T3 was grouted on February 7, 2019. The grout data logger record of pressure and volume at the grout plant is presented in Figure 5-38. Grouting was performed on two circuits, with the east circuit primed and grouted first. Grouting on the east circuit with the return valve closed was performed from 15:09 to 15:30. The grout line was switched to the northwest circuit and was grouted from 15:45 through 15:51, at which point grouting was halted. The measured volumes are not adjusted for the initial flush or grout in the lines and therefore represent an upper bound of the volumes placed at the pile base.
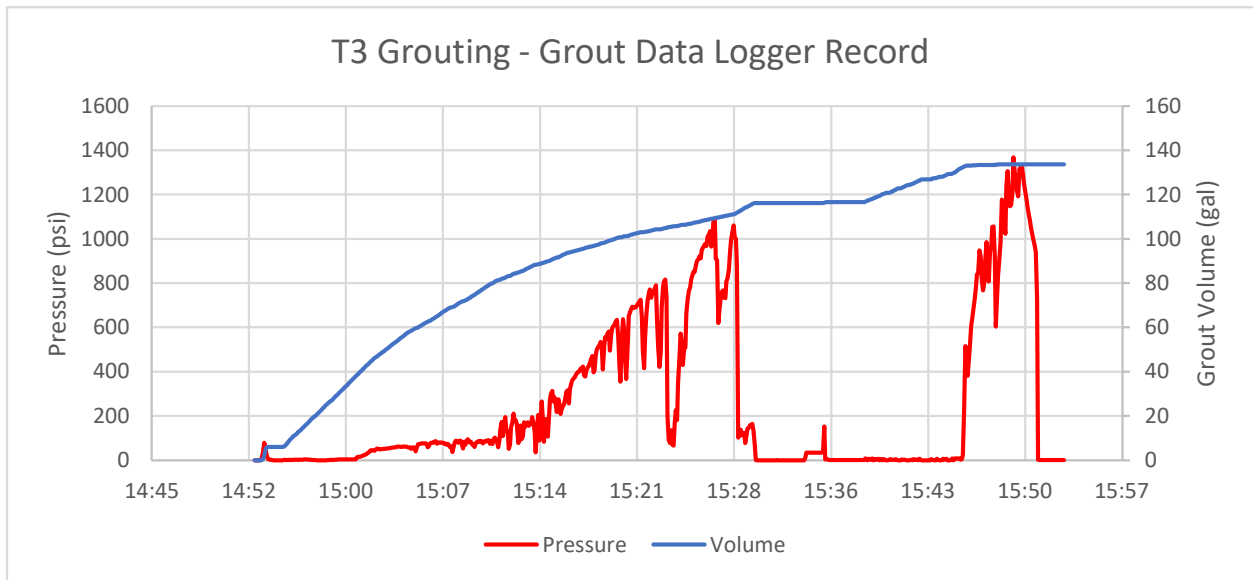
Figure 5-38:: T3 grouting, grout data logger record

The fiber optic record for shaft R3 is divided into 4 strain verticals and 2 temperature verticals. The raw frequency and segment divisions are shown in Figure 5-39.
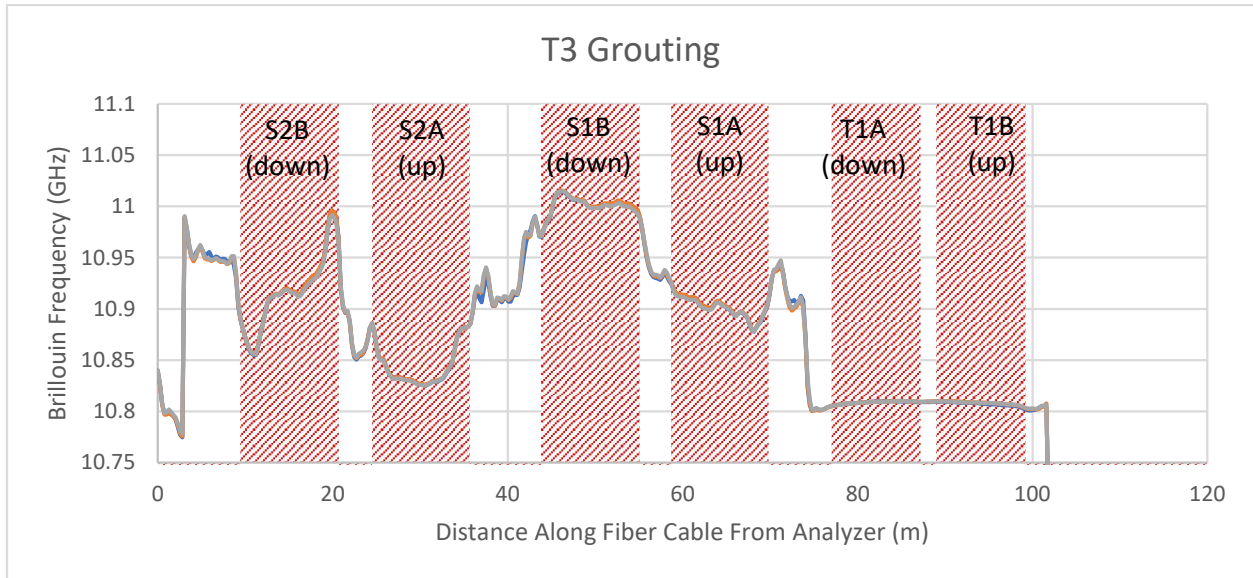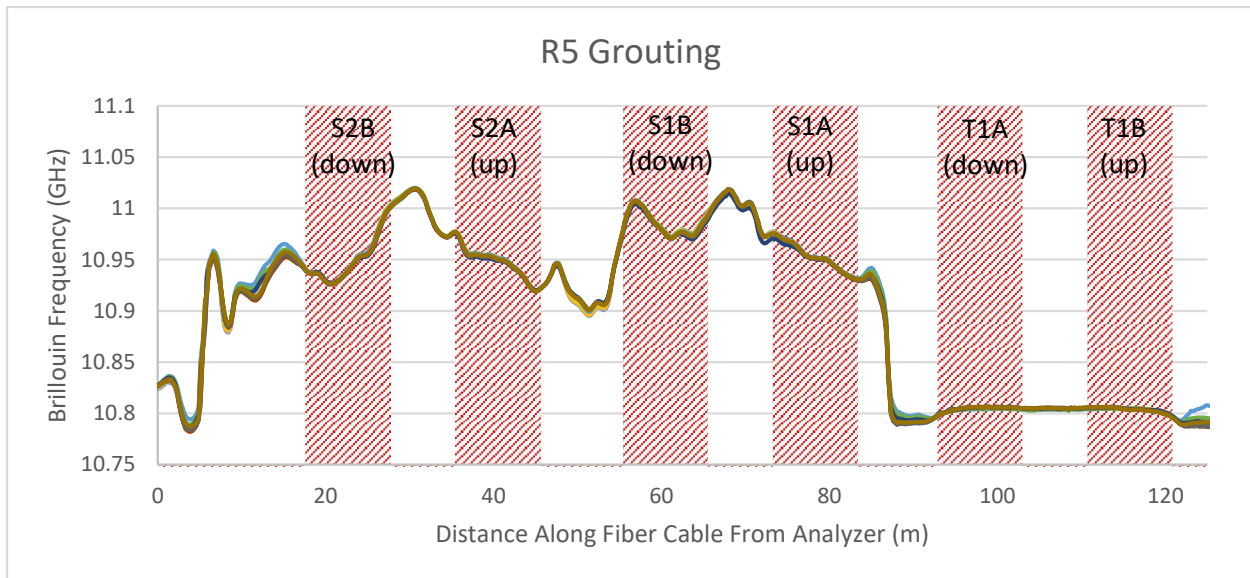
Figure 5-39: T3 grouting, raw Brillouin frequency

The measured vertical strains with time at a depth of 34.4 feet below the top of casing (TOC) are presented in Figure 5-40. The figure shows an initial peak in compressive vertical strain of approximately 87 με at 15:21 on HB1, when the associated grouting pressure was 600 psi on the east circuit. Strains on HB3 rose to 50 με at 15:47 with a pressure of 900-100 psi on the northwest circuit, just prior to halting grouting. The strains in all four verticals dropped immediately after the pressure release at 15:53, rebounding sharply before settling at an average of just below 30 με in compression at 16:27.
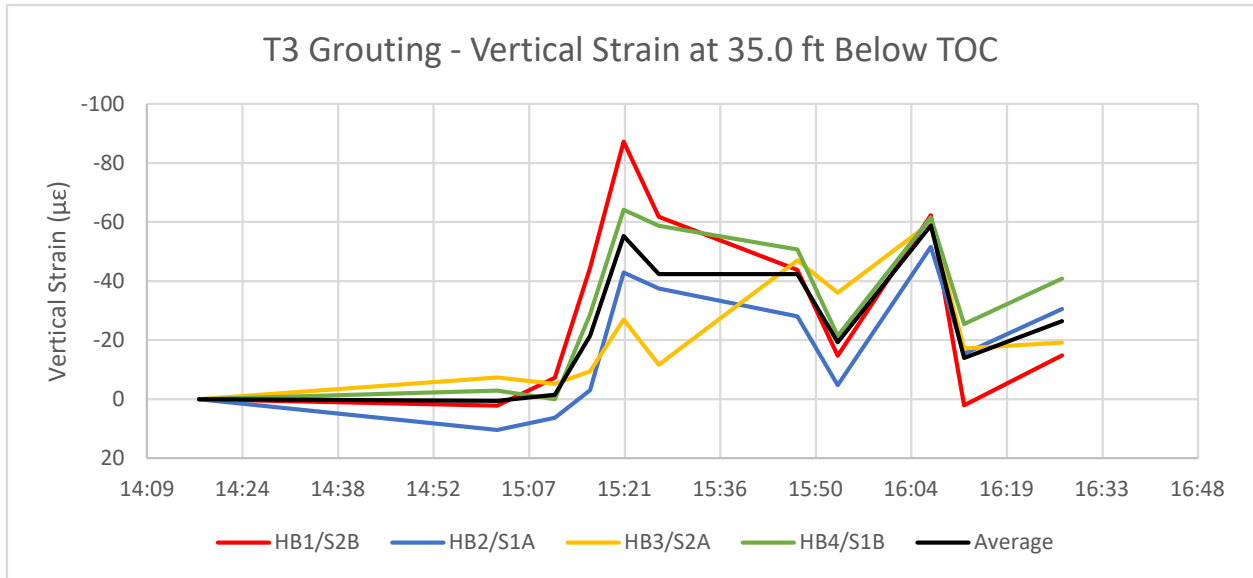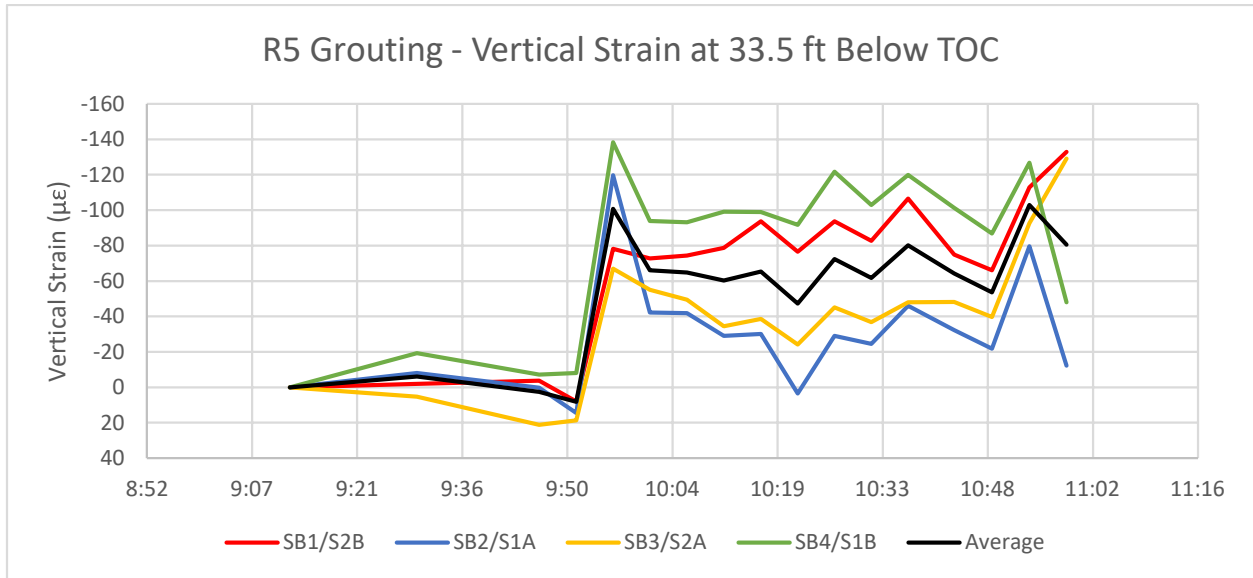
Figure 5-40: T3 grouting, vertical strains at 35.0 feet below TOC

Figure 5-41 through Figure 5-43 show the vertical strains with depth in the pile at 15:21 (~600 psi on east circuit), 15:47 (~950 psi on northwest circuit), and 16:27 (after pressure release). Figure 5-41 shows a high peak of compressive strain on HB1, with compressive strain of 114 με above the base of the pile decreasing to 0 με at 10 feet below. The other three verticals all show strains centered around 50 με. In Figure 5-42, by the time grouting had switched to the northwest circuit at 15:47, the strains at the base of the pile had decreased to at or below 50 με. In Figure 5-43, after the pressure in the grouting circuits was released, an average strain of 26 με remained above the base, extending at a constant to approximately 25 feet below TOC before fading linearly to 5 feet below TOC. In all three figures, the strain profiles increase with depth, indicating the development of some negative friction during grouting. As with earlier piles, the compressive strains at the base of the pile develop their highest values early in the grouting process and drop as grouting continues and pressure is ultimately released.
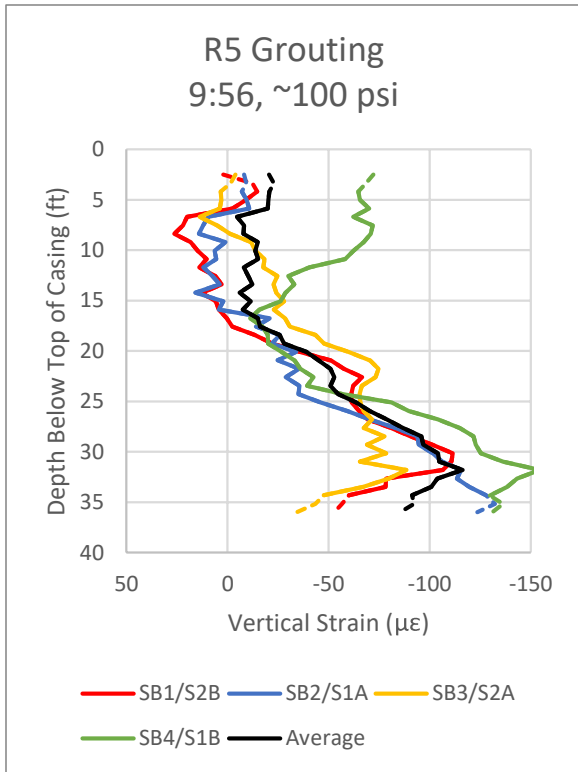
Figure 5-41: Vertical strain profile at 15:21 (~600 psi)
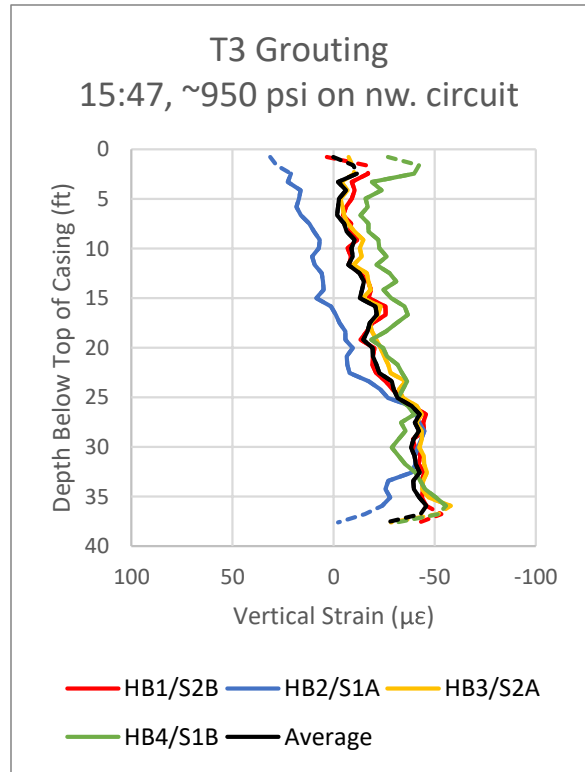
Figure 5-42: Vertical strain profile at 15:47 (~950 psi)

Figure 5-43: Vertical strain profile at 16:27 (after pressure release)

103

Closed-Type (bladder)

h) Reaction Shaft R3

Reaction Shaft R3 was grouted on February 4, 2019. The grout data logger record of pressure and volume at the grout plant is presented in Figure 5-44. All grouting was performed through a single line (of four). Connectivity between all lines was established prior to priming the system with grout. After closing the three remaining valves, grouting of the pile began at 13:44. Grouting continued until 14:15 with a peak pressure of 410 psi, after which grouting was concluded and the valve was closed. The measured volumes are not adjusted for the initial flush or grout in the lines and therefore represent an upper bound of the volumes placed at the pile base.
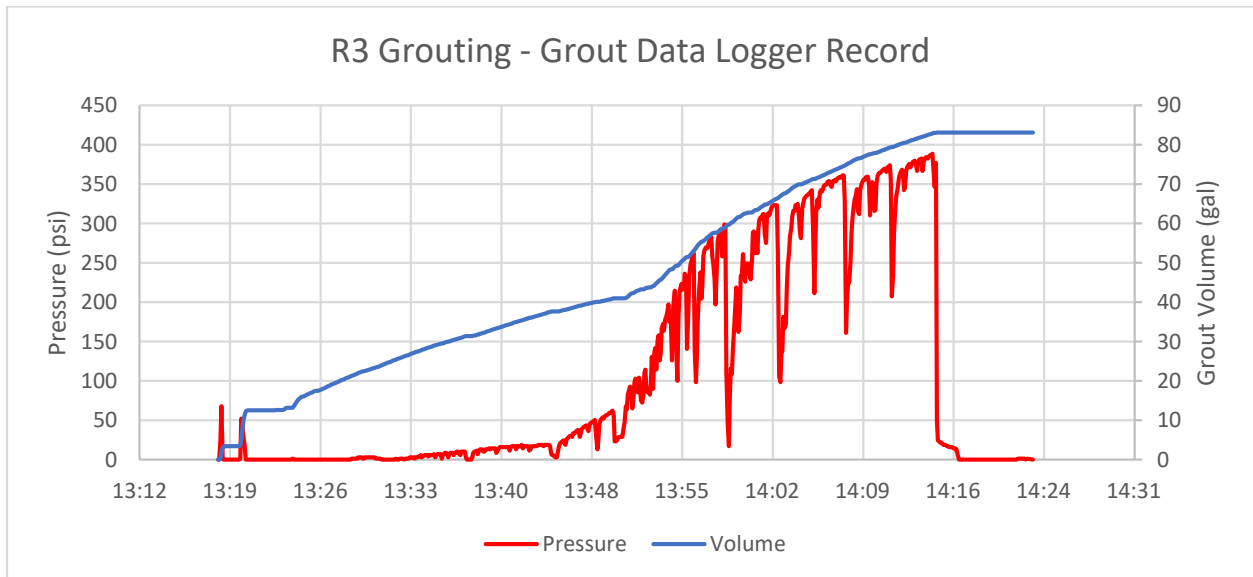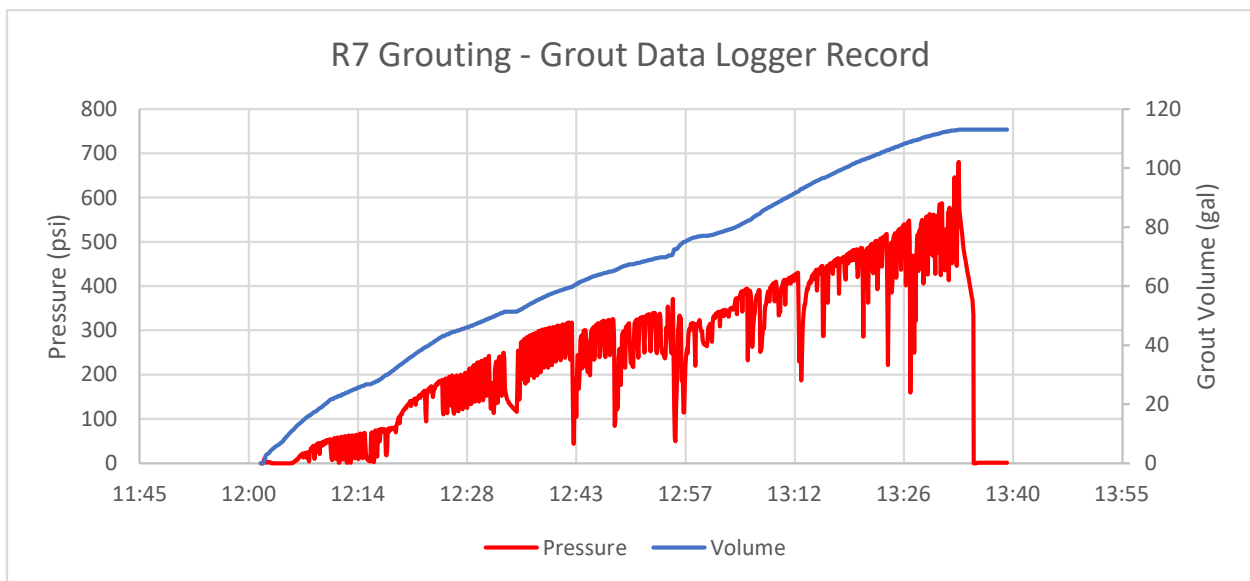

Figure 5-44: R3 grouting, grout data logger record

The fiber optic record for shaft R3 is divided into 4 strain verticals and 6 temperature verticals. The raw frequency and segment divisions are shown in Figure 5-45.
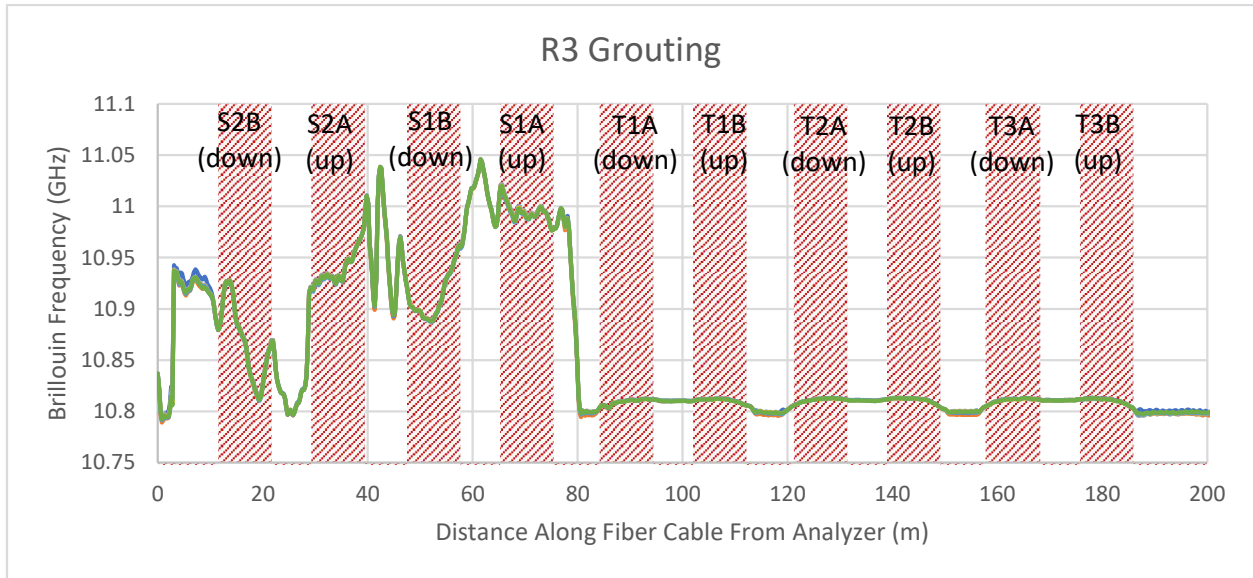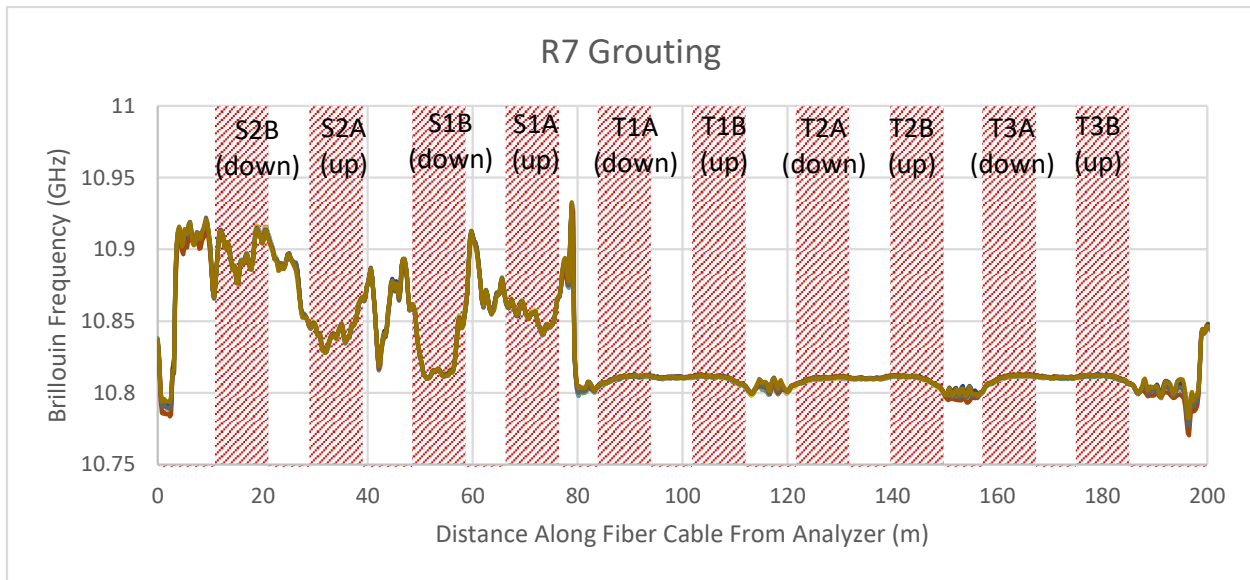
Figure 5-45: R3 grouting, raw Brillouin frequency

The measured vertical strains with time at a depth of 33.5 feet below the top of casing (TOC), approximately 1 pile diameter (5 feet) above the base, are presented in Figure 5-46. This figure shows a steady increase in vertical strain on all four verticals from the start of circuit priming at 13:22 through the highest pressure of 410 psi at 14:11. A peak strain of 63 $\mu\varepsilon$ was recorded on SB1. Once grouting was ceased at 14:15, all four verticals show a strain drop of 20-30 $\mu\varepsilon$, with the final measured compressive strains at 14:33 between 30 and 40 $\mu\varepsilon$. The strain behavior of the four verticals were similar throughout the monitoring period, indicating that the strains during grouting were roughly evenly distributed across the base of the pile.
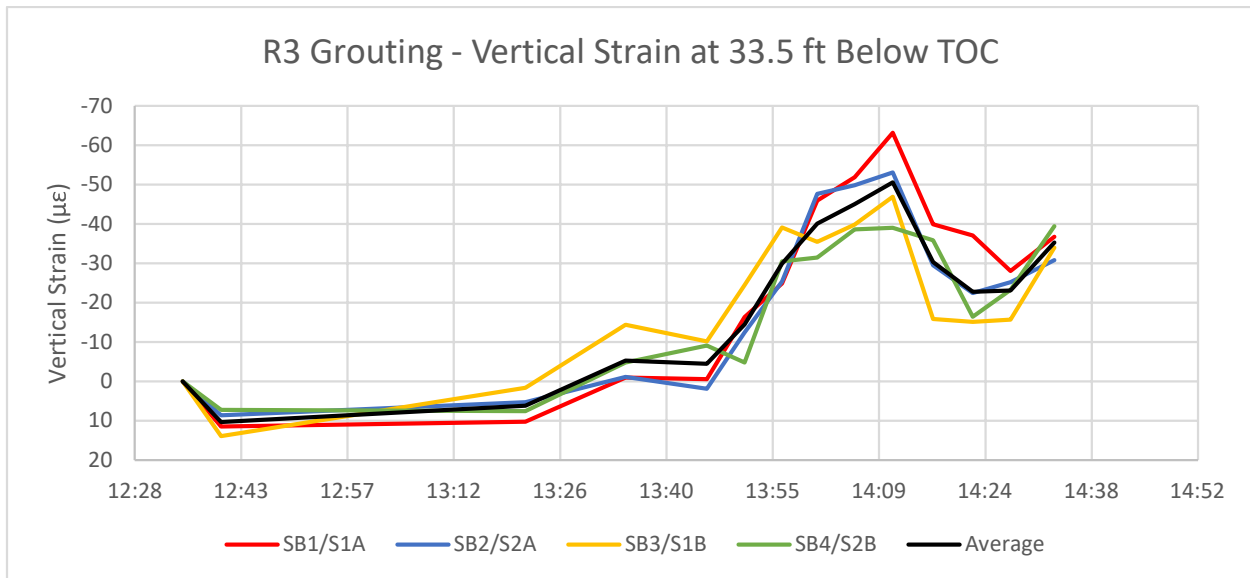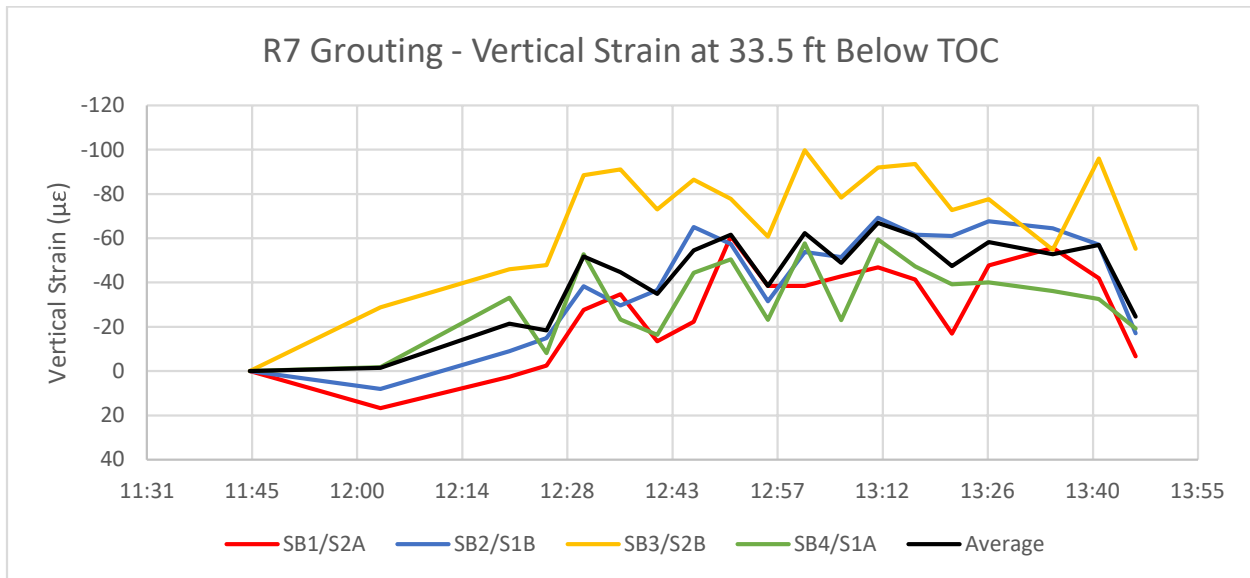
Figure 5-46: R3 grouting, vertical strains at 33.5 feet below TOC

Figure 5-47 through Figure 5-49 show the vertical strains with depth in the pile at 13:51 (~60 psi), 14:11 (~410 psi), and 14:33 (after pressure release). Figure 5-47 shows strain building on SB3 almost immediately after the start of grouting with a peak of 30 $\mu\varepsilon$ in compression at 30 feet below TOC. In Figure 5-48, at the fiber optic reading with the highest pressure at 14:11, SB1 has a peak strain of 69 $\mu\varepsilon$ at 30 feet below TOC. The other three verticals have peak compressive strains of approximately 50 $\mu\varepsilon$, with all 4 verticals having strain linearly decaying through the top of the pile. In Figure 5-49, after the pressure has been released, all of the verticals fall to below 50 $\mu\varepsilon$. SB2 shows the most dramatic drop in compression, dropping to 0 strain at 25 feet below TOC with the top 15 feet in slight tension. The remaining three verticals maintain a roughly linear strain distribution from 0 at the top of the pile to 35-45 $\mu\varepsilon$ just above the bottom of the pile. This indicates that a portion of negative skin friction developed during grouting is still present after the release of pressure.

Figure 5-47: Vertical strain profile at 13:51 (~60 psi)

Figure 5-48: Vertical strain profile at 14:11 (~410 psi)
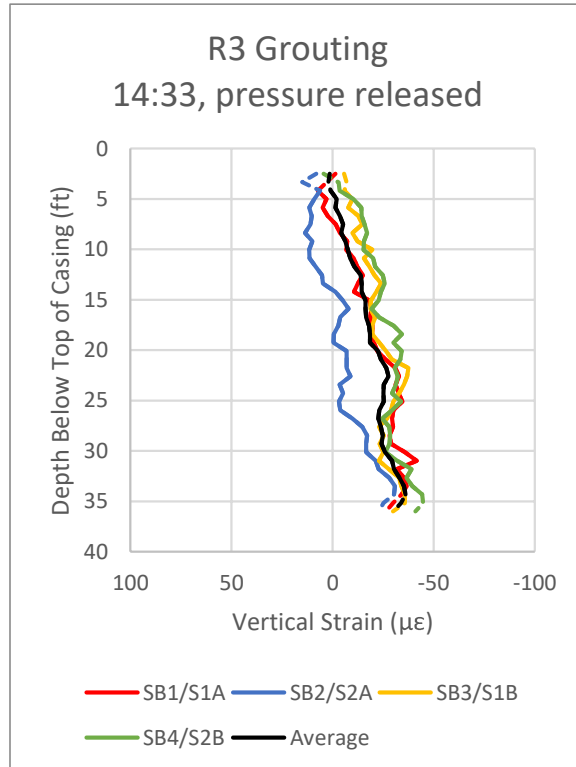
Figure 5-49: Vertical strain profile at 14:33 (after pressure release)

i) Reaction Shaft R5

Reaction Shaft R5 was grouted on February 5, 2019. The grout data logger record of pressure and volume at the grout plant is presented in Figure 5-50. All grouting was performed through a single line (of 4). Once grout return was established at the surface, all return valves were closed at 9:45 and grouting of the pile began. Grouting continued until 10:42 with an associated pressure of 410 psi, at which point the grout line was locked off and grouting was concluded. The measured volumes are not adjusted for the initial flush or grout in the lines and therefore represent an upper bound of the volumes placed at the pile base.
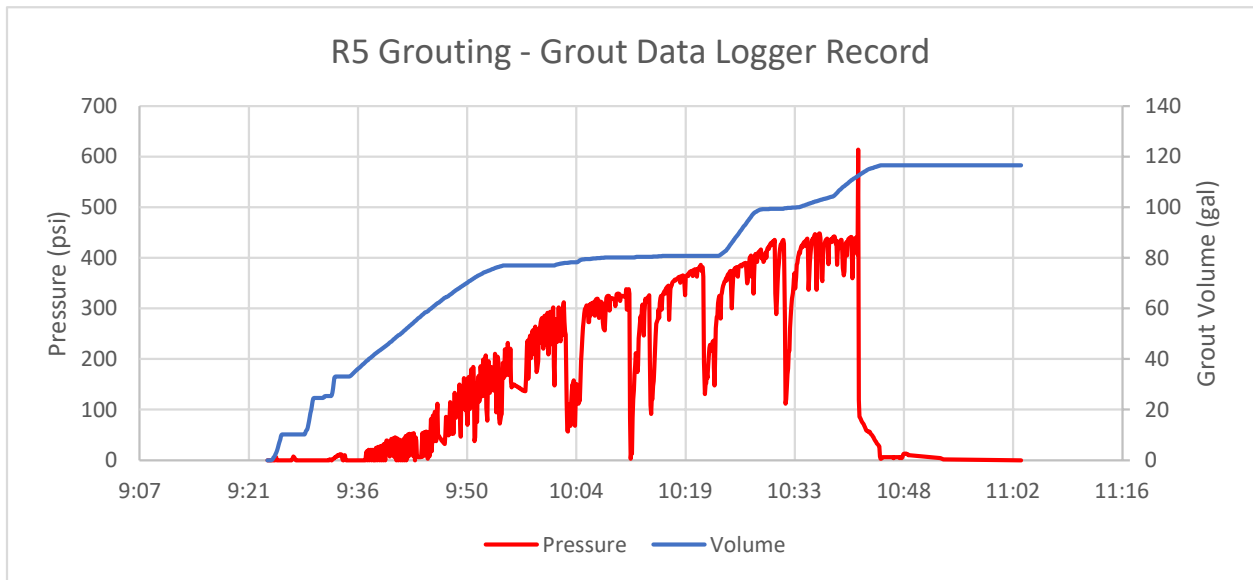
Figure 5-50: R5 grouting, grout data logger record

The fiber optic record for shaft R5 is divided into 4 strain verticals and 2 temperature verticals. The raw frequency and segment divisions are shown in Figure 5-51.

Figure 5-51: R5 grouting, raw Brillouin frequency

The measured vertical strains with time at a depth of 33.5 feet below the top of casing (TOC), approximately 1 pile diameter (5 feet) above the base, are presented in Figure 5-52. The figure shows a large increase in vertical compressive strain between 9:51 and 9:56, the second and third readings after the start of grouting at 9:45 with an associated pressure of 50 to 100 psi. After this initial rise, the strains drop to an average just above 60 με and stay roughly constant through the end of grouting at 10:42. At 10:53, just after the grout line was disconnected, all four verticals show a jump in strain of approximately 20 με. For the final read at 10:58, SB2 and SB4 show a strain decrease while SB1 and SB3 show a small strain increase with a final average strain of 80 με.

Figure 5-52: R5 grouting, vertical strains at 33.5 feet below TOC

Figure 5-53 through Figure 5-55 show the vertical strains with depth in the pile at 9:56 (~100 psi), 10:37 (~410 psi), and 10:58 (after pressure release). Figure 5-53 shows a large increase in strain very early in the grouting process, with a peak strain on SB4 of 154 με at an associated grouting pressure of 100 psi. A large compressive strain of 71 με was also observed on SB4 from the top of the pile to 10 feet below TOC. It is not clear from site observations what the cause of this shallow strain was. The remaining three verticals show a liner strain distribution from a peak value at or just below 100 με to 0 at a depth of approximately 15 feet below TOC. In the last reading before the conclusion of grouting shown in Figure 5-54, the vertical strains on SB4 at both the top and base had fallen. The average strain in the pile was roughly 93 με at a depth of 30 feet below TOC, decreasing linearly to a depth of just above 20 feet below TOC. In Figure 5-55 showing the final fiber optic reading after the pressure had been released, the strains in SB1 have increased to over 200 με at 30 feet below TOC, with strains decreasing in SB3, SB4, and SB2. Further investigation is required to determine the potential cause of the large spike in strain on SB1.

Figure 5-53: Vertical strain profile at 9:56 (~100 psi)
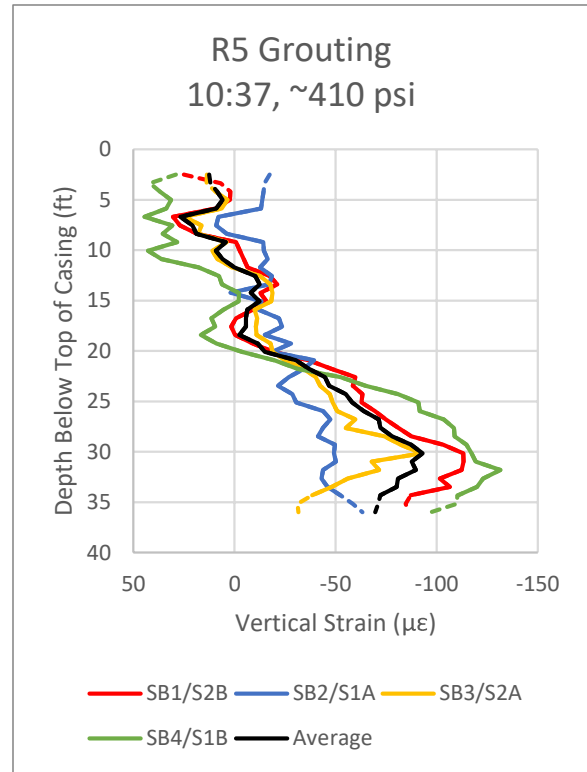
Figure 5-54: Vertical strain profile at 10:37 (~410 psi)
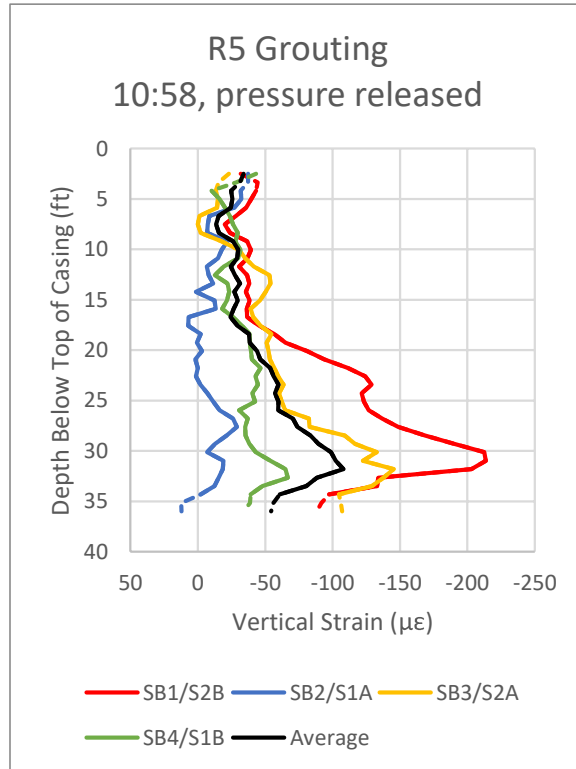
Figure 5-55: Vertical strain profile at 10:58 (after pressure release)

j) Reaction Shaft R7

Reaction Shaft R7 was grouted on February 5, 2019. The grout data logger record of pressure and volume at the grout plant is presented in Figure 5-56. All grouting was performed through a single line (of 4). Once grout return was established at the surface, all return valves were closed at 12:18 and grouting of the pile began. Grouting continued until 13:33 with an associated pressure of 520 psi, at which point the grout line was locked off and grouting was concluded. The measured volumes are not adjusted for the initial flush or grout in the lines and therefore represent an upper bound of the volumes placed at the pile base.

Figure 5-56: R7 grouting, grout data logger record

The fiber optic record for shaft R7 is divided into 4 strain verticals and 6 temperature verticals. The raw frequency and segment divisions are shown in Figure 5-57.

Figure 5-57: R7 grouting, raw Brillouin frequency

Preliminary analysis of the frequency data for R7 showed that the amplitude of the fiber optic signal was several times lower than those of a typical reading. While this loss was not apparent during the field readings, it resulted in the processed data being much noisier than a normal reading set. An example of this noise is shown in Figure 5-58 which displays the vertical strains with depth at 12:03, taken 13 minutes after the last baseline reading during the initial water flush of the grout circuits.
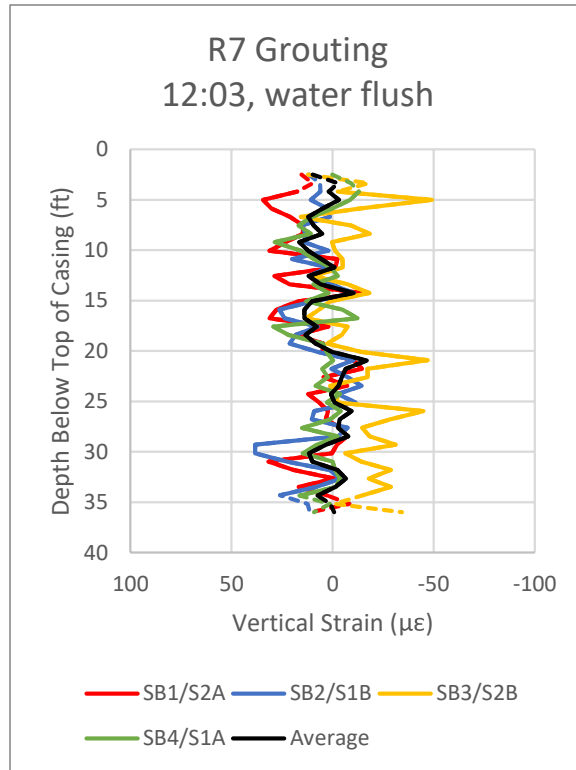
Figure 5-58: R7 grouting, strain variation during water flush due to unknown power loss in reading set

While the specific source of this power loss is unknown, it is likely that a poor connection was made either at the analyzer or the patch to the pile sensing cable. The following analysis and figures are presented with the caveat that the data contains noise of an unknown magnitude but estimated at approximately +/- 25 με. Even with this noise, the underlying trends of strain development and dissipation during and after grouting still appear to be reasonable and consistent with the observations on other piles.

The measured vertical strains with time at a depth of 33.5 feet below the top of casing (TOC), approximately 1 pile diameter (5 feet) above the base, are presented in Figure 5-59. This figure shows a general increase in strain in all four verticals throughout grouting, with the largest strains registered on SB3 with a peak value approaching 100 με. The largest single strain increase was observed from 12:25 to 12:31 with an associated grout pressure of 60 psi rising to 140 psi. Focusing on the average strain for the pile, the strain gradually increased during grouting, stayed level after the grout line was locked off at 13:33, and dropped by

approximately 30 με after the pressure in the lines was released. This drop is observed on all four verticals.
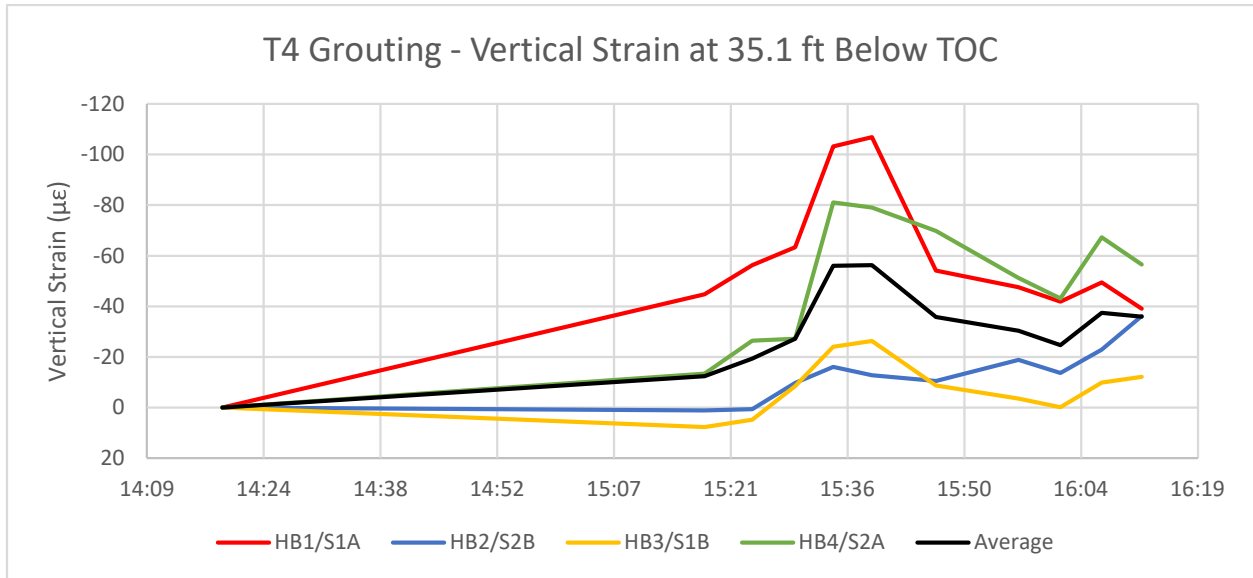

Figure 5-59: R7 grouting, vertical strains at 33.5 feet below TOC

Figure 5-60 through Figure 5-62 show the vertical strains with depth in the pile at 12:31 (~140 psi), 13:26 (~505 psi), and 13:46 (after pressure release). The high noise in the data makes direct interpretation of the strain values with depth difficult and subject to error. However, looking at the average of the four individual verticals, a trend of increasing strains over grouting can be observed. In   Figure 5-60, the average strain has a peak value of just above 60 με, decreasing linearly with depth to 15 feet below TOC before staying constant at approximately 25 με. In the final reading at 13:26 just prior to the end of grouting shown in Figure 5-61, the average strain profile is similar to that observed at 12:31; implying that little additional strain has been added into the pile. In the final reading after the pressure in the pile has been released shown in Figure 5-62, the average strain just above the base of the pile has decreased to 32 με, decreasing linearly with depth before reaching 0 at approximately 20 feet below TOC. This implies that while some negative skin friction was developed during grouting, much of the associated compressive strains were released except at the deepest portion of the pile.
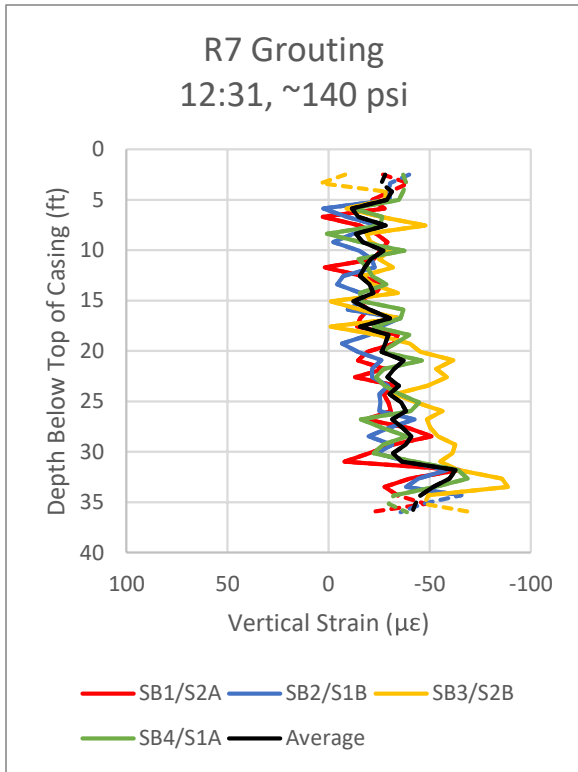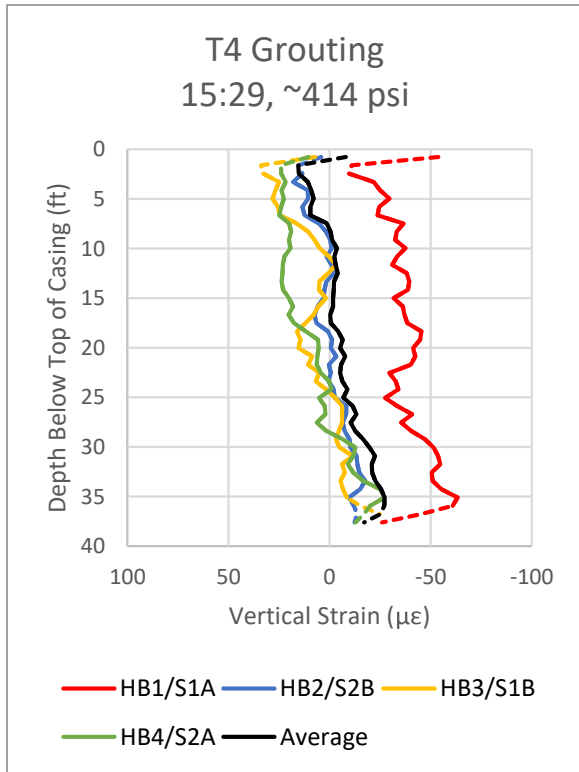
Figure 5-60: Vertical strain profile at 12:31 (~140 psi)
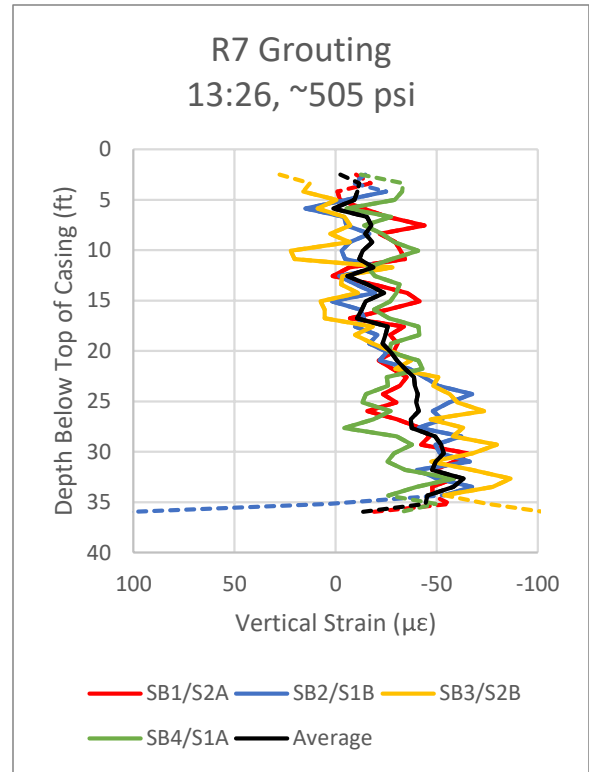
Figure 5-61: Vertical strain profile at 13:26 (~505 psi)
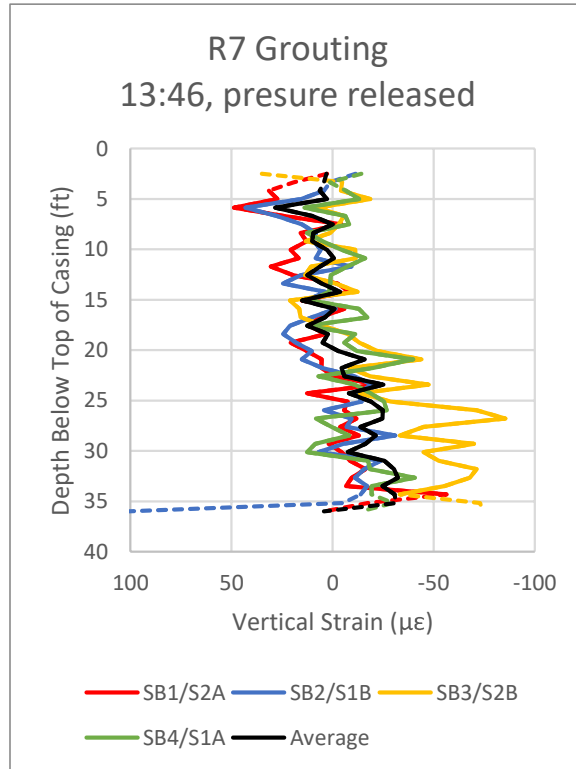
Figure 5-62: Vertical strain profile at 13:46 (after pressure release)

116

k) Reaction Shaft R9

Reaction Shaft R9 was grouted on February 4, 2019. The grout data logger record of pressure and volume at the grout plant is presented in Figure 5-63. All grouting was performed through a single line (of 4). Once grout return was established at the surface, all return valves were closed at 15:34 and grouting of the pile began. Grouting continued until 16:24 with an associated pressure of 500 psi, at which point the grout line was locked off and grouting was concluded. The measured volumes are not adjusted for the initial flush or grout in the lines and therefore represent an upper bound of the volumes placed at the pile base.
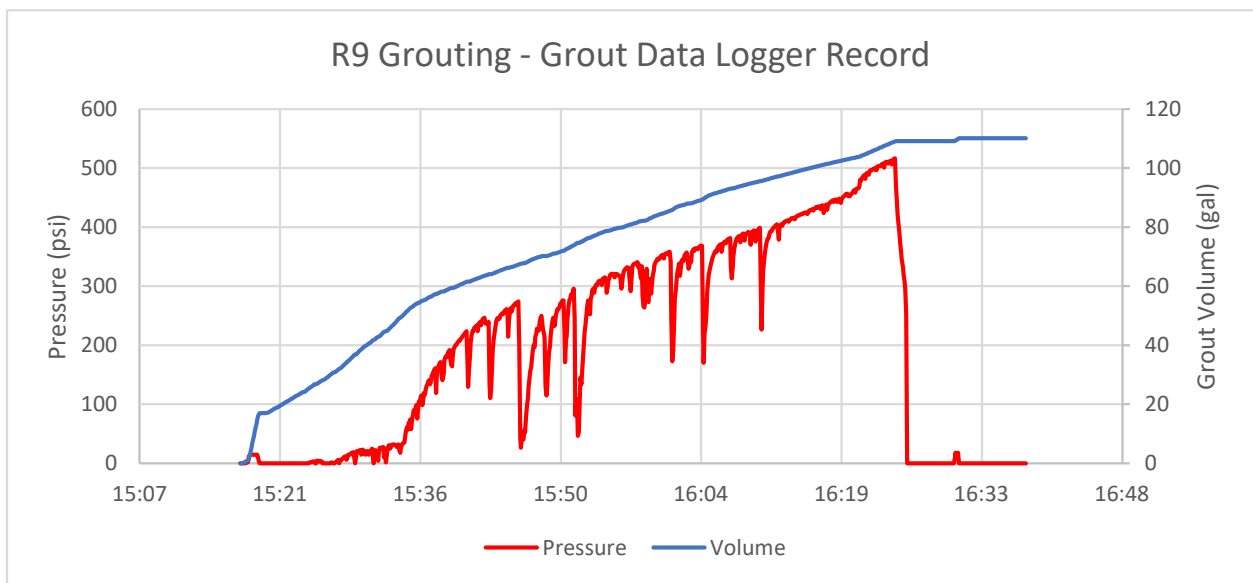
Figure 5-63: R9 grouting, grout data logger record

The fiber optic record for shaft R9 is divided into 4 strain verticals and 6 temperature verticals. The raw frequency and segment divisions are shown in Figure 5-64.
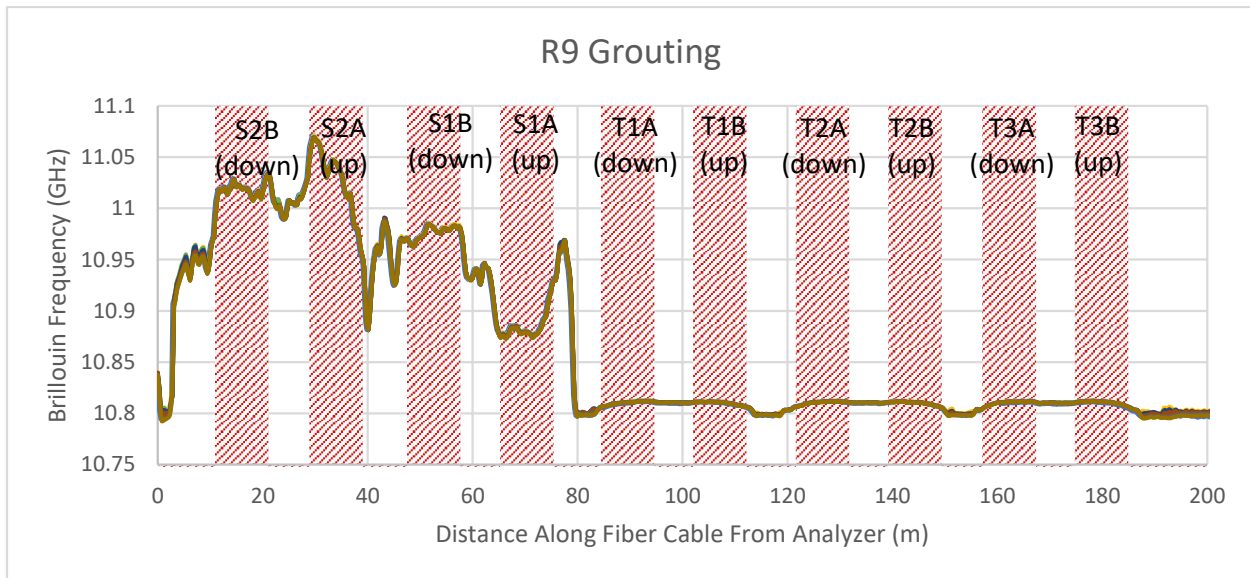
Figure 5-64: R9 grouting, raw Brillouin frequency

The measured vertical strains with time at a depth of 33.5 feet below the top of casing (TOC), approximately 1 pile diameter (5 feet) above the base, are presented in Figure 5-59. This figure shows an initial increase in strain at 15:36, corresponding with the first reading after the start of grouting. SB1, SB3 and SB4 show similar strains over the duration of grouting, with a peak value on SB4 of 66 με at 16:15 with a corresponding pressure of 420 psi. Although the pressure increased for one more reading cycle to 450 psi, the strain on all verticals dropped on the next reading, then dropped further after the end of grouting. A slight rebound was observed in the final reading at 16:53 with an average final strain of 29 με.
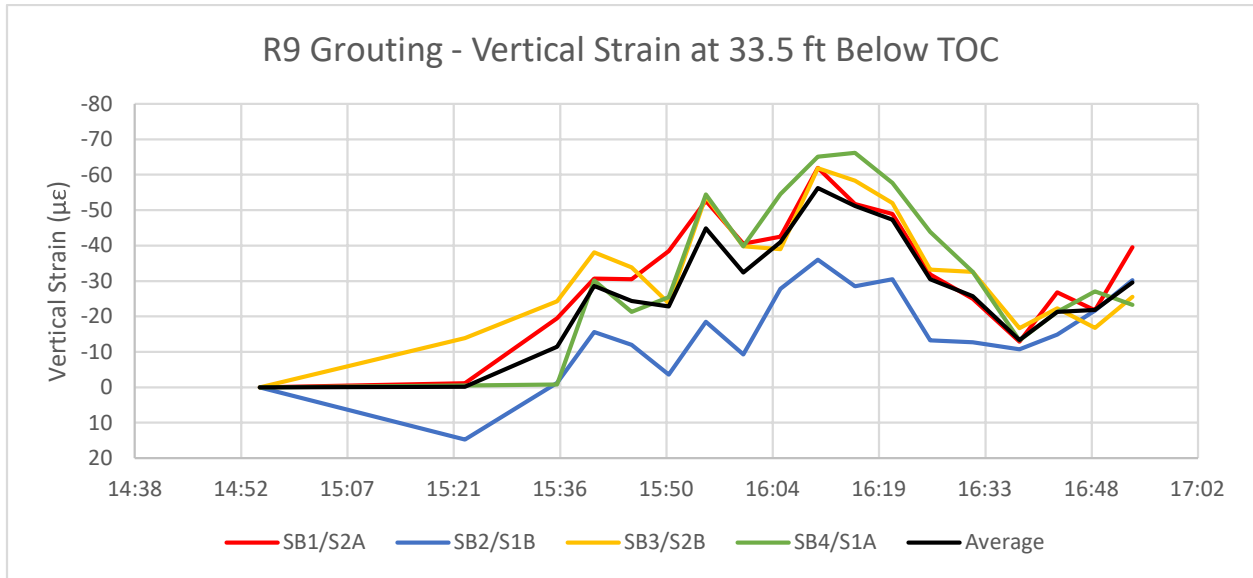
Figure 5-65: R9 grouting, vertical strains at 33.5 feet below TOC

Figure 5-66 through Figure 5-68 show the vertical strains with depth in the pile at 15:55 (~315 psi), 16:15 (~420 psi), and 16:53 (after pressure release).   Figure 5-66 shows a linear increase in strain with depth, with an average compressive strain of 46 $\mu\varepsilon$ at the base of the pile. In Figure 5-67, the average strain continues to increase to 52 $\mu\varepsilon$ at the peak grouting pressure of 420 psi. After the grouting pressure is released, in Figure 5-68, the average peak compressive strain has fallen to approximately 30 $\mu\varepsilon$. The shape of the strain curve has also changed, remaining constant from the base of the pile to 15 feet below TOC, after which it decreases linearly to the top of the pile. The shape of the strain profiles observed in these three figures show a development of negative skin friction during grouting. However, a portion of the peak value in the lower portion of the pile is released once grouted is completed.
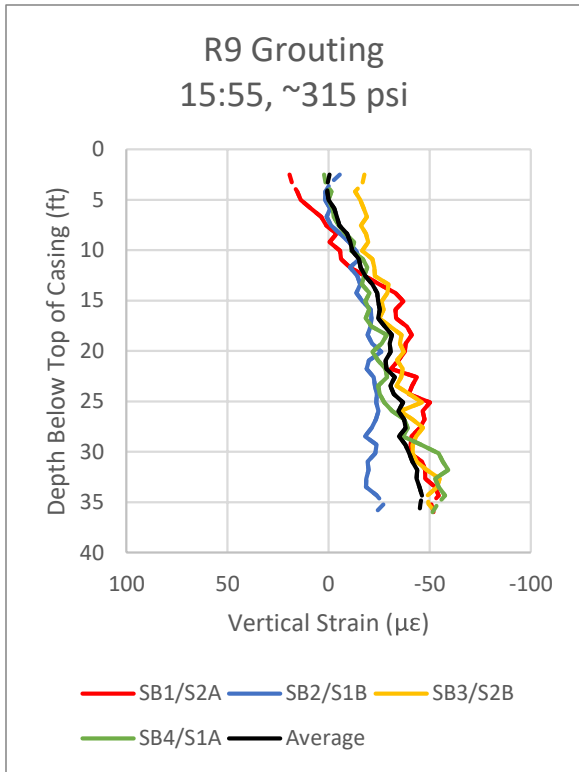
Figure 5-66: Vertical strain profile at 15:55 (~315 psi)
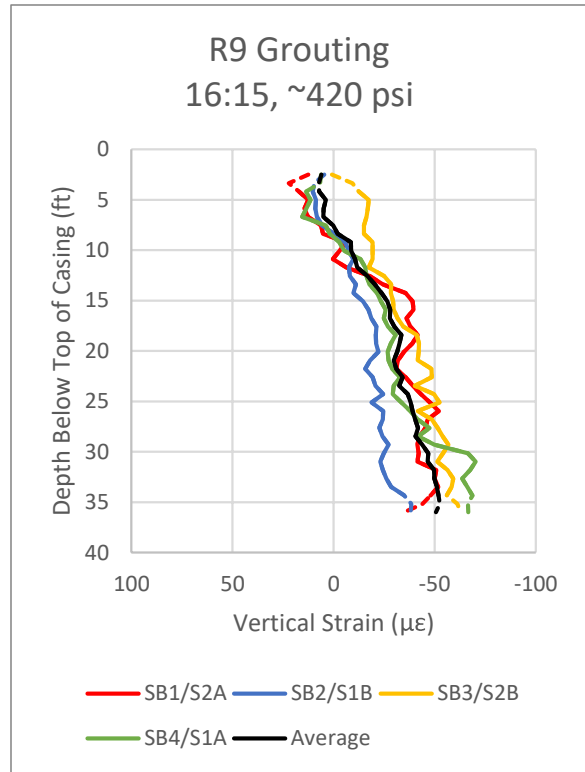
Figure 5-67: Vertical strain profile at 16:15 (~420 psi)
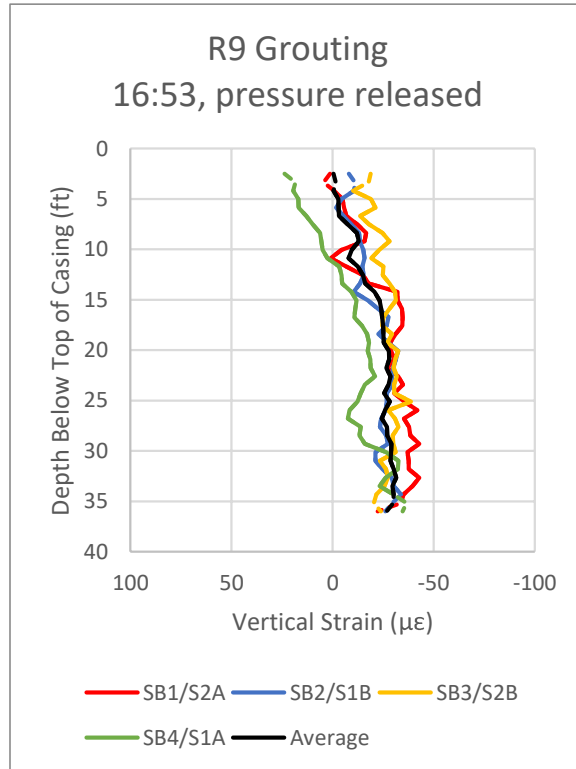
Figure 5-68: Vertical strain profile at 16:53 (after pressure release)

l)   Test Shaft T4

Test Shaft T4 was grouted on February 5, 2019. The grout data logger record of pressure and volume at the grout plant is presented in Figure 5-69. All grouting was performed through a single line. Once grout return was established at the surface, all return valves were closed at 15:14 and grouting of the pile began. Grouting continued until 15:45 with an associated pressure of 600 psi, at which point the grout line was locked off and grouting was concluded. The measured volumes are not adjusted for the initial flush or grout in the lines and therefore represent an upper bound of the volumes placed at the pile base.
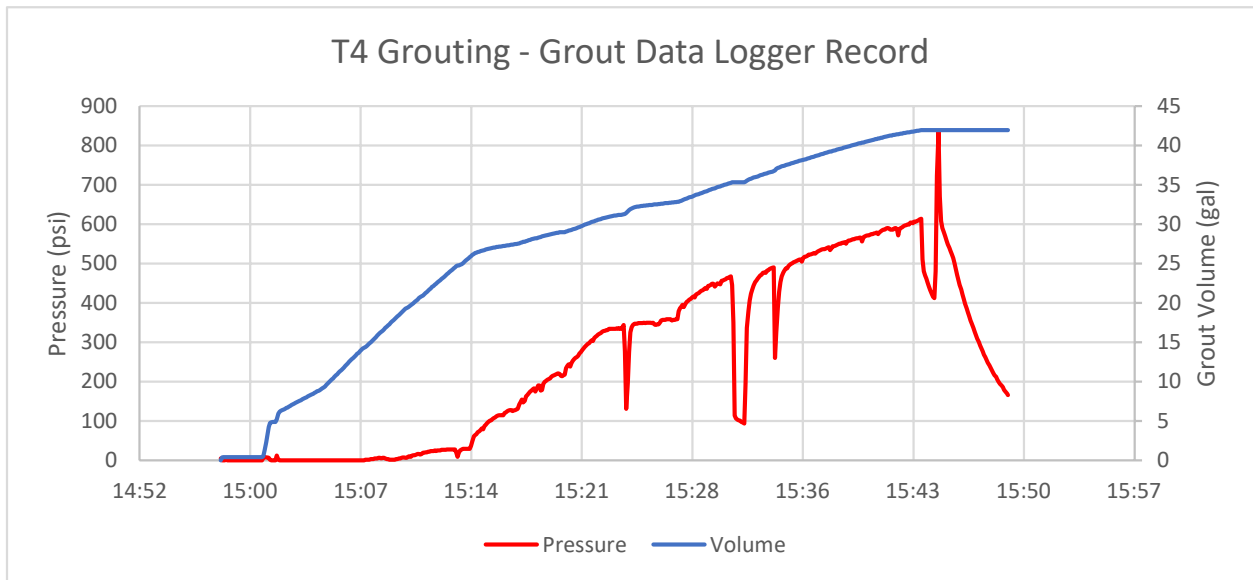
Figure 5-69: T2 grouting, grout data logger record

The fiber optic record for shaft T4 is divided into 4 strain verticals and 2 temperature verticals. The raw frequency and segment divisions are shown in Figure 5-70.
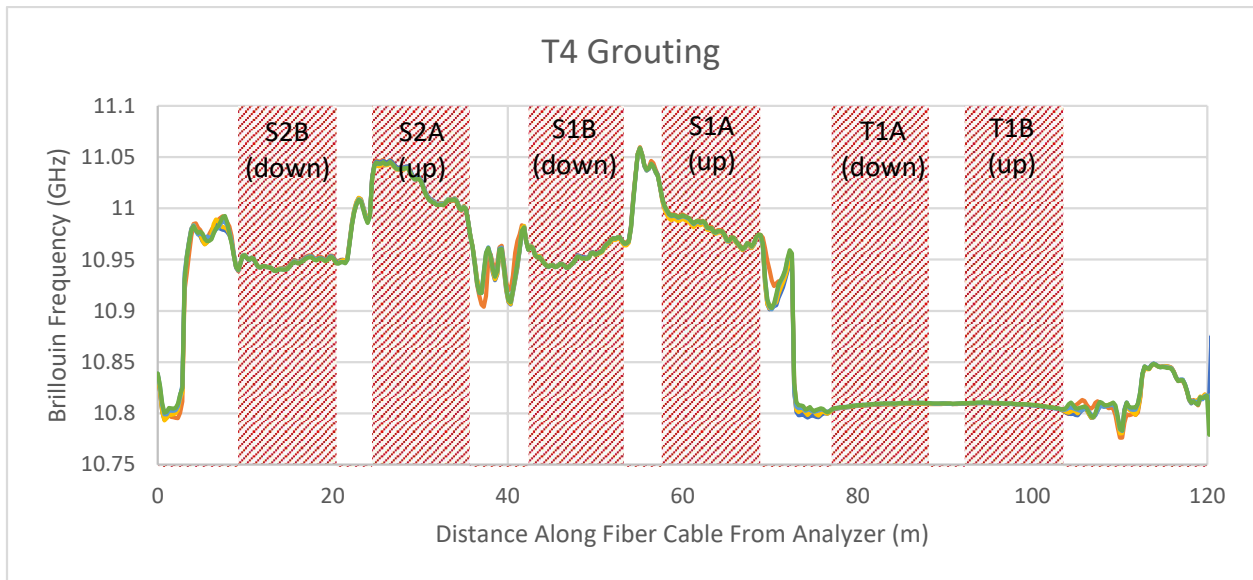
Figure 5-70: T2 grouting, raw Brillouin frequency

The measured vertical strains with time at a depth of 35.1 feet below the top of casing (TOC) are presented in Figure 5-71Figure 5-71: T2 grouting, vertical strains at 35.1 feet below TOC. This figure shows an initial increase in compressive strain on all four verticals at 15:29, followed by a large jump in strain at 13:34-13:38. The peak strain was measured at 13:38 on HB1 with 107 με in compression. At the peak, there was a wide variation in measured values across the piles with a maximum differential of over 80 με. There is a drop in strain on all verticals following the lock off of the grout lines and release of pressure at 15:46. The compressive strains continue to gradually fall until a final rise is observed prior to the final reading at 16:12 with an average compressive strain of 36 με.

Figure 5-71: T2 grouting, vertical strains at 35.1 feet below TOC

Figure 5-72 through Figure 5-74 show the vertical strains with depth in the pile at 15:29 (~414 psi), 15:38 (~540 psi), and 16:12 (after pressure release). Figure 5-72 shows a high concentration of compressive strain on HB1, with a peak strain of 63 $\mu\varepsilon$ decreasing linearly with depth to the top of the pile will a small deviation at 23 feet below TOC. The other three verticals register slight tension in the upper 20-25 feet of the pile and show a maximum compressive strain of less than 25 $\mu\varepsilon$ at the base. In Figure 5-73, at the peak strain at 15:38, the strains in HB1 at the base have increased to 107 $\mu\varepsilon$ with a rough linear decrease down to zero at the top of the pile. The strains in the other three verticals in the lower 15 feet of the pile are more evenly distributed than earlier in the grouting process, with HB4 also showing higher strains than average and HB2 and HB3 showing lower strains than average. After the pressure is released in Figure 5-74, the average strain at the base of the pile decreases to 32 $\mu\varepsilon$ with a linear trend to 0 at the top of the pile, implying that an increment of negative skin friction remains in the pile. The deviation at 20-25 feet in HB1 has increased, however the other verticals are more closely centered around the average. It is unclear what the cause of this deviation is, but it suggests an inhomogeneity in the shaft friction at this location.

123

Figure 5-72: Vertical strain profile at 15:29 (~414 psi)
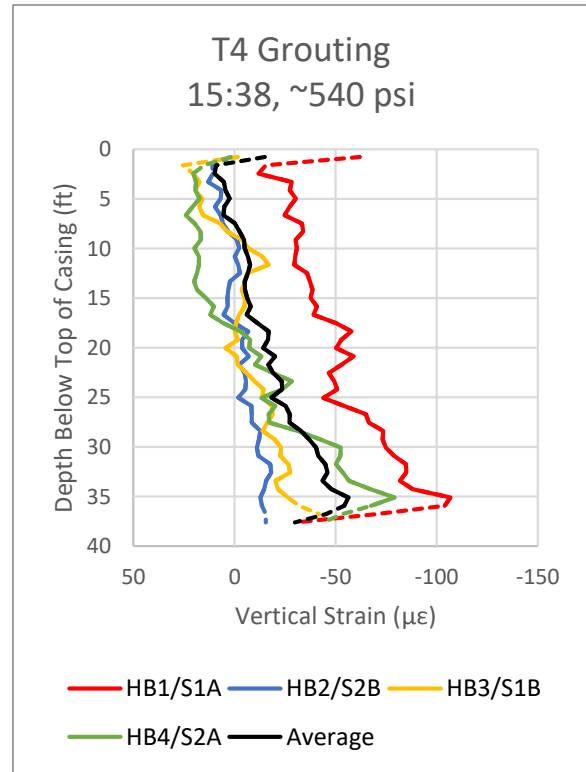
Figure 5-73: Vertical strain profile at 15:38 (~540 psi)
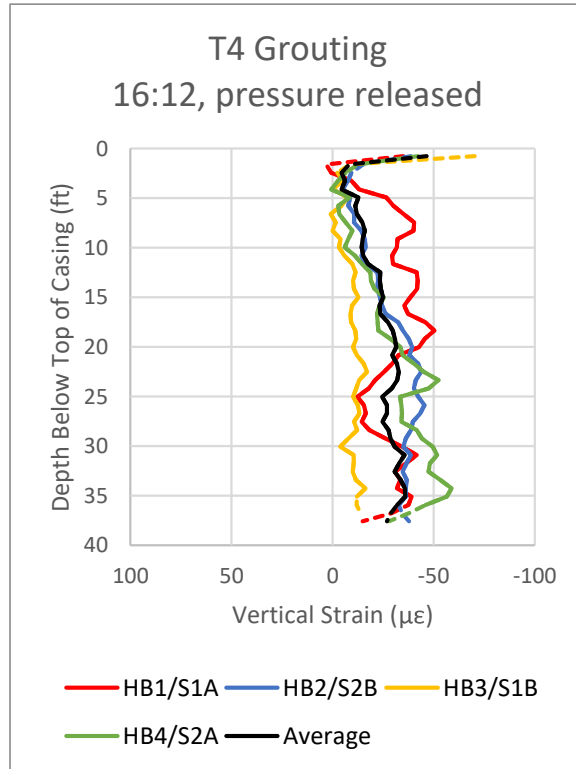
Figure 5-74: Vertical strain profile at 16:12 (after pressure release)

Summary

After reviewing the strain and temperature measurements taken during base grouting, some additional observations can be made.

- The pressure and volumes recorded at the grout plant were not directly correlated to the strains (and therefore loads) that were being applied to the pile at the base. This was the most evident for the open-type grouting system, where dramatic increases in measured grout pressure would yield associated increases in strain within the pile.
- The strains in the pile would often reach a peak relatively early in the grouting process, with an associated low pressure. Continued grouting at increasing pressures would often not result in a proportional increase in strain.
- The strains measured across the pile were often non-uniform, suggesting that the load from the grout injection was not distributed evenly across the pile base.
- Based on a subjective review, the closed-type grouting system yielded the most uniform distribution of pile strains, both across the pile area as well as reaching upwards into the pile with depth.
- For strain measurements, temperature variations during grouting were significant and needed to be accounted for in processing of the data.
- Strains in the pile decreased after the pressure was released; although several of the piles displayed continuing fluctuations in the measured strain for some time after the grouting was completed.

6. Measurements During Load Testing

Introduction

Following the conclusion of the base grouting, all four of the test piles (T1-T4) were load tested to determine their performance under axial loading. As with the base grouting, the test piles were monitored using a mix of conventional instrumentation and fiber optic sensors.

For the distributed fiber optic monitoring, the strain and temperature fiber optic loops in the test pile were connected in series with the fiber optic cables in the four reaction shafts as shown in Figure 6-1. For test piles T2-T4, all five piles (one test pile and four reaction shafts) were interrogated during each reading. Test pile T1 had the connection between the test shaft and first reaction shaft severed immediately prior to the load test and hence we were only able to interrogate the test shaft during the load test.
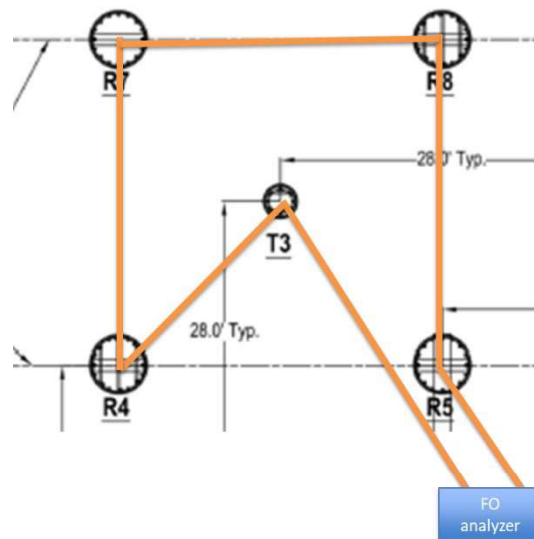
Figure 6-1: Diagram of the distributed fiber optic networking of piles during load test monitoring

Load test schedule

The load test schedule was performed in four cycles which can generally be described as follows. The first cycle was stepped up in 50 kip increments to 200 kips, then unloaded to 0 kips in 3 steps. The second cycle was stepped up back to 200 kips in 3 steps, then up to an intermediate load in 50 kip steps based on the observed displacements of the pile of

approximately a half inch, followed by unloaded to 0 kips in 3 steps. The third cycle was stepped back up to the previous maximum load in 3 steps, then up to a maximum load in 50 kip steps. The maximum load was determined collaboratively by the group based on observed displacements, loads, and the stroke capacity of the hydraulic pistons. After the maximum load was reached, the pile was unloaded to 0 kips in 3 steps. The final cycle consisted of reloaded to or just below the previous maximum load in 4-5 steps, then unloading directly to 0 kips.

The loading system was manually controlled using a hydraulic pump feeding pressure to a set of four pistons. To transition from one load to the next, the operator would increase or decrease the pressure using a manual controller, carefully timing when to stop as to end with a final load close to the nominal target as measured by the load cells. Once the operator was satisfied with the pressure, the system was held for 5 minutes. During this time, the load was observed to gradually decay over the hold time. The load decay within each 5-minute hold increased in magnitude as the total applied load increased towards the maximum load value. No additional pressure was applied during the hold times.

Fiber optic measurements

Measurements

Prior to the start of each load test, a minimum of 3 fiber optic readings were taken to serve as a baseline to compare the subsequent strain measurements to. For test piles T1, T3, and T4, a single fiber optic reading was taken during each 5-minute hold. As with the presentation of the measurements taken during grouting, the following reported data for the strain measurements during the load tests represent the readings taken over the 5-minute hold and do not represent either the average strain or the strain at a single discrete point in time. For test pile T2, the ALICIA fiber optic analyzer was used, and its readings represent discrete (near) instantaneous strain measurements of a second or less.

Data analysis

As with the results during the thermal monitoring during curing and the strain and thermal monitoring during grouting, each reading output had to be translated from a series of raw

frequency data into a variation in strain and temperature at specific locations in the monitored piles. The indexing values used in the grouting data were able to be reused for the load test data processing, with the caveat that several piles were networked together during monitoring which required the pile intervals to be shifted by a distance offset based on the cable length prior to the connection.

Temperature change effect

Prior to processing of the strain profiles, the temperature changes as measured by the thermal fiber optic lines was evaluated to determine if thermal compensation of the strain measurements was necessary. During the load test monitoring, the average spread in the thermal fiber optic cables away from the top of the pile was approximately +/- 0.3 MHz from the baseline, corresponding to a thermal fluctuation of +/- 0.27° C. Converting into strain using the coefficients for the strain cable, this corresponds to an average thermal strain of 9.7 $\mu\epsilon$ over the load test. This value is below the accuracy of the distributed fiber optic analyzers and cannot be differentiated from the noise floor; therefore, no thermal compensation of the strain values was performed on the measurements during the load tests. This is consistent with the understanding that the pile at depth (away from the ground surface) will be thermally stable during the relatively short duration of the test and is consistent with the approach taken with the conventional vibrating wire strain gauges which also did not have thermal correction applied.

The temperature variation in Test Pile T3 during the load test monitoring at the central 20 feet of the pile (10 – 30 feet below top of casing) is shown in Figure 6-2.
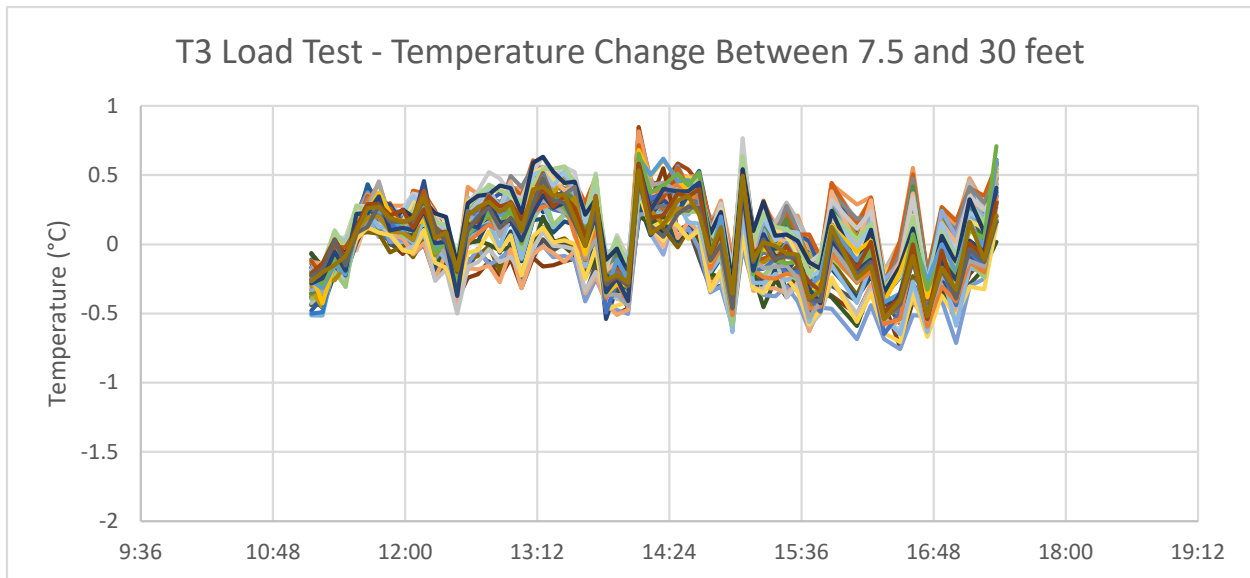
Figure 6-2: Recorded temperature variation in Test Pile T3 during load test

The average thermal fluctuation in the data is +/- 0.11° C, corresponding to an average thermal strain of 4.0 $\mu\varepsilon$. The maximum deviation was 0.81° C, with most readings during the load test falling within +/- 0.5° C of the baseline. While most of the readings are spread within a range approximately within the frequency (temperature) accuracy of the analyzer, the drop in temperature in all depths observed at 14:01 coincides with the unload cycle from ~1150 kips. This correlation suggests that the temperature cable may not be fully decoupled from the mechanical strains in the pile, with an approximate strain transfer of approximately 10 $\mu\varepsilon$, depending on how much of the observed temperature change is actually attributed to a transfer of strain. This trend is not observed elsewhere in the temperature data during the load cycle – it is possible that the rapid reversal of the loading direction resulted in the temporary transfer of strain through the thermal cable strain break.

Results

The presentation of the strain measurements during load testing are divided by the individual piles.

a) Test Pile T1, Control (no base grout)

Test pile T1, in which no base grouting was conducted, was load tested on February 23, 2019. Four load cycles were completed over just under 7 hours. The recorded load time history for

the 4 load cells is shown in Figure 6-3. The maximum load peaks of the individual cycles were 200, 900, 1750, and 1600 kips.
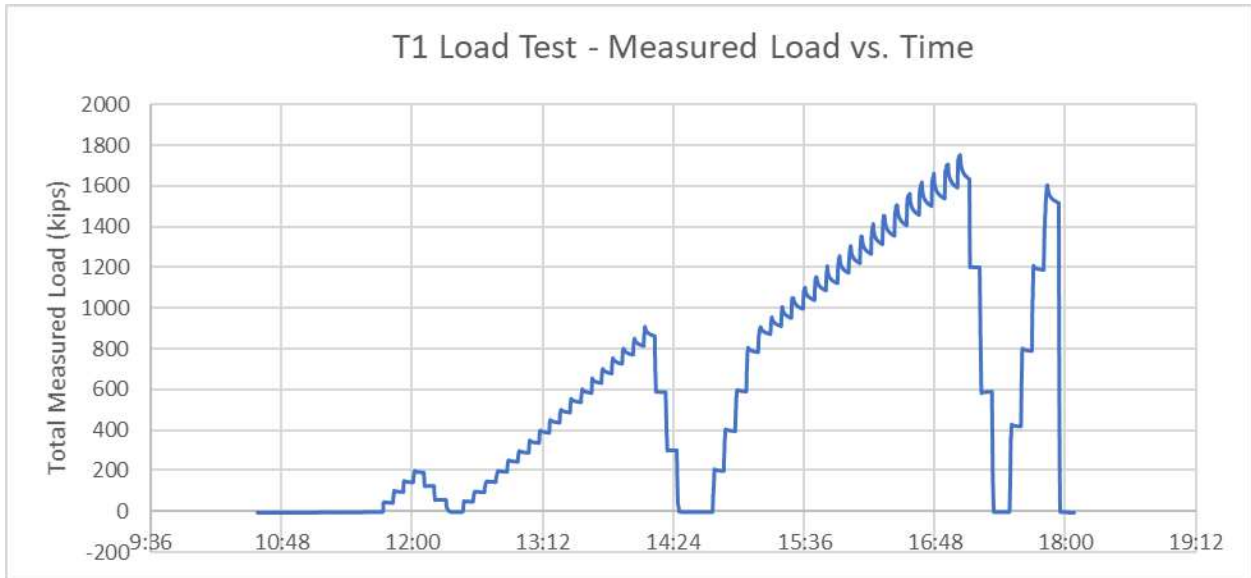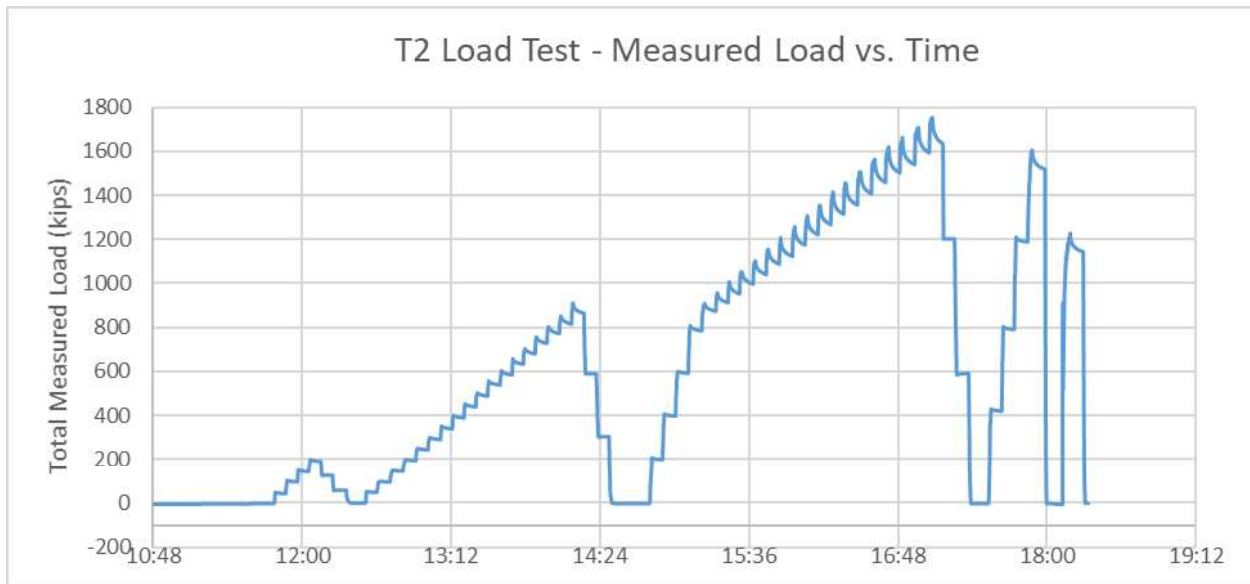

Figure 6-3: T1 load test, total load (sum of 4 individual load cells) over time

As noted earlier in the report, immediately prior to the load test, one of the test personnel tripped on the fiber optic cable connecting T1 to R1, breaking the splice and severing the connection to the four reaction shafts for the test. For this reason, the fiber optic measurements for T1 during the load test were taken using the BOTDR (single ended) mode on the Omnisens analyzer. A total of 65 distributed fiber optic readings were taken prior to, during, and after the load test. Each reading interrogated both the strain and temperature loops of the test pile. The raw frequency and segment divisions are shown in Figure 6-4.
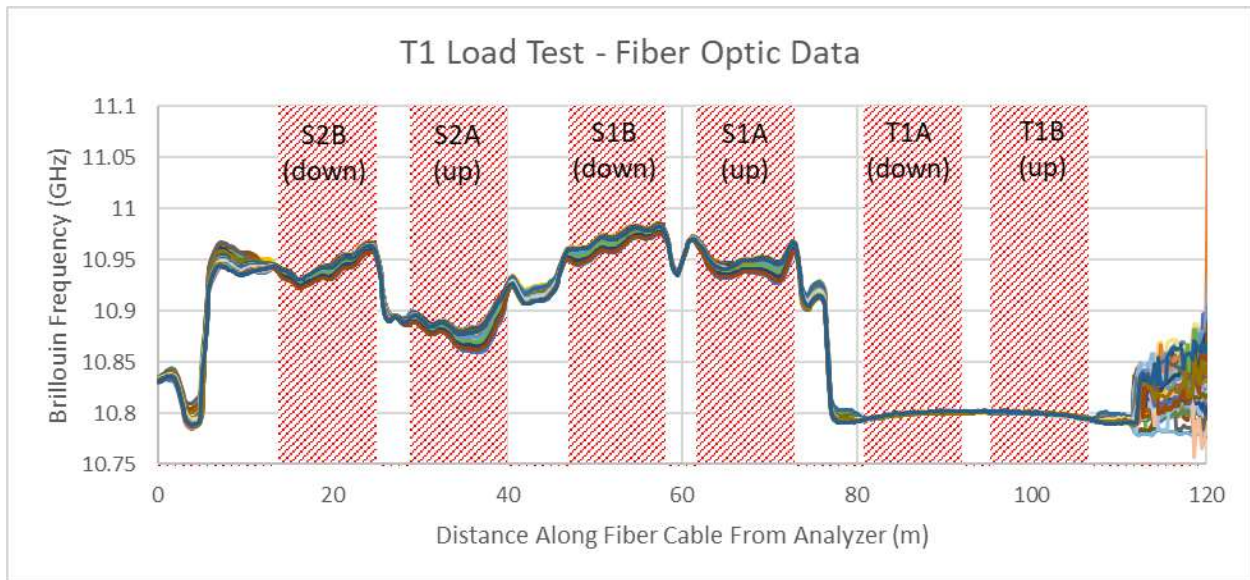
Figure 6-4: T1 load test, raw Brillouin frequency

Converting the change in frequency along the strain cable to vertical strain, the strain development within the pile at 7.5 feet below the top of casing is presented in Figure 6-5. Each data set is divided into the individual vertical portions of the cable length, designated by both the bar that they are attached to (e.g. Hollow Bar 1) as well as the strand designation (e.g. Strain 2A). The average of all 4 strain verticals is also presented. A strong difference in the strain between the sides of the pile can be observed from the spread in the strain data. HB1 experienced the highest strain during the load test, while HB3 opposite it experienced the lowest. On the perpendicular axis, HB2 and HB4 were centered close to the average, indicating that the direction of the asymmetry was close to the HB1-HB3 line.
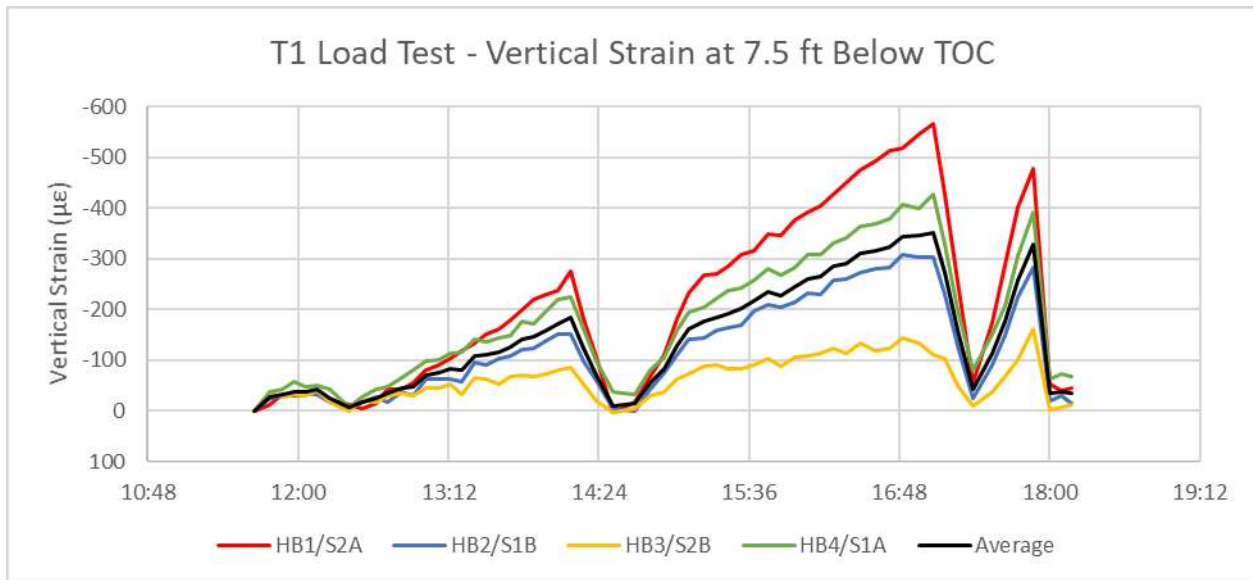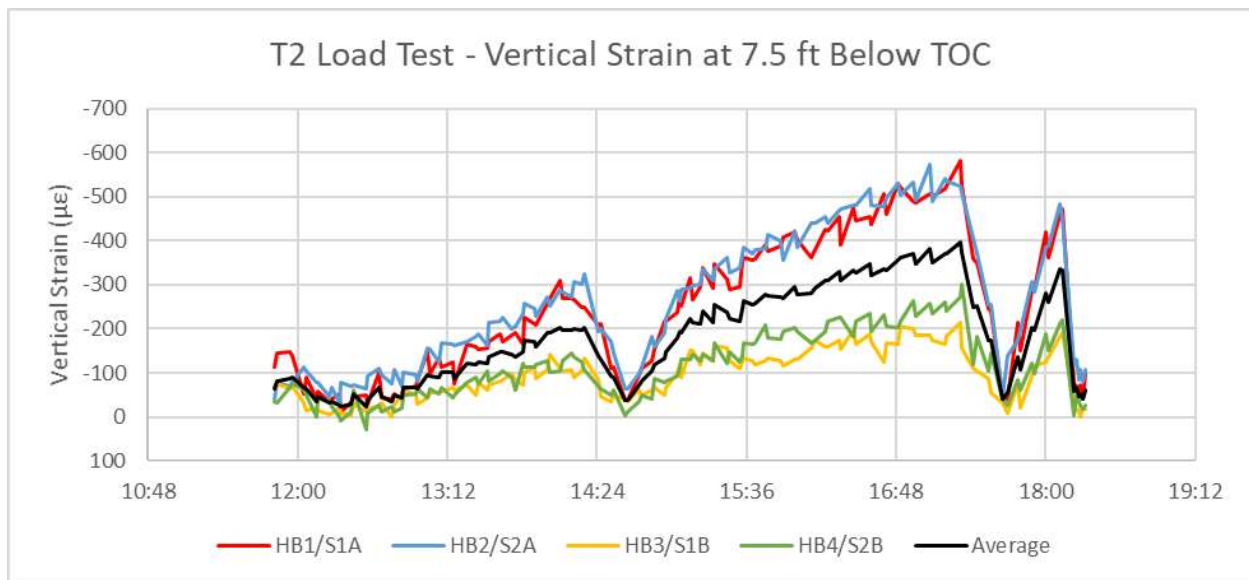
Figure 6-5: T1 vertical strain at 7.5 ft below top of casing over time

The development of strain within the pile over 6 loading increments (500 kips, 900 kips, 900 kips reload, 1500 kips, 1750 kips, and the final unload) are presented in Figure 6-6 through Figure 6-11. It is important to note that in all cases the presented load is approximate. This is due to the fact that the measured load from the load cells always had a slight deviation from the "target" load for each step, as well that the load was not constant during the approximate 5-minute hold period.
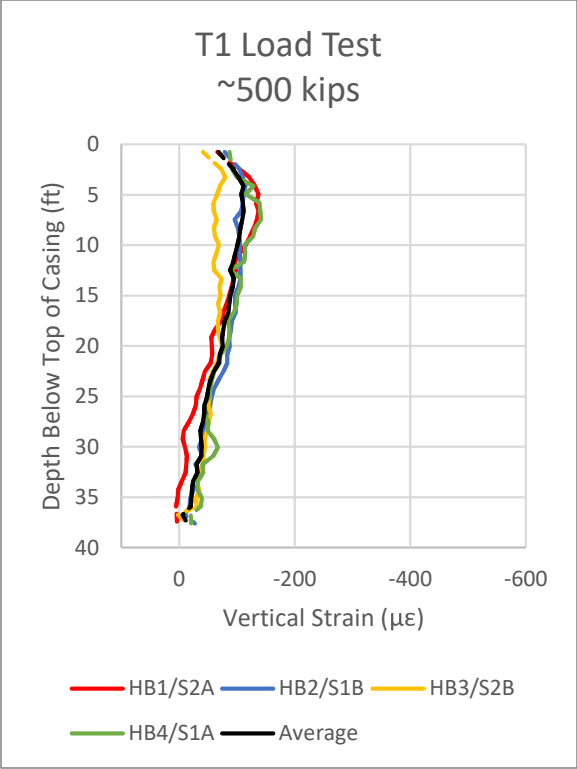
Figure 6-6: Vertical strain profile at ~500 kips load
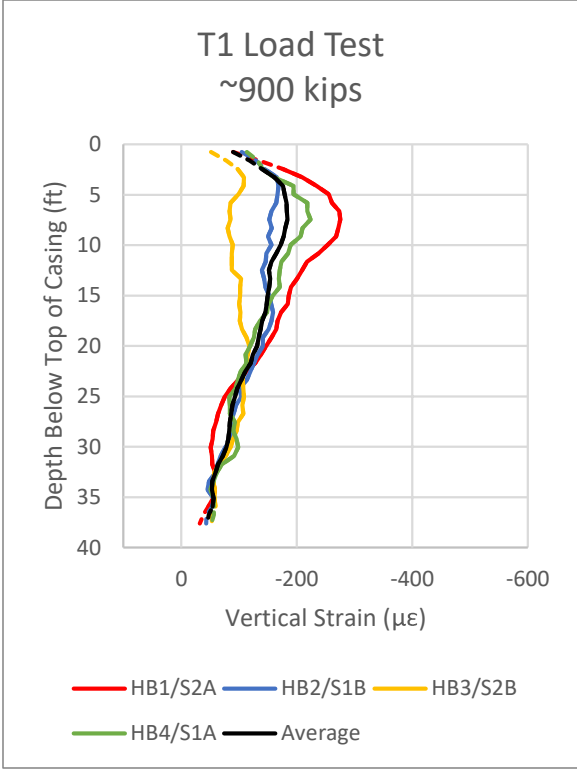
Figure 6-7: Vertical strain profile at ~900 kips load
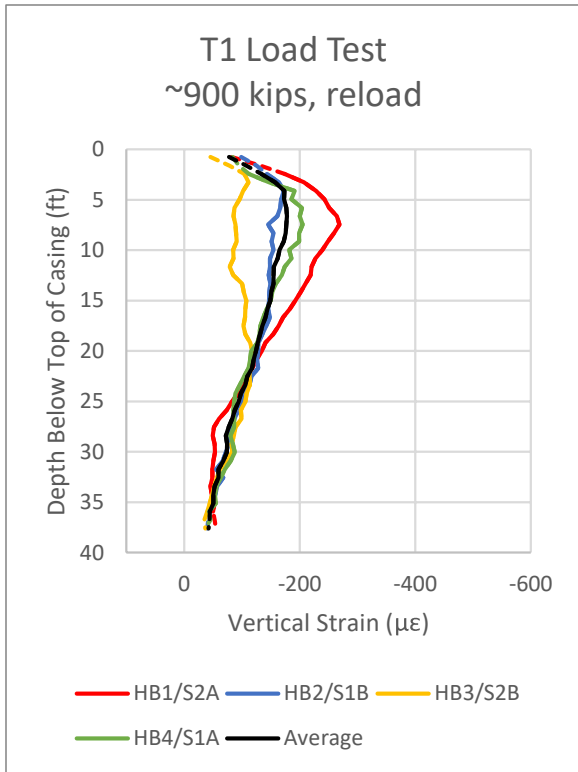
Figure 6-8: Vertical strain profile at ~900 kips reload
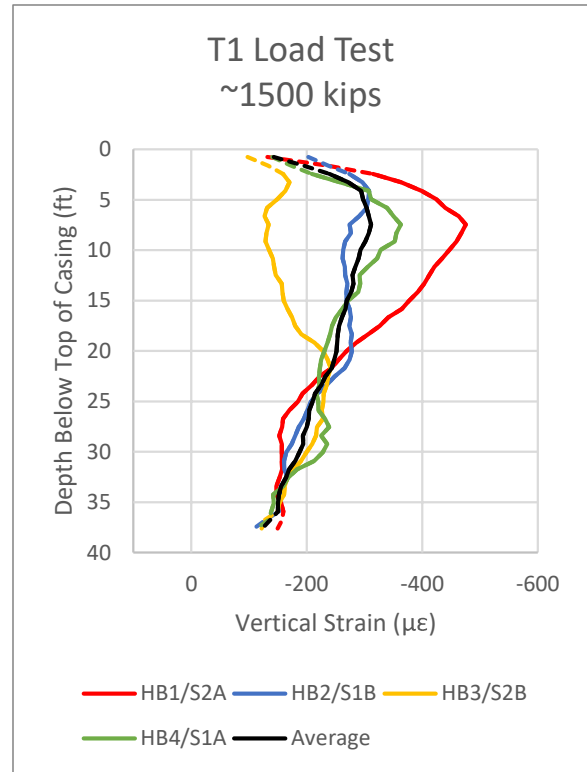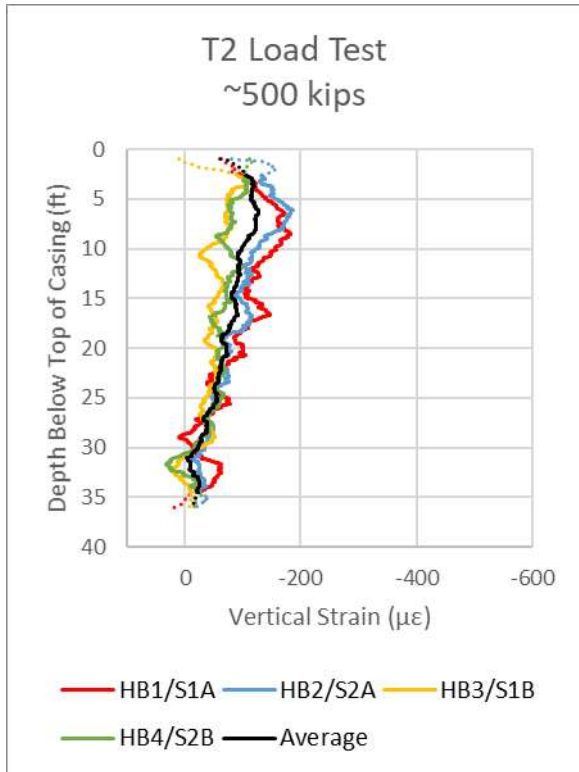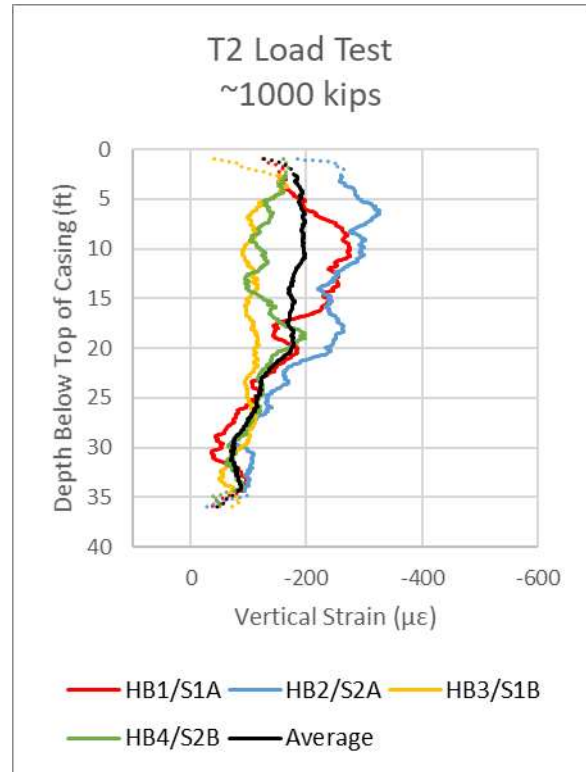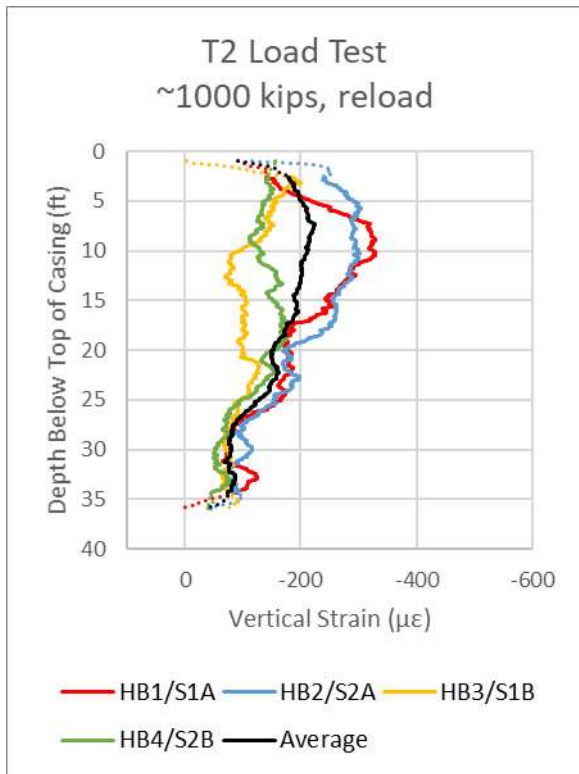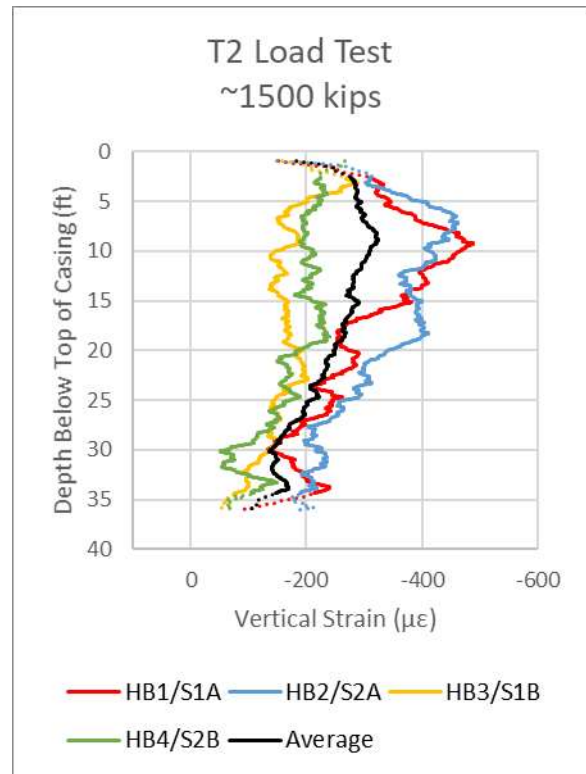

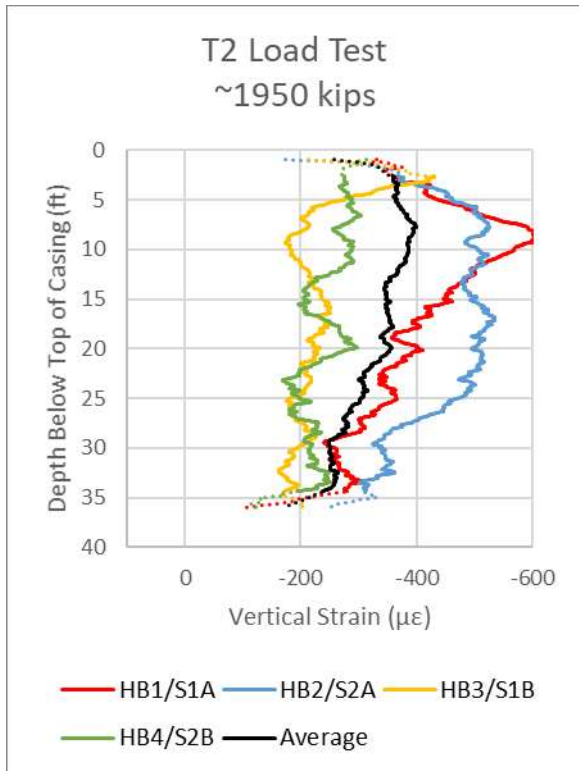*Figure 6-9: Vertical strain profile at ~1500 kips load*
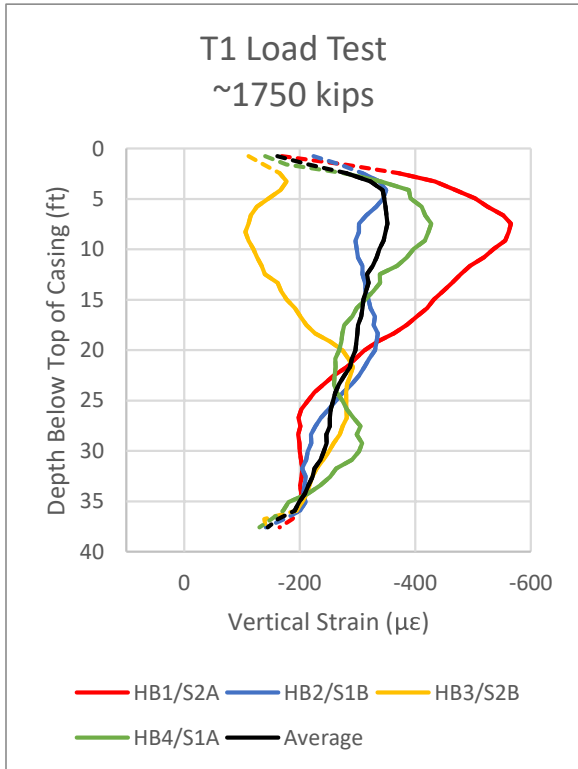
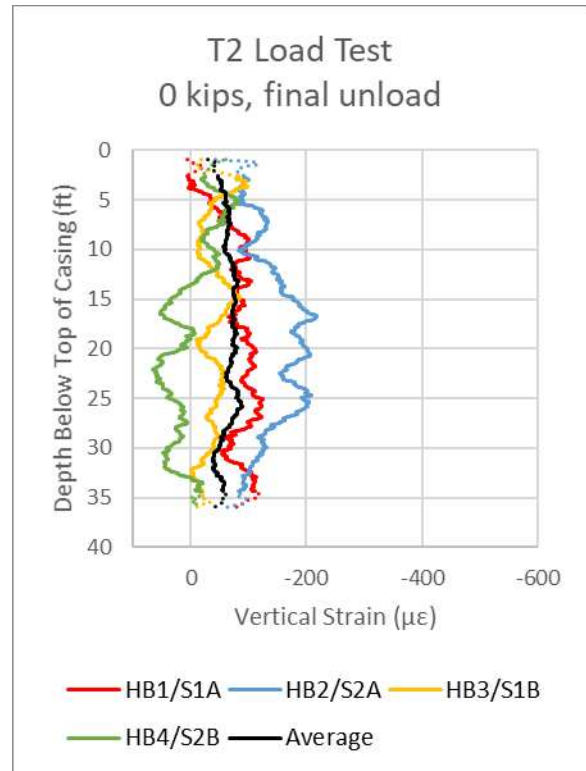*Figure 6-10: Vertical strain profile at ~1750 kips load*
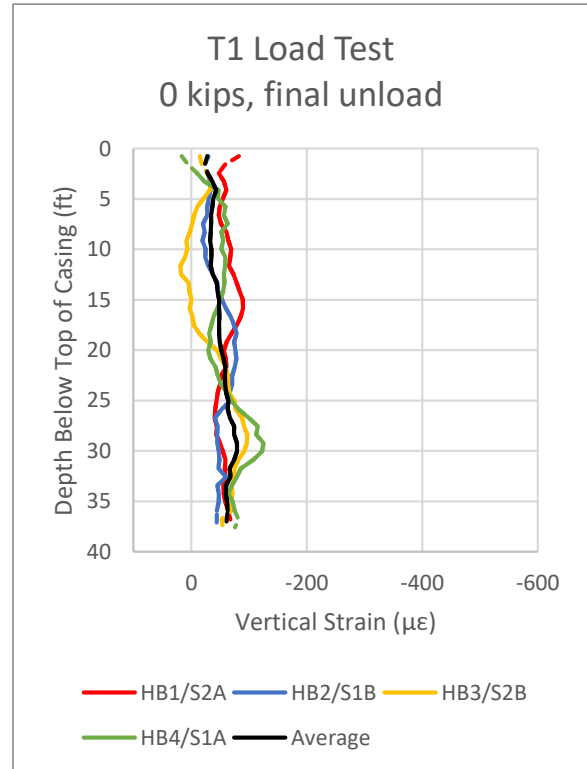
Figure 6-11: Vertical strain profile at 0 kips unload

134

Beginning in Figure 6-6 at the 500 kip interval, a developing separation in the strain between HB1 and HB3 can be observed in the top 20 feet of the pile. This separation continues to grow in magnitude through the maximum load interval of 1750 kips in Figure 6-10. The strains in HB1 show a positive curvature, developing to a maximum strain of 562 με at 8.3 feet below the top of casing. At the same time, the strains in HB3 show a negative curvature, with a minimum strain at depth of 106 με at 8.3 feet below the top of casing. These values compare to an average strain within the pile at the same depth of 348 με. The corresponding depths, with a peak at 8.3 feet and crossover at 20 feet below top of casing, and the approximate symmetry of the curvature around the average, imply that the pile is experiencing bending in the top 20 feet during the load test. This could be due to the applied load not being perfectly concentric with the center of the pile or being applied at an angle deviating from vertical during the load test. A third potential cause could be a deviation from vertical in the pile orientation itself, however this is less likely given the relative shallow depth of the pile. After removal of the load, the strains in Figure 6-11 show a small residual strain measured in the pile with an average value of approximately 50 με.

b) Test Pile T2, RIM Cell

Test Pile T2 was load tested on February 28, 2019. The pile was based grouted using a rim cell. Four load cycles were completed over just over 6 hours. The recorded load time history for the 4 load cells is shown in Figure 6-12. The maximum load peaks of the individual cycles were 200, 1000, 1950, and 1600 kips.

Figure 6-12: T2 load test, total load (sum of 4 individual load cells) over time

The fiber optic readings during the load test were taken with the Berkeley research analyzer, ALICIA. A total of 129 distributed fiber optic readings were taken prior to, during, and after the load test. Each reading interrogated both the strain and temperature loops of the test pile, as well as the four connected reaction piles (in order: T2, R6, R5, R2, R3). The raw frequency plot is presented in Figure 6-13. Focusing on the test pile, the fiber optic record was divided into the vertical strain and temperature loops as shown in Figure 6-14.
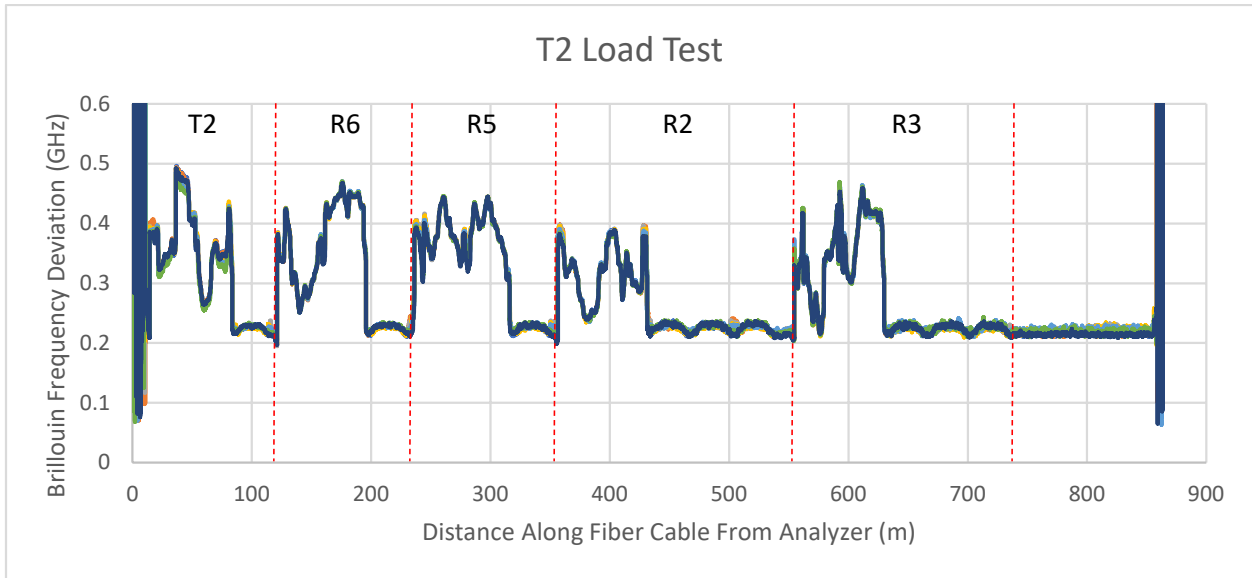
Figure 6-13: T2 load test, raw Brillouin frequency over all piles
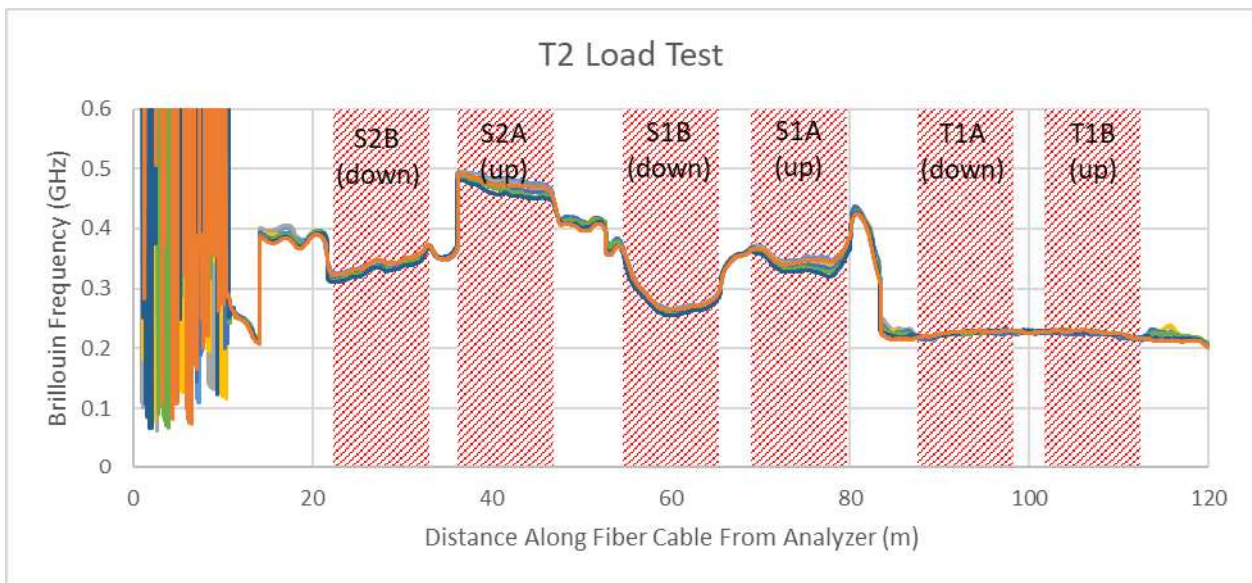
Figure 6-14: T2 load test, raw Brillouin frequency within pile T2

The development of strain over time at 7.5 feet below the top of casing in all four verticals, as well as the average strain, are shown in Figure 6-15. A difference in the strain between the sides of the pile can be observed from the spread in the strain data. HB1 and HB2 experienced the highest strain during the load test, while HB3 and HB4 on the opposite side experienced the lowest. The magnitudes of the two pairs of bars were relatively close to each other, indicating that the axis of asymmetry was approximately between HB1/2 and HB3/4, passing between

137

each of the adjacent bar pairs. It can also be observed from the data that the linear trends during the increasing and decreasing loads displayed more noise than the corresponding reads on the other test piles using the Omnisens analyzer. This noise is likely attributed to the performance of the ALICIA analyzer in terms of its frequency resolution and repeatability, with the errors for any individual reading being higher that the more expensive Omnisens analyzer. The data is centered approximately +/- 20 µε from a linear fit of the data for each strand, indicating that the repeatability is banded roughly within this magnitude. This is supported by the known optical limitations of the ALICIA analyzer and can be improved or relaxed by changing the selected optical components within its construction, depending on if higher or lower strain resolution is needed for monitoring applications.

Figure 6-15: T2 vertical strain at 7.5 ft below top of casing over time

The development of strain within the pile over 6 loading increments (500 kips, 1000 kips, 1000 kips reload, 1500 kips, 1950 kips, and the final unload) are presented in Figure 6-16 through Figure 6-21. The plotted strain represents the fiber optic readings taken just after the target load stabilized at each increment (additional load was no longer being added). However, the load is still presented as approximate due to the deviation of the actual measured load versus the target.

Figure 6-16: Vertical strain profile at ~500 kips load

Figure 6-17: Vertical strain profile at ~1000 kips load

139

Figure 6-18: Vertical strain profile at ~1000 kips reload

Figure 6-19: Vertical strain profile at ~1500 kips load

Figure 6-20: Vertical strain profile at ~1950 kips load

Figure 6-21: Vertical strain profile at 0 kips unload

Beginning in Figure 6-16 at the 500 kip interval, a developing separation in the strain between HB1/2 and HB3/4 can be observed in the top 15 feet of the pile. This separation continues to grow in magnitude and also extend in depth through the maximum load interval of 1950 kips in Figure 6-20. The shape and magnitude of the HB1 and HB2 strain curves are similar through the maximum load, at which point HB1 displays a much sharper peak and strain decay with depth while HB2 shows a more gradual but rounded strain curve above the average. Likewise, the shape and magnitude of HB3 and HB4 are also similar through the maximum load, at which point HB3 develops a mild peak as compared to HB4. As with the strain profiles in Test Pile T1, the curvatures roughly mirror each other, with HB1/2 displaying positive curvature with a peak strain on HB1 of 600 με at a depth of 9.2 feet below the top of casing. HB3/4 display negative curvature in the same area with a local minimum strain of 178 με at a depth of 9.2 feet below the top of casing. The cause of the difference in strain between the sides of the pile are likely due to bending within the pile introduced during the load test. Looking at the residual strains in Figure 6-21 after the load on the pile has been removed, there is still a significant spread in the strains within the pile, with HB2 displaying strains of approximately 200 με between 15 and 25 feet below top of casing.

In addition to the distributed fiber optic strain measurements, strain measurements were also taken on the point-based FBG sensor string installed on HB3. The strain development over time of the 10 discrete measurement points is shown below. The sensor labels count up with depth from top to bottom, with FBG11 at 6.3 feet below the top of casing and FBG20 at the base of the pile at approximately 35.8 ft below the top of casing. Figure 6-22 shows the changes in FBG strains with time.
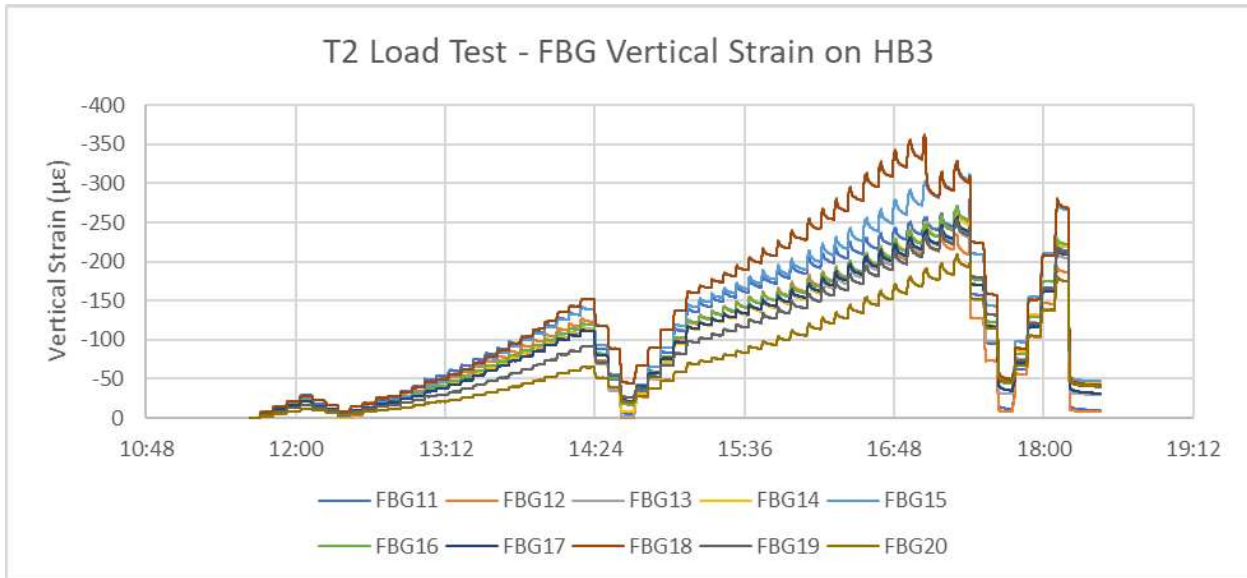
Figure 6-22: T2 load test FBG fiber optic strain readings over time

For comparison, the development of strain in the FBG sensor at approximately 9.5 feet below the top of casing is shown with the corresponding measurement from the distributed fiber optic reading at the same point, as shown in Figure 6-23. The distributed vertical strain is from the individual cable section installed on the same HB3 bar as the FBG sensor string.
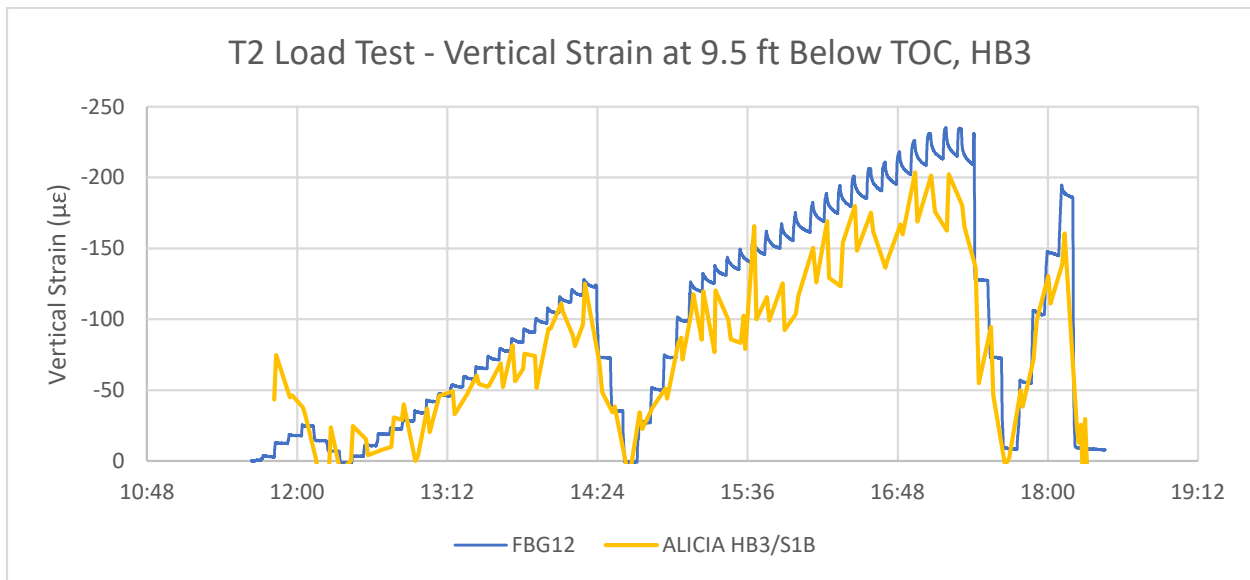
Figure 6-23: Point and distributed T2 vertical strain at 9.5 ft below top of casing over time

The FBG data shows much finer time and strain sensitivity. The Micron Optics analyzer was sampling at a 1 second interval, with a strain resolution of under 1 με. This allows the individual

142

peak and decay within each load interval to clearly be seen in the shape of the plotted data, with the peak and decay becoming more pronounced at the higher load intervals. The distributed fiber optic data follows the same trend but the noise previously discussed within the linear portions of the data cause the data to fluctuate above and below the likely "true" strain value at the same reading times. In general, the distributed fiber optic readings closely followed the FBG strain readings, with a slight deviation observed in the final load cycle of approximately 20-30 με. The strain readings with depth for the FBG string and the corresponding distributed readings at the maximum load interval are presented in Figure 6-24.
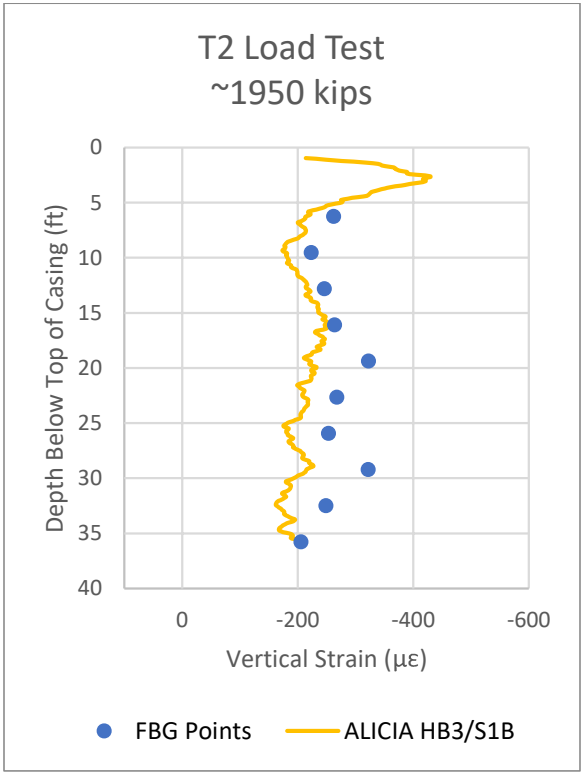
Figure 6-24: Point and distributed T2 vertical strain with depth at 1950 kips

As with the time-series plot of the comparable strains at 9.5 feet in Figure 6-23, the strains in Figure 6-24 show a similar strain shape between the FBG and distributed readings, with the FBG strains generally having a larger magnitude than the distributed readings from ALICIA at the same depth.

c) Pile T3, Open-Type (tube-à-manchette)

143

Pile T3 was load tested on March 4, 2019. The pile was base grouted using tube-à-manchette. Four load cycles were completed in approximately 8.5 hours. The recorded load time history forT3 load test, total load (sum of 4 individual load cells) over timeis shown in Figure 6-25. The maximum load peaks of the individual cycles were 200, 1150, 2027, and 1600 kips.
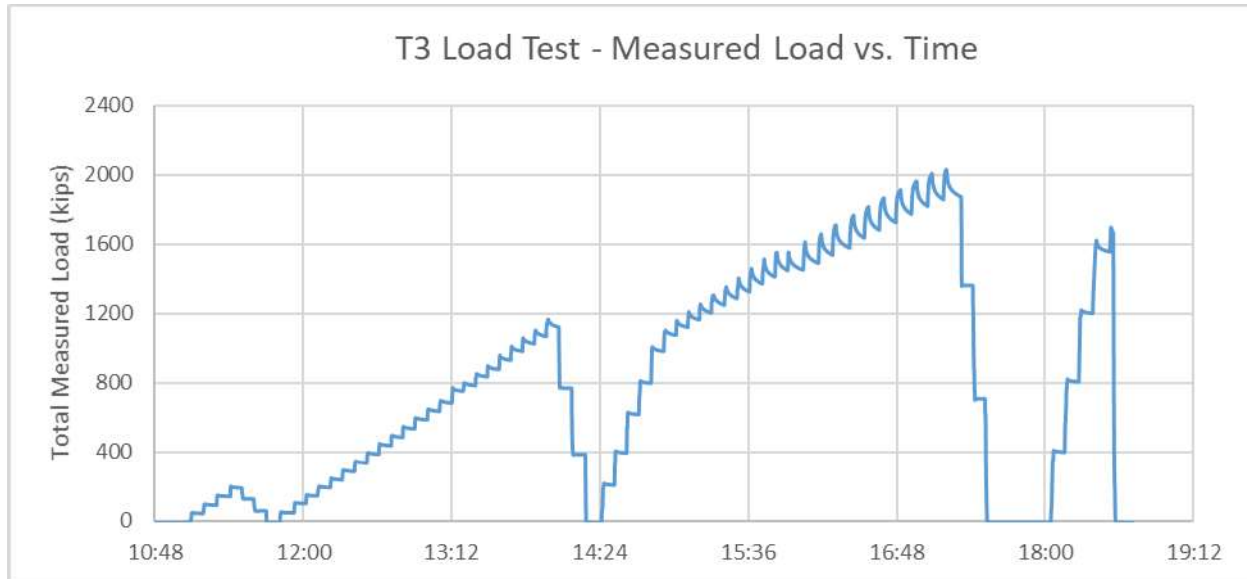
Figure 6-25: T3 load test, total load (sum of 4 individual load cells) over time

The fiber optic readings during the load test were taken in BOTDA mode (full loop) using the Omnisens analyzer. A total of 60 distributed fiber optic readings were taken prior to, during, and after the load test. Each reading interrogated both the strain and temperature loops of the test pile, as well as the four connected reaction piles (in order: T3, R5, R8, R9, R2). The raw frequency plot is presented in Figure 6-26. Focusing on the test pile, the fiber optic record was divided into the vertical strain and temperature loops, as shown in Figure 6-27.
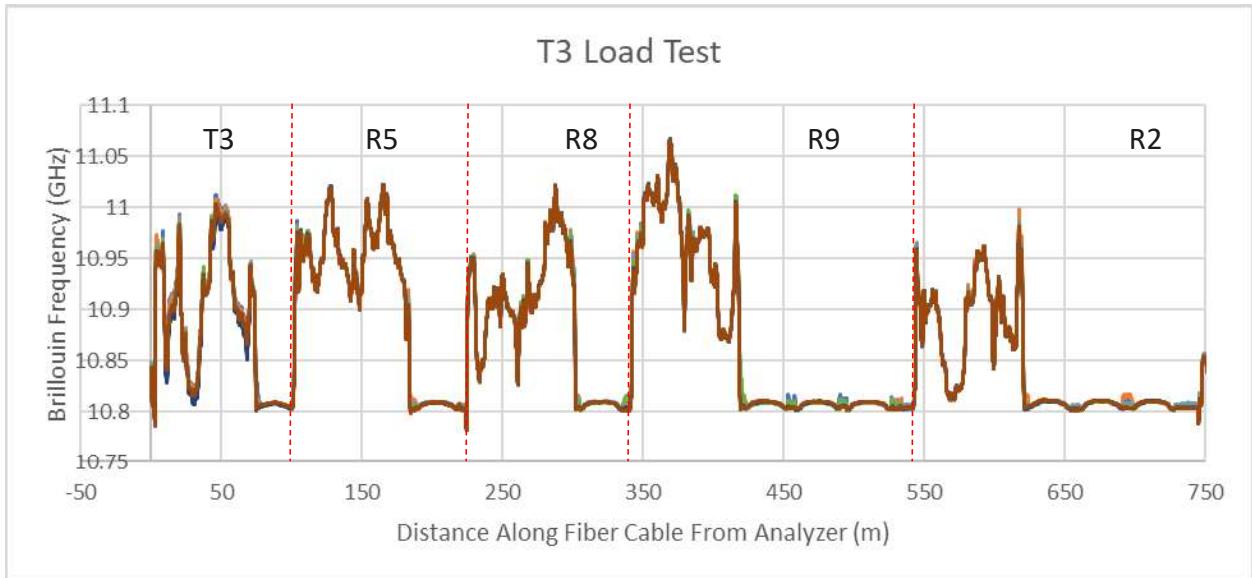
Figure 6-26: T3 load test, raw Brillouin frequency over all piles
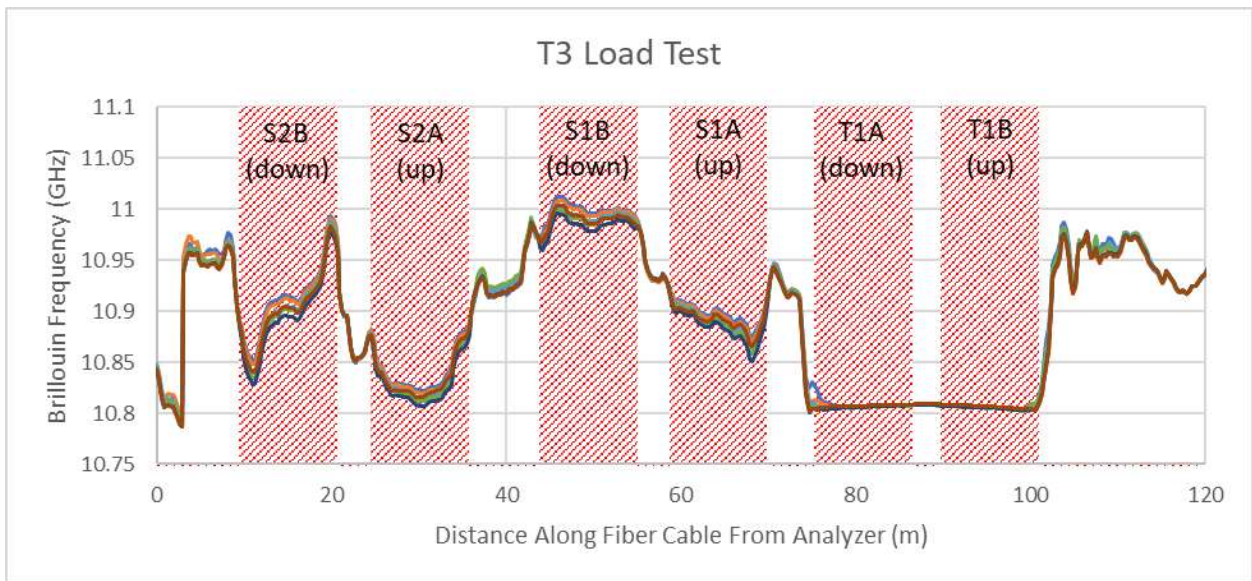
Figure 6-27: T3 load test, raw Brillouin frequency within pile T3

The development of strain over time at 7.5 feet below the top of casing in all four verticals, as well as the average strain, are shown in Figure 6-28. The distributed fiber optic record stops just prior to the penultimate unload. This is due to the fiber optic cable between R5 and R8 being severed as the reaction frame settled back to the ground as the load was released. Since no BOTDR (single-ended) baseline was taken prior to the load test, further readings in the final reload were taken but cannot be directly compared to the earlier record. Comparing the BOTDA

145

record up to the point of the fiber optic cable break, the results are generally comparable to the BOTDR readings taken on T1 using the Omnisens analyzer and are less noisy than the BOTDR readings taken on T2 using the ALICIA analyzer.
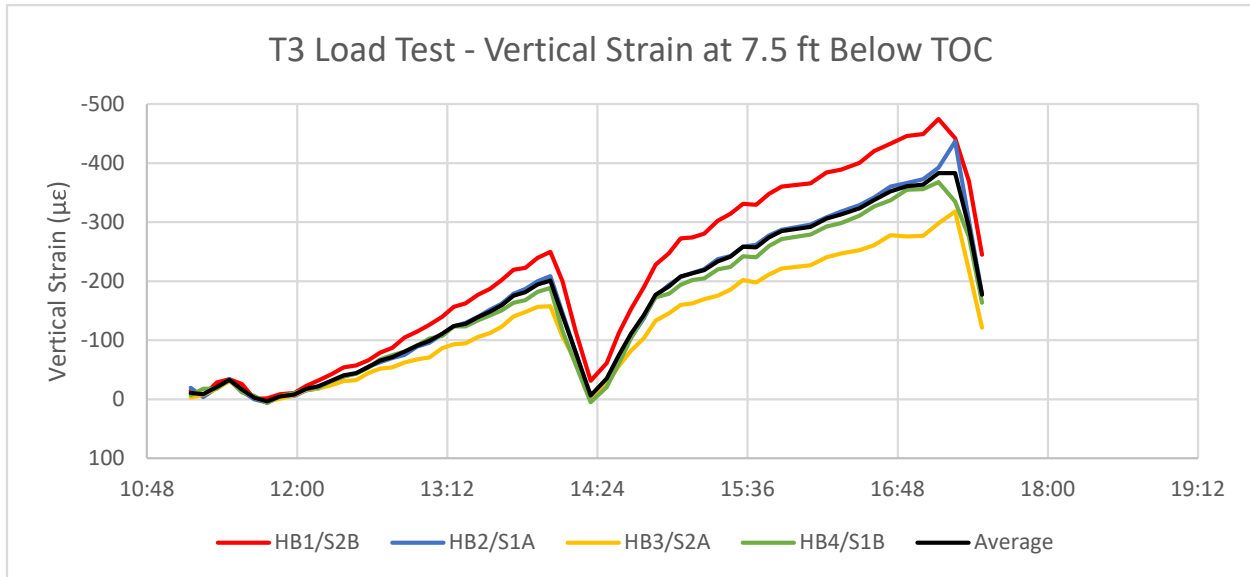
Figure 6-28: T3 vertical strain at 7.5 ft below top of casing over time

A difference between the strain in the sides of the piles can be observed in the spread in the strain data in Figure 6-28. HB1 experienced the highest strain during the load test, while HB3 opposite it experienced the lowest. On the perpendicular axis, HB2 and HB4 were centered close to the average, indicating that the direction of the asymmetry was close to the HB1-HB3 line.

The development of strain within the pile over 6 loading increments (500 kips, 1150 kips, 1150 kips reload, 1500 kips, 2027 kips, and the final reading before the cable breakage at 700 kips) are presented in Figure 6-29 through Figure 6-34. As with the readings in T1, the presented load is approximate due to the deviation in the applied load from the "target" load and the variable load decay during the 5-minute fiber optic reading.
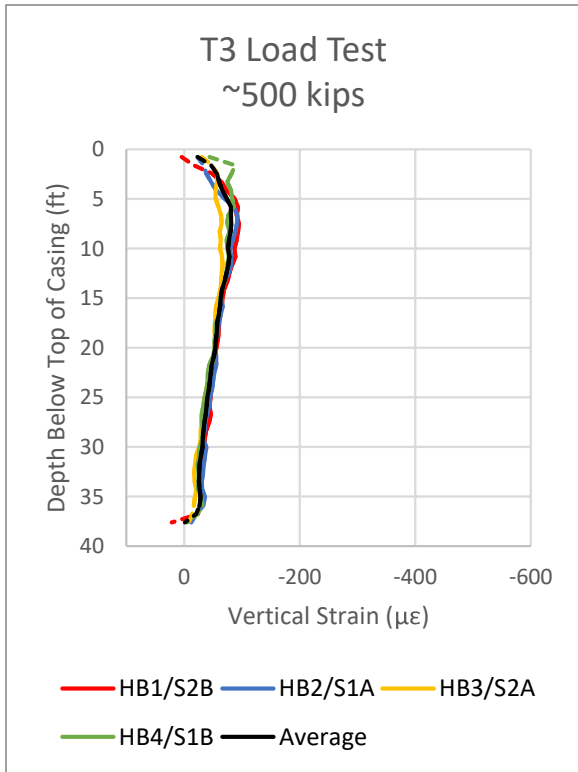
Figure 6-29: Vertical strain profile at ~500 kips load
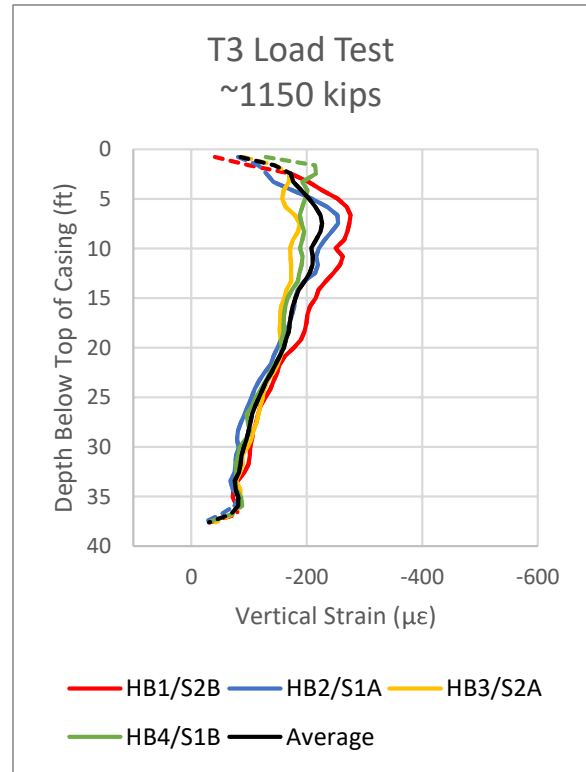
Figure 6-30: Vertical strain profile at ~1150 kips load
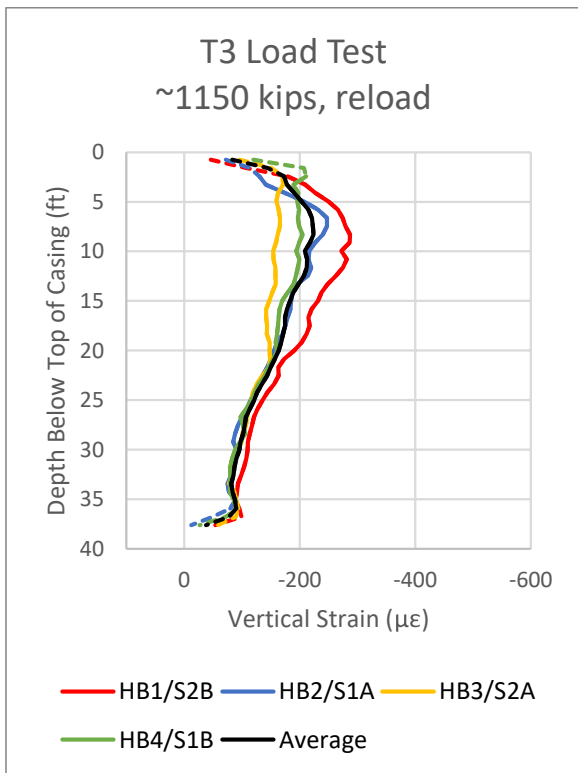
Figure 6-31: Vertical strain profile at ~1150 kips reload
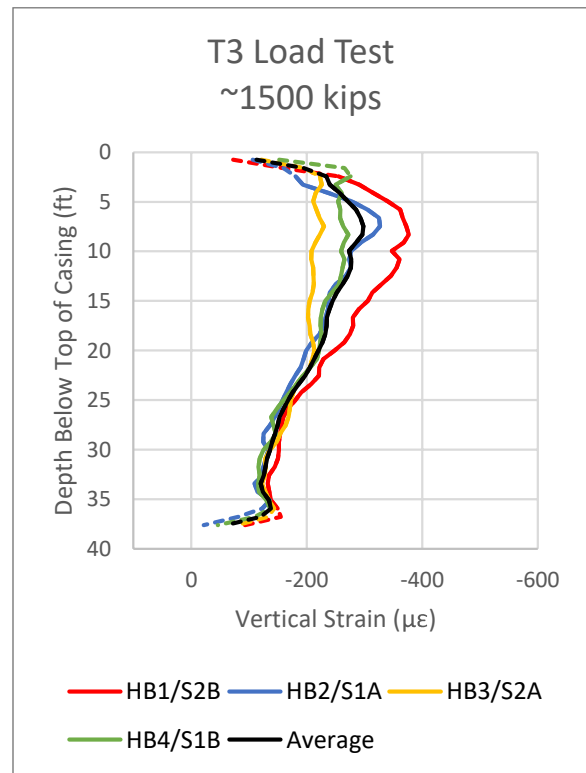
Figure 6-32: Vertical strain profile at ~1500 kips load
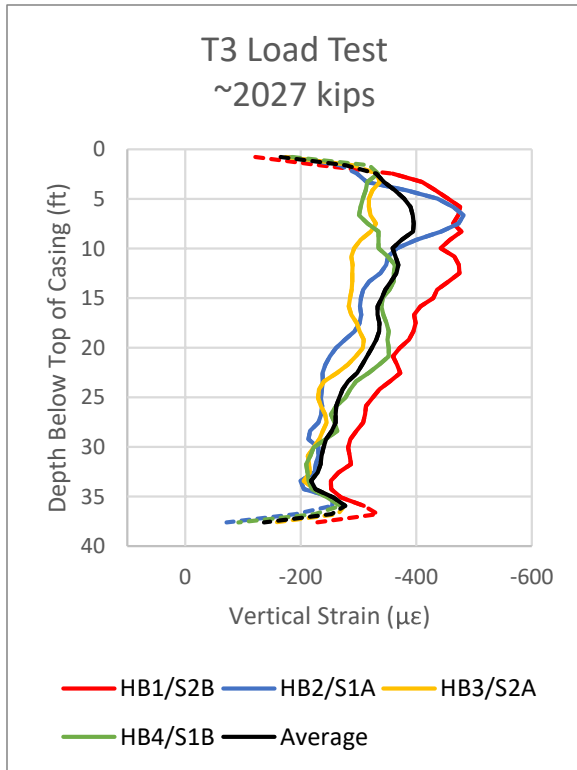
Figure 6-33: Vertical strain profile at ~2027 kips load   Figure 6-34: Vertical strain profile at ~700 kips unload
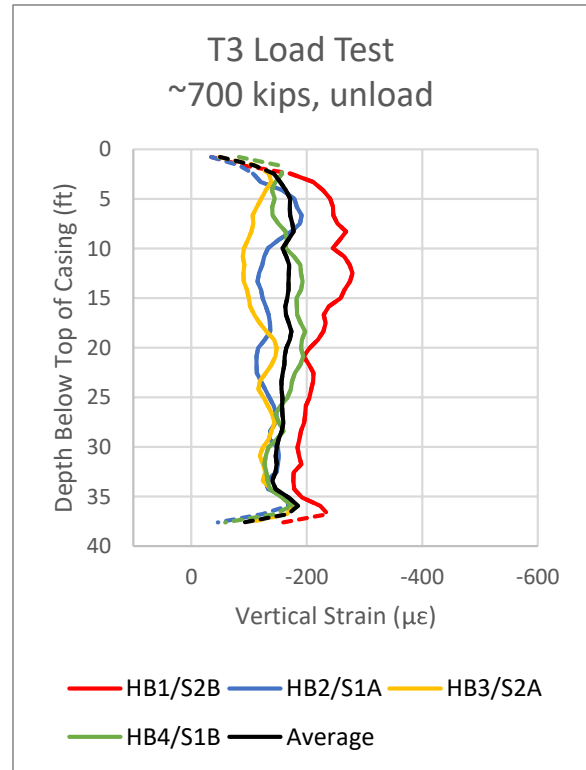
In comparison to the strain profiles in piles T1 and T2, the strain differential across the pile in T3 is of a much lower magnitude. The separation in strain is not apparent in Figure 6-29 at the 500 kip interval. The separation begins to appear in Figure 6-30 at 1150 kips, although the magnitude is relatively low compared to the results from the other test piles. The separation grows slightly in magnitude in the subsequent figures to the maximum load interval of 2027 kips in Figure 6-33. The strains in HB1 show a positive curvature, developing to a maximum strain of 474 με at 7.4 feet below the top of casing. The strains in HB3 do not display a clear negative curvature in the same depth, slowly decreasing in compressive strain linearly from 330 με at 7.5 feet to 297 με at 17.5 feet below the top of casing. The relatively small spread between the maximum and minimum strains and the lack of clear curvature symmetry implies that the bending in T3 during the load test was of a lower magnitude than that observed in piles T1 and T2.

d)   Pile T4, Closed-Type (bladder)

Pile T4 was load tested on February 21, 2019. The pile was base grouted using the bladder system. Four load cycles were completed in just over 7 hours. The recorded load time history for total load (sum of 4 individual load cells) is shown in Figure 6-35. The maximum load peaks of the individual cycles were 200, 1050, 1750, and 1600 kips.
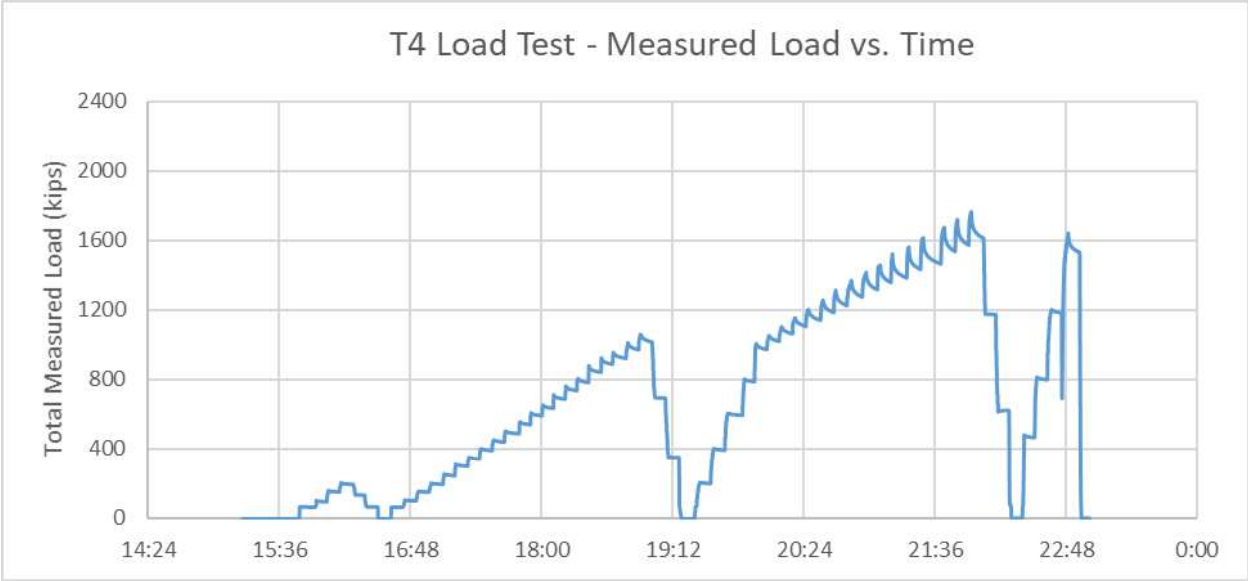
Figure 6-35: T4 load test, total load (sum of 4 individual load cells) over time

The fiber optic readings during the load test were taken in BOTDA mode (full loop) using the Omnisens analyzer. A total of 62 distributed fiber optic readings were taken prior to, during, and after the load test. Each reading interrogated both the strain and temperature loops of the test pile, as well as the four connected reaction piles (in order: T4, R4, R7, R8, R6). The raw frequency plot is presented in Figure 6-36. Focusing on the test pile, the fiber optic record was divided into the vertical strain and temperature loops, as shown in Figure 6-37.
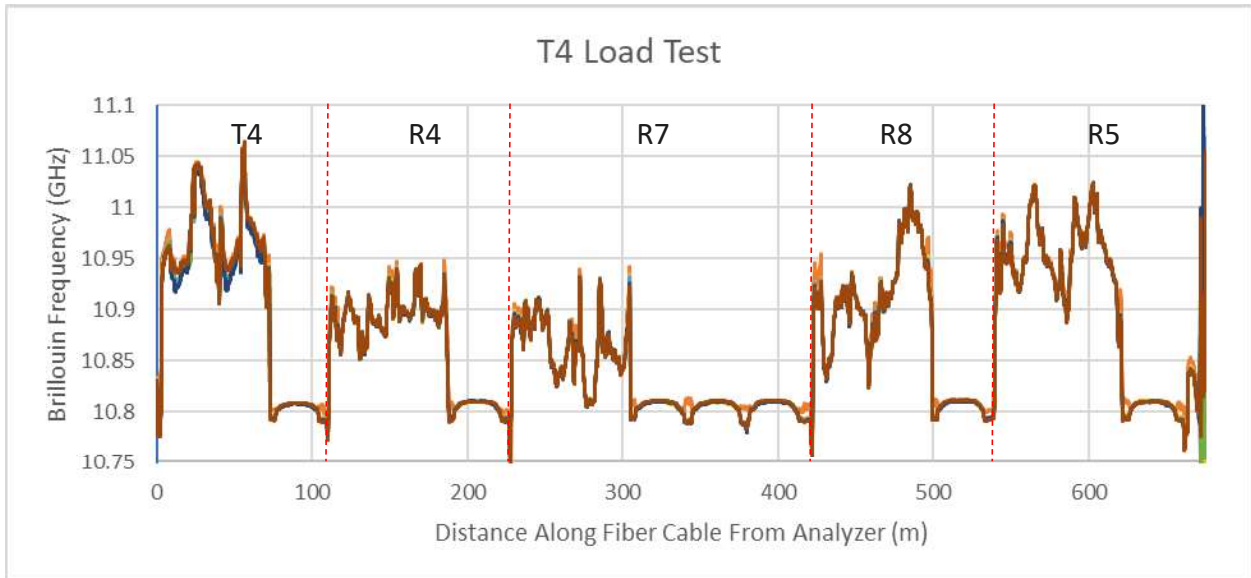
Figure 6-36: T4 load test, raw Brillouin frequency over all piles
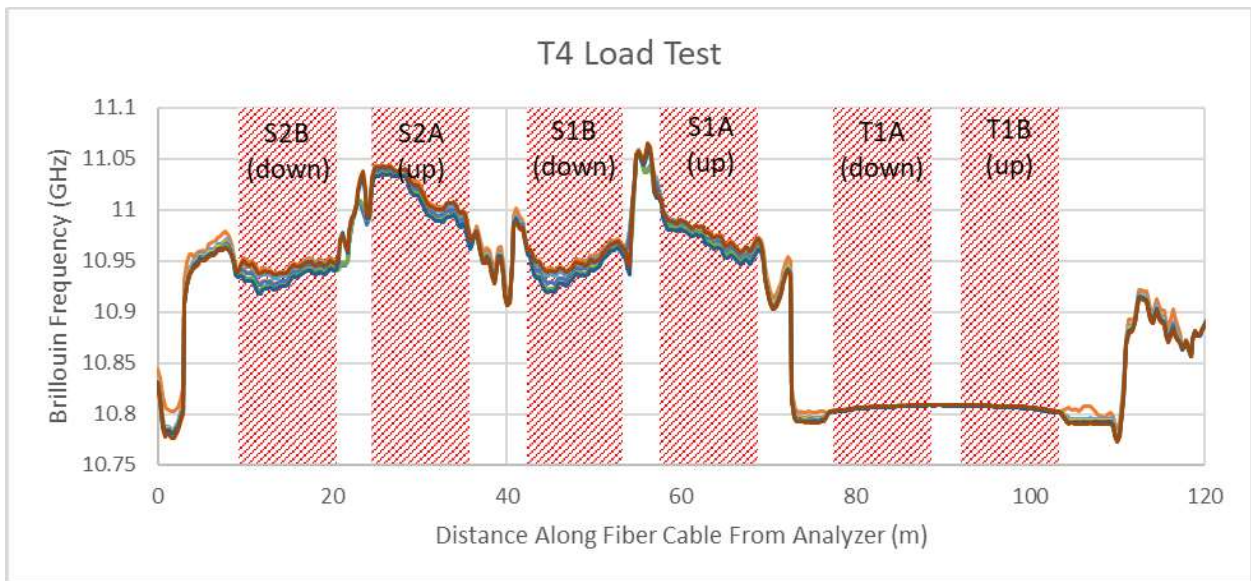
Figure 6-37: T4 load test, raw Brillouin frequency within pile T4

The development of strain over time at 7.5 feet below the top of casing in all four verticals, as well as the average strain, are shown in Figure 6-38. A difference in the strain across the pile can be observed from the spread in the strain data. HB2 and HB3 experienced the highest strain during the load test, while HB1 and HB4 on the opposite side experienced the lowest. The magnitudes of the strains observed on the coordinating pairs of bars were relatively close to

each other, indicating that the axis of asymmetry was approximately between HB2/3 and HB1/4, passing between each of the adjacent bar pairs.
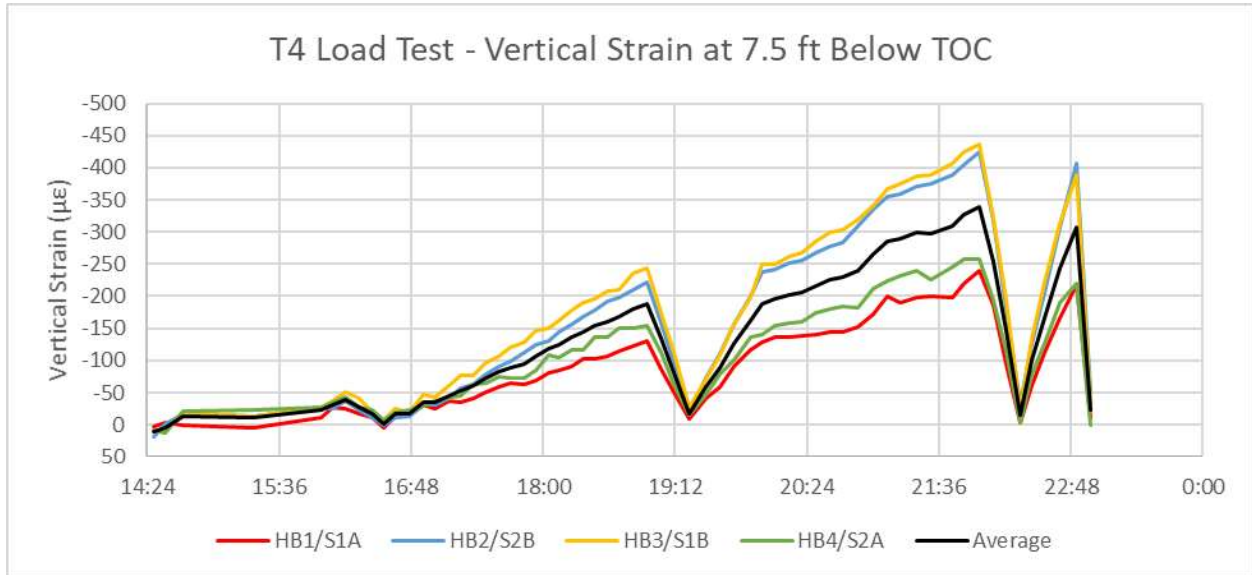
Figure 6-38: T3 vertical strain at 7.5 ft below top of casing over time

The development of strain within the pile over 6 loading increments (500 kips, 1050 kips, 1050 kips reload, 1500 kips, 1750 kips, and the final unload) are presented in Figure 6-39 through Figure 6-44. As with the readings in T1 and T3, the presented load is approximate due to the deviation in the applied load from the "target" load and the variable load decay during the 5-minute fiber optic reading.
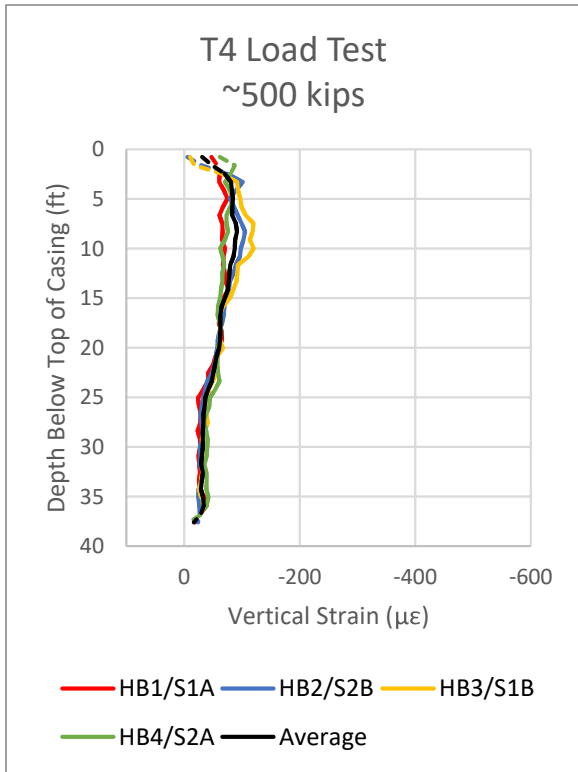
Figure 6-39: Vertical strain profile at ~500 kips load
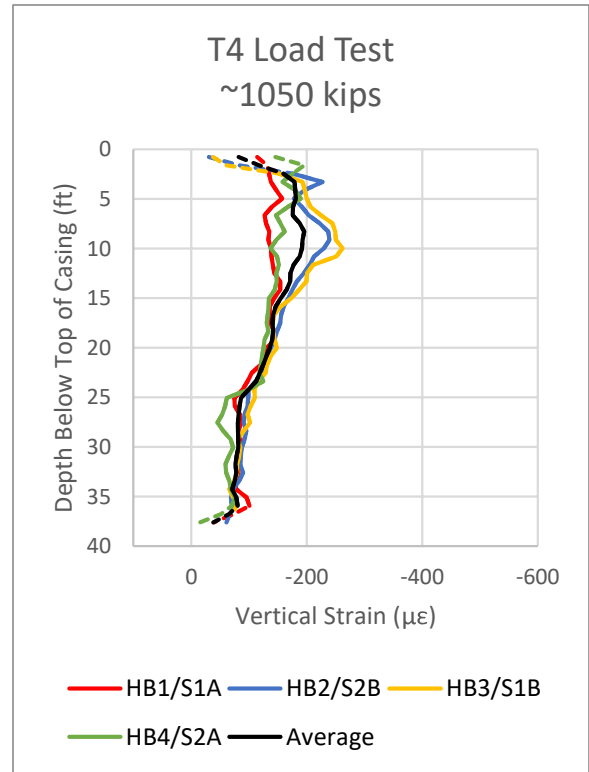
Figure 6-40: Vertical strain profile at ~1050 kips load
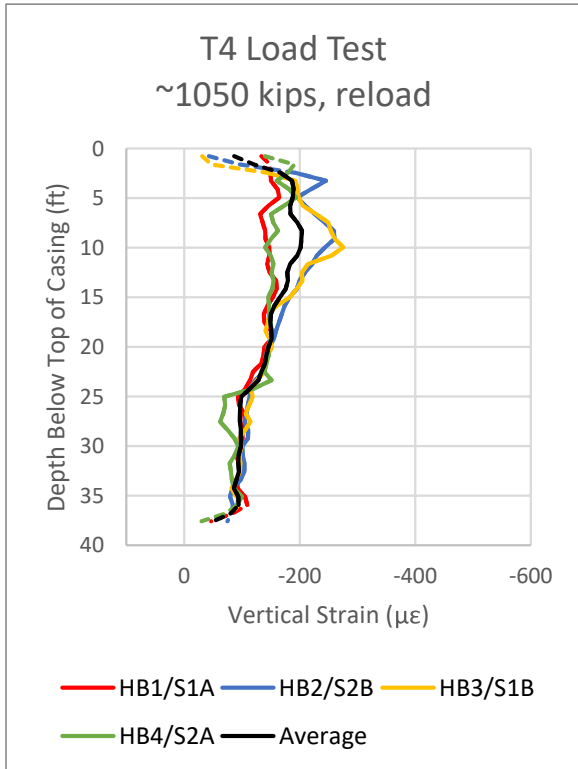
Figure 6-41: Vertical strain profile at ~1050 kips reload
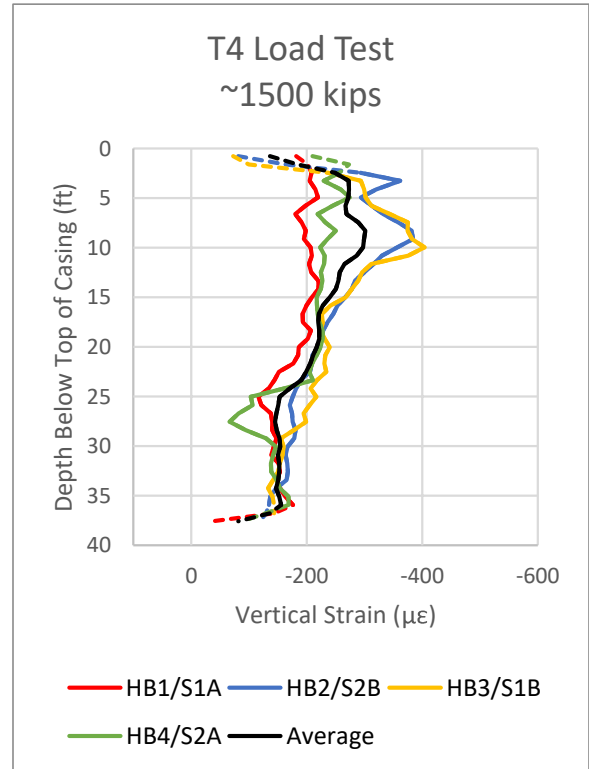
Figure 6-42: Vertical strain profile at ~1500 kips load

152
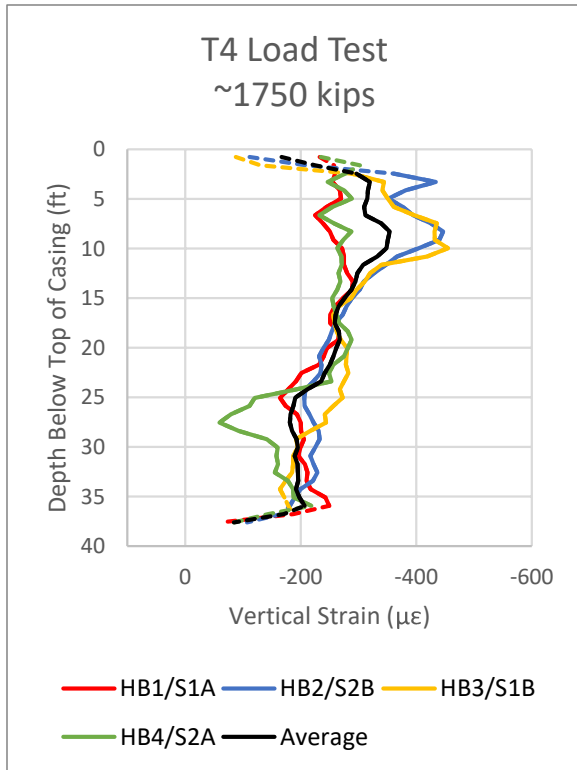
Figure 6-43: Vertical strain profile at ~1750 kips load
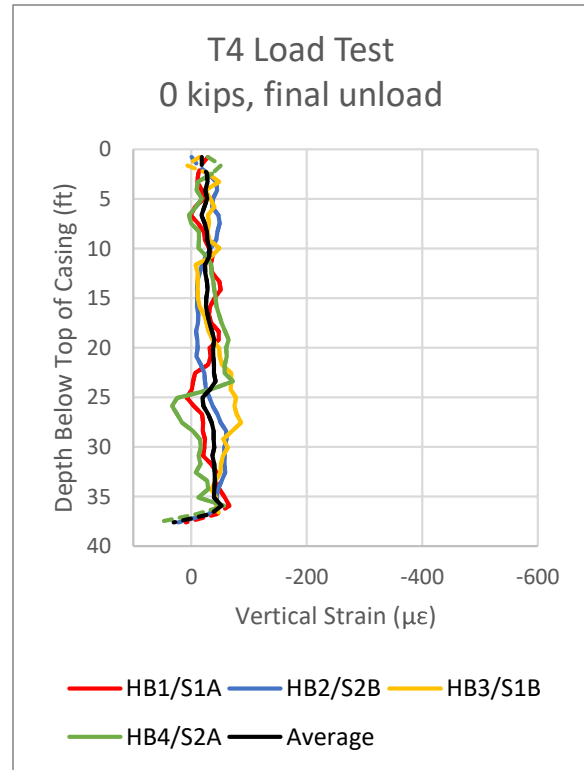
Figure 6-44: Vertical strain profile at 0 kips unload

At the 500 kip interval in Figure 6-39, a small separation in the strain between HB2/3 and HB1/4 can be observed in the top 15 feet of the pile. The separation grows in magnitude in the subsequent figures, peaking at the maximum load interval of 1750 kips in Figure 6-43. The shape and magnitude of the HB2 and HB3 strain curves are similar through all of the loading intervals with a positive concavity and a peak strain of 455 $\mu\varepsilon$ on HB3 at a depth of 10 feet below top of casing. Likewise, the shape and magnitude of HB1 and HB4 are also similar through the maximum load, displaying a slight negative concavity above 15 feet below top of casing. A semi-defined negative peak is observed at 6.6 feet below top of casing with a magnitude of 232 $\mu\varepsilon$. Due to the lack of a well-defined peak on the HB1/4 pair, the symmetry is not as pronounced as that observed on test piles T1 and T2. It is therefore likely that, as with T3, there was less bending introduced into T4 during the load test. The average strain in Figure 6-44 after removal of the load show a residual strain of approximately 30 $\mu\varepsilon$.

Summary

A brief summary of the fiber optic strain data from the load test is presented below.

153

- Non-uniform strains around the cross section of the pile were observed in all the tests. Based on the shape of the strain profiles, this is likely due to bending forces being introduced into the pile during the load test. In most cases, the strongest differential was confined to the top 20 feet of the pile.
- Comparing the average strain at the bottom of the "main" fiber optic profile in each pile (the final section of the solid line before spatial resolution from the base could affect the reading), the strain values were in the range of 190 – 277 με. The actual values are listed in Table 6-1.

Table 6-1: Load test final load and base strain

Pile	Grout System	Final Load	Final Base Avg. Compressive Strain
T1	None	~1750 kips	191 με
T2	RIM Cell	~1950 kips	239 με
T3	Open-type	~2027 kips	277 με
T4	Closed-type	~1750 kips	207 με

- Of the piles with a final reading at 0 kips, all the readings showed average residual strains with a value on the order of 30-50 με.

7. Discussion

Following the completion of the lab and field testing, three topics were identified as requiring further discussion. These include a direct comparison in the strain measurements between the distributed fiber optic system and the conventional vibrating wire strain gauges (SG), an evaluation of the magnitude of the strain-shift in the fiber optic data caused by the changing strains during the reading interval, and a framework specification for distributed fiber optic monitoring for piles.

Strain Measurement Comparison Between DFOS and VWSG

Six levels of vibrating wire strain gauges were included in each of the project test shafts, installed and read by the University of Missouri team. The quantity and plan location varied between the levels and did not directly correspond to the four verticals of distributed strain fiber optic cable. The levels, number of sensors, and average depth are presented in Table 7-1. Note that the average depth is an average between the four test shafts – within each given test shafts all strain gauges for each level were installed at the same depth.

Table 7-1: Test pile vibrating wire strain gauge levels

Level	Number of SGs	Average Depth, ft. BTOC
1	4	36.6
2	3	30.9
3	3	23.9
4	3	17.0
5	3	10.0
6	2	1.9

Due to the variable strain changes within the pile observed during grouting, the strain comparison between the two measurement systems was performed on the data generated during load testing. Since the SGs and fiber optic strain cables were not installed in the same plan location within the piles, a direct comparison between the data at specific gauge locations is not possible. Instead, a comparison between all WGs and all four distributed strain fiber optic verticals is presented at the six representative load increments selected in the Results section

155

of Chapter 6. The average strain at each reading level between the two systems is separately plotted for each load increment.

a)   Test Pile T1, Control (no base grout)

The strain measurement results for the distributed fiber optic system and the SGs in pile T1 are presented in Figure 7-1 to Figure 7-12. Beginning in Figure 7-1, the spread of the individual SGs are approximately enveloped by the four fiber optic strain verticals. This trend continues in the other four load increments as well as the final unload reading presented in Figure 7-11. Of particular note are the low SG readings at 10.3 feet in the pile, most clearly apparent in Figure 7-7 and Figure 7-9. Absent the fiber optic data, it is plausible that this low data point may have been discarded as an invalid reading during evaluation of the strain data. However, the distributed strain readings of the fiber optic system show that this strain readings is valid and should be included in any subsequent evaluation of the pile load test. Turning to the plots of the measured strain average with depth, the two measurement sets show good agreement both in magnitude and the shape of the strain profile. Excluding readings at the bottom of the pile where the spatial resolution constraints of the fiber optic system affected the readings (represented by the dashed lines at the bottom of the pile), the maximum difference between the two averages was on the order of 30 $\mu\varepsilon$.
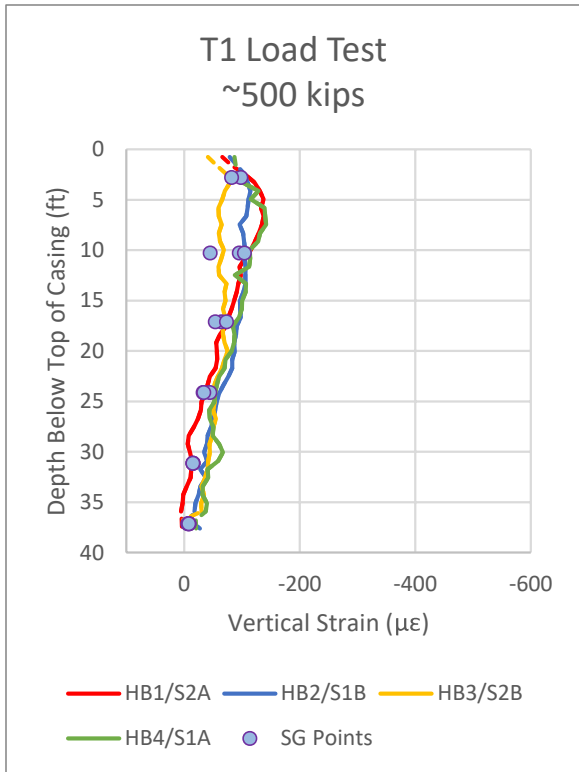
Figure 7-1: Vertical strain profile at ~500 kips load
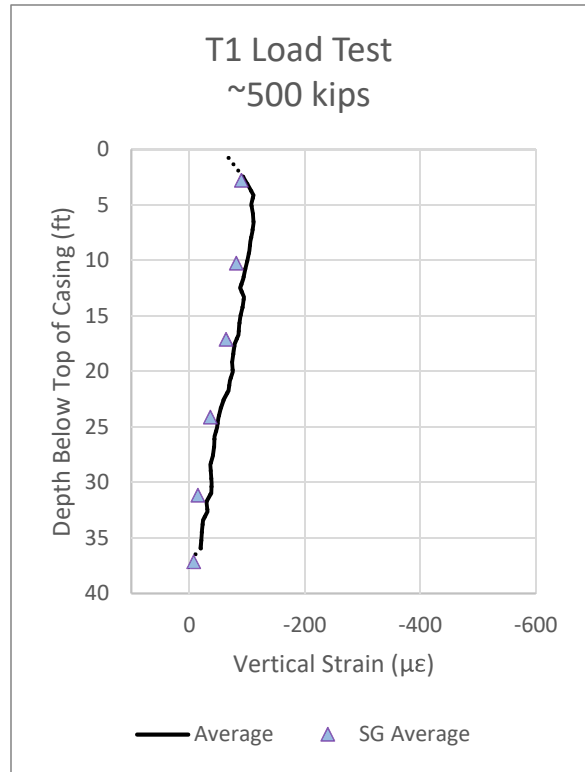
Figure 7-2: Average strain profile at ~500 kips load
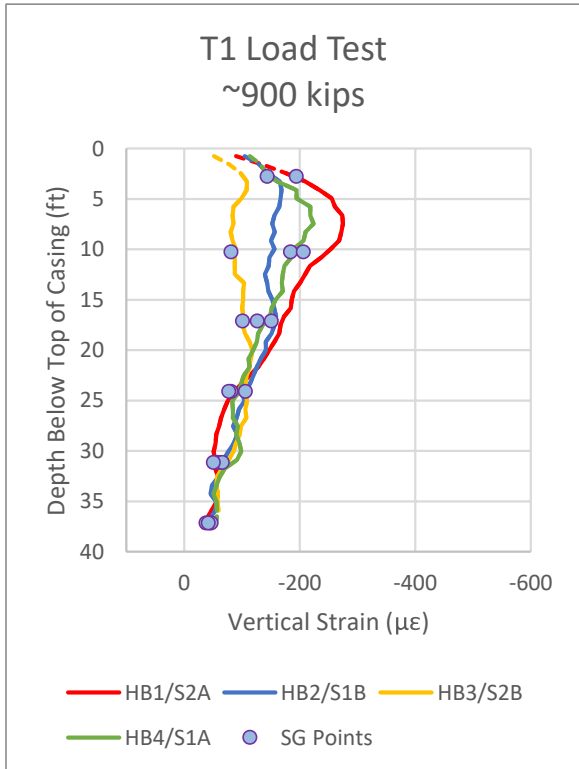
Figure 7-3: Vertical strain profile at ~900 kips load
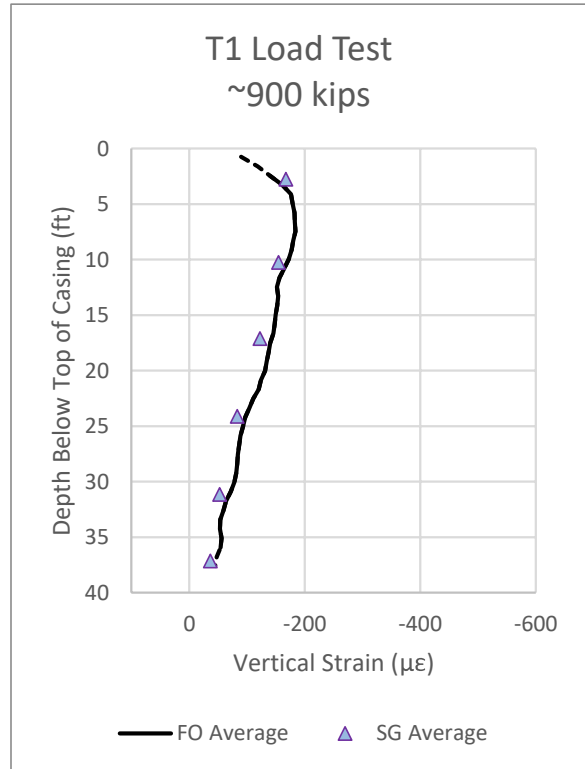
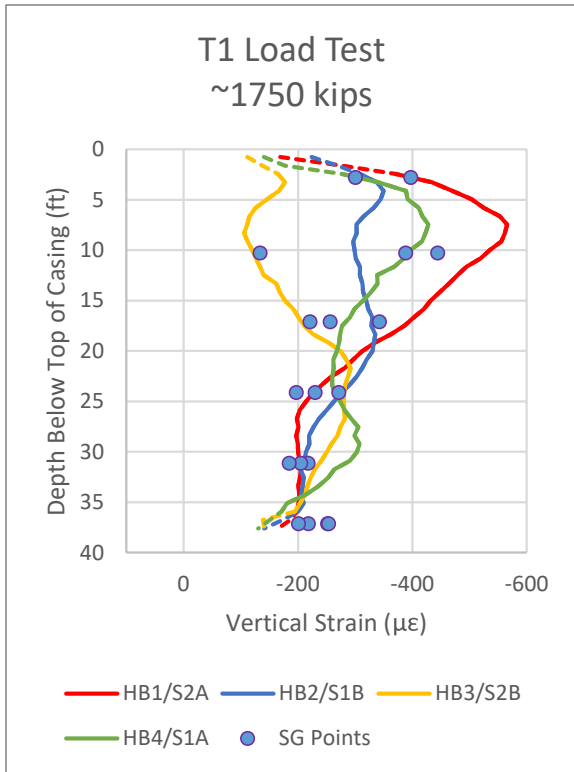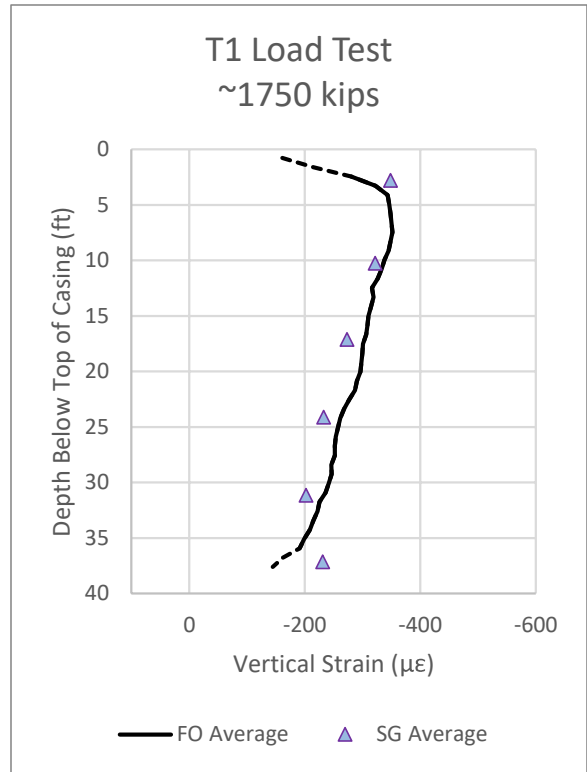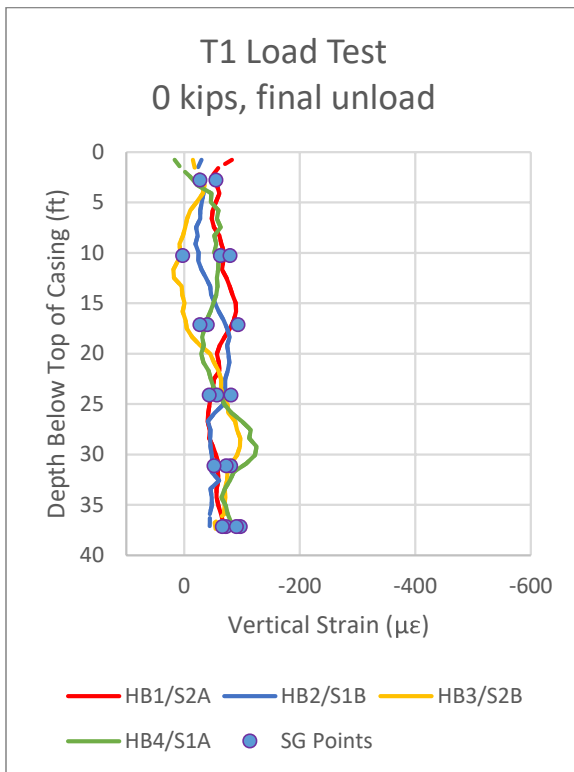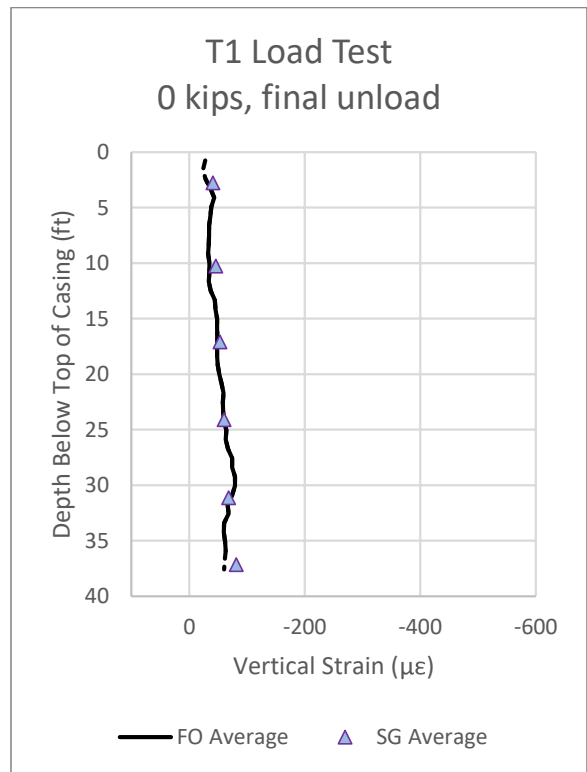*Figure 7-4: Average strain profile at ~900 kips load*

157
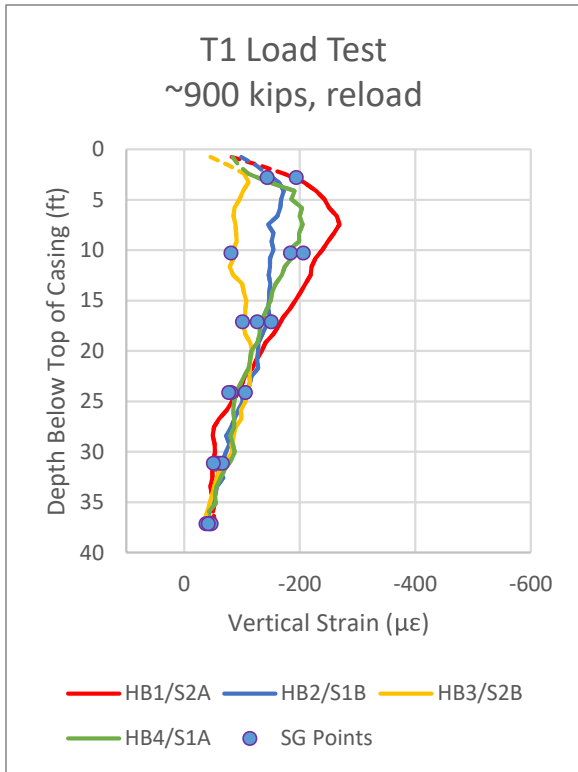
Figure 7-5: Vertical strain profile at ~900 kips reload
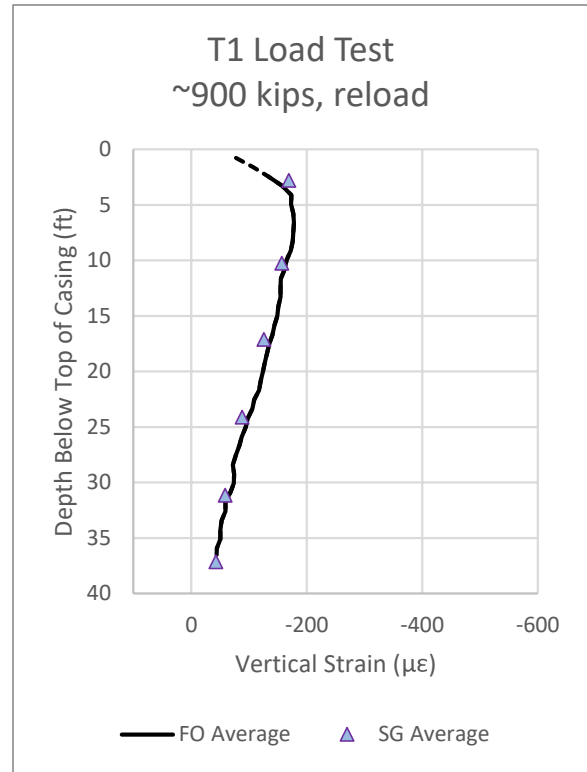
Figure 7-6: Average strain profile at ~900 kips reload
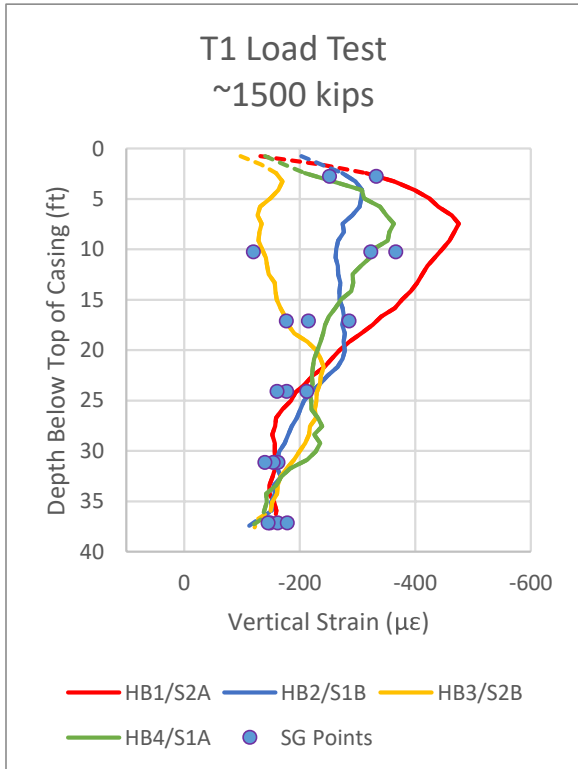
Figure 7-7: Vertical strain profile at ~1500 kips load
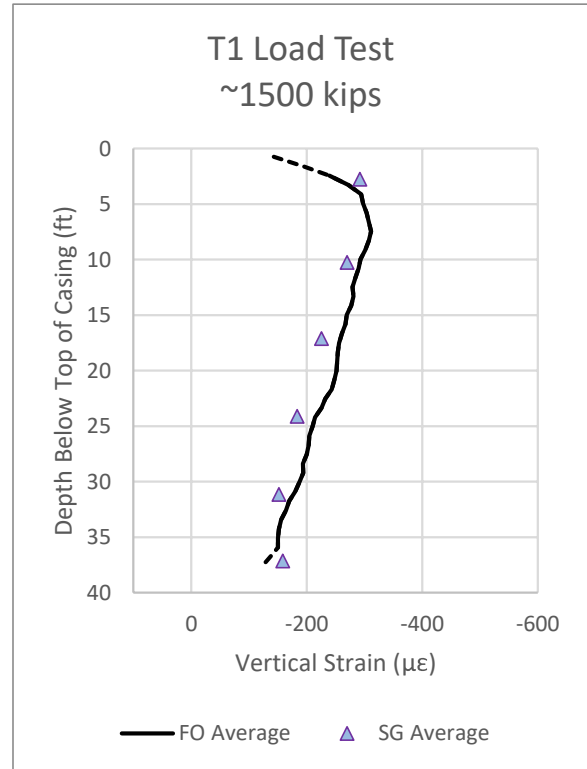
Figure 7-8: Average strain profile at ~1500 kips load

Figure 7-9: Vertical strain profile at ~1750 kips load

Figure 7-10: Average strain profile at ~1750 kips load

Figure 7-11: Vertical strain profile at 0 kips unload

Figure 7-12: Average strain profile at 0 kips unload

159

b) Test Pile T2, RIM Cell

The strain measurement results for the distributed fiber optic system and the SGs in pile T2 are presented in Figure 7-13 to Figure 7-24. Similar to the results from pile T1, the individual SG readings at each level are approximately enveloped by the four strain gauge verticals. It is noted that the peak strain values measured by the SG are lower than the highest readings in the fiber optic strands, a trend most apparent in Figure 7-21 at the peak load increment of ~1950 kips. This difference is also observed in the plots of the strain averages, where the SG readings are up to approximately 75 $\mu\epsilon$ below the corresponding fiber optic average. One potential explanation for this difference is that the plan orientation of the strain gauges within the pile were such that a gauge was not located on the axis of peak strain within the pile, likely associated with bending within the top portion of the pile. By being shifted off this axis, the SG readings would potentially register lower strains at each elevation within the top portion of the pile. A second potential cause of the difference could be an overestimation of the strain within the fiber optic cable due to an error with the ALICIA fiber optic analyzer. However, since the SG and fiber optic readings agree closer in value at the bottom portion of the pile, it is not thought that the ALICIA analyzer is the cause of the observed strian difference.
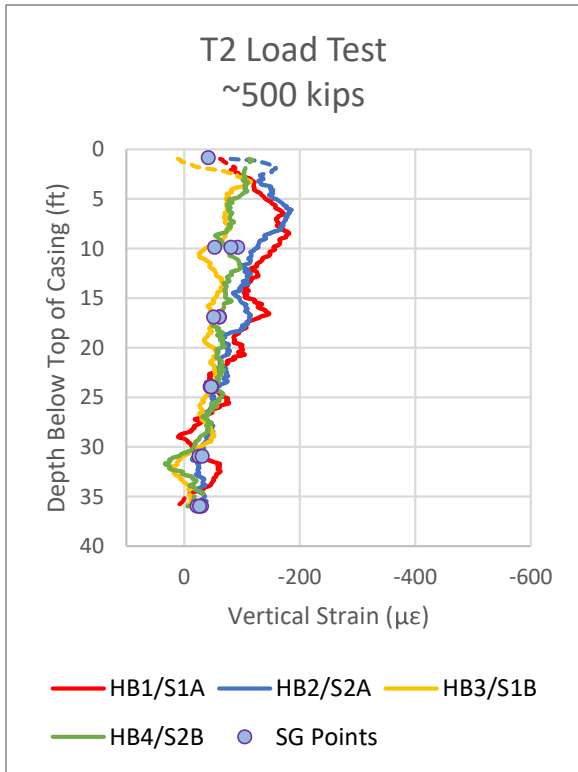
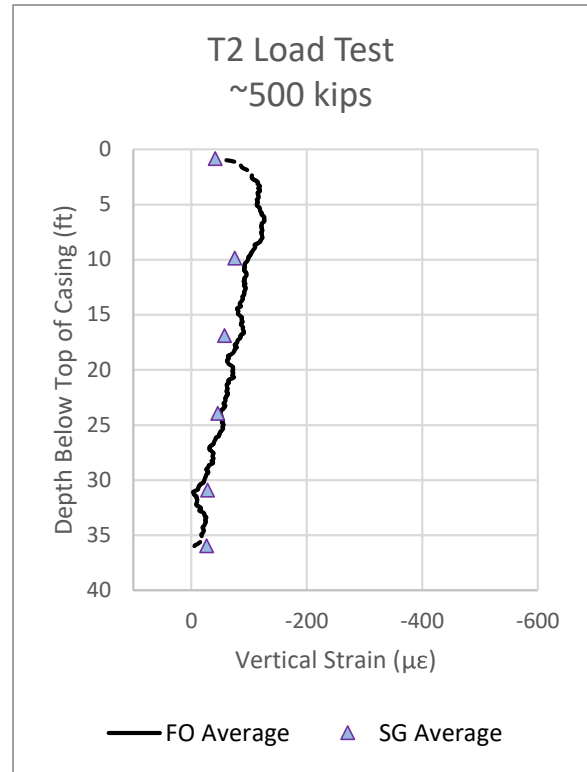Figure 7-13: Vertical strain profile at ~500 kips load

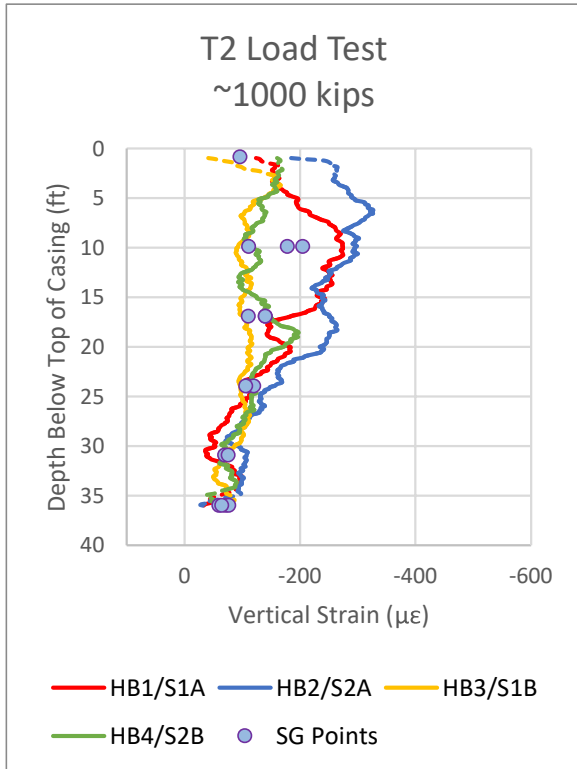Figure 7-14: Average strain profile at ~500 kips load

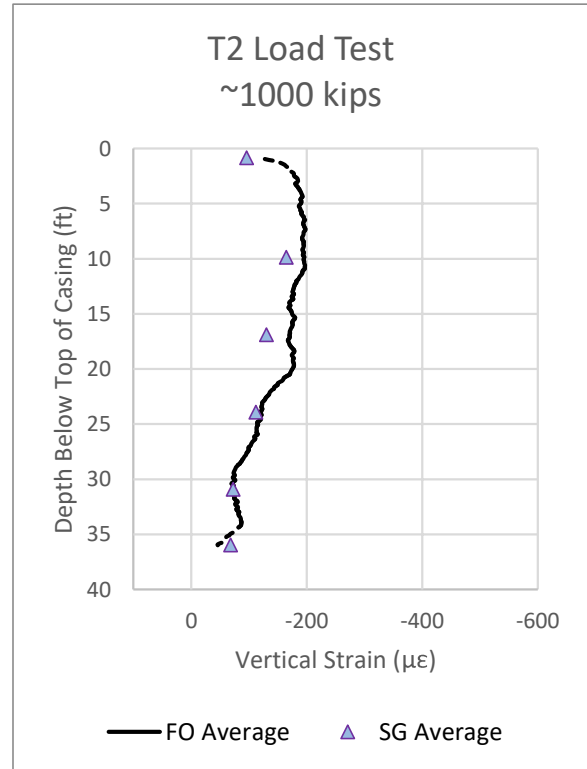Figure 7-15: Vertical strain profile at ~1000 kips load

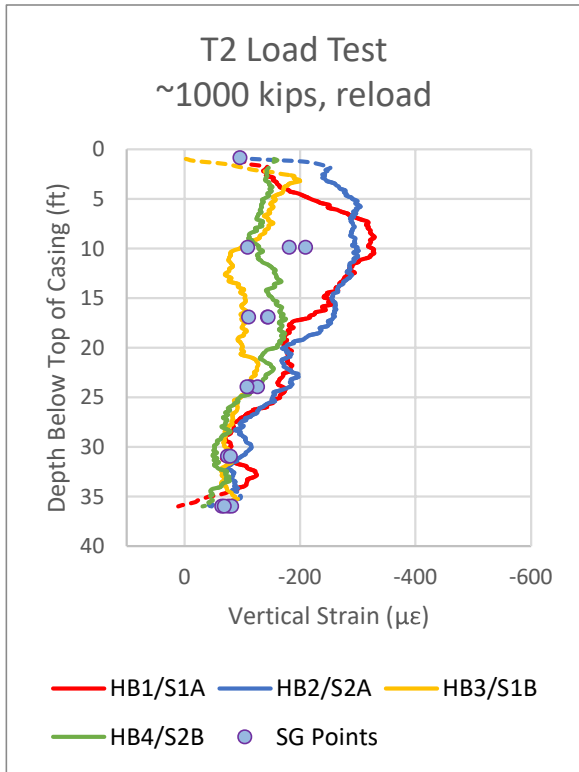Figure 7-16: Average strain profile at ~1000 kips load

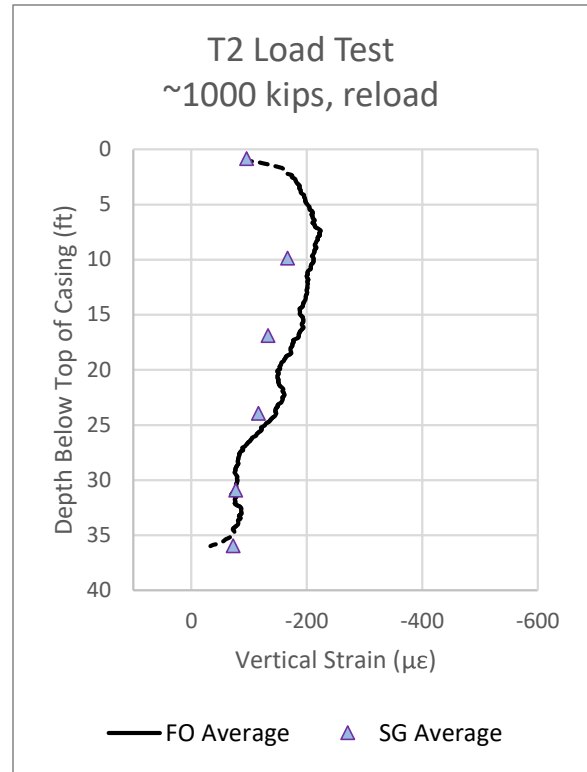*Figure 7-17: Vertical strain profile at ~1000 kips reload*

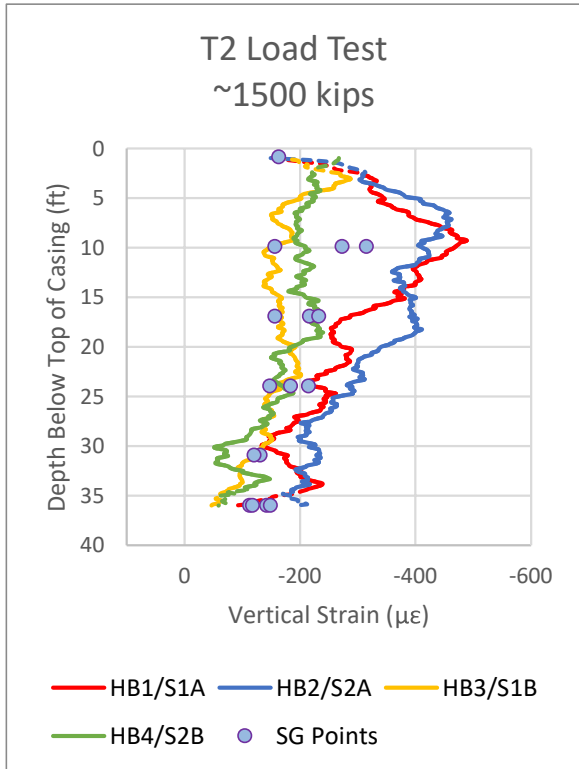*Figure 7-18: Average strain profile at ~1000 kips reload*

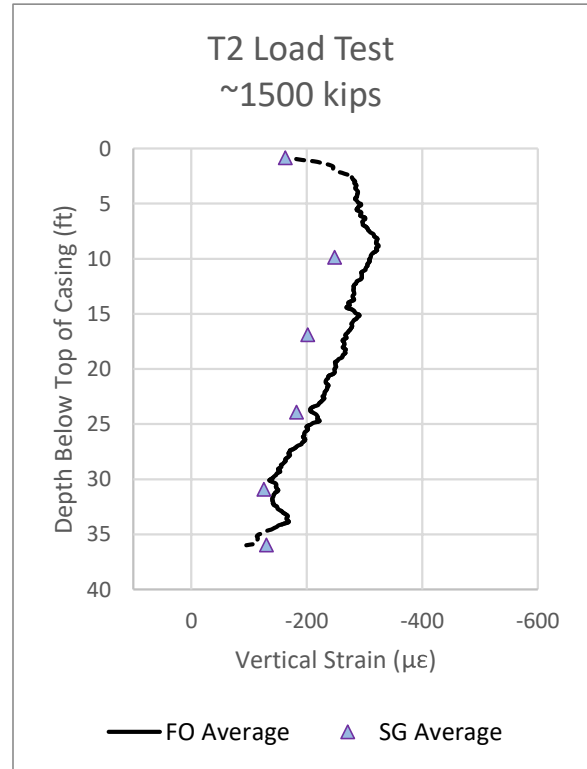*Figure 7-19: Vertical strain profile at ~1500 kips load*

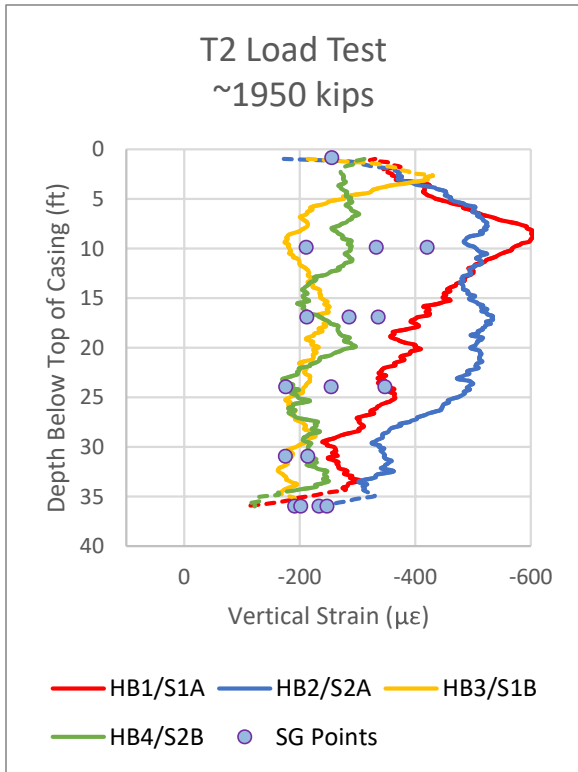*Figure 7-20: Average strain profile at ~1500 kips load*

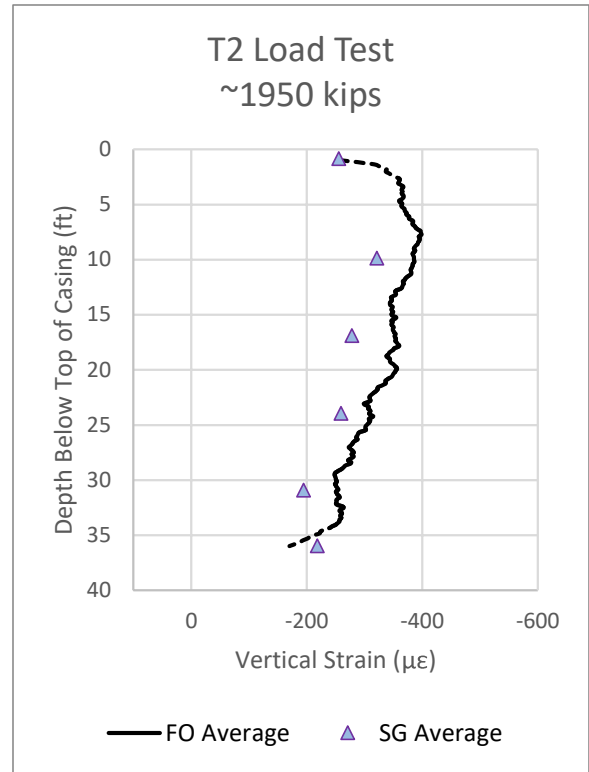Figure 7-21: Vertical strain profile at ~1950 kips load

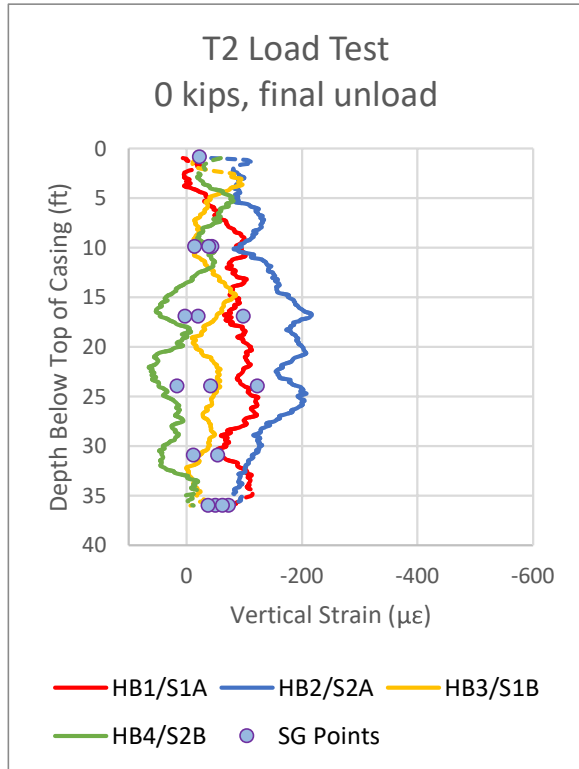Figure 7-22: Average strain profile at ~1950 kips load

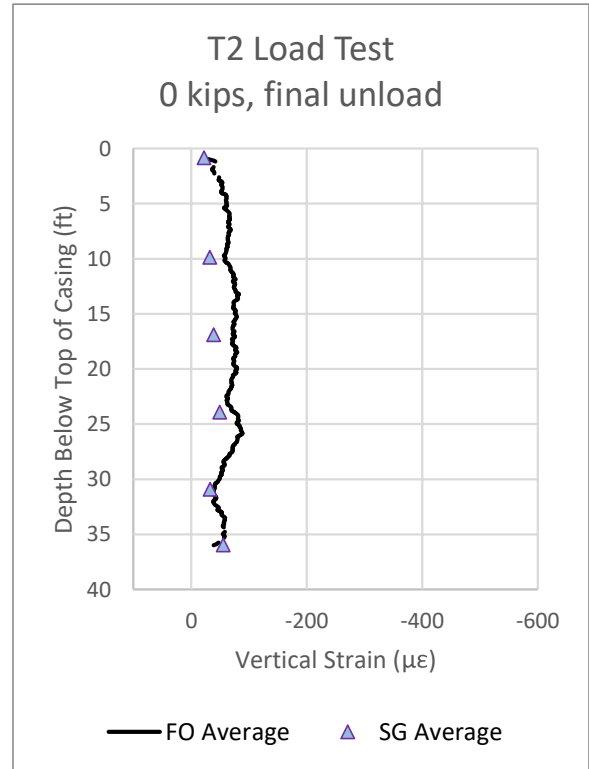Figure 7-23: Vertical strain profile at 0 kips unload

Figure 7-24: Average strain profile at 0 kips unload

c) Pile T3, Open-Type (tube-à-manchette)

The strain measurement results for the distributed fiber optic system and the SGs in pile T3 are presented in Figure 7-25 to Figure 7-36. Similar to the results from T1 and T2, the SG readings are approximately enveloped by the four fiber optic verticals. The range of strain magnitudes at each reading elevation between the two measurement systems are relatively similar, a trend most apparent at the peak load of ~2027 kips shown in Figure 7-33. Looking at the figures comparing the average strain with depth between the two systems, there is close agreement in both the magnitude and shape of the strain profile between the two systems. The maximum difference between the caluclated averages was approximately 20 µε, observed in the final profile in Figure 7-36 at ~700 kips during the unload just prior to the fiber optic cable being severed.
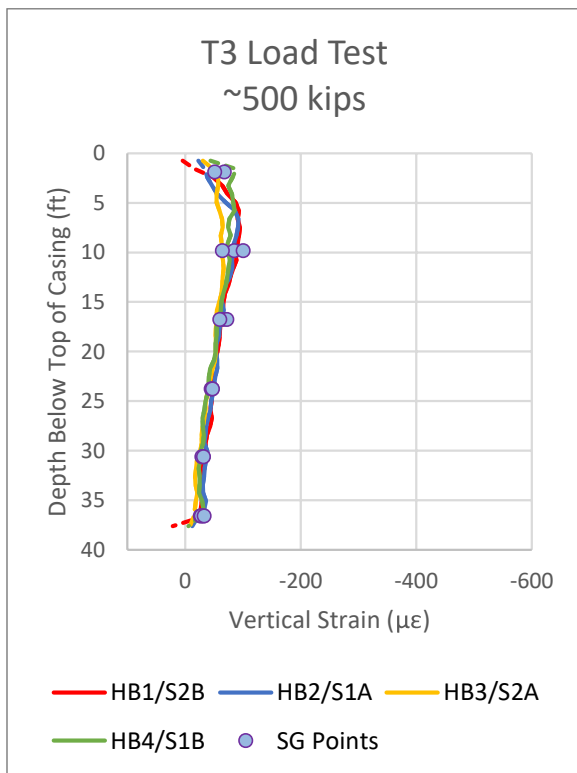

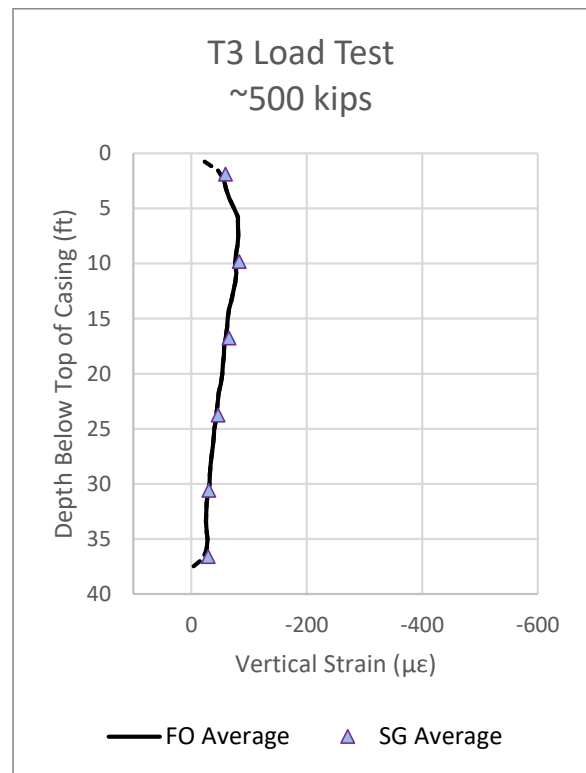Figure 7-25: Vertical strain profile at ~500 kips load

Figure 7-26: Average strain profile at ~500 kips load

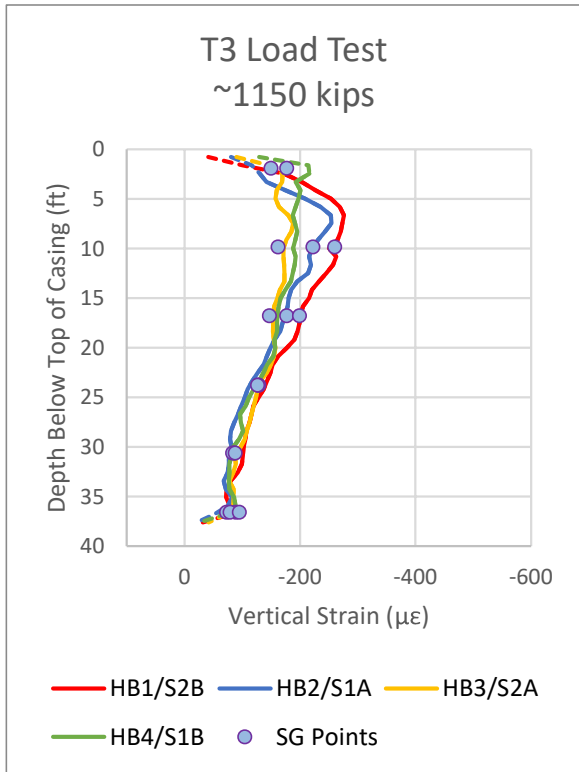*Figure 7-27: Vertical strain profile at ~1150 kips load*

Figure 7-28: Average strain profile at ~1150 kips load

Figure 7-29: Vertical strain profile at ~1150 kips reload

Figure 7-30: Average strain profile at ~1150 kips reload

165

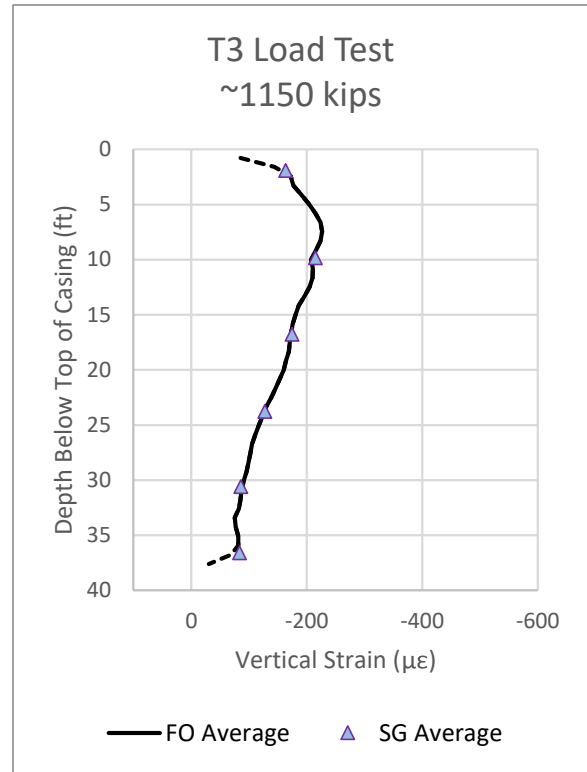*Figure 7-31: Vertical strain profile at ~1500 kips load*

Figure 7-32: Average strain profile at ~1500 kips load

Figure 7-33: Vertical strain profile at ~2027 kips load

Figure 7-34: Average strain profile at ~2027 kips load

166

Figure 7-35: Vertical strain profile at 0 kips unload

Figure 7-36: Average strain profile at 0 kips unload

d) Pile T4, Closed-Type (bladder)

The strain measurement results for the distributed fiber optic system and the SGs in pile T4 are presented in Figure 7-37 to Figure 7-48. As with the other test piles, the range of the individual SG readings are approximately enveloped by the fiber optic verticals. A small deviation is observed at the 10- and 17-foot levels, where the lowest SG magnitude is consistently lower than the corresponding lowest fiber optic reading. This slight shift, as well as the peak SG values at the same levels consistently being below the peak in the fiber optic data, may explain the sight difference observed at the same depths in the average strain profiles between the SG and fiber optic data. A maximum difference in the two average strains of 46 µε was observed at the peak load of ~1750 kips, shown in Figure 7-46.

167

Figure 7-37: Vertical strain profile at ~500 kips load

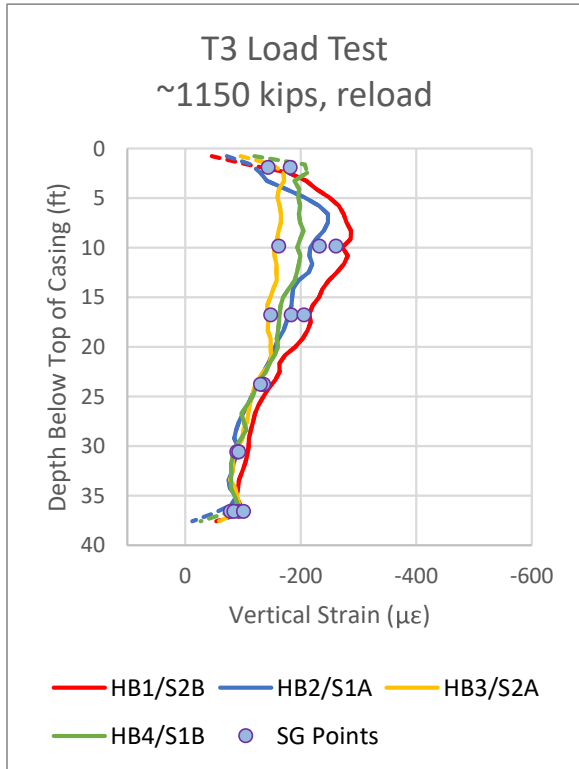*Figure 7-38: Average strain profile at ~500 kips load*

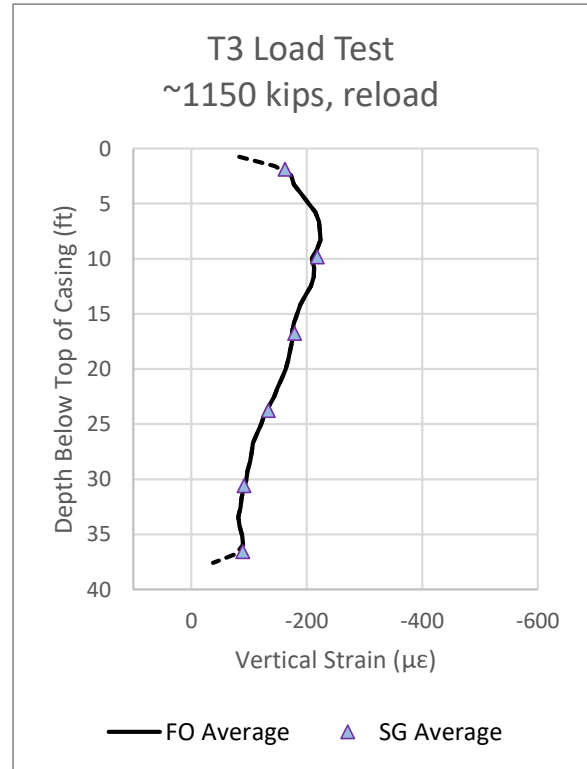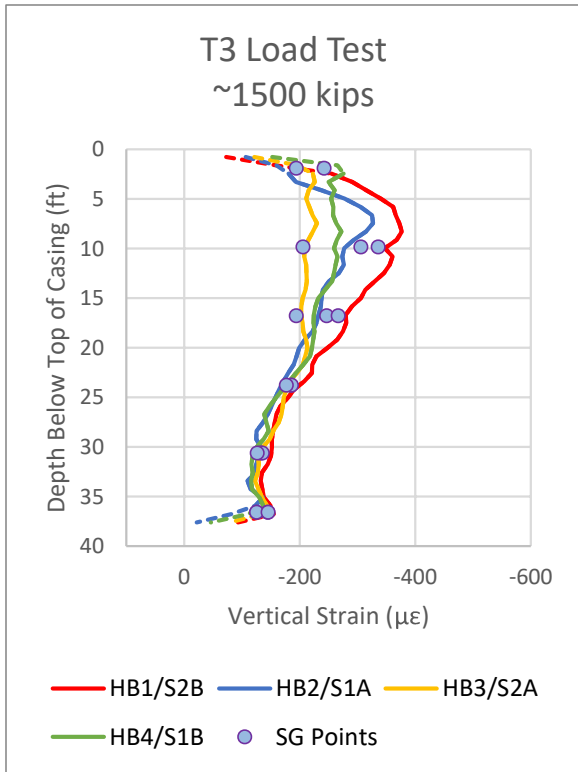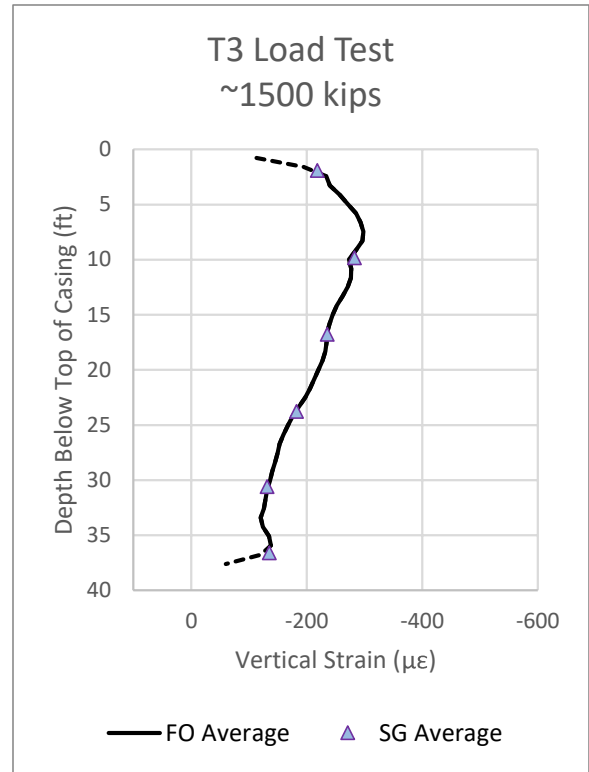*Figure 7-39: Vertical strain profile at ~1050 kips load*

Figure 7-40: Average strain profile at ~1050 kips load

Figure 7-41: Vertical strain profile at ~1050 kips reload

Figure 7-42: Average strain profile at ~1050 kips reload

Figure 7-43: Vertical strain profile at ~1500 kips load
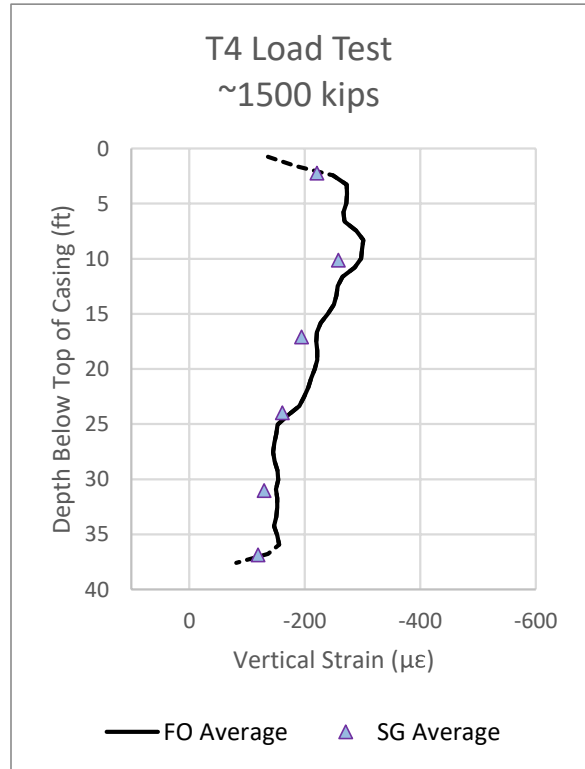
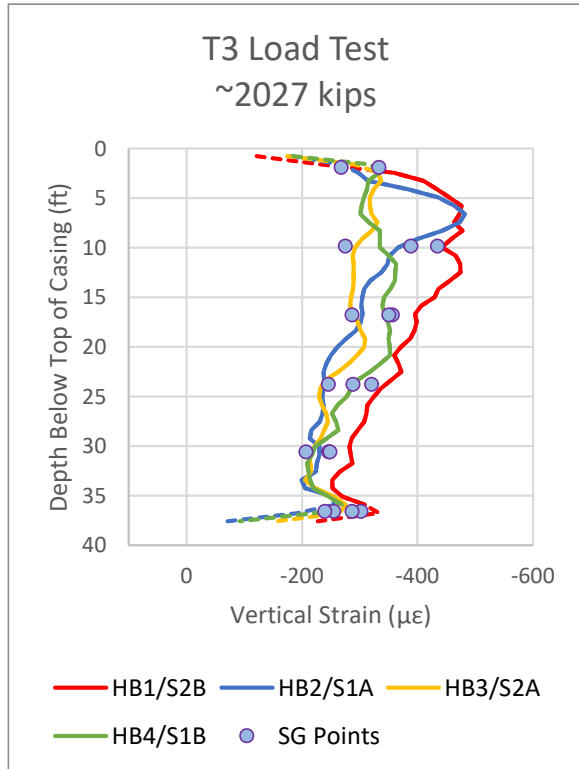*Figure 7-44: Average strain profile at ~1500 kips load*

169
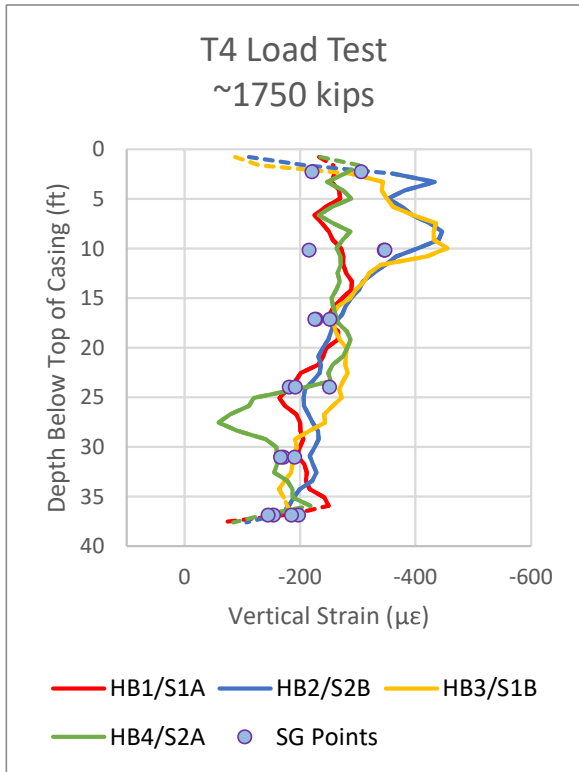
Figure 7-45: Vertical strain profile at ~1750 kips load
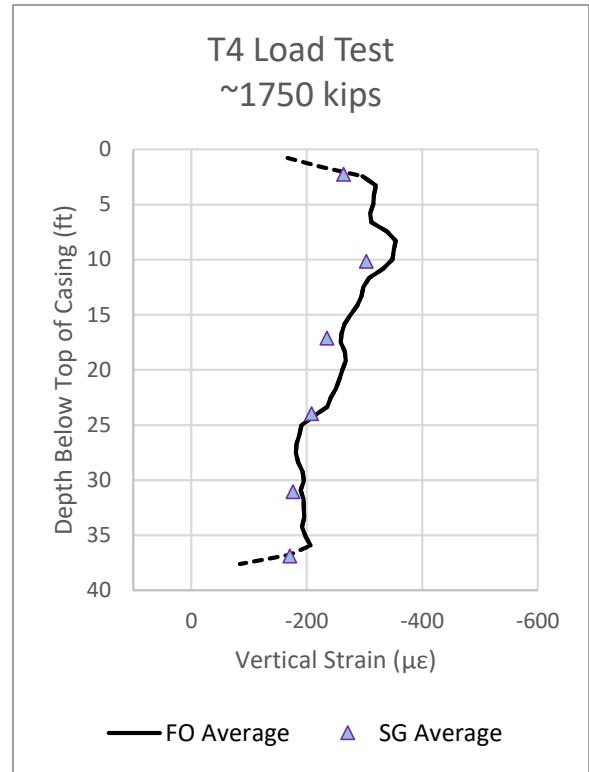
Figure 7-46: Average strain profile at ~1750 kips load
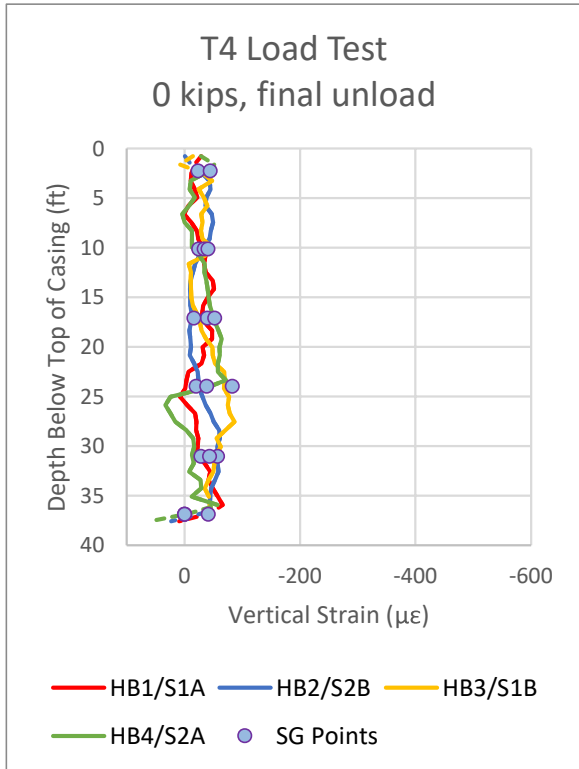
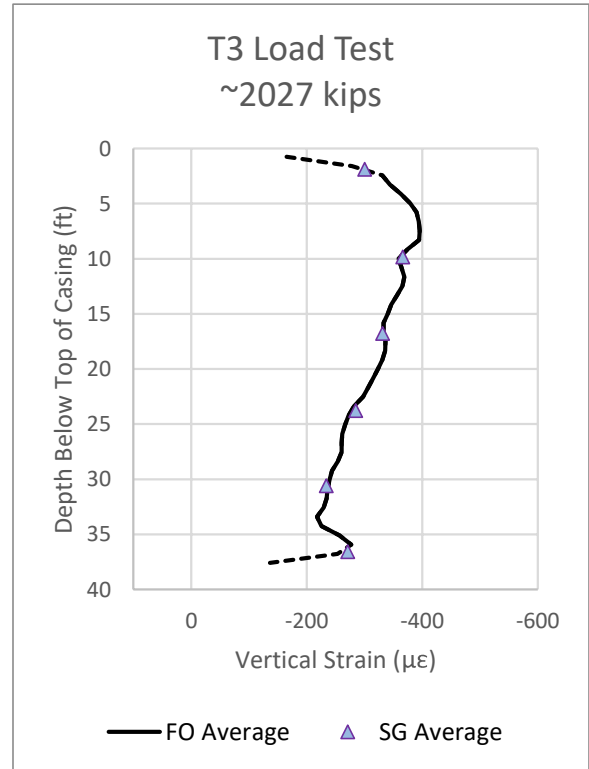*Figure 7-47: Vertical strain profile at 0 kips unload*

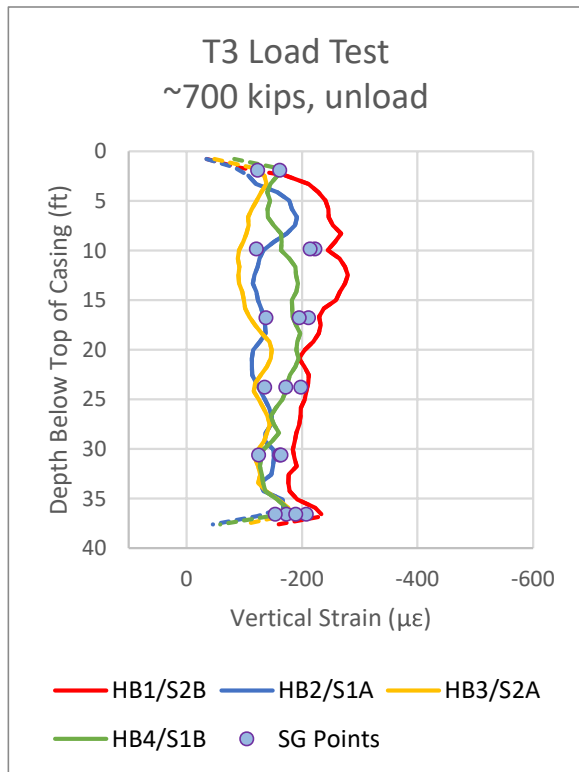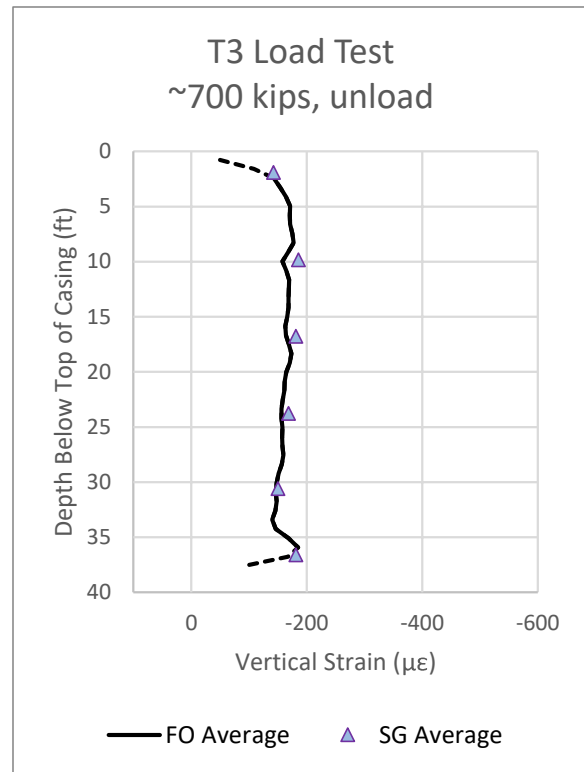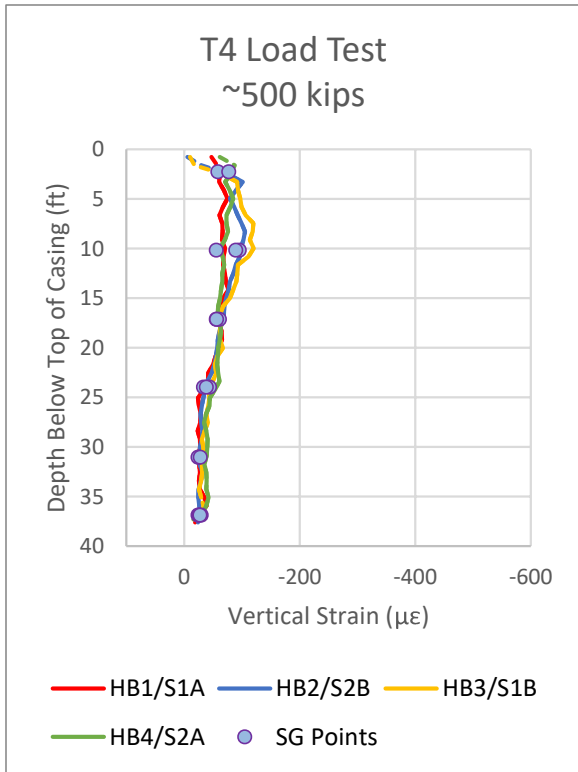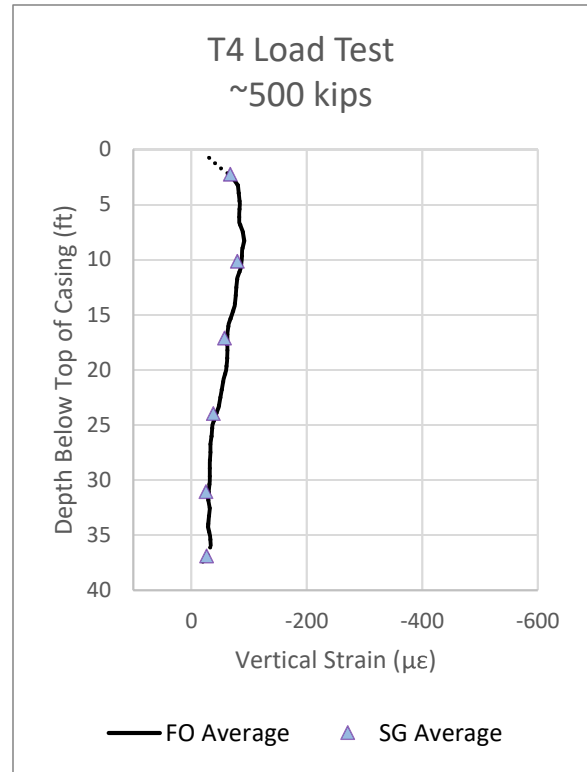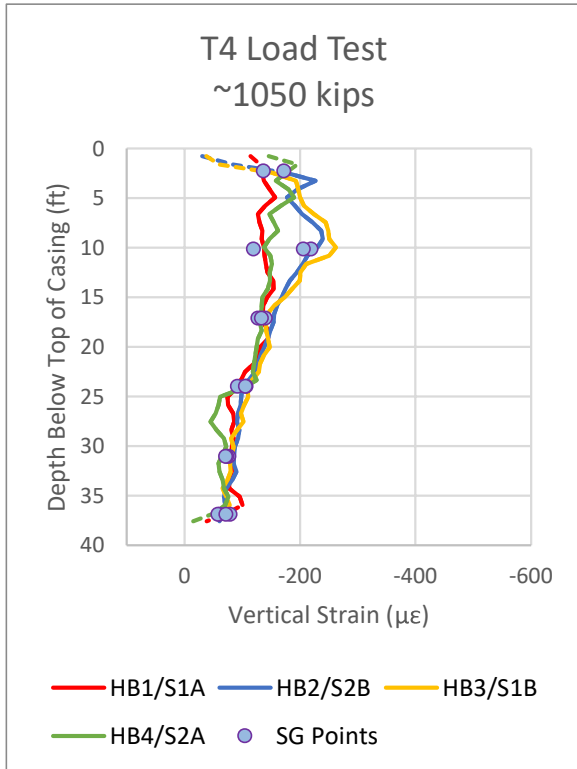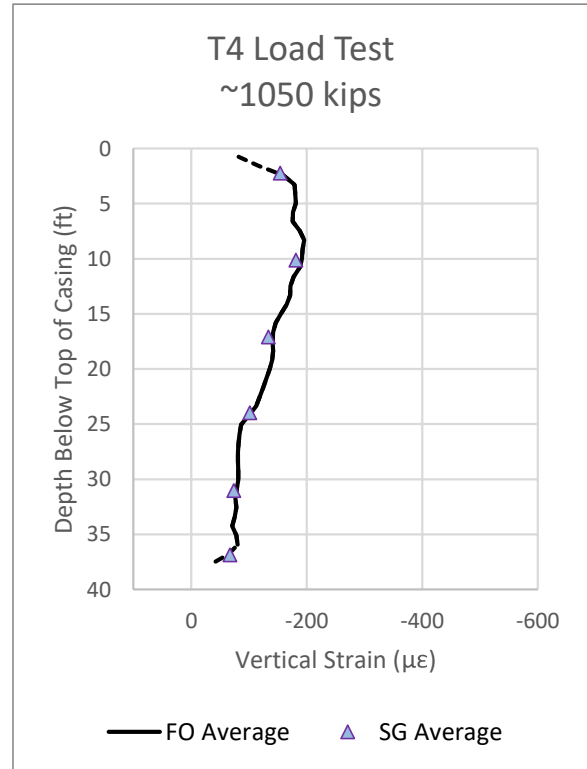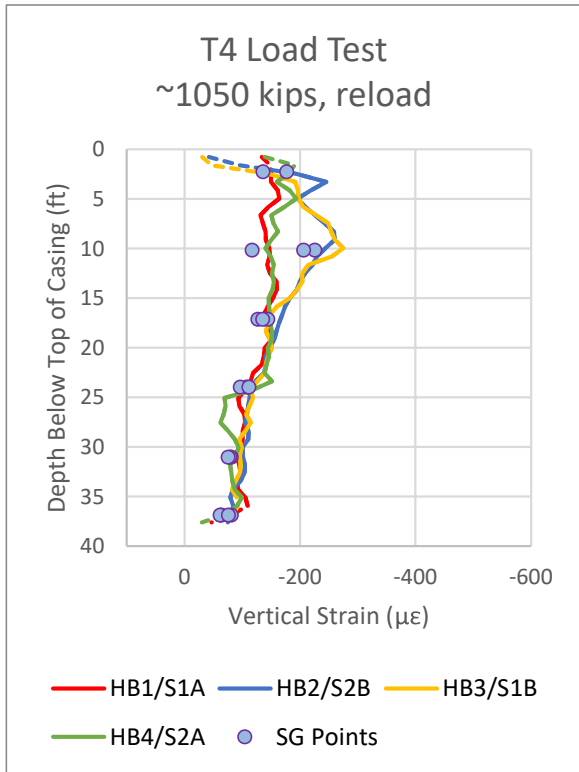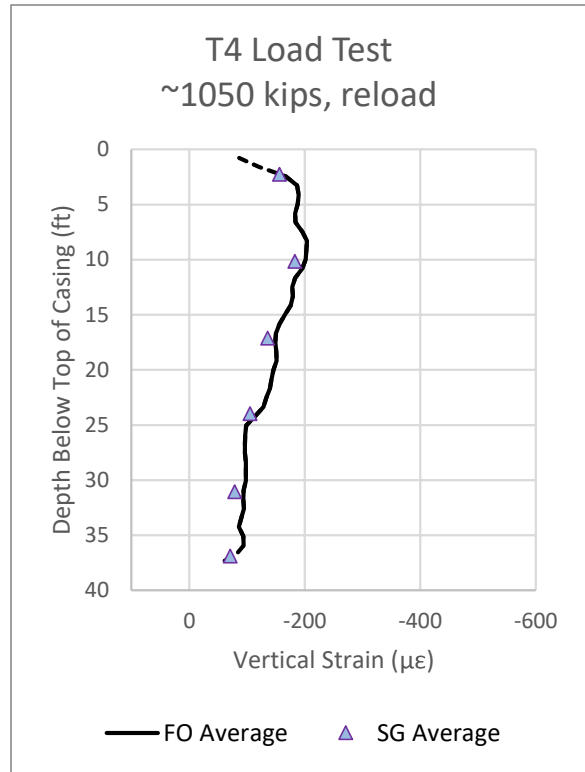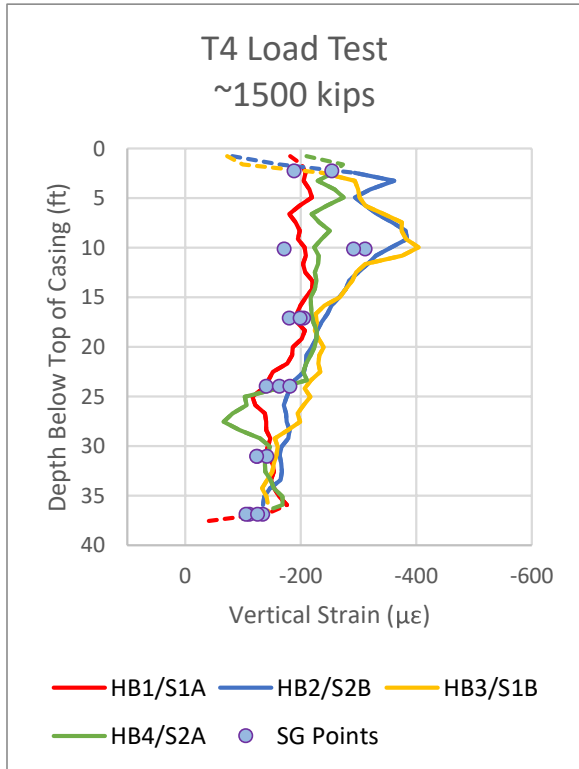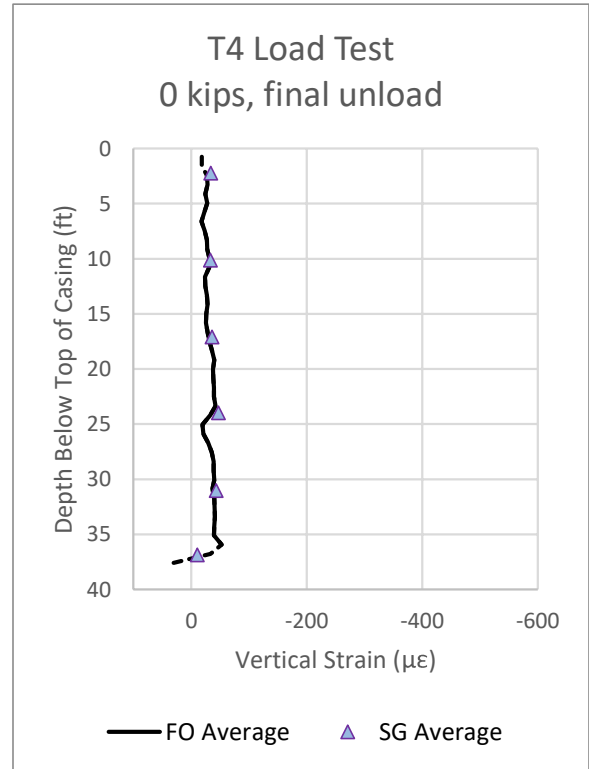*Figure 7-48: Average strain profile at 0 kips unload*

Reviewing the strain comparison over the four test shaft load results, the strain measurements produced by the distributed fiber optic system were comparable to the conventional vibrating wire strain gages. Differences in individual readings can be partially explained by the difference in placement within the pile at each elevation, an effect exacerbated by the non-uniform strain profiles associated with potential bending in the top portions of the piles. The average strain profiles were consistently within close agreement between the two measurement systems, both in magnitude as well as in the shape of the strain profile. The distributed fiber optic strain readings offer a benefit over the point-based strain gauges in that they generate a (near) continuous strain profile along the pile length, allowing variations in strain at a given elevation to be understood in a more complete context as compared to discrete reading elevations. This benefit is most apparent in the case of individual outlier measurements, which absent a complete strain profile might otherwise be discarded in evaluation of the results.

Quantification of Variable Strain Effect on Fiber Optic Readings

Based on the lab testing in Chapter 3 and the understanding that the load in the piles were not constant throughout the fiber optic reading intervals (apart from ALICIA) during base grouting and the load tests, the fiber optic strain profiles presented in this report represent a temporal sampling of the strains in the pile during the approximate five-minute reading. The reading architecture used in the commercial Omnisens analyzer "sweeps" the range of frequencies within the reading window, from lowest to highest. Where each frequency peak along the fiber falls within the scan determines the specific time within the reading that the strain at that point is registered.

For the study in this discussion, the highest load increment during load testing was chosen for analysis. This corresponds to the peak load of 2027 kips applied during the load test of test shaft T3. Using the load cell data at the top of the pile, recorded every 5-6 seconds, the fiber optic strain readings can be approximately corrected to a single point in time and associated load. This process quantifies the effect of the analyzer architecture on the resulting strain profile. The approach requires adopting the assumption that the strains within the length of the

pile are linearly dependent on the applied load in the analysis period. While this assumption is not strictly valid for all load cases, it forms an upper limit for the potential shift in strain resulting from the load decay during the hold period.

During each hold period during the load test of T3, a single fiber optic reading was taken, taking on average just under 5 minutes. During this time, the load applied to the pile would decay from its initial peak as the pressure in the actuators gradually reduced (the reduction is understood to be attributed partially to pressure losses within the system, as well as the vertical movement of the pile head away from the reaction frame under higher loads). In the peak load interval for T3, the fiber optic reading was started at a maximum registered load of 2027.7 kips. During the 294.7 seconds to complete the fiber optic reading, the measured load dropped 7% to 1885.7 kips. The load decay curve, as well as the start and stop of the fiber optic reading, is shown in Figure 7-49.
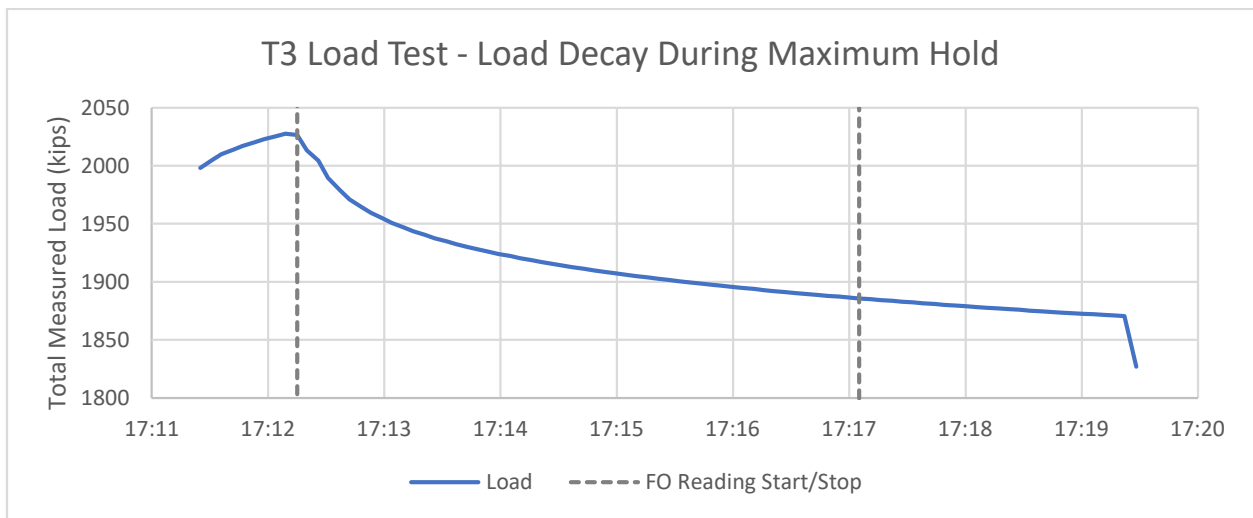
Figure 7-49: Load decay during peak interval in T3 load test

The start and stop of the fiber optic reading are shown in Figure 7-49. As can be seen, the reading started just following the peak load after the load test operator reported that they had stopped adding pressure to the actuators.

The raw frequency profile of the 2027 kip fiber optic reading is shown in Figure 7-50. The lower and upper scanning frequency bounds, set within the analyzer configuration, are shown in dashed black lines at 10.7 GHz and 11.1 GHz, respectively.
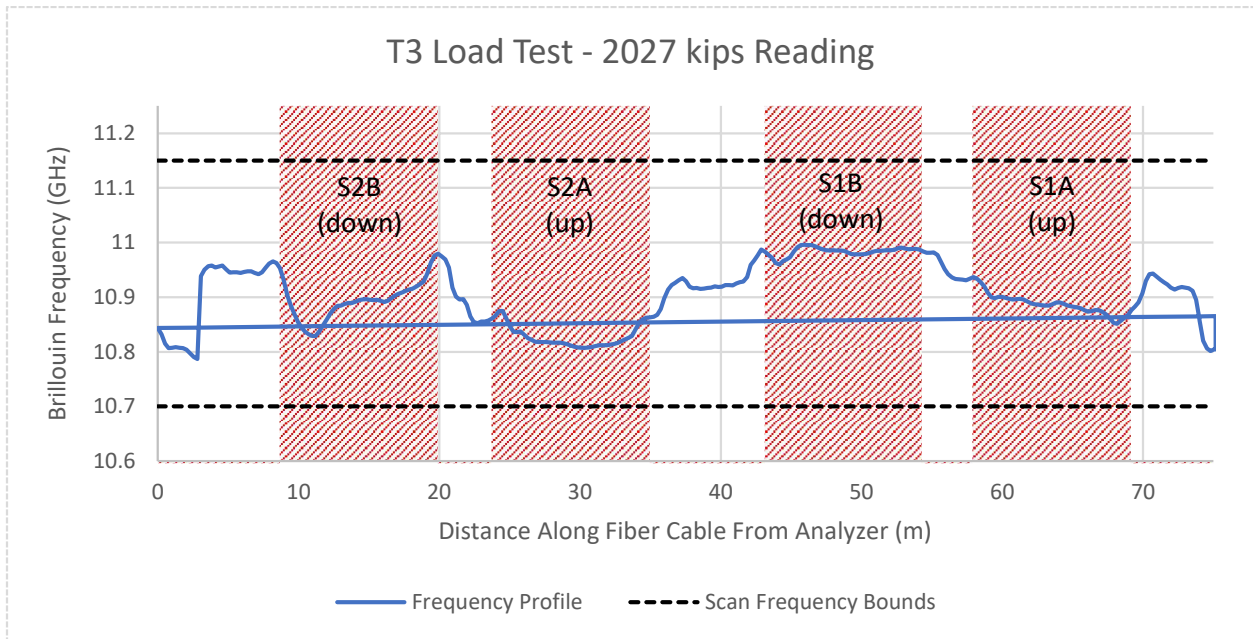
Figure 7-50: Raw frequency profile of 2027 kip fiber optic strain reading

Using the baseline readings taken prior to the start of the load test and the calibration factors for the strain cable, the frequency profile above can be processed into four individual strain profiles with depth. This was originally presented in Figure 6-33 and is reproduced as Figure 7-51.
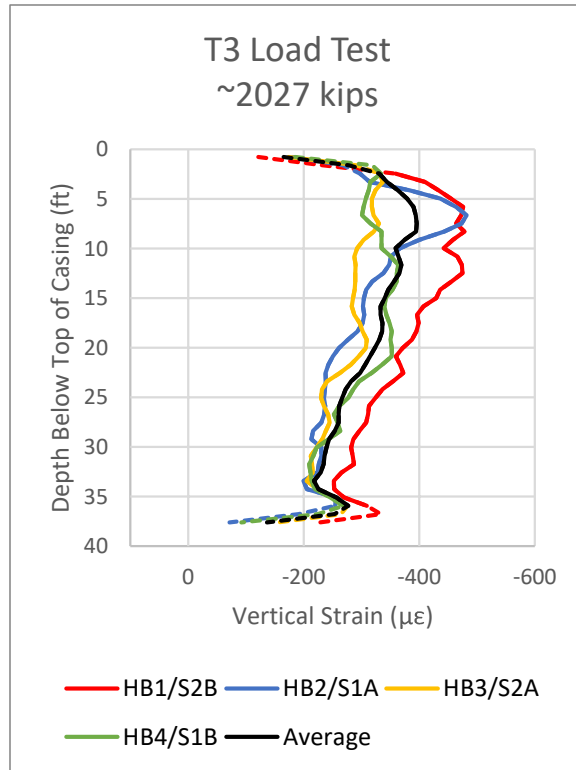
Figure 7-51: T3 load test vertical strain with depth at maximum applied load (uncorrected)

Within the configuration of the analyzer, a frequency step for the reading was set at 0.0005 GHz (0.5 MHz). Between the bottom and top frequency, this means that 901 individual frequency scans were taken during the reading. Dividing the recorded reading time of 294.699 seconds by the number of steps, 3.057 steps were completed each second, with a corresponding shift in frequency of 0.0015 GHz/second. Using this frequency rate, the approximate scan frequency that the analyzer was reading for each second of the total read time can be calculated. Inverting this approach and applying it to the raw frequency profile of the strain reading, the nearest second when each measurement point within the pile was interrogated during the total reading was estimated. The scan time of each strain measurement point within the pile is shown in Figure 7-52.
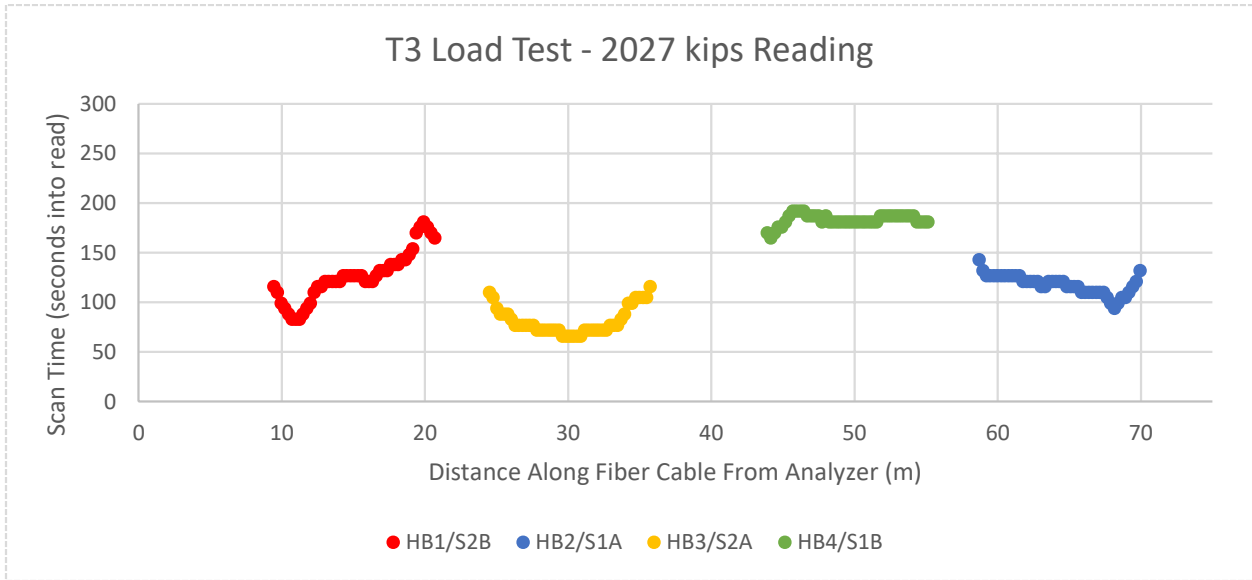
Figure 7-52: Scan time of each reading point within the 4 strain verticals

As shown in Figure 7-52, there was not only variation in the time when the individual measurements were taken during the total scan, both within and between the individual strain verticals; the first strain measurement did not take place until 66 seconds into the reading. Using the calculated time when each reading point was interrogated and synchronizing the start of the reading to the associated load measurement in the pile, the approximate load at the top the pile when each reading was taken is evaluated. This is presented in Figure 7-53.
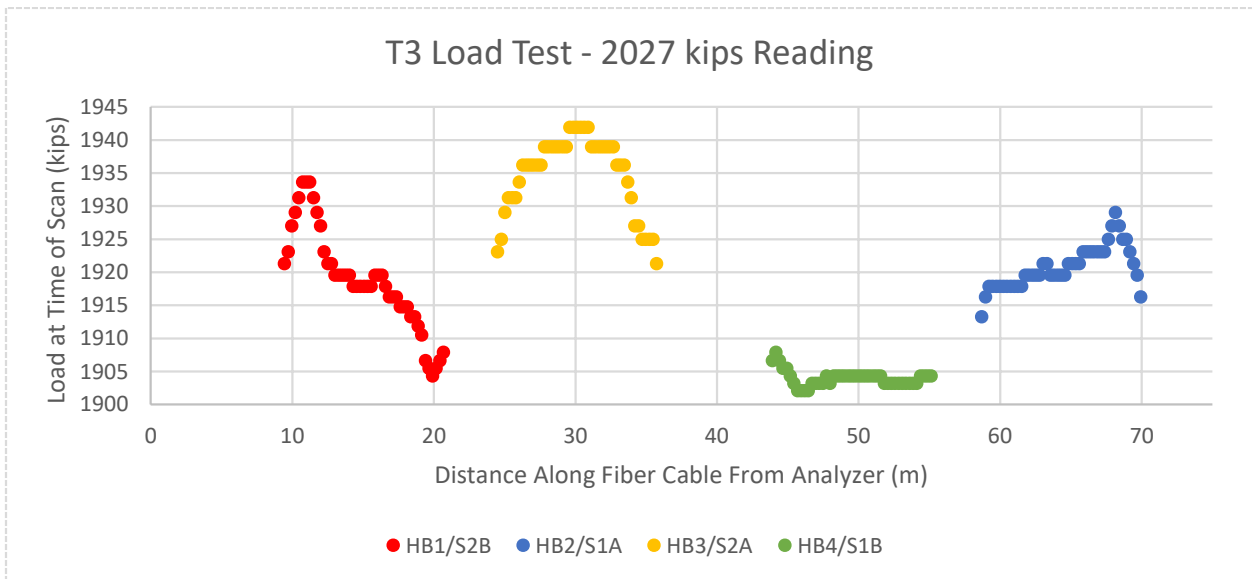
Figure 7-53: Measured load at top of pile for each reading point scan time

175

Once the measured load at the top of the pile has been determined for each measurement point within the fiber optic profile, the measured strain can be normalized (scaled up) by the corresponding percentage of the maximum load at each point. This provides an upper bound approximation of what the instantaneous strain profile within the pile would have been at the start of the reading when the maximum load was applied. The applied normalization equation is presented below.

$$\varepsilon_{i,0} = \frac{\varepsilon_{i,t}\ P_0}{P_t}$$

where

$\varepsilon_{0,i}$ = the equivalent strain at point i at time 0 (max load)

$\varepsilon_{t,i}$ = the measured strain at point i at associated reading time t

P_0 = the measured applied load at the top of the pile at time 0 (max load)

P_t = the measured applied load at the top of the pile at time t

The original and normalized strain profiles for the four strain verticals and the average strain are presented in Figure 7-54 to Figure 7-58.
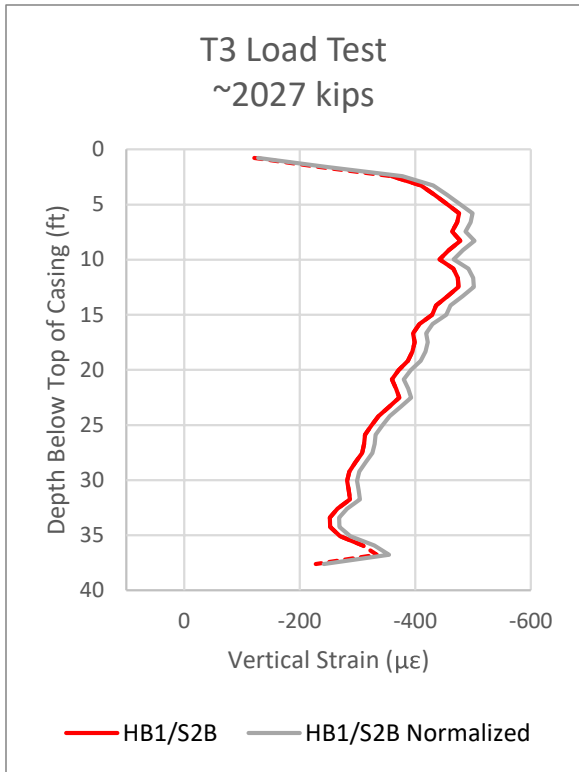
Figure 7-54: Normalized strain profile HB1
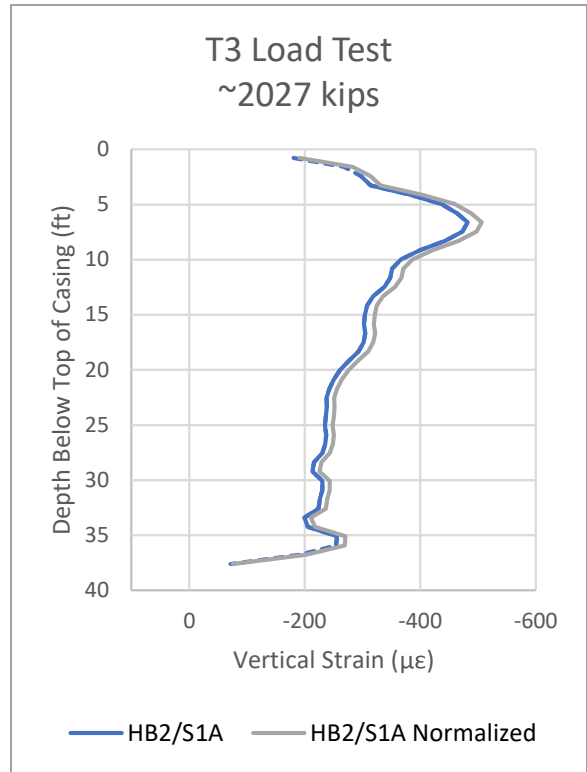
Figure 7-55: Normalized strain profile HB2
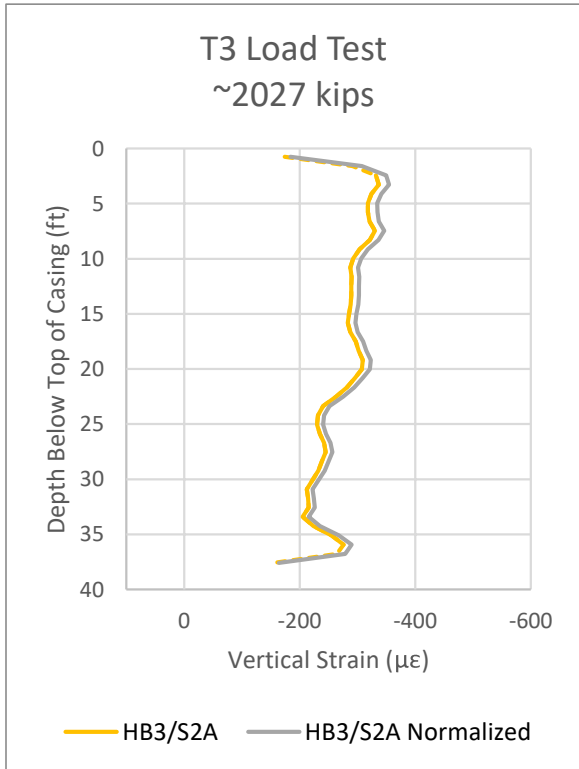
Figure 7-56: Normalized strain profile HB3
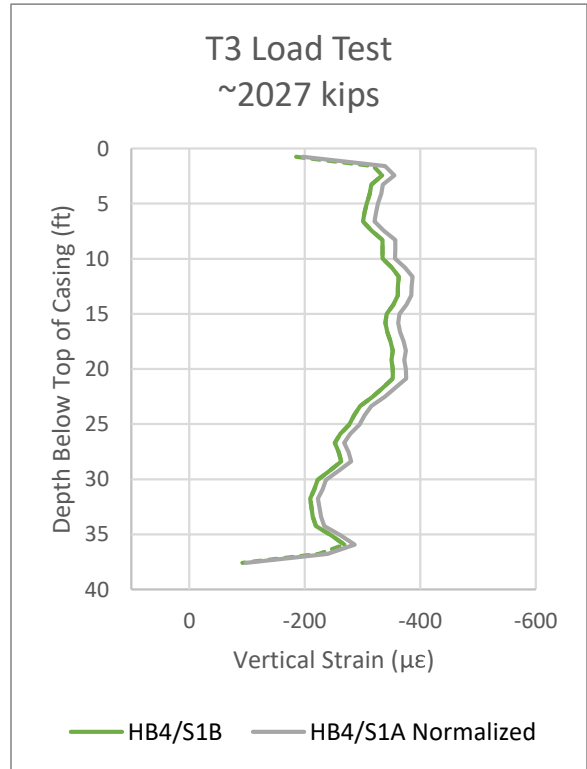
Figure 7-57: Normalized strain profile HB4

177
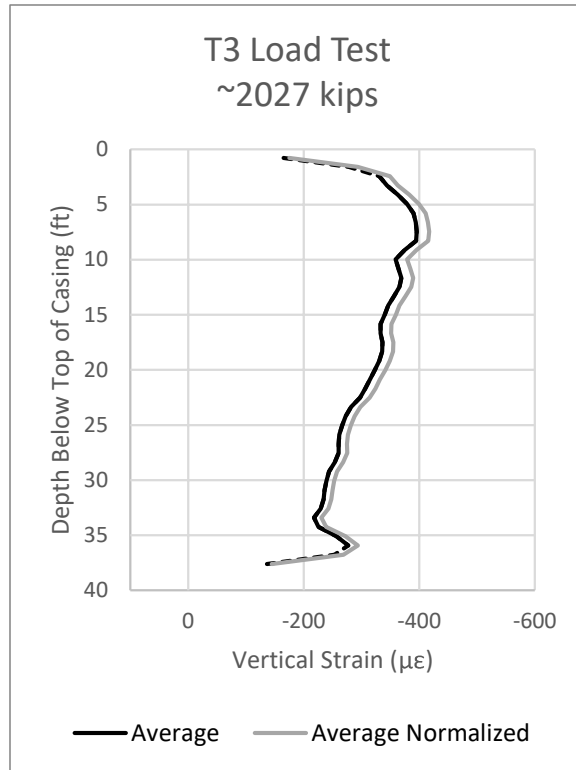
Figure 7-58: Average normalized strain profile

As can be seen in Figure 7-54 through Figure 7-58, the relative difference between the original and normalized strain profile is relatively small compared to the total magnitude of the measured strain. The maximum strain correction made in the normalization process across all four verticals had a magnitude of 26.7 µε, with an average correction value of 17.0 µε.

Based on the laboratory testing summarized in Chapter 3 and the above analysis and normalization, it is possible to correct for the effect of the temporal variation of strain along the fiber optic cable during the analyzer reading duration. Evaluating this effect and correction on the maximum load and decay observed within the load test data set for the project, the effect is relatively small with a magnitude just above the overall accuracy of the system of 15 µε. However, for future monitoring projects where the strain variation during readings is of a large enough magnitude that the effect on the strain profile is significant, the correction procedure above can be applied so long as a detailed record of the applied load is available, the fiber optic and load readings can be synchronized, and the change in load during the reading interval can be approximated as proportional to the strain change during the same time.

8. Conclusion

Distributed fiber optic sensing offers a direct, cost-effective way to incorporate a high density of strain and temperature measurements into deep foundation construction, grouting, and load testing While base grouting has observed to be a successful method to improve the capacity of large diameter drilled shafts in a variety of field studies, the variation and uncertainty associated with the grout delivery, distribution, and pressures at the bottom of the pile remain a source of variability in reliably modeling the capacity of the improved foundations.

Quality assurance and control (QA/C) on production base grouting of piles is commonly achieved by monitoring the grout pressure and volumetric flow at the top of the pile. However, as evident in the strain results during base grouting presented in Chapter 5 of this report, the vertical strains observed in the pile during grouting do not always correspond to the grout delivery behavior at the surface. Distributed fiber optic sensing can be incorporated into the QA/C program of base grouted piles to provide a wealth of data about the behavior of the pile during grouting without adding significant time or cost to the construction. The parameters that can be directly observed include the distribution of strains around the footprint of the base of the pile, the magnitude and extent to which these strains are manifest upwards from the base, the correlation of strains to the grout pumping at the ground surface, and direct measurement of the short- and long-term dissipation of strains after grouting is complete. This level information, while not currently available on most production base grouting projects, can provide valuable information to decrease the uncertainty associated with the grouting process and improve the specification and engineering design of base grouting programs.

Several of the benefits, as well as the potential limitations, of distributed fiber optic monitoring of strains in deep foundations were discussed in this report. Some of the major takeaways are summarize below:

- Cable selection: It is important to select a cable package, applicable for either strain or temperature cable, that is robust enough to survive installation and handling on site while also performs linearly over the temperature/strain ranges of interest on the project.
- Installation: The fiber optic cable installation is relatively quick when compared to the welding of conventional sister bar or embedded strain gauges. However, two important

considerations should be kept in mind. The first is to include a thermal cable to allow for temperature compensation of the data within the pile. This is particularly important for base grouting or embedded load cell tests when the introduction of fluid into the pile can locally affect the temperature of nearby strain cable. The second is to ensure to protect the cable through all phases of the installation. This includes handling of the reinforcement cages on the ground, picking of the cage from horizontal to vertical, installation into the bore, concreting, and curing.

- Analyzer selection: Since the grouting pressures (and therefore potentially the associated strains) where highly variable during the grouting process, it is recommended to use a fiber optic analyzer with a fast interrogation time. While discussion was provided of ways to correct for the averaging during a fiber optic reading in Chapter 7, this method requires a directly correlated data set proportional to the strain (in our case – the load cells) which the grouting pressure or volume has proven not to be reliable for. It is therefore simpler to take shorter, more frequent strain measurements rather than rely on the analyzer algorithm to create a temporal average of the peaks.

- Processing: Distributed fiber optic data, by its nature, creates a high density of data readings. Organizing, processing, and interpreting this data can become challenging, especially when incorporated into a limited time or budget project. It is recommended that data reduction and processing be automated through code wherever possible, especially if the approach will be repeated across multiple piles and/or projects. This can allow the data to be presented in a similar time and level of effort to conventional instruments, while providing the benefits of continuous strain and temperature profiles within the pile.

Distributed fiber optics can offer many benefits in the QA/C of base grouted piles and address some of the hurdles or misconceptions about base grouting that came up in the European Survey responses in Chapter 2. One of the major challenges posed to base grouting is a lack of understanding of how it improves the pile. While introducing strain measurements in the pile during production can only partially address that, it can help offer a much more in-depth data set on pile performance during base grouting that can hopefully build a case history catalogue to increase confidence within the industry, at least in the US. The knock-on benefit of this data set would be the ability to refine design and construction methodologies for base grouting projects, both in terms of site selection, delivery design, grout schedule, and incorporating the benefits back into a load-resistance design framework. Ultimately, this cycle can result in the practice of base grouting becoming more accepted on a widespread basis, which in turn will help motivate further research to continue to optimize the practice.

9. References

ASTM Standard D1143/D1143M (2020). "Standard Test Methods for Deep Foundation Elements Under Static Axial Compressive Load," ASTM International. https://www.astm.org/Standards/D1143.htm

ASTM Standard D7949 (2014). "Standard Test Methods for Thermal Integrity Profiling of Concrete Deep Foundations," ASTM International. https://www.astm.org/Standards/D7949.htm

ASTM Standard F3079-14 (2020), "Standard Practice for Use of Distributed Optical Fiber Sensing Systems for Monitoring the Impact of Ground Movements During Tunnel and Utility Construction on Existing Underground Utilities," ASTM International. https://www.astm.org/Standards/F3079.htm

Day, T. J., Boeckmann, A. Z., & Loehr, J. E. (2015, March). Separating Contributions from Pre-Mobilization and Ground Improvement for Post-Grouted Drilled Shafts. *IFCEE 2015*. https://doi.org/10.1061/9780784479087.086

FHWA, Brown, D. A., Turner, J. P., Castelli, R. J., & Loehr, E. J. (2018, September). *Drilled Shafts: Construction Procedures and Design Methods* (FHWA-NHI 18–024). Federal Highway Administration.

FHWA, Loehr, J. E., Marinucci, A., Duffy, P. H., Gomez, J., Robinson, H., Day, T., Boeckmann, A., & Cadden, A. (2017, March). *Evaluation and Guidance Development for Post-Grouted Drilled Shafts for Highways* (FHWA-HIF-17-024). Federal Highway Administration. https://www.fhwa.dot.gov/engineering/geotech/pubs/hif17024.pdf

Institution of Civil Engineers. (2017). *ICE Specification for Piling and Embedded Retaining Walls* (3rd ed.). ICE Publishing.

Kechavarzi, C., Soga, K., Battista, N., Fidler, P., Pelecanos, L., Elshafie, M., & Mair, R. J. (2016). *Distributed Optical Fibre Sensing for Monitoring Geotechnical Infrastructures - A Practical Guide*. ICE Publishing.

Mullins, G. (2016). Construction QA/QC Methods for Postgrouting Drilled Shafts. *Journal of Performance of Constructed Facilities*, *30*(4), 04015085–1-04015085–10. https://doi.org/10.1061/(asce)cf.1943-5509.0000827

Ruiz, M. E., & Pando, M. A. (2009, March). Load Transfer Mechanisms of Tip Post-Grouted Drilled Shafts in Sand. *Contemporary Topics in Deep Foundations*. https://doi.org/10.1061/41021(335)3

Soga, K., & Luo, L. (2018). Distributed fiber optics sensors for civil engineering infrastructure sensing. *Journal of Structural Integrity and Maintenance*, *3*(1), 1–21. https://doi.org/10.1080/24705314.2018.1426138

Appendix

Appendix A: European Post Grouting Practitioner Survey

[text reproduced from original Google Doc survey]

<u>European Post-Grouting Practitioner Survey</u>

Thank you for taking the time to complete this survey. This survey relates to post-grouting of drilled shafts/bored piles, sometimes referred to as base grouting. The author, Andrew Yeskoo, is a PhD student at UC Berkeley studying strain monitoring of post-grouted shafts. As the state of practice in post-grouting in Europe is relatively mature compared to that in the United States, this survey was conceived to attempt to capture the approaches taken in the European deep foundation industry.

During the survey, if a question does not apply to you or you do not understand the question, please feel free to answer as such or suggest any useful clarification.

All responses will be anonymized in the final report. We ask the following identification questions to capture the background of the survey participants to track differences in opinions across different fields and titles.

- Name
- Company
- Field (multiple choice)
    - Engineering / design
    - Contractor / construction
    - Academia
    - Other…
- Job title

I. General Approach

- Please provide a brief overview of your background with post-grouting. Roughly how many projects/piles have you worked on with post-grouting employed? What role have you had on these projects?
- In your own words, what is the benefit of post-grouting?
- What is your understanding of the mechanism(s) of improvement provided by post-grouting? If multiple mechanisms are contributing, please rank your choices in order of importance.
- Under what project context would you consider or recommend post-grouting? Why? Are there any situations in which you would not recommend post-grouting? Why?
- In what soil conditions do you feel post-grouting is most effective? Are there soil conditions where you would not recommend post-grouting? Please explain.

II. Geotechnical Design

- What approach do you use in your design of post-grouted piles? Are there empirical relationships that you use to inform your calculations? What field/soil testing parameters do you use in your design (e.g. pressuremeter, cone penetration test, standard penetration test, etc.)?
- Are there codes and/or published design guidance which you employ in your design of post-grouted piles?
- Does the use of post-grouting result in any differences in the assessment of geotechnical resistance / application of safety factors versus a non- post-grouted shaft?
- Do you rely on past pile load test data in your design of post-grouted piles? How similar (soil conditions, dimensions, etc.) must a load test result be for you to consider it applicable?
- Do you include a prescriptive load testing program as part of your design? If yes, are tested piles sacrificial or can they be used in the final structure? If tests are performed on production piles, what percentage of production piles are specific for testing?
- What are the specifications/requirements as to the timing of grouting activities during construction?

III. Grouting System Approach

- What post-grout delivery systems have you used on projects (e.g. tube-a-manchette, rubber bladder, jacking plates, drilling and grouting, etc.)?
- What post-grout delivery systems do you recommend, and why?
- Are there any grout-delivery systems which you would not recommend? Why?
- Who on the project team is responsible for the design of the grout delivery system, once the system type has been chosen? What are the most important parameters to consider in the design and layout of the system? Example parameters could include hose length from the grout plant to the pile, grout pipe diameter within the pile, elbow/valve/fitting types, aperture size and orientation at the grout delivery ports, port layout, etc.
- What are your chief concerns during the grouting process? What do you feel is important to watch for?

IV.   Grout Mix Design

- Who on the project team is responsible for the specification of the grout mix design?
- What ranges of water-cement ratios do you use? On what basis do you select the water-cement ratio?
- Do you recommend the use of bentonite in the grout? If yes, in what proportion?
- Do you recommend the use of any admixtures in the grout (e.g. plasticizers, etc.)? At what proportion?
- Is any grout testing or approval required prior to construction in the design/preconstruction phase? What types of tests/parameters are required?
- Do you vary the grout mixture during the post-grouting phase? If yes, what are the milestones or triggers of when you alter the mix?

- Do you recommend different grout mixtures based on soil type?
- What tests do you perform on the grout during post-grouting? How often are the tests performed? What are the acceptable ranges for each test?

V.   Monitoring During Grouting

- Please indicate what monitoring is performed during post-grouting on the list below. *(multiple choice)*
    - Pile tip movement
    - Pile head movement
    - Pile strains
    - Grouting volume
    - Minimum grouting pressure
    - Maximum grouting pressure
    - Residual pressure/time
    - Grout flow
    - Other…
- If a monitoring value listed above is used for acceptance or has a minimum/maximum value, please state that criteria.
- If grout volume is monitored, what approach do you use to calculate the volume of the grout in the soil or grouting zone?
- What approach do you use for pressure monitoring? Where in the system are the pressure readings taken (location of dial gauges or pressure transducers)? Is the effective pressure at the toe of the pile/injection point calculated (and using what method)?
- If strains within the piles are measured, what type of measuring system is used? Where within the pile are the measurement points located?
- What approach is taken to monitoring data? Are data taken manually or is an automated system employed? At what frequency is data taken?
- Do you recommend the use of multiple stages of grouting on the same pile? What is the approach? What is the timing of staged grout injections (either on multiple circuits or re-injection on previous circuits)?
- What do you do in the event that a shaft fails to satisfy the grouting criteria?

VI.   Closing

- What do you think are the primary barriers preventing a more widespread adoption of post-grouting in the industry?
- Is there any thing of importance (either in design, construction, or monitoring) which was not covered in this survey?
- Would you be willing to be contacted for any follow-up questions? *(yes/no)*
- If yes, please provide your e-mail address.

Thank you for your participation!

If you have any questions or comments on this survey, please feel free to contact Andrew

Yeskoo at rayeskoo@berkeley.edu

Appendix B: Specification Considerations for Fiber Optic Monitoring of Drilled Shafts

The following is intended to serve as a framework for the creation of a specification for the use of fiber optic sensing for large diameter drilled shafts. While the specific language can be modified within each section to match the content and tone of the larger specification package, the intent of each section is to provide a suggested list of requirements which will help maximize the chances of success of the monitoring program. The focus of this specification section is on the use of Brillouin distributed fiber optic systems for strain and temperature monitoring. Where appropriate, distinctions are made between the two metrics when different performance requirements apply. For the specification of Fiber Bragg Grating (FBG) or other point-based fiber optic sensors, it is recommended that these replicate the specifications of a conventional vibrating wire or resistance-based strain or temperature monitoring system, with minimal modification to address the specific equipment proposed for use.

In cases where the fiber optic monitoring is being procured by a bid process, a submittal is recommended to be required documenting the responsive firms' qualifications and instrumentation plan so that it can be checked against the specification requirements recommended below.

References

The following documents were referenced in the creation of this document. While no single sample specification document yet exists for distributed fiber optic monitoring of drilled shafts, these documents provide additional background and guidance for foundation monitoring and can be incorporated, in part or in their entirety, as the project demands. Full references for the documents below can be found in the References section of this report.

ASTM Standard D1143/D11436M, 2020. "Standard Test Methods for Deep Foundation
    Elements Under Static Axial Compressive Load."

ASTM Standard D7949, 2014. "Standard Test Methods for Thermal Integrity Profiling of
    Concrete Deep Foundations."

ASTM Standard F3079, 2014 (2020), "Standard Practice for Use of Distributed Optical Fiber

Sensing Systems for Monitoring the Impact of Ground Movements During Tunnel and Utility

Construction on Existing Underground Utilities."

Distributed Fibre Optic Strain Sensing for Monitoring Civil Infrastructure – A Practical Guide.

Cambridge Centre for Smart Infrastructure & Construction. 2016.

Drilled Shafts: Construction Procedures and Design Methods. Publication No. FHWA-NHI 18-

024. September 2018.

ICE Specification for Piling and Embedded Retaining Walls. (3rd ed). Institution of Civil

Engineers. December 2016.

Qualifications

The design, installation, monitoring, and reporting of the fiber optic monitoring data should be

performed by a qualified contractor with previous experience with fiber optic monitoring for

civil infrastructure, ideally within CIDH deep foundations.

It is recommended that a submittal response contain a summary narrative of at least three

previous fiber optic monitoring projects, including the following information:

- Monitoring scope, parameters under measurement
- List of key personnel, and who will be involved in the project
- List of equipment used, and which will be used in the project
- List of any breakages or system failures encountered during installation or monitoring
- Project reference

Quality Assurance and Control

The contractor should establish and document a quality assurance and control program for the

project delivery, including any inspection, documentation, testing and test records of all fiber

optic system materials, equipment, and cables.

Equipment

It is recommended that the specific equipment proposed for use in the foundation monitoring

be outlined in the submittal response. This should include the following information:

189

Fiber optic analyzer

A data sheet for the specific model of fiber optic analyzer should be provided for review. In addition, the following performance metrics should be outlined in the submittal. For many analyzers, these metrics are co-dependent; that is, there is a tradeoff in these functions when maximizing one at the cost of reducing another. For all metrics, the compatible performance should be presented for the system settings proposed for the monitoring project.

- Measurement resolution – recommended +/- 20 $\mu\varepsilon$ or +/- 1 degree Celsius or better
- Sensing distance range – should be suitable for the entire sensing cable length, including any surface routing to monitoring point
- Readout (sampling) interval – recommended 0.25 m or better
- Spatial resolution – recommended 1 m or better
- Acquisition time – depends on the application; for load testing it should be compared to the planned hold time
- Optical budget – should be compared to the total optical losses within the planned sensing cable length, including cable losses, splices, and connectors
- Long-term stability – include any requirements for temperature stability or compensation at the analyzer location
- Range of strain/temperature able to be measured
- Requirement for single-ended or double-ended cable access

The above metrics, when taken together, should be reviewed for suitability in fulfilling the monitoring program's goals. If there are specific values or limits that are required for the monitoring project, these should be listed as requirements within the specification section.

In addition to the performance characteristics of the analyzer, the submittal should also include the processing workflow whereby the raw analyzer output is processed into strain or temperature data. This should include the format of the output data, the equations used to process the data into engineering units, and the format of the final output.

Fiber Optic Cables

The sensing fiber optic cables should be chosen to balance the sensing performance with survivability and workability during installation. The cables should be resistant to crushing, tension, kinking, and other types of physical forces that would be likely to occur during handling on site. Since the fiber optic cables themselves act as the sensing elements in a distributed fiber optic monitoring program, their selection and performance should be carefully documented in

the response submittal. A data sheet for each cable type should be submitted, including the following information:

- Manufacturer, part number, and description of the fiber optic cable, including a schematic cross section
- Single-mode or multi-mode, number of cores within the cable
- Tight buffer (strain sensing) or loose tube (temperature sensing)
- Thermal coefficient for both strain and temperature cable
- Strain coefficient for strain cable
- Allowable installation bending radius
- Calibration testing over expected strain/temperature range and documentation if behavior becomes non-linear at extremes (eg. slippage in strain cable)
- Upper and lower limits of monitored parameter ranges
- Demonstration of bonding of strain cable within concrete

As with the fiber optic analyzer, the above performance metrics should be reviewed for suitability in fulfilling the monitoring program's goals.

Installation

Cable Splicing and Connectors

All splicing and cable preparation should be performed by a qualified worker using fusion splicing. It is recommended that the optical attenuation for each splice not exceed 0.02dB. All splices should be protected within a waterproof housing that provides strain relief as to protect the splice during installation. The monitoring loops should be designed so that no splice points, including connectors, are located within the pile itself. In addition, a splicer and materials to perform a cable repair should be present on-site during installation in the case of a breakage.

Cable Integrity Testing

Cable, splice, and connector integrity should be tested periodically during installation using an OTDR fiber optic tester. In the event that a breakage is detected, the installation should be halted if feasible and the point of breakage inspected and ascertained for a potential field repair.

Cable Layout

For thermal integrity testing, it is recommended that approximately one thermal fiber optic cable be installed for every foot of diameter, rounding up to the nearest even number for loop-based systems, with the cables evenly spaced around the circumference of the reinforcing cage. For strain monitoring, it is recommended that at least four strain verticals be placed at 90-degree intervals around the cage. For larger diameter piles, additional strain verticals can be incorporated but it is recommended to keep them opposed at 180° apart as to allow for measurement of bending within the pile. For piles where only strain monitoring is being performed, it is recommended to incorporate at least one set of thermal cables to measure the temperature during the load test and confirm that the temperature is stable during testing and thermal compensation is not required.

Cable Attachment

The fiber optic sensing cable should be attached to the reinforcement cage to maintain a vertical alignment once installed in the pile bore. The cables should be snuggly held to the cage using zip ties every 3-6 feet. The zip ties should be applied at locations as to not cause kinks or sharp bends within the fiber optic cables. The cables should be maintained taught and in as straight alignment as is feasible. In the case when the fibers are attached to the cage when it is horizontal, sufficient slack should be allowed in the cables as to accommodate the bending and deformation of the cage as it is picked up and rotated to vertical, with any excess slack then pulled out during the lowering of the cage into the bore. All bends and curves in the cable should be installed at a radius equal to or greater than that recommended for the cable. All bends or direction changes, such as the turn-around at the bottom of the pile, should be installed with physical constraints (zip ties, conduit guides, etc.) to prevent the bending radius from decreasing during installation and tensioning.

Protection of the Cables

Special effort should be spent by all members of the project team to protect and avoid damaging the fiber optic cables. This includes protection during installation, moving of the reinforcement cage, installation within the pile bore, during concreting, and after concreting but prior to the load test. When the fiber optic cables are not being actively interrogated by the

analyzer, it is recommended that the excess cable be neatly coiled and placed in a plastic bag for protection.

Thermal Monitoring

A temperature baseline should be taken as soon as possible after concreting. The baseline should consist of a minimum of three consecutive readings, after which they should be compared with each other to ensure that the system is functioning properly. If site access and safety allow, the baseline can be taken prior to concrete placement, with periodic thermal readings taken during the pour. The readings should continue periodically until well after the concrete temperature peaks within the entire pile. If site conditions and security allow, the monitoring should be performed continuously at a recommended reading interval of 15 minutes through the monitoring period.

Criteria to establish the end of monitoring or total monitoring duration should be provided by the structural engineer, based on the specific concrete mix, volume, and expected cure time of the concrete.

The reported data should be presented in tabular form as separate tables for each vertical cable, with depth in the pile on the vertical axis and each reading time on the horizontal axis. It is recommended that the data be presented as relative temperature change from the initial baseline; however, Brillouin systems allow for an approximation of the absolute temperature along the cable with careful calibration testing of the peak frequency. This reporting is considered less accurate than the differential temperature measurement and should be caveated as such.

Strain Monitoring

A strain baseline should be taken prior to the load test or the start of any long-term strain monitoring. The baseline should consist of a minimum of three consecutive readings, after which they should be compared with each other to ensure that the system is functioning properly. For load test monitoring, the strain readings should be taken during scheduled hold times. For analyzers with a long (>10 second) interrogation time, the load should be held as constant as possible during the reading interval to maximize the accuracy of the reading.

The reported data should be presented in tabular form as separate tables for each vertical cable, with depth in the pile on the vertical axis and each reading time on the horizontal axis. It is recommended that the data be presented as relative strain change from the initial baseline. As with thermal monitoring, Brillouin systems allow for an approximation of the absolute strain along the cable. However, this can often be affected by strains not related to the pile load testing, including those resulting from the cable manufacturing and installation. This reporting is therefore not recommended unless a highly concentrated strain is observed at baseline that exceeds the common magnitude of background strain variation within the cable.